



# PHYSIOLOGICAL, PATHOLOGICAL ROLES AND PHARMACOLOGY OF INSULIN REGULATED AMINOPEPTIDASE

EDITED BY: Efstratios Stratikos, Siew Yeen Chai and Hugo Gutiérrez De Teran  
PUBLISHED IN: *Frontiers in Molecular Biosciences*,  
*Frontiers in Cell and Developmental Biology* and  
*Frontiers in Pharmacology*



# frontiers

## Frontiers eBook Copyright Statement

The copyright in the text of individual articles in this eBook is the property of their respective authors or their respective institutions or funders. The copyright in graphics and images within each article may be subject to copyright of other parties. In both cases this is subject to a license granted to Frontiers.

The compilation of articles constituting this eBook is the property of Frontiers.

Each article within this eBook, and the eBook itself, are published under the most recent version of the Creative Commons CC-BY licence.

The version current at the date of publication of this eBook is CC-BY 4.0. If the CC-BY licence is updated, the licence granted by Frontiers is automatically updated to the new version.

When exercising any right under the CC-BY licence, Frontiers must be attributed as the original publisher of the article or eBook, as applicable.

Authors have the responsibility of ensuring that any graphics or other materials which are the property of others may be included in the CC-BY licence, but this should be checked before relying on the CC-BY licence to reproduce those materials. Any copyright notices relating to those materials must be complied with.

Copyright and source acknowledgement notices may not be removed and must be displayed in any copy, derivative work or partial copy which includes the elements in question.

All copyright, and all rights therein, are protected by national and international copyright laws. The above represents a summary only. For further information please read Frontiers' Conditions for Website Use and Copyright Statement, and the applicable CC-BY licence.

ISSN 1664-8714

ISBN 978-2-88966-902-8

DOI 10.3389/978-2-88966-902-8

## About Frontiers

Frontiers is more than just an open-access publisher of scholarly articles: it is a pioneering approach to the world of academia, radically improving the way scholarly research is managed. The grand vision of Frontiers is a world where all people have an equal opportunity to seek, share and generate knowledge. Frontiers provides immediate and permanent online open access to all its publications, but this alone is not enough to realize our grand goals.

## Frontiers Journal Series

The Frontiers Journal Series is a multi-tier and interdisciplinary set of open-access, online journals, promising a paradigm shift from the current review, selection and dissemination processes in academic publishing. All Frontiers journals are driven by researchers for researchers; therefore, they constitute a service to the scholarly community. At the same time, the Frontiers Journal Series operates on a revolutionary invention, the tiered publishing system, initially addressing specific communities of scholars, and gradually climbing up to broader public understanding, thus serving the interests of the lay society, too.

## Dedication to Quality

Each Frontiers article is a landmark of the highest quality, thanks to genuinely collaborative interactions between authors and review editors, who include some of the world's best academicians. Research must be certified by peers before entering a stream of knowledge that may eventually reach the public - and shape society; therefore, Frontiers only applies the most rigorous and unbiased reviews.

Frontiers revolutionizes research publishing by freely delivering the most outstanding research, evaluated with no bias from both the academic and social point of view. By applying the most advanced information technologies, Frontiers is catapulting scholarly publishing into a new generation.

## What are Frontiers Research Topics?

Frontiers Research Topics are very popular trademarks of the Frontiers Journals Series: they are collections of at least ten articles, all centered on a particular subject. With their unique mix of varied contributions from Original Research to Review Articles, Frontiers Research Topics unify the most influential researchers, the latest key findings and historical advances in a hot research area! Find out more on how to host your own Frontiers Research Topic or contribute to one as an author by contacting the Frontiers Editorial Office: [frontiersin.org/about/contact](http://frontiersin.org/about/contact)

# PHYSIOLOGICAL, PATHOLOGICAL ROLES AND PHARMACOLOGY OF INSULIN REGULATED AMINOPEPTIDASE

Topic Editors:

**Efstratios Stratikos**, National and Kapodistrian University of Athens, Greece

**Siew Yeen Chai**, Monash University Melbourne, Australia

**Hugo Gutiérrez De Teran**, Uppsala University, Sweden

**Citation:** Stratikos, E., Chai, S. Y., de Teran, H. G., eds. (2021). Physiological, Pathological Roles and Pharmacology of Insulin Regulated Aminopectidase. Lausanne: Frontiers Media SA. doi: 10.3389/978-2-88966-902-8

# Table of Contents

- 04 Editorial: Physiological, Pathological Roles and Pharmacology of Insulin Regulated Aminopeptidase**  
Siew Yeen Chai, Hugo Gutiérrez-de-Terán and Efstratios Stratikos
- 07 The Type of Fat in the Diet Influences the Behavior and the Relationship Between Cystinyl and Alanyl Aminopeptidase Activities in Frontal Cortex, Liver, and Plasma**  
Ana Belén Segarra, Isabel Prieto, Inmaculada Banegas, Magdalena Martínez-Cañamero, Marc de Gasparo, Patrick Vanderheyden, Stefan Zorad and Manuel Ramírez-Sánchez
- 14 Reciprocal Expression Patterns of Placental Leucine Aminopeptidase/Insulin-Regulated Aminopeptidase and Vasopressin in the Murine Brain**  
Yoshikuni Goto, Takahiro J. Nakamura, Kenji Ogawa, Akira Hattori and Masafumi Tsujimoto
- 21 The Discovery of Insulin-Regulated Aminopeptidase (IRAP) Inhibitors: A Literature Review**  
Dimitris Georgiadis, Angeliki Ziotopoulou, Eleni Kaloumenou, Angelos Lelis and Antonia Papasava
- 29 IRAP Inhibitors: M1-Aminopeptidase Family Inspiration**  
Nicholas Barlow and Philip E. Thompson
- 37 Is There an Interplay Between the Functional Domains of IRAP?**  
Anika Vear, Tracey Gaspari, Philip Thompson and Siew Yeen Chai
- 47 From Angiotensin IV to Small Peptidemimetics Inhibiting Insulin-Regulated Aminopeptidase**  
Mathias Hallberg and Mats Larhed
- 63 The Role of Insulin Regulated Aminopeptidase in Endocytic Trafficking and Receptor Signaling in Immune Cells**  
Delphyne Descamps, Irini Evnouchidou, Vivien Caillens, Carole Drjac, Sabine Riffault, Peter van Endert and Loredana Saveanu
- 77 Insulin-Regulated Aminopeptidase Inhibition Ameliorates Metabolism in Obese Zucker Rats**  
Katarina Krskova, Lucia Balazova, Viktoria Dobrocsyova, Rafal Olszanecki, Maciej Suski, Siew Yeen Chai and Štefan Zorad
- 87 IRAP Endosomes Control Phagosomal Maturation in Dendritic Cells**  
Mirjana Weimershaus, François-Xavier Mauvais, Irini Evnouchidou, Myriam Lawand, Loredana Saveanu and Peter van Endert
- 100 Serum IRAP, a Novel Direct Biomarker of Prediabetes and Type 2 Diabetes?**  
Candice Trocmé, Nicolas Gonnet, Margaux Di Tommaso, Hanen Samouda, Jean-Luc Cracowski, Claire Cracowski, Stéphanie Lambert-Porcheron, Martine Laville, Estelle Nobécourt, Chiraz Gaddhab, Allan Le Lay, Torsten Bohn, Christine Poitou, Karine Clément, Fahd Al-Mulla, Milad S. Bitar and Serge P. Bottari
- 110 Structural Basis of Inhibition of Human Insulin-Regulated Aminopeptidase (IRAP) by Benzopyran-Based Inhibitors**  
Sudarsana Reddy Vanga, Johan Åqvist, Anders Hallberg and Hugo Gutiérrez-de-Terán





# Editorial: Physiological, Pathological Roles and Pharmacology of Insulin Regulated Aminopeptidase

Siew Yeen Chai<sup>1</sup>, Hugo Gutiérrez-de-Terán<sup>2</sup> and Efstratios Stratikos<sup>3\*</sup>

<sup>1</sup> Department of Physiology, Monash Biomedicine Discovery Institute, Monash University, Clayton, VIC, Australia,

<sup>2</sup> Department of Cell and Molecular Biology, Uppsala University, Uppsala, Sweden, <sup>3</sup> Biochemistry Laboratory, Department of Chemistry, National and Kapodistrian University of Athens, Athens, Greece

**Keywords:** aminopeptidase, metabolism, trafficking, immune system, peptide hormones, central nervous system, glucose, fibrosis

## Editorial on the Research Topic

### Physiological, Pathological Roles, and Pharmacology of Insulin Regulated Aminopeptidase

Insulin-Regulated Aminopeptidase (IRAP) is a transmembrane zinc metalloprotease with several reported biological functions. IRAP belongs to the M1 family of aminopeptidases (EC 3.4.11.3) and is also known as cystinyl aminopeptidase, placental leucine aminopeptidase (PLAP), and oxytocinase. The reported biological functions of IRAP include: (i) the regulation of trafficking of glucose transporter 4 (Keller, 2003), (ii) the generation of antigenic peptides for cross-presentation (Saveanu et al., 2009), (iii) T-cell receptor signaling (Evnouchidou et al., 2020), (iv) the regulation of placental oxytocin levels (Tsujiimoto et al., 1992), (v) not well-understood roles in cognition and other central nervous system functions possibly through the regulation of oxytocin and vasopressin levels in the brain (Herbst et al., 1997; Albiston et al., 2011; Bernstein et al., 2017) or altered glucose uptake (Fernando et al., 2008; Albiston et al., 2011; Ismail et al., 2017), and (vi) the regulation of organ fibrosis (T. Gaspari, personal communication). All these roles have been associated with at least one of the two functional components of IRAP: an extracellular *C-terminal* domain that contains the M1 exopeptidase catalytic site and a 110 amino-acid long cytosolic *N-terminal* domain, connected by a single transmembrane-spanning region. The *C-terminal* domain underlies the ability of IRAP to trim antigenic peptides and peptide hormones, whereas the *N-terminal* domain appears to control intracellular trafficking and signaling events. The structure of the extracellular domain has been recently solved and resembles several other enzymes of the M1 family of aminopeptidases, featuring a large internal cavity adjacent to the catalytic center, which can accommodate peptide substrates (Mpakali et al., 2015) (**Figure 1**). The *C-terminal* domain can dimerize and change conformations upon ligand binding (Mpakali et al., 2017). Very little is currently known about the structure and molecular interactions of the *N-terminal* domain.

The important biological functions in which IRAP participates are attracting increased attention for possible pharmacological interventions. The primary function targeted to date has been the aminopeptidase activity, for which both functional and structural knowledge exists. In particular, IRAP inhibitors have been pursued as potential therapeutics for cognitive disorders (Chai et al., 2008; Andersson and Hallberg, 2012; Diwakarla et al., 2016), immune modulators (Kokkala et al., 2016), and more recently as anti-fibrotic agents.

In this special issue “Physiological, Pathological Roles and Pharmacology of Insulin Regulated Aminopeptidase,” we present a series of reviews and research papers written from leading authors in the field of IRAP, covering most aspects of the state-of-the-art research for this enzyme.

## OPEN ACCESS

### Edited and reviewed by:

Cecilia Giulivi,  
University of California, Davis,  
United States

### \*Correspondence:

Efstratios Stratikos  
estratikos@chem.uoa.gr

### Specialty section:

This article was submitted to  
Cellular Biochemistry,  
a section of the journal  
Frontiers in Molecular Biosciences

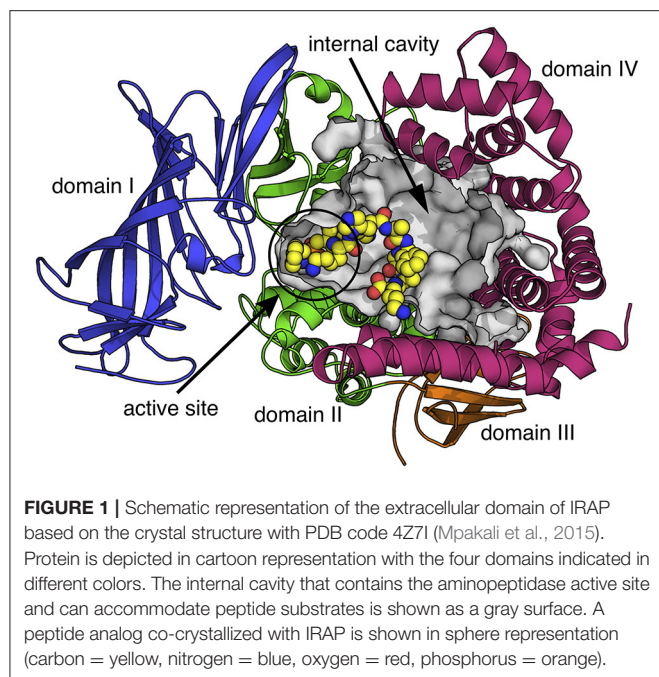
**Received:** 24 March 2021

**Accepted:** 30 March 2021

**Published:** 23 April 2021

### Citation:

Chai SY, Gutiérrez-de-Terán H and  
Stratikos E (2021) Editorial:  
Physiological, Pathological Roles and  
Pharmacology of Insulin Regulated  
Aminopeptidase.  
Front. Mol. Biosci. 8:685101.  
doi: 10.3389/fmolb.2021.685101



With regards to the role of IRAP in metabolism, Trocmé et al. explore the possibility of using serum IRAP as a novel biomarker of prediabetes and type 2 diabetes, Krskova et al. demonstrate that IRAP inhibition improves glucose clearance in obese Zucker rats and Segarra et al. demonstrate how different types of dietary fat intake can affect IRAP and Alanyl aminopeptidase activities in the frontal cortex of the brain, the liver, and plasma. Exploring the role of IRAP in the immune system, Weimershaus et al. demonstrate how IRAP endosomes control phagosomal maturation in dendritic cells and Descamps et al. explore the role of IRAP in endocytic trafficking and receptor signaling in immune cells. Related to the role of IRAP in the central nervous system, Goto et al. describe a reciprocal relationship between IRAP expression and vasopressin levels in the murine brain.

## REFERENCES

- Albiston, A. L., Diwakarla, S., Fernando, R. N., Mountford, S. J., Yeatman, H. R., Morgan, B., et al. (2011). Identification and development of specific inhibitors for insulin-regulated aminopeptidase as a new class of cognitive enhancers. *Br. J. Pharmacol.* 164, 37–47. doi: 10.1111/j.1476-5381.2011.01402.x
- Andersson, H., and Hallberg, M. (2012). Discovery of inhibitors of insulin-regulated aminopeptidase as cognitive enhancers. *Int. J. Hypertens.* 2012:789671. doi: 10.1155/2012/789671
- Bernstein, H. G., Müller, S., Dobrowolny, H., Wolke, C., Lendeckel, U., Bukowska, A., et al. (2017). Insulin-regulated aminopeptidase immunoreactivity is abundantly present in human hypothalamus and posterior pituitary gland, with reduced expression in paraventricular and suprachiasmatic neurons in chronic schizophrenia. *Eur. Arch. Psychiatry Clin. Neurosci.* 267, 427–443. doi: 10.1007/s00406-016-0757-7
- Chai, S. Y., Yeatman, H. R., Parker, M. W., Ascher, D. B., Thompson, P. E., Mulvey, H. T., et al. (2008). Development of cognitive enhancers based on

In view of the two functional domains of IRAP, Vear et al. explore the under-studied relationship between the *N-terminal* cytosolic and the *C-terminal* catalytic domains of IRAP and how the localization of IRAP may play an important role in defining its physiological or pathological functions. Finally, a number of articles explore the development of IRAP inhibitors with potential pharmacological and chemical biology applications: Georgiadis et al. provide a broad review on the development of IRAP inhibitors, Barlow and Thompson focus on efforts to develop inhibitors inspired by other members of the M1 family of aminopeptidases, Hallberg et al. review the development of angiotensin IV inspired small peptidemimetic inhibitors for IRAP and Vanga et al. explore the structural basis of inhibition of IRAP by benzopyran-based compounds.

It is becoming clear that the important biological functions played by IRAP will undoubtedly sustain scientific interest on this enzyme in the coming years, especially in view of newly discovered functions with poorly understood molecular mechanisms. However, its multitude of biological roles could also act as a deterrent for drug development efforts. Likely, IRAPs tractability as a pharmaceutical target will greatly depend on detailed mechanistical analysis and prioritization of its biological functions, an aspect in which this Special Issue contributes. On the other hand, solid pre-existing progress in inhibitor design and development could incentivize drug development efforts as highlighted by contributed articles to this Special Issue. The possible effect of active-site inhibitors to IRAP's trafficking functions needs to be carefully addressed, an aspect that will certainly benefit from further work on the interplay of the two domains of IRAP. Regardless of these potential caveats, one thing is clear: the coming together of IRAP researchers from different fields and the continued frank and honest discussion that ensues will ensure that progress will be made, paving the way for the validation of IRAP as a tractable therapeutic target in the future.

## AUTHOR CONTRIBUTIONS

All authors contributed to the writing of the editorial and have approved the final version.

- inhibition of insulin-regulated aminopeptidase. *BMC Neurosci.* 9(Suppl. 2):S14. doi: 10.1186/1471-2202-9-S2-S14
- Diwakarla, S., Nylander, E., Gronbladh, A., Vanga, S. R., Khan, Y. S., Gutierrez-de-Teran, H., et al. (2016). Binding to and inhibition of insulin-regulated aminopeptidase by macrocyclic disulfides enhances spine density. *Mol. Pharmacol.* 89, 413–424. doi: 10.1124/mol.115.102533
- Evnouchidou, I., Chappert, P., Benadda, S., Zucchetti, A., Weimershaus, M., Bens, M., et al. (2020). IRAP-dependent endosomal T cell receptor signalling is essential for T cell responses. *Nat. Commun.* 11:2779. doi: 10.1038/s41467-020-16471-7
- Fernando, R. N., Albiston, A. L., and Chai, S. Y. (2008). The insulin-regulated aminopeptidase IRAP is colocalised with GLUT4 in the mouse hippocampus—potential role in modulation of glucose uptake in neurones? *Eur. J. Neurosci.* 28, 588–598. doi: 10.1111/j.1460-9568.2008.06347.x
- Herbst, J. J., Ross, S. A., Scott, H. M., Bobin, S. A., Morris, N. J., Lienhard, G. E., et al. (1997). Insulin stimulates cell surface aminopeptidase activity toward vasopressin in adipocytes. *Am. J. Physiol.* 272, E600–E606. doi: 10.1152/ajpendo.1997.272.4.E600

- Ismail, M. A. M., Mateos, L., Maioli, S., Merino-Serrais, P., Ali, Z., Lodeiro, M., et al. (2017). 27-Hydroxycholesterol impairs neuronal glucose uptake through an IRAP/GLUT4 system dysregulation. *J. Exp. Med.* 214, 699–717. doi: 10.1084/jem.20160534
- Keller, S. R. (2003). The insulin-regulated aminopeptidase: a companion and regulator of GLUT4. *Front. Biosci.* 8, s410–s420. doi: 10.2741/1078
- Kokkala, P., Mpakali, A., Mauvais, F.-X., Papakyriakou, A., Daskalaki, I., Petropoulou, I., et al. (2016). Optimization and structure–activity relationships of phosphinic pseudotriptide inhibitors of aminopeptidases that generate antigenic peptides. *J. Med. Chem.* 59, 9107–9123. doi: 10.1021/acs.jmedchem.6b01031
- Mpakali, A., Saridakis, E., Harlos, K., Zhao, Y., Kokkala, P., Georgiadis, D., et al. (2017). Ligand-induced conformational change of insulin-regulated aminopeptidase: insights on catalytic mechanism and active site plasticity. *J. Med. Chem.* 60:2963–2972. doi: 10.2210/pdb5mj6/pdb
- Mpakali, A., Saridakis, E., Harlos, K., Zhao, Y., Papakyriakou, A., Kokkala, P., et al. (2015). Crystal structure of insulin-regulated aminopeptidase with bound substrate analogue provides insight on antigenic epitope precursor recognition and processing. *J. Immunol.* 195, 2842–2851. doi: 10.4049/jimmunol.1501103
- Saveanu, L., Carroll, O., Weimershaus, M., Guernonprez, P., Firat, E., Lindo, V., et al. (2009). IRAP identifies an endosomal compartment required for MHC Class I cross-presentation. *Science* 325, 213–217. doi: 10.1126/science.1172845
- Tsujimoto, M., Mizutani, S., Adachi, H., Kimura, M., Nakazato, H., and Tomoda, Y. (1992). Identification of human placental leucine aminopeptidase as oxytocinase. *Arch. Biochem. Biophys.* 292, 388–392. doi: 10.1016/0003-9861(92)90007-J

**Conflict of Interest:** The authors declare that the research was conducted in the absence of any commercial or financial relationships that could be construed as a potential conflict of interest.

Copyright © 2021 Chai, Gutiérrez-de-Terán and Stratikos. This is an open-access article distributed under the terms of the Creative Commons Attribution License (CC BY). The use, distribution or reproduction in other forums is permitted, provided the original author(s) and the copyright owner(s) are credited and that the original publication in this journal is cited, in accordance with accepted academic practice. No use, distribution or reproduction is permitted which does not comply with these terms.



# The Type of Fat in the Diet Influences the Behavior and the Relationship Between Cystinyl and Alanyl Aminopeptidase Activities in Frontal Cortex, Liver, and Plasma

Ana Belén Segarra<sup>1</sup>, Isabel Prieto<sup>1</sup>, Inmaculada Banegas<sup>1</sup>,  
Magdalena Martínez-Cañamero<sup>1</sup>, Marc de Gasparo<sup>2</sup>, Patrick Vanderheyden<sup>3</sup>,  
Stefan Zorad<sup>4</sup> and Manuel Ramírez-Sánchez<sup>1\*</sup>

<sup>1</sup> Department of Health Sciences, University of Jaen, Jaen, Spain, <sup>2</sup> Cardiovascular & Metabolic Syndrome Adviser, Rossemaison, Switzerland, <sup>3</sup> Department of Molecular and Biochemical Pharmacology, Vrije Universiteit Brussel, Brussels, Belgium, <sup>4</sup> Biomedical Research Center, Institute of Experimental Endocrinology, Slovak Academy of Sciences, Bratislava, Slovakia

## OPEN ACCESS

### Edited by:

Siew Yeen Chai,  
Monash University, Australia

### Reviewed by:

Paul Richard Gard,  
University of Brighton,  
United Kingdom  
Vincenzo Tufarelli,  
University of Bari Aldo Moro, Italy  
Gina Cavaliere,  
University of Naples Federico II, Italy

### \*Correspondence:

Manuel Ramírez-Sánchez  
msanchez@ujaen.es

### Specialty section:

This article was submitted to  
Cellular Biochemistry,  
a section of the journal  
Frontiers in Molecular Biosciences

**Received:** 26 January 2020

**Accepted:** 22 April 2020

**Published:** 15 May 2020

### Citation:

Segarra AB, Prieto I, Banegas I,  
Martínez-Cañamero M, de  
Gasparo M, Vanderheyden P, Zorad S  
and Ramírez-Sánchez M (2020) The  
Type of Fat in the Diet Influences the  
Behavior and the Relationship  
Between Cystinyl and Alanyl  
Aminopeptidase Activities in Frontal  
Cortex, Liver, and Plasma.  
Front. Mol. Biosci. 7:94.  
doi: 10.3389/fmolb.2020.00094

Insulin-regulated aminopeptidase (IRAP, cystinyl aminopeptidase, CysAP) and aminopeptidase M (alanyl aminopeptidase, AlaAP) are closely related enzymes involved in cognitive, metabolic, and cardiovascular functions. These functions may be modulated by the type of fat used in the diet. In order to analyze a possible coordinated response of both enzymes we determined simultaneously their activities in frontal cortex, liver, and plasma of adult male rats fed diets enriched with fats differing in their percentages of saturated, mono or polyunsaturated fatty acids such as sesame, sunflower, fish, olive, Iberian lard, and coconut. The systolic blood pressure, food intake, body and liver weight as well as glucose and total cholesterol levels in plasma were measured. The type of fat in the diet influences the enzymatic activities depending on the enzyme and its location. These results suggest cognitive improvement properties for diets with predominance of polyunsaturated fatty acids. Physiological parameters such as systolic blood pressure, food intake, and biochemical factors such as cholesterol and glucose in plasma were also modified depending on the type of diet, supporting beneficial properties for diets rich in mono and polyunsaturated fatty acids. Inter-tissue correlations between the analyzed parameters were also modified depending on the type of diet. If the type of fat used in the diet modifies the behavior and relationship between CysAP and AlaAP in and between frontal cortex, liver and plasma, the functions in which they are involved could also be modified.

**Keywords:** diet, fatty acids, cystinyl-aminopeptidase, alanyl-aminopeptidase, renin-angiotensin system

## INTRODUCTION

Ang III at the final steps of the cascade of the renin-angiotensin system (**Figure 1A**) is metabolized to Ang IV, through the action of alanyl aminopeptidase (AlaAP, EC. 3.4.11.2). Ang IV is further metabolized to Ang 4-8 by the action of AlaAP. By its binding to the AT<sub>4</sub> receptor, identified as insulin-regulated aminopeptidase (IRAP or cystinyl aminopeptidase, CysAP, EC. 3.4.11.3, AT<sub>4</sub>),

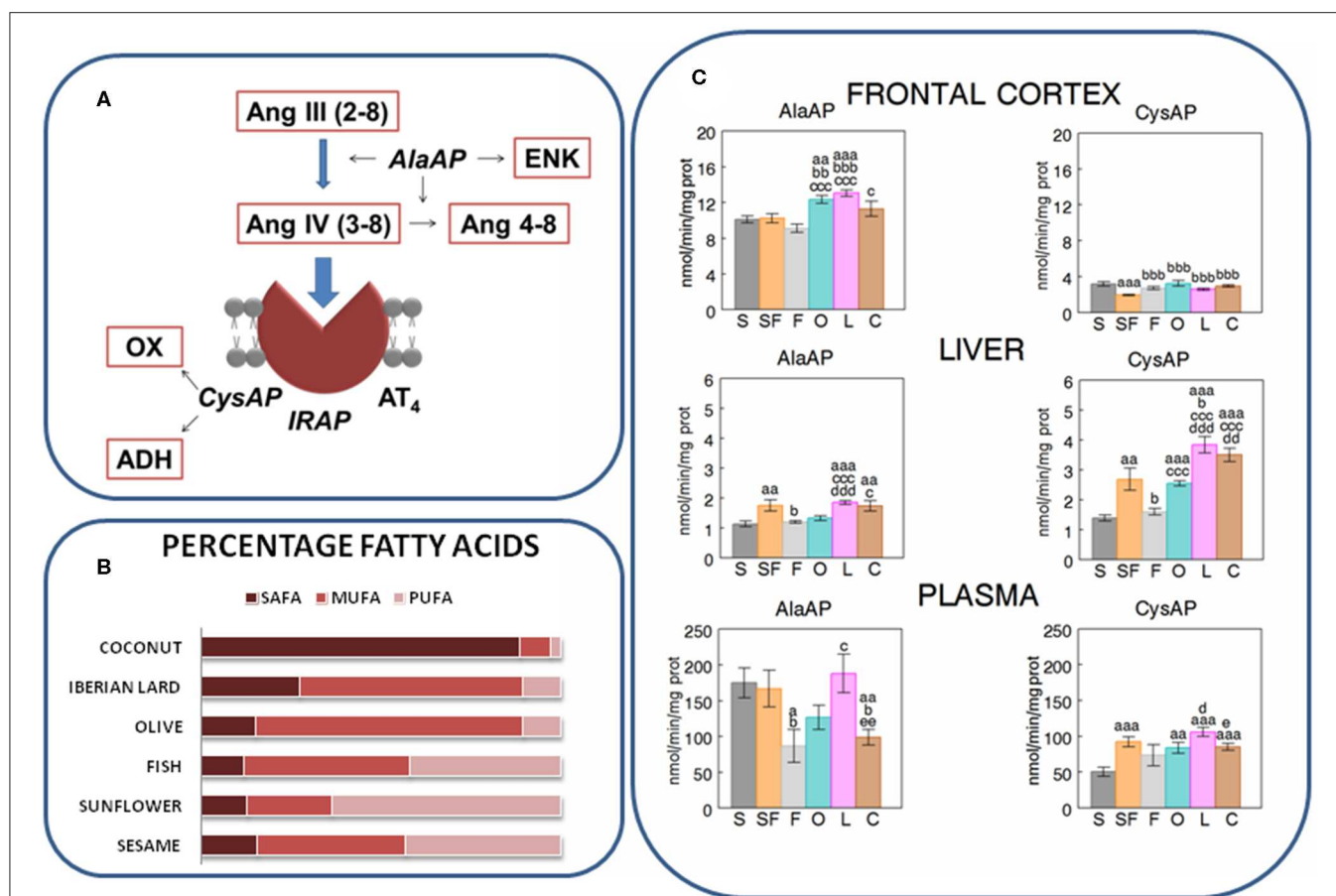


**FIGURE 1 | (A)** Partial scheme of the last steps of the renin-angiotensin system in which appear the enzymatic activities measured in the present work: alanyl-aminopeptidase (AlaAP) and cystinyl-aminopeptidase (CysAP), reported to be identical to insulin-regulated aminopeptidase (IRAP) and to the AT<sub>4</sub> receptor. The scheme also represents the susceptible endogenous substrates, other than angiotensins. ENK, enkephalin; OX, oxytocin; ADH, antidiuretic hormone (vasopressin) (Ramírez-Sánchez et al., 2013). **(B)** Relative percentages of saturated (SAFA), monounsaturated (MUFA), and polyunsaturated (PUFA) fatty acids in the oils used in the present study to enrich the different types of diets: Respectively (SAFA, MUFA, PUFA), for sesame- (15.7, 41, 43.4), sunflower- (12, 22.4, 60.7), fish- (12, 45.8, 41.6), olive- (13.2, 73.2, 8.9), Iberian lard- (27.6, 62, 9.4), and coconut-oil (86.5, 5.8, 1.8) (Segarra et al., 2008). **(C)** Mean  $\pm$  S.E.M. levels ( $n = 8$ ) of AlaAP and CysAP activities (nmol/min/mg prot) obtained in frontal cortex, liver and plasma of male rats fed during 16 weeks with diets enriched with sesame- (S, charcoal), sunflower- (SF, rose), fish- (F, gray), olive- (O, cyan), Iberian lard- (L, magenta) and coconut-oil (C, brown). (a) indicates a significant difference in comparison with S; (b) significant difference with SF; (c) significant difference with F; (d) significant difference with O; (e) significant difference with L. Single letter,  $P < 0.05$ ; double letter,  $P < 0.01$ ; triple letter,  $P < 0.001$ .

Ang IV may be involved in cognitive and cardiovascular functions as well as in glucose metabolism. Its role in glucose uptake in brain is region-specific and dependent on a high colocalization of IRAP and the glucose transporter GLUT4 (Fernando et al., 2008). However, the effects of Ang IV on glucose uptake and the IRAP function may be independent (De Bundel et al., 2009). On the other hand, AlaAP may also hydrolyze enkephalins whereas CysAP hydrolyzes oxytocin and vasopressin (reviewed in Ramírez-Sánchez et al., 2013). The inhibition of both AlaAP (Ismail et al., 2017) and IRAP (Diwakarla et al., 2016; Seyer et al., 2019) have been proposed as strategies to improve cognitive functions such as memory processes. Therefore, both AlaAP and CysAP activities might act in concert to affect the cognitive, cardiovascular and metabolic functions in which they have been involved.

The type of fat in the diet modifies the profile of fatty acids and the levels of certain neuropeptidase activities in frontal cortex (Segarra et al., 2011, 2019a) as well as the levels of cholesterol in plasma (Segarra et al., 2008). In addition, the type of fat in the diet affects the correlation between some neuropeptidase activities and certain fatty acids in frontal cortex (Segarra et al., 2011, 2019a). Changes of the fatty acids profile in cells may affect the fluidity of membranes and consequently the association between the enzyme and the membrane as well as the binding of the enzyme with its endogenous substrates (Youdim et al., 2000; Segarra et al., 2011). Therefore, if the proteolytic activities change, the levels and functions in which their endogenous substrates are involved, such as cognitive functions, may also be modified.

Furthermore, different types of diets affect the metabolism of lipids, carbohydrates, and proteins on target organs such as



the liver particularly involved in glucose metabolism, where they can influence glucose levels and fatty acids, and the brain, where they can modulate cognitive processes. The study of the effect of various saturated and unsaturated fats in the diet should give us an overview of the behavior of neuropeptidases and therefore, on the functional status of their endogenous substrates. These effects on the hepatic, cerebral and plasma response of such enzymes could be produced through a gut-brain-liver direct axis (Wang et al., 2008) or by indirect action linked to the induction of the development of different types of microbiota (Mayer et al., 2015; Martínez et al., 2019).

Tissues do not function as independent compartments: they interact among each other to offer an integrated response to changes in the internal and/or external environment (Samdani et al., 2015; Segarra et al., 2019b). If the level of activity of each enzyme in each tissue can be differentially modified depending on the type of diet, a possible interaction between such intra and inter-tissue activities could also be modified. In order to contrast the influence of the degree of saturation of fat on the diet (Figure 1B) and to better understand a neurovisceral integrative response to the effect of specific diets, it is necessary not only to determinate the profile of the response to selective diets at different locations but also to obtain information on the intra- and inter-tissue interactions between these locations (Samdani et al., 2015) and enzymes. Therefore, AlaAP and CysAP activities were determined in frontal cortex (FC), liver (LI), and plasma (PL) of male rats fed diets enriched with sesame oil (S), sunflower oil (SF), fish oil (F), olive oil (O), Iberian lard (L), or coconut oil (C). Systolic blood pressure (SBP), food intake (FI), body weight (BW), liver weight (LW), as well as total cholesterol (TCH) and glucose (GLU) levels in plasma were also measured.

## MATERIALS AND METHODS

Forty eight adult male Wistar rats, weighing 200–250 g (aged 3–4 months) at the beginning of the study, were divided in six groups ( $n = 8$  each), individually housed in metabolic cages and kept under standard environmental conditions. To ensure a full effect of the diets on experimental animals and based on the average length of the diet used in the literature, each group was fed during 16 weeks with isocaloric diets supplemented with 10% of the different oils studied: S, SF, F, O, L, and C (Segarra et al., 2008). At the end of the feeding period, the rats were weighed and their systolic blood pressure recorded by plethysmography (Segarra et al., 2008). Under equithesin anesthesia, blood samples were obtained from the left cardiac ventricle and then, the animals were totally perfused with saline. Their brains were quickly removed and cooled in dry ice. The livers were removed, weighed and samples from the left lateral lobe were obtained and cooled in dry ice. From brains, the frontal lobes (11.20 mm anterior to the interaural line) were dissected according to the stereotaxic atlas of Paxinos and Watson (1998). Plasma was isolated by centrifugation of blood samples for 10 min at 2,000 g using heparin as an anticoagulant and stored at  $-20^{\circ}\text{C}$ . TCH and GLU were determined colourimetrically in plasma using kits supplied, respectively, by Sigma (St Louis,

MO) and Spinreact (Girona, Spain) and expressed as mg/dL (Segarra et al., 2019b). In order to avoid its possible influence on the studied factors such as CysAP (Habtemichael et al., 2015), fasting conditions were not included in the study. Although it has been reported the influence of equithesin anesthesia on glucose levels (Bola and Kiyatkin, 2016), all groups were treated in the same conditions, which permit to discriminate the effects of the different diets on the studied factors. All experimental procedures were in accordance with the European Communities Council Directive 86/609/EEC. Enzymatic assays were performed as previously described Ramírez et al. (2011). Briefly, brain and liver samples were homogenized in 400  $\mu\text{l}$  of 10 mM HCl-Tris buffer (pH 7.4) and ultracentrifuged at  $100,000 \times g$  for 30 min at  $4^{\circ}\text{C}$ . To obtain the particulate fraction, the pellets were re-homogenized in HCl-Tris buffer (pH 7.4) plus 1% Triton-X-100. After centrifugation ( $100,000 \times g$ , 30 min,  $4^{\circ}\text{C}$ ), the supernatants were shaken in an orbital rotor for 2 h at  $4^{\circ}\text{C}$  with the polymeric adsorbent Bio-Beads SM-2 (100 mg/ml) to remove the detergent from the sample. After bio-beads removal, these supernatants were used to measure AlaAP and CysAP activities as well as protein content in triplicate (Ramírez et al., 2011). AlaAP and CysAP levels were measured using Ala- or Cys- $\beta$ -naphthylamide as substrates. Ten microlitre of each supernatant and plasma were incubated for 30 min at  $25^{\circ}\text{C}$  with 1 ml of the substrate solution, i.e., 2.14 mg/100 ml of Ala- $\beta$ -naphthylamide or 5.53 mg/100 ml of Cys- $\beta$ -naphthylamide, 10 mg/100 ml BSA, and 10 mg/100 ml DTT in 50 mM of phosphate buffer (pH 7.4 for AlaAP) and 50 mM HCl-Tris buffer (pH 6 for CysAP). The reactions were terminated by the addition of 1 ml of 0.1 mol/l of acetate buffer, pH 4.2. The amount of -naphthylamine released as a result of the enzymatic activity was measured fluorometrically at a 412 nm emission wavelength with an excitation wavelength of 345 nm. Proteins were quantified in triplicate (Bradford, 1976) with BSA as a standard. Specific activities were expressed as pmol of the corresponding substrate hydrolyzed per min per mg of protein. Fluorogenic assays were linear with respect to time of hydrolysis and protein content. For statistical analysis, to analyze differences between groups, one-way analysis of variance (ANOVA) was used. *Post-hoc* comparisons were made using the Student's *t*-test. Pearson's coefficient of correlation was computed to study the possible intra- and inter-tissue association of the parameters studied. Computations were performed using SPSS 13.0 and STATA 9.0. P-values below 0.05 were considered significant.

## RESULTS

The results are indicated in Figures 1, 2 and in Tables 1, 2. The levels of TCH and SBP (Segarra et al., 2008) as well as AlaAP activity with F, O and C diets (Segarra et al., 2019a) were previously reported. In *frontal cortex*, O and L diets exhibited higher levels of AlaAP activity than after the S diet, SF and F diets ( $p < 0.01$  and  $p < 0.001$ ) and C diet induced higher levels of AlaAP activity than F diet ( $p < 0.05$ ). CysAP had lower activity with the SF diet than with the other diets ( $p < 0.001$ ). In contrast, C diet demonstrated higher CysAP activity levels than the F diet ( $p < 0.05$ ). In *liver*, the S diet caused lower levels of AlaAP activity

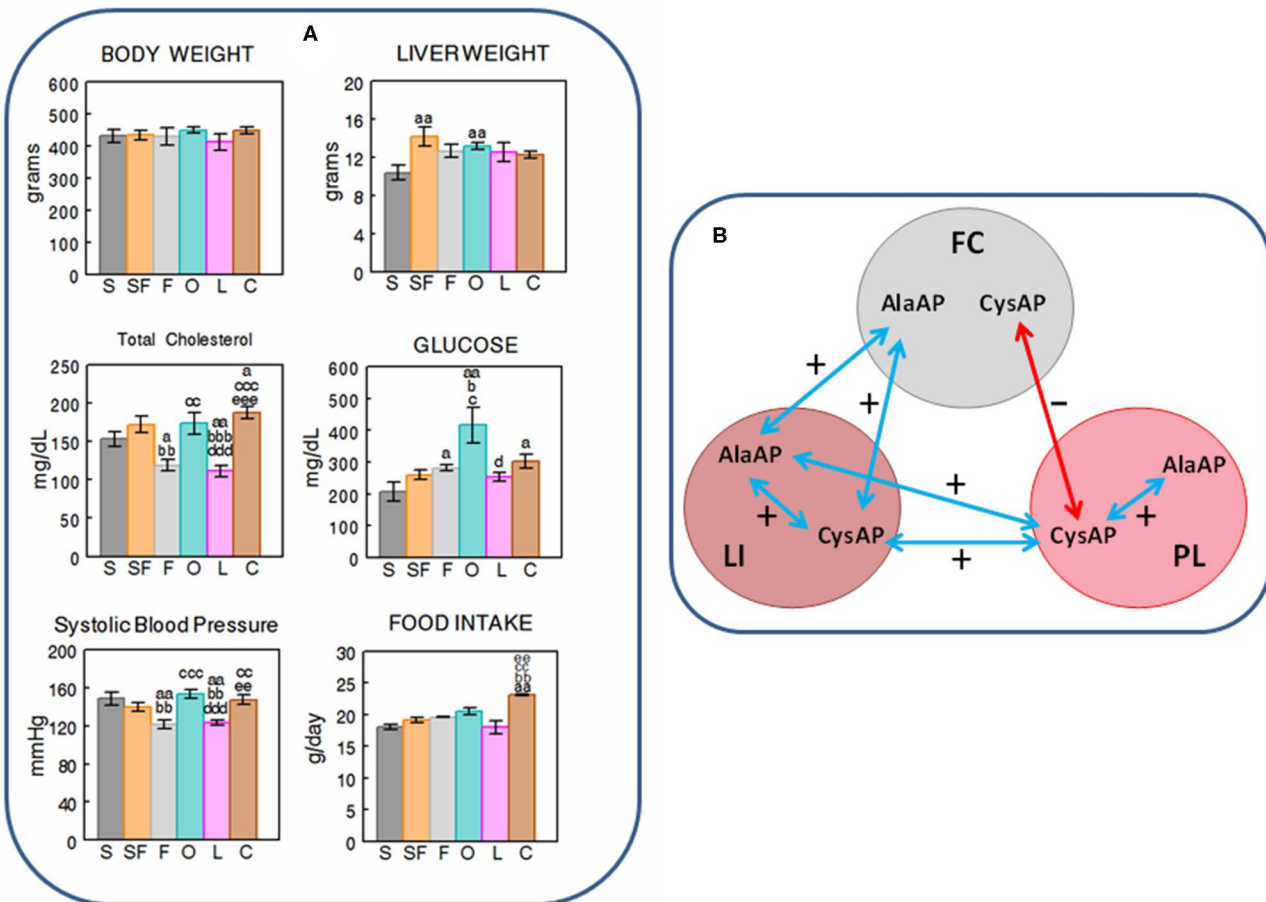


**FIGURE 2 | (A)** Mean  $\pm$  S.E.M. levels ( $n = 8$ ) of body and liver weight (grams), total cholesterol and glucose levels in plasma (mg/dL), systolic blood pressure levels (mmHg) and food intake (g/day), obtained at the end of the feeding period in male rats fed during 16 weeks with diets enriched with sesame- (S, charcoal), sunflower- (SF, rose), fish- (F, gray), olive- (O, cyan), Iberian lard- (L, magenta), and coconut-oil (C, brown). (a) indicates a significant difference in comparison with S; (b) significant difference with SF; (c) significant difference with F; (d) significant difference with O; (e) significant difference with L. Single letter,  $P < 0.05$ ; double letter,  $P < 0.01$ ; triple letter,  $P < 0.001$ . **(B)** Simplified scheme showing the intra- and inter-tissue significant correlations between the enzymatic activities. Blue arrows denote positive correlations. Red arrow denotes negative correlation. FC, frontal cortex; LI, liver; PL, plasma.

than the SF ( $p < 0.01$ ), L ( $p < 0.001$ ), and C ( $p < 0.01$ ) diets. Further, L had higher levels of AlaAP activity than S, F and O ( $p < 0.001$ ). C was also higher than S ( $p < 0.01$ ) and F ( $p < 0.05$ ) for AlaAP activity. In liver, CysAP had higher levels of activity with L diet than with S ( $p < 0.001$ ), SF ( $p < 0.05$ ), F ( $p < 0.001$ ), and O diet ( $p < 0.001$ ) whereas C was higher than S ( $p < 0.001$ ), F ( $p < 0.001$ ) and O ( $p < 0.01$ ) diets and S was lower than SF ( $p < 0.01$ ), O, L, and C ( $p < 0.001$ ). In plasma, AlaAP activity was lower with F than with S, SF, and L diets ( $p < 0.05$ ), C was also lower than S ( $p < 0.01$ ), SF ( $p < 0.05$ ), and L ( $p < 0.01$ ) diets. In plasma, CysAP activity was also lower with S diet than with SF ( $p < 0.001$ ), O ( $p < 0.01$ ), L ( $p < 0.001$ ), and C ( $p < 0.001$ ) diets. O and C diets had lower levels of CysAP activity than L ( $p < 0.05$ ) (Figure 1C).

While weight gain (data not shown) and body weight demonstrated no differences between the different types of diets at the end of the feeding period, the liver weight showed to have lower levels with the S diet than with SF and O diets ( $p < 0.01$ ).

Total cholesterol in plasma demonstrated lower levels with F and L diets than with the rest of diets, and glucose was higher with O than with S, SF, F and L diets. The S diet had lower levels of plasma glucose than F, O and C diets. Systolic blood pressure exhibited the same profile than TCH: lower levels of SBP with F and L diets than with the rest. FI was higher ( $p < 0.01$ ) with the C diet than with the rest of diets except with O (Figure 2A).

When we analyzed the data for the search of intra- and inter-tissue correlations with each of the diets studied, significant inter-tissue correlations between enzymatic activities were only obtained with S (between FC vs. PL: FC CysAP vs. PL AlaAP and FC CysAP vs. PL CysAP) and with O (between FC vs. LI: FC CysAP vs. LI AlaAP). There were negative correlations with S and positive with O. SBP correlates negatively with GLU in the diet enriched with S and positively in the diet enriched with L. Glucose also correlates negatively with CysAP activity from LI in the O diet. Intra-tissue correlations between both enzymatic activities were observed in FC with O and L diets, in LI with SF, L



**TABLE 1 |** Intra- and inter-tissue significant correlations (paired data) of the different parameters measured into and between the tissues analyzed: Frontal cortex (FC), liver (LI), and plasma (PL) in each one of the diets studied ( $n = 8$ ).

Sesame			Sunflower			Fish		
Correlation	<i>r</i>	<i>P</i>	Correlation	<i>r</i>	<i>P</i>	Correlation	<i>r</i>	<i>P</i>
FC CysAP vs. PL AlaAP	−0.772	0.02	LI AlaAP vs. LI CysAP	+0.881	0.003	LI AlaAP vs. LI CysAP	+0.775	0.02
FC CysAP vs. PL CysAP	−0.798	0.01				PL AlaAP vs. PL CysAP	+0.935	0.0006
PL AlaAP vs. PL CysAP	+0.816	0.01						
SBP vs. Glucose	−0.777	0.02						

Olive			Iberian lard			Coconut		
FC CysAP vs. LI AlaAP	+0.708	0.04	FC AlaAP vs. FC CysAP	+0.795	0.01	No correlations		
FC AlaAP vs. FC CysAP	+0.884	0.003	LI AlaAP vs. LI CysAP	+0.813	0.01			
Glucose vs. LI CysAP	−0.767	0.02	SBP vs. Glucose	+0.803	0.01			

Negative correlations with rose background. Positive correlations with blue background. The values of *r* and *P* are indicated.

**TABLE 2 |** Values of *r* for significant correlations (paired data) obtained between the different physiological and biochemical parameters determined at each location (Frontal cortex, FC; Liver, LI; Plasma, PL), considering together all the data ( $n = 48$ ) obtained with the six groups designed (sesame, sunflower, fish, olive, Iberian lard, coconut).

	Body wt	Liver wt	SBP	FI	Total Ch	Glucose	FC AlaAP	FC CysAP	LI AlaAP	LI CysAP	PL AlaAP	PL CysAP
Body wt	1	+0.642			+0.359				+0.290			+0.352
Liver wt		1						−0.312	+0.391			+0.560
SBP			1		+0.518							
FI				1								
Total Ch					1							
Glucose						1						
FC AlaAP							1		+0.425	+0.575		
FC CysAP								1				−0.389
LI AlaAP									1	+0.803		+0.366
LI CysAP										1		+0.464
PL AlaAP											1	+0.469
PL CysAP												1

Blue background for positive values and rose background for negative ones.

and F diets and in PL with the F diet. No significant correlations were observed in the C diet (Table 1).

Considering together the data obtained with the six diets studied ( $n = 48$ ), we observed significant positive correlations between BW vs. LW and TCH but also with LI AlaAP and PL CysAP activities. LW correlates negatively with FC CysAP and positively with LI AlaAP and PL CysAP activities. SBP correlates positively with TCH. While FC AlaAP correlates positively with LI AlaAP and LI CysAP activities, FC CysAP correlates negatively with PL CysAP activity. LI AlaAP correlates positively with LI CysAP and PL CysAP activities, and PL CysAP correlates positively with LI CysAP and with PL AlaAP activities (Table 2 and Figure 2B).

## DISCUSSION

AlaAP and CysAP activities are involved in the metabolism of enkephalins, oxytocin and vasopressin as well as in the glucose metabolism. Changes in enzyme activities depending on the type

of fat in the diet may be related to changes in the functions they exert in the locations studied: FC, LI, and PL. Consequently we could expect modulations in cognitive and metabolic functions in which these enzymes are involved (Ramírez-Sánchez et al., 2013). However, since we have not included a parallel study using specific IRAP inhibitors, the CysAP activity measured in the present work using an arylamide derivative as substrate does not necessarily corresponds to IRAP activity and therefore the interpretation of the results should be considered with caution.

It has been reported that the AT<sub>4</sub> receptor was identified as IRAP being also co-localized with the glucose transporter GLUT4. It was proposed that the binding of Ang IV to AT<sub>4</sub> results in the inhibition of its enzymatic activity, reducing the catabolism of their endogenous substrates (vasopressin, oxytocin) and consequently increasing their availability and extending their action. Therefore, through its high affinity binding to the AT<sub>4</sub> receptor, Ang IV might modulate cognitive and metabolic functions via neuropeptide processing or local blood flows. In

this context, since AlaAP activity is involved in Ang III and Ang IV metabolism and it also acts as enkephalinase, this enzyme may as well be involved in these cognitive and metabolic regulations (Ramírez-Sánchez et al., 2013; Ismail et al., 2017).

In FC, the high difference between diets for AlaAP and CysAP activities suggests a role for the type of fatty acids on these enzymatic activities and therefore on their substrates. For example the low levels of both activities with SF (rich in polyunsaturated fatty acids) may suggest longer action for the AlaAP substrates enkephalins and Ang III and a longer action for the CysAP substrate oxytocin. Polyunsaturated fatty acids enriched diet has been proposed to improve cognitive functions (Chalon et al., 2001). Enkephalins (Henry et al., 2017), and oxytocin (Wagner and Echterhoff, 2018) were also reported as cognitive improving neuropeptides. If a diet enriched in polyunsaturated fatty acids results in reduced levels of enkephalinase and oxytocinase activities in comparison with other diets, both neuropeptides may prolong their beneficial effects in frontal cortex. As previously indicated, the specific fatty acids membrane pattern induced by this type of diet may affect membrane fluidity and the association with the membrane-bound enzyme and so influence the hydrolytic capability of the enzyme (Youdim et al., 2000; Segarra et al., 2011). These results are compatible with an improvement of cognitive functions such as memory processes (Diwakarla et al., 2016; Seyer et al., 2019) for enriched diets in polyunsaturated fatty acids such as SF. In LI, with S and F (rich in mono and polyunsaturated fatty acids) there were lower levels of AlaAP and CysAP activities which may suggest an increase in local blood flow. In PL, for example, there was a clear difference between AlaAP and CysAP with the S diet: whereas AlaAP exhibited high activity levels (suggesting high metabolism of Ang III, Ang IV and enkephalins), CysAP had low levels of activity, suggesting longer action of vasopressin.

With the diet enriched with O, there was a negative correlation between GLU and CysAP activity in liver: The lower CysAP activity in liver, the higher GLU in PL and vice versa. This could be interpreted as a direct influence of the O diet on the glucose transporter and/or a compensatory response of CysAP in liver to the increase in plasma of GLU (Figure 2B). Other authors have described diverse influences of diets on plasma glucose. For example, Buettner et al. (2006), analyzing diets enriched with lard, olive, coconut and fish oil reported high levels of plasma glucose in olive, in comparison with the rest of diets. Dulloo et al. (1995), studying diets enriched with lard, coconut, olive, sunflower and fish did not observe differences for glucose levels between diets. Giron et al. (1999) reported lower glucose levels in plasma of animals fed a diet enriched with fish oil than the ones enriched with olive and sunflower oils. Interestingly, it has been discovered that upper intestinal lipids activate a gut-brain-liver axis that regulates liver glucose homeostasis (Wang et al., 2008). In addition, hypercholesterolemia has been associated with cognitive disorders linked to GLUT4 expression and modulated by CysAP and aminopeptidase N activities (Ismail et al., 2017). Our results are therefore in agreement with these observation: changes in the levels of cholesterol, depending on the type of diet, may influence the cognitive processes. In this sense, the

low levels of TCH and SBP obtained with diets enriched with F or L (Figure 2A) suggest a beneficial role for mono and polyunsaturated fatty acids.

Interestingly, with a diet enriched with S (rich in monounsaturated and polyunsaturated fat), there was a negative correlation between SBP vs. GLU but in contrast, with L (rich mainly in monounsaturated fat) this correlation was positive which supports the importance of the type of diet in the adjustment of physiologic processes. Furthermore, both if we consider individually the type of diet (S and O) (Table 1), and if we consider together the data of all diets (Table 2), the relationship of FC with PL was *negative* while that of FC with LI was *positive*, just as it is also *positive* between LI and PL. In particular, considering only the S-enriched diet (Table 1), FC CysAP correlated *negatively* with PL AlaAP and PL CysAP and also *negatively* with PL CysAP considering all data (Table 2). In contrast, FC CysAP correlated *positively* with LI AlaAP and LI CysAP with an O-enriched diet (Table 1) and FC AlaAP correlated *positively* with LI AlaAP and LI CysAP (Table 2). In addition, AlaAP and CysAP from LI, correlated *positively* with AlaAP and CysAP from PL (Table 2). From a general perspective (Figure 2B), we observed some form of *positive* feedback between FC AlaAP with LI AlaAP and CysAP, a *positive* feedback between LI AlaAP and CysAP with PL but a *negative* feedback between FC CysAP with PL CysAP. Also, while in LI and PL there was a *positive* relationship between AlaAP and CysAP, there was no correlation in FC. Whether such changes relate to the amount of enzyme present ( $V_{max}$ ) or the conformation of the enzyme ( $K_m$ ) remains to be analyzed.

As we could expect, the results demonstrated significant positive correlations for BW vs. LW and vs. TCH as well as for SBP vs. TCH (Table 2). These results support the validity of our observation. In conclusion, the present results apparently do not show a clear systematic profile of response depending on the type of diet but they could be considered as preliminary results which support a distinctive influence of the saturation of the fatty acids in the diet that may result in changes in cognitive and metabolic functions which deserve further specific research.

## DATA AVAILABILITY STATEMENT

The raw data supporting the conclusions of this article will be made available to any qualified researcher.

## ETHICS STATEMENT

The animal study was reviewed and approved by Ethics committee of the University of JAÉN.

## AUTHOR CONTRIBUTIONS

AS and IP contributed equally to the work with the acquisition, analysis, and interpretation of data. MR-S contributed to the acquisition, analysis and interpretation of data and wrote the first manuscript draft. MM-C,

IB, PV, SZ, and MG participated in the analysis and interpretation of data and revised critically the final form of the manuscript. All authors have approved the final manuscript.

## REFERENCES

- Bola, R. A., and Kiyatkin, E. A. (2016). Robust brain hyperglycemia during general anesthesia: relationships with metabolic brain inhibition and vasodilation. *Front. Physiol.* 7:39. doi: 10.3389/fphys.2016.00039
- Bradford, M. M. (1976). A rapid and sensitive method for the quantitation of microgram quantities of protein utilizing the principle of protein-dye binding. *Anal. Biochem.* 72, 248–254. doi: 10.1016/0003-2697(76)90527-3
- Buettner, R., Parhofer, K. G., Woenckhaus, M., Wrede, C. E., Kunz-Schughart, L. A., Schölmerich, J., et al. (2006). Defining high-fat-diet rat models: metabolic and molecular effects of different fat types. *J. Mol. Endocrinol.* 36, 485–501. doi: 10.1677/jme.1.01909
- Chalon, S., Vancassel, S., Zimmer, L., Guilloteau, D., and Durand, G. (2001). Polyunsaturated fatty acids and cerebral function: focus on monoaminergic neurotransmission. *Lipids* 36, 937–944. doi: 10.1007/s11745-001-0804-7
- De Bundel, D., Smolders, I., Yang, R., Albiston, A. L., Michotte, Y., and Chai, S. Y. (2009). Angiotensin IV and LVV-haemorphin 7 enhance spatial working memory in rats: effects on hippocampal glucose levels and blood flow. *Neurobiol. Learn. Mem.* 92, 19–26. doi: 10.1016/j.nlm.2009.02.004
- Diwakarla, S., Nylander, E., Grönbladh, A., Vanga, S. R., Khan, Y. S., Gutiérrez-de-Terán, H., et al. (2016). Aryl sulfonamide inhibitors of insulin-regulated aminopeptidase enhance spine density in primary hippocampal neuron cultures. *ACS Chem. Neurosci.* 7, 1383–1392. doi: 10.1021/acschemneuro.6b00146
- Dulloo, A. G., Mensi, N., Seydoux, J., and Girardier, L. (1995). Differential effects of high-fat diets varying in fatty acid composition on the efficiency of lean and fat tissue deposition during weight recovery after low food intake. *Metabolism* 44, 273–279. doi: 10.1016/0026-0495(95)90277-5
- Fernando, R. N., Albiston, A. L., and Chai, S. Y. (2008). The insulin-regulated aminopeptidase IRAP is colocalised with GLUT4 in the mouse hippocampus—potential role in modulation of glucose uptake in neurones?. *Eur. J. Neurosci.* 28, 588–598. doi: 10.1111/j.1460-9568.2008.06347.x
- Giron, M. D., Sanchez, F., Hortelano, P., Periago, J. L., and Suarez, M. D. (1999). Effects of dietary fatty acids on lipid metabolism in streptozotocin-induced diabetic rats. *Metabolism* 48, 455–460. doi: 10.1016/S0026-0495(99)90103-8
- Habtemichael, E. N., Alcázar-Román, A., Rubin, B. R., Grossi, L. R., Belman, J. P., Julca, O., et al. (2015). Coordinated regulation of vasopressin inactivation and glucose uptake by action of TUG protein in muscle. *J. Biol. Chem.* 290, 14454–14461. doi: 10.1074/jbc.C115.639203
- Henry, M. S., Gendron, L., Tremblay, M. E., and Drolet, G. (2017). Enkephalins: endogenous analgesics with an emerging role in stress resilience. *Neural Plast.* 2017, 1546125. doi: 10.1155/2017/1546125
- Ismail, M. A., Mateos, L., Maioli, S., Merino-Serrais, P., Ali, Z., Lodeiro, M., et al. (2017). 27-Hydroxycholesterol impairs neuronal glucose uptake through an IRAP/GLUT4 system dysregulation. *J. Exp. Med.* 214, 699–717. doi: 10.1084/jem.20160534
- Martínez, N., Prieto, I., Hidalgo, M., Segarra, A. B., Martínez-Rodríguez, A. M., Cobo, A., et al. (2019). Refined versus extra virgin olive oil high-fat diet impact on intestinal microbiota of mice and its relation to different physiological variables. *Microorganisms* 7:E61. doi: 10.3390/microorganisms7020061
- Mayer, E. A., Tillisch, K., and Gupta, A. (2015). Gut/brain axis and the microbiota. *J. Clin. Invest.* 125, 926–938. doi: 10.1172/JCI76304
- Paxinos, G., and Watson, C. (1998). *The Rat Brain in Stereotaxic Coordinates*. 4th Edn. London: Academic Press.
- Ramírez, M., Prieto, I., Banegas, I., Segarra, A. B., and Alba, F. (2011). Neuropeptidases. *Methods Mol. Biol.* 789, 287–294. doi: 10.1007/978-1-61779-310-3\_18
- Ramírez-Sánchez, M., Prieto, I., Wangenstein, R., Banegas, I., Segarra, A. B., Villarejo, A. B., et al. (2013). The renin-angiotensin system: new insight into old therapies. *Curr. Med. Chem.* 20, 1313–1322. doi: 10.2174/0929867311320100008
- Samdani, P., Singhal, M., Sinha, N., Tripathi, P., Sharma, S., Tikoo, K., et al. (2015). A comprehensive inter-tissue crosstalk analysis underlying progression and control of obesity and diabetes. *Sci. Rep.* 5:12340. doi: 10.1038/srep12340
- Segarra, A. B., Prieto, I., Martínez-Cañamero, M., Ruiz-Sanz, J. I., Ruiz-Larrea, M. B., De Gasparo, M., et al. (2019a). Enkephalinase activity is modified and correlates with fatty acids in frontal cortex depending on fish, olive or coconut oil used in the diet. *Endocr. Regul.* 53, 59–64. doi: 10.2478/enr-2019-0007
- Segarra, A. B., Prieto-Gomez, I., Banegas, I., Martínez-Cañamero, M., Luna, J. D., de Gasparo, M., et al. (2019b). Functional and neurometabolic asymmetry in SHR and WKY rats following vasoactive treatments. *Sci. Rep.* 9:16098. doi: 10.1038/s41598-019-52658-9
- Segarra, A. B., Ramírez, M., Banegas, I., Alba, F., Vives, F., de Gasparo, M., et al. (2008). Dietary fat influences testosterone, cholesterol, aminopeptidase A, and blood pressure in male rats. *Horm. Metab. Res.* 40, 289–291. doi: 10.1055/s-2008-1046800
- Segarra, A. B., Ruiz-Sanz, J. I., Ruiz-Larrea, M. B., Ramírez-Sánchez, M., de Gasparo, M., Banegas, I., et al. (2011). The profile of fatty acids in frontal cortex of rats depends on the type of fat used in the diet and correlates with neuropeptidase activities. *Horm. Metab. Res.* 43, 86–91. doi: 10.1055/s-0030-1269855
- Seyer, B., Diwakarla, S., Burns, P., Hallberg, A., Grönbladh, A., Hallberg, M., et al. (2019). Insulin-regulated aminopeptidase inhibitor-mediated increases in dendritic spine density are facilitated by glucose uptake. *J. Neurochem.* 293, 14880–14890. doi: 10.1111/jnc.14880
- Wagner, U., and Echterhoff, G. (2018). When does oxytocin affect human memory encoding? the role of social context and individual attachment style. *Front. Hum. Neurosci.* 12:349. doi: 10.3389/fnhum.2018.00349
- Wang, P. Y., Caspi, L., Lam, C. K., Chari, M., Li, X., Light, P. E., et al. (2008). Upper intestinal lipids trigger a gut-brain-liver axis to regulate glucose production. *Nature* 452, 1012–1016. doi: 10.1038/nature06852
- Youdim, K. A., Martin, A., and Joseph, J. A. (2000). Essential fatty acids and the brain: possible health implications. *Int. J. Dev. Neurosci.* 18, 383–399. doi: 10.1016/S0736-5748(00)00013-7

## FUNDING

This research was supported by a grant from the University of Jaén (ref. UJA2003-015).

**Conflict of Interest:** The authors declare that the research was conducted in the absence of any commercial or financial relationships that could be construed as a potential conflict of interest.

Copyright © 2020 Segarra, Prieto, Banegas, Martínez-Cañamero, de Gasparo, Vanderheyden, Zorad and Ramírez-Sánchez. This is an open-access article distributed under the terms of the Creative Commons Attribution License (CC BY). The use, distribution or reproduction in other forums is permitted, provided the original author(s) and the copyright owner(s) are credited and that the original publication in this journal is cited, in accordance with accepted academic practice. No use, distribution or reproduction is permitted which does not comply with these terms.



# Reciprocal Expression Patterns of Placental Leucine Aminopeptidase/Insulin-Regulated Aminopeptidase and Vasopressin in the Murine Brain

Yoshikuni Goto<sup>1\*</sup>, Takahiro J. Nakamura<sup>2</sup>, Kenji Ogawa<sup>3</sup>, Akira Hattori<sup>4</sup> and Masafumi Tsujimoto<sup>1</sup>

<sup>1</sup> Faculty of Pharmaceutical Sciences, Teikyo Heisei University, Nakano, Japan, <sup>2</sup> Laboratory of Animal Physiology, School of Agriculture, Meiji University, Kawasaki, Japan, <sup>3</sup> Laboratory of Veterinary Epizootiology, Department of Veterinary Medicine, Nihon University, Fujisawa, Japan, <sup>4</sup> Department of System Chemotherapy and Molecular Sciences, Graduate School of Pharmaceutical Sciences, Kyoto University, Kyoto, Japan

## OPEN ACCESS

### Edited by:

Efstathios Stratikos,  
National Centre of Scientific Research  
“Demokritos”, Greece

### Reviewed by:

Tracey Gaspari,  
Monash University, Australia  
Loredana Saveanu,  
Institut National de la Santé et de la  
Recherche Médicale (INSERM),  
France

### \*Correspondence:

Yoshikuni Goto  
y.goto@thu.ac.jp

### Specialty section:

This article was submitted to  
Cellular Biochemistry,  
a section of the journal  
Frontiers in Molecular Biosciences

**Received:** 24 April 2020

**Accepted:** 01 July 2020

**Published:** 24 July 2020

### Citation:

Goto Y, Nakamura TJ, Ogawa K,  
Hattori A and Tsujimoto M (2020)  
Reciprocal Expression Patterns  
of Placental Leucine  
Aminopeptidase/Insulin-Regulated  
Aminopeptidase and Vasopressin  
in the Murine Brain.  
Front. Mol. Biosci. 7:168.  
doi: 10.3389/fmolb.2020.00168

Placental leucine aminopeptidase/insulin-regulated aminopeptidase (P-LAP/IRAP) regulates vasopressin and oxytocin levels in the brain and peripheral tissues by controlled degradation of these peptides. In this study, we determined the relationship between P-LAP/IRAP and vasopressin levels in subregions of the murine brain. P-LAP/IRAP expression was observed in almost all brain regions. The expression patterns of P-LAP/IRAP and vasopressin indicated that cells expressing one of these protein/peptide were distinct from those expressing the other, although there was significant overlap between the expression regions. In addition, we found reciprocal diurnal rhythm patterns in P-LAP/IRAP and arginine vasopressin (AVP) expression in the hippocampus and pituitary gland. Further, synchronously cultured PC12 cells on treatment with nerve growth factor (NGF) showed circadian expression patterns of P-LAP/IRAP and enzymatic activity during 24 h of incubation. Considering that vasopressin is one of the most efficient peptide substrates of P-LAP/IRAP, these results suggest a possible feedback loop between P-LAP/IRAP and vasopressin expression, that regulates the function of these substrate peptides of the enzyme *via* translocation of P-LAP/IRAP from intracellular vesicles to the plasma membrane in brain cells. These findings provide novel insights into the functions of P-LAP/IRAP in the brain and suggest the involvement of these peptides in modulation of brain AVP functions in hyperosmolality, memory, learning, and circadian rhythm.

**Keywords:** placental leucine aminopeptidase, insulin-regulated aminopeptidase, aminopeptidase, vasopressin, circadian rhythm, brain

## INTRODUCTION

Placental leucine aminopeptidase (P-LAP) was first purified from retroplacental serum as a soluble protein (Tsujimoto et al., 1992). Subsequent cloning and sequence analysis of its cDNA revealed that the enzyme is a type II membrane protein localized in intracellular vesicles (Rogi et al., 1996). During pregnancy, P-LAP is synthesized as a vesicular membrane protein in the placenta,



cleaved by ADAM12, and then secreted into the maternal serum (Ito et al., 2004). P-LAP activity in the maternal serum remains low in the first trimester, rises progressively during the second and third trimesters, and then declines rapidly after parturition (Yamahara et al., 2000). Therefore, serum P-LAP level has been reported to be a viable predictor of fetal death (Tian et al., 2016). In female Bornean orangutans that gave stillbirths, the P-LAP concentration in urine failed to increase; whereas in those that gave live births, the average P-LAP concentration in urine showed a progressive increase till delivery (Kinoshita et al., 2017). P-LAP is believed to prevent the premature onset of uterine contractions by degrading oxytocin, thereby playing a role in the maintenance of normal pregnancy (Yamahara et al., 2000).

Keller et al. (1995) have reported the cloning of insulin-regulated membrane aminopeptidase (IRAP), which is a rat ortholog of P-LAP and co-localizes with the glucose transporter 4 (GLUT4) in intracellular vesicles. Microinjection of a GST fusion protein containing the cytoplasmic domain of IRAP was shown to cause the translocation of GLUT4-containing vesicles to the plasma membrane in 3T3-L1 adipocytes, suggesting that the N-terminal region of IRAP plays a role in the distribution of these vesicles for glucose uptake into the cells (Ross et al., 1996). However, the pathophysiological significance of IRAP (hereafter referred to as P-LAP/IRAP) in diabetes remains elusive (Keller, 2004; Bogan, 2012).

Placental leucine aminopeptidase/insulin-regulated aminopeptidase (P-LAP/IRAP) is a multifunctional enzyme that plays several pathophysiological roles. This enzyme can act as a receptor for angiotensin IV (Ang IV), which facilitates memory retention and retrieval (Albiston et al., 2001). Since Ang IV is an inhibitor of P-LAP/IRAP ligands to the Ang IV receptor are considered to exert memory-enhancing effects by modulating the enzymatic activity of P-LAP/IRAP. Similar to the case of GLUT4-containing vesicles, P-LAP/IRAP is involved in vesicular trafficking of the somatostatin type 2A receptor to the plasma membrane in hippocampal neurons and thus exerts an inhibitory effect on seizure activity (De Bundel et al., 2015). Although P-LAP/IRAP and oxytocin are co-expressed in hypothalamic neuronal cells, these are packaged in separate vesicles (Tobin et al., 2014). Inhibition of P-LAP/IRAP activity in the hypothalamus leads to increased frequency of milk ejection reflexes due to enhancement in oxytocin concentration. These results indicate that P-LAP/IRAP plays important roles in the modulation of several brain functions. This enzyme is also an important player in host defense systems, such as antigen cross-presentation, and Toll-like receptor 9 signaling (Saveanu et al., 2009; Babdor et al., 2017). P-LAP/IRAP trims antigenic peptides presented by MHC class I molecules, and also modulates Toll-like receptor 9 trafficking to lysosomes *via* interaction with FHOD4 (Saveanu et al., 2009; Babdor et al., 2017).

We have earlier reported the expression of P-LAP/IRAP in the brain (Matsumoto et al., 2001). We also identified several neuronal peptide substrates of the enzyme, including dynorphin A, vasopressin, oxytocin, and somatostatin (Tsujimoto et al., 1992; Matsumoto et al., 2000). However, the relationship between the expression levels and activity of P-LAP/IRAP

and the expression levels of its substrates in each sub-region of the brain remains unknown. In this study, we examined the roles of this enzyme in the brain. We identified reciprocal rhythmic increases and decreases in P-LAP/IRAP and arginine vasopressin (AVP) levels in several regions of the brain. Vasopressin is known to play multiple roles in distinct regions of the brain, related to hyperosmolality, memory, learning, and circadian rhythm (Johnston, 1985; Alescio-Lautier and Soumireu-Mourat, 1998; Ingram et al., 1998). The functional significance of the present results is discussed in the context of vasopressin being one of the most efficient peptide substrates of P-LAP/IRAP (Tsujimoto et al., 1992; Matsumoto et al., 2000).

## MATERIALS AND METHODS

### Animals

Male C57BL/6J mice were obtained from the Charles River Laboratories, Japan (Yokohama, Japan). Animal husbandry and all animal experiments were conducted in accordance with the guidelines of the Science Council of Japan and were approved by the Institutional Animal Care and Use Committee of Teikyo-Heisei University. The animals were maintained in a controlled environment (room temperature:  $24 \pm 1^\circ\text{C}$ ; humidity:  $50 \pm 5\%$ ), with food and water available *ad libitum*, and were housed under a light/dark (LD) cycle of 12 h of light (light intensity: 200–300 lux), and 12 h of darkness until sacrifice.

### Preparation of Brain Extracts

Male mice aged 4–6 months were euthanized at zeitgeber time (ZT) 8–10. ZT is a 24-h normalized notation of the phase in a circadian cycle entrained to the LD condition, with lights on from ZT 0 to ZT 12. The olfactory bulb, pituitary gland, cerebrum, cerebellum, hippocampus, hypothalamus, and thalamus were surgically collected and stored at  $-80^\circ\text{C}$  for processing. Brain extracts were prepared by homogenizing the whole brain with 0.5% Triton X-100 in 4 mL of cold phosphate-buffered saline (PBS) using a Dounce homogenizer. The homogenate was centrifuged at  $15,000 \times g$  for 30 min at  $4^\circ\text{C}$ , and the supernatant was stored at  $-80^\circ\text{C}$  until use.

### Immunofluorescence Staining

Whole brains from C57BL/6J mice aged 4–6 months were washed once with cold PBS, fixed by treatment with 4% paraformaldehyde for 24 h at  $4^\circ\text{C}$ , and cryoprotected in 30% sucrose in PBS for 48 h. Brain sections were prepared from free-floating coronal brain slices obtained from the middle of the rostrocaudal axis with a CM3050 S cryostat (Leica Biosystems, Richmond Hill, ON, Canada). The sections were washed thrice with PBS containing 0.5% Triton X-100 for 5 min each and then blocked with 5% donkey serum (Sigma-Aldrich) for 2 h at room temperature. Next, they were incubated overnight with anti-vasopressin antibody (Catalog No. 20069, ImmunoStar, Hudson, WI, United States) in PBS containing 5% donkey serum. The peptide was counterstained with Alexa Fluor 488-labeled anti-rabbit secondary antibody overnight in PBS

containing 5% donkey serum. After unbound dye molecules were washed off with PBS, the sections were incubated overnight with anti-IRAP (D7C5) XP<sup>®</sup> rabbit monoclonal antibody (Catalog No. 6918, Cell Signaling Technology, MA, United States) labeled with allophycocyanin labeling kit – SH (Dojindo Molecular Technologies, Kumamoto, Japan). The stained samples were dried on glass slides and mounted on cover slips with FluorSave Reagent (Calbiochem, San Diego, CA, United States). Images were acquired on a FV3000 confocal laser scanning microscope (Olympus, Tokyo, Japan) using 488 and 647 nm lasers as excitation light sources.

## Quantification of AVP

The levels of AVP in the brain were measured using an Arg<sup>8</sup>-vasopressin ELISA kit (ab205928, Abcam, Cambridge, United Kingdom) according to the manufacturer's instructions.

## Cell Culture, Differentiation, and Rhythmic Synchronization

PC12 (pheochromocytoma) cells were cultured in DMEM medium (Nacalai Tesque, Kyoto, Japan) containing heat-inactivated (56°C, 30 min) fetal bovine serum at 37°C in humidified air containing 5% CO<sub>2</sub>. The cells were differentiated with 100 ng/mL of murine NGF-2.5S from Sigma-Aldrich (St. Louis, MO, United States) for 5 days. For synchronization, cells were treated with 50% (v/v) horse serum for 2 h, in accordance with a reported method (Balsalobre et al., 1998), and then kept in the DMEM containing 10% fetal bovine serum medium.

## Western Blot Analysis

A 10-μg aliquot of total protein in the tissue and cell extracts was analyzed by western blotting to detect P-LAP/IRAP (a monoclonal antibody termed GOH-1 was prepared by immunizing mice with recombinant human P-LAP/IRAP), IRAP (D7C5) XP<sup>®</sup> rabbit monoclonal antibody, IRAP (3E1) mouse monoclonal antibody (Catalog No. 9876, Cell Signaling Technology), and GAPDH (Santa Cruz, CA, United States). Protein blots were probed using an anti-P-LAP antibody followed by an HRP-labeled secondary antibody. The protein bands were detected using an ImageQuant LAS 4000 Mini Luminescent Image Analyzer (GE Healthcare, Chicago, IL, United States) and ECL Prime Western Blotting Detection Kit (GE Healthcare). Densitometric analysis of the antibody response was performed using the ImageJ software.

## Measurement of Cystinyl-Aminopeptidase Activity

Cystinyl-aminopeptidase (CAP) activity was determined using S-benzyl-cysteine-4-methylcoumaryl-7-amide (Bzl-Cys-MCA; Bachem, Bubendorf, Switzerland) by modifying a previously described method (Matsumoto et al., 2000). Briefly, 25 μL lysate was mixed with 25 μL PBS containing 200 μM Bzl-Cys-MCA, and incubated at 37°C for 15 min. The concentration of 7-amino-4-methylcoumarin was measured using an SH-9000 Lab multi-microplate reader (Hitachi High Tech, Tokyo,

Japan) at excitation and emission wavelengths of 380 and 460 nm, respectively. The measured fluorescence intensities were converted to enzymatic activities using a standard curve generated with 7-amino-4-methylcoumarin.

## Statistical Analysis

All the data reported here are representative of at least 3 independent experiments and are presented as mean ± SE. Statistical analysis was conducted using the Student's *t*-test and one-way ANOVA; *p* < 0.05 was considered statistically significant. The mean values of each group were compared using the Tukey–Kramer multiple comparison test.

## RESULTS AND DISCUSSION

Initially, we compared the specificity of GOH-1 with 2 commercially available anti-P-LAP/IRAP monoclonal antibodies (D7C5 and 3E1) by western blot analysis (Pan et al., 2019; Evnouchidou et al., 2020). As shown in **Figure 1**, GOH-1, and D7C5 recognized the same protein with a molecular weight of 140–165 kDa, which was expected to be P-LAP/IRAP. As shown previously (Matsumoto et al., 2001), P-LAP/IRAP in the brain has a lower molecular weight than that in the heart, and the liver is associated with minimal expression of the enzyme. On the other hand, 3E1 recognized several unidentified proteins in addition to P-LAP/IRAP. Therefore, we concluded that the GOH-1 monoclonal antibody was suitable for western blot analysis.

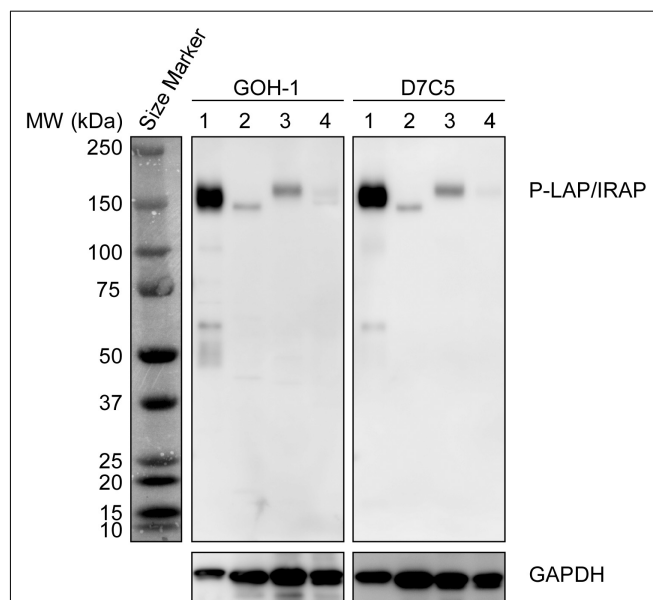


**FIGURE 1** | Specific recognition of P-LAP/IRAP by the anti-P-LAP/IRAP antibodies employed in this study. Western blot analyses of PC12 cell lysate and tissue lysates prepared from C56BL/6J mice [detection of P-LAP/IRAP (top) and GAPDH (bottom) as an internal control]. Lane 1: PC12 cells, lane 2: brain, lane 3: heart, and lane 4: liver.

## Expression Patterns of P-LAP/IRAP and AVP in Several Murine Brain Sub-regions

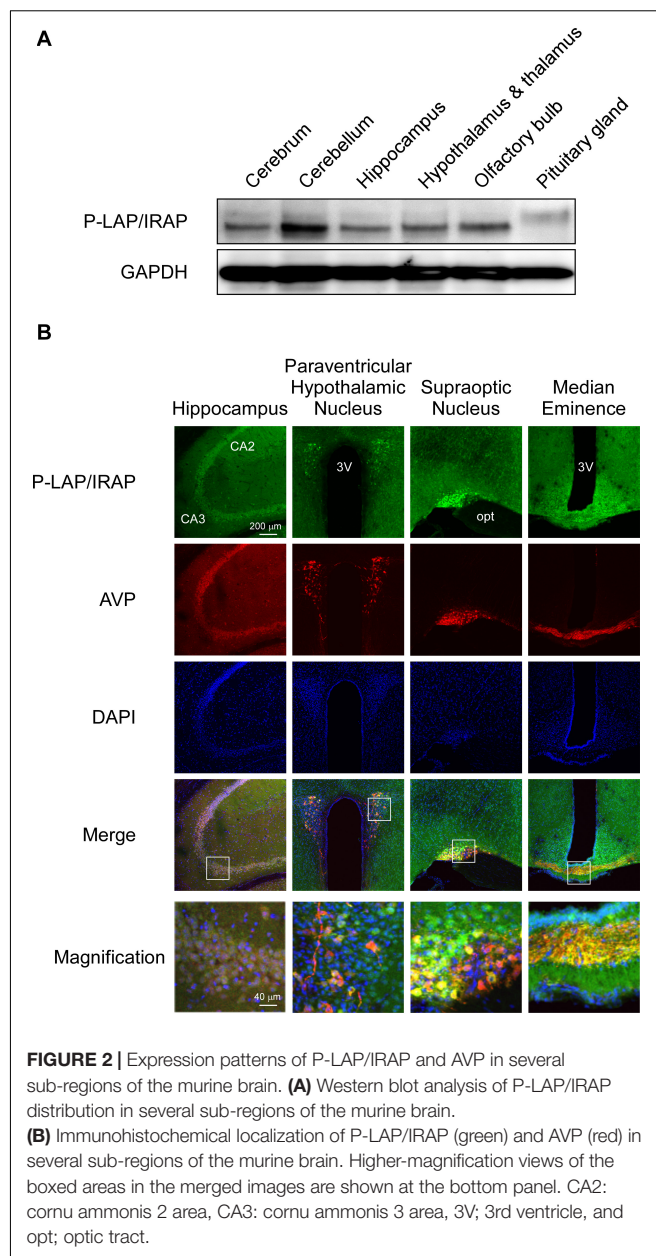
Placental leucine aminopeptidase/insulin-regulated aminopeptidase is known to cleave several peptide substrates located in the brain (Matsumoto et al., 2000). Among those tested, vasopressin was the most efficiently cleaved. Furthermore, vasopressin was the first reported physiological substrate of this enzyme (Wallis et al., 2007). Therefore, in this study, we attempted to elucidate the relationship between the expression pattern and levels of P-LAP/IRAP and vasopressin in several sub-regions of the murine brain, with the overall objective of elucidating the roles of P-LAP/IRAP in the brain.

**Figure 2A** shows the expression levels of P-LAP/IRAP in several sub-regions of the murine brain. A P-LAP/IRAP immunoreactivity band at a molecular mass of 140 kDa was detected in all the sub-regions except the pituitary gland, which expressed a 165 kDa peptide. We have previously reported the expression of P-LAP/IRAP in several human tissues, including the heart, small intestine, kidney, and brain (Matsumoto et al., 2001). The molecular mass of the enzyme expressed in the brain was slightly lower than that of the enzymes expressed in other tissues. Since the primary sequence of the enzyme contains 18 potential *N*-glycosylation sites (Rogi et al., 1996), differential glycosylation could have led to the observed differences in the molecular mass of the enzyme. Hence, we speculated that, in the murine brain, only the pituitary gland expressed a high-molecular-weight enzyme, presumably because of higher *N*-glycosylation levels. However, we could not exclude the possibility of amino acid deletions from the enzyme expressed in sub-regions of the brain other than the pituitary gland. In fact, we have previously reported 4 amino-acid deletions from the *N*-terminal end of the recombinant human P-LAP/IRAP expressed in CHO cells (Matsumoto et al., 2000).

Next, we performed immunohistochemical analyses using D7C5 to rule out the possibility of non-specific interaction between GOH-1 and sample proteins prepared from several sub-regions of the brain. Frequent usage of D7C5 for immunohistochemical analysis has been previously established (Sun et al., 2014; Evnouchidou et al., 2020).

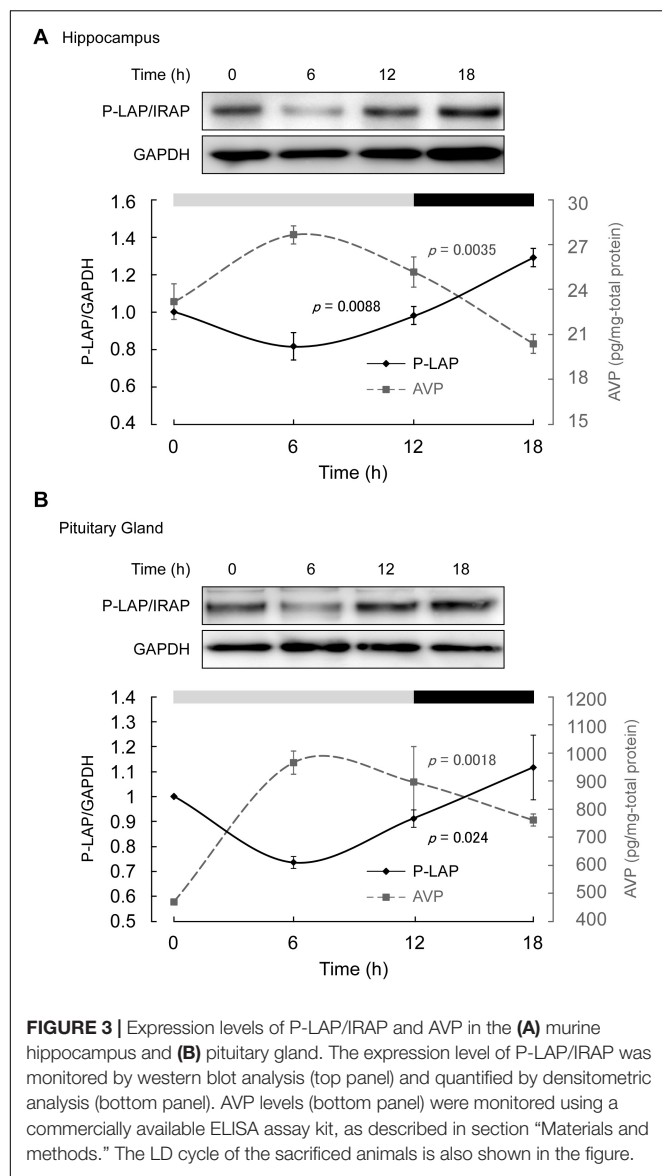
**Figure 2B** shows the immunohistochemical localization of P-LAP/IRAP and AVP in various regions of the murine brain.

In the hippocampus, expression patterns of P-LAP/IRAP and AVP exhibited large overlaps. The merged magnified image suggested that a substantial portion of P-LAP/IRAP was co-expressed with AVP, and this co-expression was typically seen in the CA3 to CA2 areas. In the paraventricular hypothalamic nucleus, P-LAP/IRAP was expressed ubiquitously, and strong expression was observed as patches where AVP-producing cells were co-localized with P-LAP/IRAP-expressing ones. A close look at the merged image suggested that higher expression of P-LAP/IRAP in these cells tended to be associated with lower AVP expression and *vice versa*. In the supraoptic nucleus, P-LAP/IRAP- and AVP-expressing cells were also concentrated in the same area. There were two



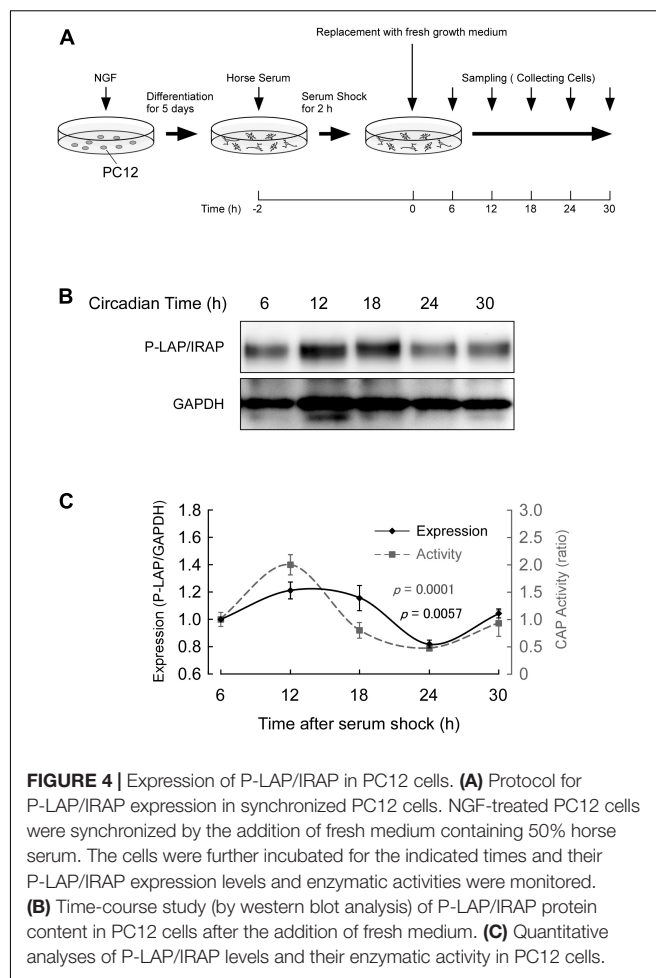
areas showing apparently differential expression patterns, out of which showed both P-LAP/IRAP and AVP expression (as judged by the yellow color in the merged image), and the other predominantly expressed AVP. It was thus plausible that in the former area, P-LAP/IRAP and AVP were co-expressed in the same cells, and in the latter, cells dominantly expressing AVP were localized. P-LAP/IRAP-expressing cells were distributed in a diffused manner throughout the median eminence, whereas the localization of AVP-expressing cells was restricted to neural fibers at its center. Merged images suggested the co-expression of P-LAP/IRAP and AVP in the same cells in the central area. Taken together, although expression patterns of immunostained P-LAP/IRAP and mature AVP showed appreciable overlaps, non-overlapping staining





patterns were also observed in several sub-regions of the murine brain. Considering our previous work showing that neuronal cells, but not glial cells, in the brain expresses the enzyme (Matsumoto et al., 2000), it is tempting to speculate that significant portions of neuronal cells co-expressed P-LAP/IRAP and AVP in several sub-regions of the murine brain. In addition, neuronal cells dominantly expressing AVP were also localized adjacent to the co-expressing cells in certain regions.

In the suprachiasmatic nucleus of the hypothalamus that contains a circadian pacemaker, circadian rhythms in vasopressin expression have been reported (Ingram et al., 1998; Mieda et al., 2015). Under LD conditions, AVP levels in the suprachiasmatic nucleus show diurnal rhythmic variations with a peak in the early light phase and a broad trough during the dark phase. Considering that vasopressin is one of the best substrates of P-LAP/IRAP, we compared the expression



patterns of the latter with that of vasopressin in the brain hippocampus and pituitary gland. Vasopressin-synthesizing neurons in the paraventricular and supraoptic nuclei in the hypothalamus are known to project to the posterior pituitary (Swaab et al., 1975).

## Diurnal Patterns of P-LAP/IRAP and AVP Expression in the Hippocampus and Pituitary Gland

Mice maintained under controlled environmental conditions with an LD cycle (12 h light, 12 h dark) were employed, as described in section “Materials and methods.” As expected, in the middle of the light phase, higher expression level of AVP was observed in both the hippocampus and pituitary gland. On the other hand, the AVP levels tended to decrease in the dark phase (Figure 3). One-way ANOVA revealed diurnal expression patterns of AVP in both the hippocampus and pituitary gland ( $p = 0.0035$  and  $0.0018$ , respectively). These results support the notion that although the experimental period in this study was rather short, diurnal rhythms in vasopressin content in both the hippocampus and pituitary gland could be detected.

On the other hand, P-LAP/IRAP levels in the hippocampus and pituitary gland showed a trend opposite to that of AVP, reaching a minimum value in the middle of the light phase (**Figure 3**). In the dark phase, an increase in P-LAP/IRAP expression was noted. One-way ANOVA revealed diurnal expression patterns of P-LAP/IRAP levels in both the hippocampus and pituitary ( $p = 0.0088$  and  $0.024$ , respectively). Since the P-LAP/IRAP-expressing cells in the hippocampus were located near the AVP-producing ones, it is tempting to speculate that the expression level of P-LAP/IRAP might have affected the level of AVP secreted into the extracellular milieu. When P-LAP/IRAP levels were high, the levels of AVP secreted from the neighboring cells were low, and *vice versa*. Hence, we concluded that the expression of P-LAP/IRAP and AVP showed an antiphasic pattern. In addition, vasopressin mRNA levels in the brain have been reported to be rhythmically dominated by clock genes (Carter and Murphy, 1992; Garbarino-Pico and Green, 2007). To our knowledge, our findings constitute one of the first evidences to suggest that P-LAP/IRAP may contribute to post-translational rhythms in vasopressin expression levels by mediating proteolytic degradation. These results therefore suggest that P-LAP/IRAP modulates the physiological functions of vasopressin in hyperosmolality, memory, learning, and circadian rhythm.

## Circadian Patterns of P-LAP/IRAP in PC12 Cells

In our previous work, we observed that nerve growth factor (NGF) treatment induced the differentiation of rat PC12 cells into neuronal cells and characteristic neurite outgrowth was observed within 2 days (Matsumoto et al., 2001). Additionally, an increase in the expression of P-LAP/IRAP in these cells was observed during differentiation. Considering the diurnal expression pattern of P-LAP/IRAP in the brain, we speculated that the enzyme expression and activity were regulated by the circadian clock in neurons. Therefore, we examined the expression and enzymatic activity patterns of P-LAP/IRAP in differentiated PC12 cells.

Cells were treated with NGF for 5 days and further incubated in the presence of 50% horse serum for 2 h. After serum shock, these cells were cultured in fresh culture medium (DMEM containing 10% fetal bovine serum) to start the synchronous culture. Then, the cells were collected every 6 h after replacement of the media (**Figure 4A**) and P-LAP/IRAP expression and CAP activity, which represents P-LAP/IRAP activity, were determined.

**Figure 4B** shows the changes in immunoreactivity of P-LAP/IRAP in NGF-treated PC12 cells up to 30 h after the serum shock. As expected, an immunoreactivity band at a molecular mass of 140 kDa was clearly detectable. In addition, we repeatedly observed a clear oscillation of the reactivity, with a peak between 12 and 18 h and a trough at 24 h after the serum shock. **Figure 4C** shows the quantified expression levels of P-LAP/IRAP normalized using the GAPDH level, confirming the changes in the expression level of the enzyme within 30 h after the serum shock. We also monitored CAP activity in these cells

and observed an in-phase rhythmic variation of the activity with P-LAP/IRAP expression. These results suggest that the expression of P-LAP/IRAP in NGF-treated neuronal cells shows circadian rhythmicity with synchronized oscillation for at least 30 h after the serum shock. Considering the possible substrates of P-LAP/IRAP in the brain reported so far (Matsumoto et al., 2000; Wallis et al., 2007), this rhythmic pattern in its enzymatic activity may have regulatory roles in neuronal cell processes involving the modulation of the functions of its substrates, such as vasopressin.

In this study, we report possible autonomous expression of P-LAP/IRAP in the hippocampus and pituitary gland of the brain for the first time. Rhythmicity was also observed in NGF-treated PC12 cells, suggesting that it is an intrinsic property of neuronal cells that affects the expression levels of peptide substrates such as vasopressin, somatostatin, and oxytocin in the brain. Reciprocal rhythmic increases and decreases in P-LAP/IRAP and AVP levels in several regions of the brain support the notion that this enzyme regulates peptide levels *via* its enzymatic activity. In addition, it has also been reported that peptide substrates such as vasopressin and oxytocin increase the cell surface expression of P-LAP/IRAP in human umbilical vein endothelial cells and rat kidney cells, respectively, Nakamura et al. (2000), Masuda et al. (2003). It is therefore tempting to postulate a feedback loop between P-LAP/IRAP expression in neuronal cells and AVP secreted from same or neighboring cells. Alternatively, it is also possible that the intrinsic rhythmicity of P-LAP/IRAP expression in these cells solely facilitates its localization in the plasma membrane and thus modulates the level of extracellular AVP produced by these or adjacent cells. More studies are required to elucidate the roles of this rhythmic expression pattern of P-LAP/IRAP in the brain.

## DATA AVAILABILITY STATEMENT

The raw data supporting the conclusions of this article will be made available by the authors, without undue reservation.

## ETHICS STATEMENT

The animal study was reviewed and approved by Committee of Teikyo-Heisei university.

## AUTHOR CONTRIBUTIONS

YG, TN, and MT conceived the study and prepared the manuscript. YG performed all the experiments. KO and AH prepared the monoclonal antibody against P-LAP/IRAP. All authors have read and approved the manuscript.

## FUNDING

This work was supported in part by JSPS KAKENHI, Grant Number 19K07405.

## REFERENCES

- Albiston, A. L., McDowall, S. G., Matsacos, D., Sim, P., Clune, E., Mustafa, T., et al. (2001). Evidence that the angiotensin IV (AT(4)) receptor is the enzyme insulin-regulated aminopeptidase. *J. Biol. Chem.* 276, 48623–48626. doi: 10.1074/jbc.c100512200
- Alescio-Lautier, B., and Soumireu-Mourat, B. (1998). Role of vasopressin in learning and memory in the hippocampus. *Prog. Brain Res.* 119, 501–521. doi: 10.1016/s0079-6123(08)61590-3
- Babdor, J., Descamps, D., Adiko, A. C., Tohme, M., Maschalidi, S., Evnouchidou, I., et al. (2017). IRAP(+) endosomes restrict TLR9 activation and signaling. *Nat. Immunol.* 18, 509–518. doi: 10.1038/ni.3711
- Balsobre, A., Damiola, F., and Schibler, U. (1998). A serum shock induces circadian gene expression in mammalian tissue culture cells. *Cell* 93, 929–937. doi: 10.1016/s0092-8674(00)81199-x
- Bogan, J. S. (2012). Regulation of glucose transporter translocation in health and diabetes. *Annu. Rev. Biochem.* 81, 507–532. doi: 10.1146/annurev-biochem-060109-094246
- Carter, D. A., and Murphy, D. (1992). Nuclear mechanisms mediate rhythmic changes in vasopressin mRNA expression in the rat suprachiasmatic nucleus. *Brain Res. Mol. Brain Res.* 12, 315–321. doi: 10.1016/0169-328x(92)90133-v
- De Bundel, D., Fafouri, A., Csaba, Z., Loyens, E., Lebon, S., El Ghoulzi, V., et al. (2015). Trans-modulation of the somatostatin type 2A receptor trafficking by insulin-regulated aminopeptidase decreases limbic seizures. *J. Neurosci.* 35, 11960–11975. doi: 10.1523/jneurosci.0476-15.2015
- Evnouchidou, I., Chappert, P., Benadda, S., Zucchetti, A., Weimershaus, M., Bens, M., et al. (2020). IRAP-dependent endosomal T cell receptor signalling is essential for T cell responses. *Nat. Commun.* 11, 2779.
- Garbarino-Pico, E., and Green, C. B. (2007). Posttranscriptional regulation of mammalian circadian clock output. *Cold Spring Harb. Symp. Quant. Biol.* 72, 145–156. doi: 10.1101/sqb.2007.72.022
- Ingram, C. D., Ciobanu, R., Coculescu, I. L., Tanasescu, R., Coculescu, M., and Mihai, R. (1998). Vasopressin neurotransmission and the control of circadian rhythms in the suprachiasmatic nucleus. *Prog. Brain Res.* 119, 351–364. doi: 10.1016/s0079-6123(08)61580-0
- Ito, N., Nomura, S., Iwase, A., Ito, T., Kikkawa, F., Tsujimoto, M., et al. (2004). ADAMs, a disintegrin and metalloproteinases, mediate shedding of oxytocinase. *Biochem. Biophys. Res. Commun.* 314, 1008–1013. doi: 10.1016/j.bbrc.2003.12.183
- Johnston, C. I. (1985). Vasopressin in circulatory control and hypertension. *J. Hypertens.* 3, 557–569. doi: 10.1097/00004872-198512000-00001
- Keller, S. R. (2004). Role of the insulin-regulated aminopeptidase IRAP in insulin action and diabetes. *Biol. Pharm. Bull.* 27, 761–764. doi: 10.1248/bpb.27.761
- Keller, S. R., Scott, H. M., Mastick, C. C., Aebersold, R., and Lienhard, G. E. (1995). Cloning and characterization of a novel insulin-regulated membrane aminopeptidase from Glut4 vesicles. *J. Biol. Chem.* 270, 23612–23618. doi: 10.1074/jbc.270.40.23612
- Kinoshita, K., Sano, Y., Takai, A., Shimizu, M., Kobayashi, T., Ouchi, A., et al. (2017). Urinary sex steroid hormone and placental leucine aminopeptidase concentration differences between live births and stillbirth of Bornean orangutans (*Pongo pygmaeus*). *J. Med. Primatol.* 46, 3–8. doi: 10.1111/jmp.12249
- Masuda, S., Hattori, A., Matsumoto, H., Miyazawa, S., Natori, Y., Mizutani, S., et al. (2003). Involvement of the V2 receptor in vasopressin-stimulated translocation of placental leucine aminopeptidase/oxytocinase in renal cells. *Eur. J. Biochem.* 270, 1988–1994. doi: 10.1046/j.1432-1033.2003.03570.x
- Matsumoto, H., Nagasaka, T., Hattori, A., Rogi, T., Tsuruoka, N., Mizutani, S., et al. (2001). Expression of placental leucine aminopeptidase/oxytocinase in neuronal cells and its action on neuronal peptides. *Eur. J. Biochem.* 268, 3259–3266. doi: 10.1046/j.1432-1327.2001.02221.x
- Matsumoto, H., Rogi, T., Yamashiro, K., Kodama, S., Tsuruoka, N., Hattori, A., et al. (2000). Characterization of a recombinant soluble form of human placental leucine aminopeptidase/oxytocinase expressed in Chinese hamster ovary cells. *Eur. J. Biochem.* 267, 46–52. doi: 10.1046/j.1432-1327.2000.00949.x
- Mieda, M., Ono, D., Hasegawa, E., Okamoto, H., Honma, K., Honma, S., et al. (2015). Cellular clocks in AVP neurons of the SCN are critical for interneuronal coupling regulating circadian behavior rhythm. *Neuron* 85, 1103–1116. doi: 10.1016/j.neuron.2015.02.005
- Nakamura, H., Itakura, A., Okamura, M., Ito, M., Iwase, A., Nakanishi, Y., et al. (2000). Oxytocin stimulates the translocation of oxytocinase of human vascular endothelial cells via activation of oxytocin receptors. *Endocrinology* 141, 4481–4485. doi: 10.1210/endo.141.12.7832
- Pan, X., Meriin, A., Huang, G., and Kandror, K. V. (2019). Insulin-responsive amino peptidase follows the Glut4 pathway but is dispensable for the formation and translocation of insulin-responsive vesicles. *Mol. Biol. Cell* 30, 1536–1543. doi: 10.1091/mbc.e18-12-0792
- Rogi, T., Tsujimoto, M., Nakazato, H., Mizutani, S., and Tomoda, Y. (1996). Human placental leucine aminopeptidase/oxytocinase. A new member of type II membrane-spanning zinc metallopeptidase family. *J. Biol. Chem.* 271, 56–61. doi: 10.1074/jbc.271.1.56
- Ross, S. A., Scott, H. M., Morris, N. J., Leung, W. Y., Mao, F., Lienhard, G. E., et al. (1996). Characterization of the insulin-regulated membrane aminopeptidase in 3T3-L1 adipocytes. *J. Biol. Chem.* 271, 3328–3332. doi: 10.1074/jbc.271.6.3328
- Saveanu, L., Carroll, O., Weimershaus, M., Guernonprez, P., Firat, E., Lindo, V., et al. (2009). IRAP identifies an endosomal compartment required for MHC class I cross-presentation. *Science* 325, 213–217. doi: 10.1126/science.1172845
- Sun, K., Park, J., Gupta, O. T., Holland, W. L., Auerbach, P., Zhang, N., et al. (2014). Endotrophin triggers adipose tissue fibrosis and metabolic dysfunction. *Nat. Commun.* 5:3485.
- Swaab, D. F., Pool, C. W., and Nijveldt, F. (1975). Immunofluorescence of vasopressin and oxytocin in the rat hypothalamo-neurohypophyseal system. *J. Neural Transm.* 36, 195–215. doi: 10.1007/bf01253126
- Tian, C., Huang, Z., and Wen, Z. (2016). Associations between serum placental leucine aminopeptidase and pregnancy outcomes. *Int. J. Gynaecol. Obstet.* 135, 255–258. doi: 10.1016/j.ijgo.2016.05.016
- Tobin, V. A., Arechaga, G., Brunton, P. J., Russell, J. A., Leng, G., Ludwig, M., et al. (2014). Oxytocinase in the female rat hypothalamus: a novel mechanism controlling oxytocin neurones during lactation. *J. Neuroendocrinol.* 26, 205–216. doi: 10.1111/jne.12141
- Tsujimoto, M., Mizutani, S., Adachi, H., Kimura, M., Nakazato, H., and Tomoda, Y. (1992). Identification of human placental leucine aminopeptidase as oxytocinase. *Arch. Biochem. Biophys.* 292, 388–392. doi: 10.1016/0003-9861(92)90007-j
- Wallis, M. G., Lankford, M. F., and Keller, S. R. (2007). Vasopressin is a physiological substrate for the insulin-regulated aminopeptidase IRAP. *Am. J. Physiol. Endocrinol. Metab.* 293, E1092–E1102.
- Yamahara, N., Nomura, S., Suzuki, T., Itakura, A., Ito, M., Okamoto, T., et al. (2000). Placental leucine aminopeptidase/oxytocinase in maternal serum and placenta during normal pregnancy. *Life Sci.* 66, 1401–1410. doi: 10.1016/s0024-3205(00)00451-3

**Conflict of Interest:** The authors declare that the research was conducted in the absence of any commercial or financial relationships that could be construed as a potential conflict of interest.

Copyright © 2020 Goto, Nakamura, Ogawa, Hattori and Tsujimoto. This is an open-access article distributed under the terms of the Creative Commons Attribution License (CC BY). The use, distribution or reproduction in other forums is permitted, provided the original author(s) and the copyright owner(s) are credited and that the original publication in this journal is cited, in accordance with accepted academic practice. No use, distribution or reproduction is permitted which does not comply with these terms.



# The Discovery of Insulin-Regulated Aminopeptidase (IRAP) Inhibitors: A Literature Review

Dimitris Georgiadis\*, Angeliki Ziotopoulou, Eleni Kaloumenou, Angelos Lelis and Antonia Papasava

Laboratory of Organic Chemistry, Department of Chemistry, National and Kapodistrian University of Athens, Athens, Greece

## OPEN ACCESS

### Edited by:

Efstathios Stratikos,  
National Centre of Scientific Research  
Demokritos, Greece

### Reviewed by:

Mats Lars-Erik Larhed,  
Uppsala University, Sweden  
Artur Mucha,  
Wrocław University of Science and  
Technology, Poland

### \*Correspondence:

Dimitris Georgiadis  
dgeorgia@chem.uoa.gr

### Specialty section:

This article was submitted to  
Experimental Pharmacology  
and Drug Discovery,  
a section of the journal  
Frontiers in Pharmacology

**Received:** 21 July 2020

**Accepted:** 24 August 2020

**Published:** 23 September 2020

### Citation:

Georgiadis D, Ziotopoulou A,  
Kaloumenou E, Lelis A and  
Papasava A (2020) The Discovery of  
Insulin-Regulated Aminopeptidase  
(IRAP) Inhibitors: A Literature Review.  
Front. Pharmacol. 11:585838.  
doi: 10.3389/fphar.2020.585838

Insulin-Regulated Aminopeptidase (IRAP, EC 3.4.11.3) is a multi-tasking member of the M1 family of zinc aminopeptidases. Among its diverse biological functions, IRAP is a regulator of oxytocin levels during late stages of pregnancy, it affects cellular glucose uptake by trafficking of the glucose transporter type 4 and it mediates antigen cross-presentation by dendritic cells. Accumulating evidence show that pharmacological inhibition of IRAP may hold promise as a valid approach for the treatment of several pathological states such as memory disorders, neurodegenerative diseases, etc. Aiming to the investigation of physiological roles of IRAP and therapeutic potential of its regulation, intense research efforts have been dedicated to the discovery of small-molecule inhibitors. Moreover, reliable structure-activity relationships have been largely facilitated by recent crystal structures of IRAP and detailed computational studies. This review aims to summarize efforts of medicinal chemists toward the design and development of IRAP inhibitors, with special emphasis to factors affecting inhibitor selectivity.

**Keywords:** inhibitor, insulin-regulated aminopeptidase, inhibitor selectivity, aminopeptidase, structure-activity relationships

## INTRODUCTION

Insulin-regulated aminopeptidase (IRAP, oxytocinase, EC 3.4.11.3) is a type II transmembrane Zn-protease that belongs to the M1 family of aminopeptidases (Rogi et al., 1996; Laustsen et al., 1997; Nomura et al., 2013). IRAP was so named because it was first identified in specialized vesicles in fat and muscle cells co-localized with the glucose transporter GLUT4. Upon insulin receptor stimulation these vesicles translocate to plasma membrane to facilitate glucose uptake into the cells (Keller et al., 1995). IRAP is also called oxytocinase since it was also isolated from the placenta and was found to regulate the levels of circulating oxytocin during the later stages of human pregnancy (Rogi et al., 1996). IRAP is highly expressed in brain regions associated with cognition (Fernando et al., 2005) and is able to degrade macrocyclic peptides, such as oxytocin and vasopressin, which are known to influence favorably cognitive functions (Gulpinar and Yegen, 2004; Wallis et al., 2007; Rimmele et al., 2009; Albiston et al., 2011). Moreover, IRAP is inhibited by angiotensin IV (AngIV), hence IRAP was recognized as a potential target for the treatment of cognitive disorders during the last decade (Albiston et al., 2001; Lew et al., 2003; Albiston et al., 2008; Albiston et al., 2011; Andersson and Hallberg, 2012). Except from IRAP's association to



glucose metabolism and cognition-related functions, it is also involved in the generation of antigenic MHC peptides for cross-presentation (Saveanu et al., 2009; Saveanu and Van Endert, 2012), in the trafficking of T-cell receptors (Evnouchidou et al., 2020) and in the progress of cardiac and renal fibrosis (Gaspari et al., 2018a; Gaspari et al., 2018b). Although the development of IRAP inhibitors was initially aiming to the development of cognitive enhancers, applications in the regulation of immune responses or as antifibrotic agents are also emerging fields of pharmacological interest. In this mini-review, we present the different classes of IRAP inhibitors, we briefly discuss key interactions that govern inhibitor binding and we provide selectivity profile data and possible interpretation of observed selectivity. We must note that  $K_i$  or  $IC_{50}$  values of inhibitors mentioned in this review may have been estimated using different types of assays. Regardless of the methodology, general conclusions on the comparison of inhibition profiles are not significantly affected by this discrepancy.

## TYPES OF IRAP INHIBITORS

### AngIV Peptidic Analogs and Peptidomimetics

Undoubtedly, a strong inspiration toward the development of the first IRAP inhibitors came from the breakthrough discovery that IRAP is identified as the  $AT_4$  receptor (Albiston et al., 2001). Based on prior work of Harding and Wright on AngIV analogs with high affinity for  $AT_4$  (Sardinia et al., 1993; Sardinia et al., 1994; Krishnan et al., 1999), Lew et al. demonstrated that  $AT_4$  receptor ligands, such as  $Nle^1$ -AngIV, divalinal-AngIV, decapeptide LVVYPWTQRF (LVV-hemorphin-7) and the parent peptide AngIV, inhibit the proteolytic activity of IRAP in HEK293T cell membranes with  $K_i$  values between 113 nM and 2.3  $\mu$ M (Lew et al., 2003). In 2003, Lee et al. produced several truncated or alanine-substituted analogs of LVV-hemorphin-7 and evaluated their binding affinity in competition studies with  $^{125}I$ -AngIV in sheep adrenal and cerebellar membranes (Lee et al., 2003). The authors also estimated the  $K_i$  values in an enzyme inhibition assay for selected truncated LVV-hemorphin-7 analogs which revealed that  $N$ -terminal amino acid deletion can be tolerated up to  $Val^3$  whereas  $C$ -terminal deletion does not significantly affect binding affinity up to  $Pro^6$ . Interestingly, tripeptide VYP is only three time less potent inhibitor ( $K_i$  = 620 nM) than the parent decapeptide ( $K_i$  = 196 nM), highlighting the importance of hydrophobic residues for binding affinity against IRAP.

In 2006, the research group of Hallberg designed and evaluated a series of disulfide-cyclized AngIV analogs based on the assumption that macrocyclization would confer metabolic stability toward enzymatic degradation while retaining the high affinity of AngIV for IRAP (Axén et al., 2006). Indeed, compound 1 (Figure 1) was identified which encompasses an 11-membered, conformationally flexible ring, displays similar inhibitory potency toward IRAP as AngIV and is characterized by reduced susceptibility against proteolysis. The significance of

proper positioning of disulfide linkage within the peptide became evident after detailed evaluation of several suitably designed AngIV analogs, which revealed that only cyclization at the  $C$ -terminal region of AngIV can lead to inhibitors equipotent to AngIV. This observation led to the conclusion that the  $Cys^4$ - $Pro^5$ - $Cys^6$  moiety in compound 1 adopts an inverse  $\gamma$ -turn conformation that possibly resembles the bioactive conformation of AngIV, as it was further supported by conformational analysis. These findings triggered subsequent studies by the same group aiming to the gradual transition from AngIV peptide analogs to more “drug-like”, designed peptidomimetics. In a 2007 report, it was proposed that the conformational characteristics of the  $C$ -terminal sequence  $His^4$ - $Pro^5$ - $Phe^6$  of AngIV (or the  $Cys^4$ - $Pro^5$ - $Cys^6$  tail of compound 1) can be mimicked by a non-peptidic 2-(aminomethyl) phenylacetic acid (AMPAA) moiety which optimally positions the terminal carboxylate for efficient enzyme recognition (Axén et al., 2007). Compound 2 (Figure 1) showed considerably higher metabolic stability against metalloproteases present in CHO-K1 cell membranes than AngIV and it was able to induce proliferation of adult neural stem cells. Moreover, compound 2 was almost twice more selective for IRAP versus APN than the disulfide analog 2, which validates furthermore Hallberg’s rigidification approach.

In 2008, Hallberg and co-workers extended their previous studies on backbone modification of AngIV by introducing additional non-cleavable amino acid surrogates, in order to increase metabolic stability of IRAP inhibitors (Andersson et al., 2008). Among the various peptidomimetics developed, compound 3 (Figure 1) showed the highest potency for IRAP ( $K_i$  = 1.4  $\mu$ M), albeit 23-fold lower than AngIV. As compared to AngIV structure,  $Tyr^2$  was replaced by a 4-hydroxydiphenylmethane scaffold and  $C$ -terminal sequence  $His^4$ - $Pro^5$ - $Phe^6$  was replaced by an AMPAA moiety. A conceptually similar approach was employed by Lukaszuk et al. who produced analogs of AngIV with  $\beta^2$ - or  $\beta^3$ -amino acid substitutions in order to enhance potency, stability and IRAP/APN selectivity (Lukaszuk et al., 2008). Compound AL-11 (Figure 1) was particularly interesting to that respect since it was able to inhibit IRAP with a  $K_i$  value of 27.5 nM, it displayed a ~200-fold selectivity for APN and it was completely stable in the presence of CHO-K1 cell membranes. The development of AL-11 was based on the observation that the introduction of  $\beta^2$ - $hVal^1$  and  $\beta^3$ - $hPhe^6$  substitutions contribute to the metabolic stability and the suppression of binding to  $AT_1$ , respectively, whereas the synergy of both substitutions is responsible for the reported selectivity for IRAP versus APN. The same research team managed to improve inhibitory potency for IRAP by replacing  $His^4$ - $Pro^5$  of AngIV by  $Aia^4$ - $Gly^5$  ( $Aia$ : 4-amino-1,2,4,5-tetrahydro-indolo[2,3-*c*]-azepin-3-one) while maintaining the  $\beta^2$ - $hVal^1$  substitution (AL-40, Figure 1) (Lukaszuk et al., 2009). Evidently, the introduction of a constrained Trp analog instead of  $His^4$  is responsible for a substantial conformational transformation of AL-40 which boosts binding affinity for IRAP. Similar replacements of  $Tyr^2$  by constrained amino acids had a deleterious effect on potency whereas such modifications for  $Pro^4$  and  $Phe^6$  are well tolerated, albeit without surpassing the efficiency of AL-40 (Lukaszuk et al., 2011). Finally, screening of  $\alpha$ -substituted amino acids in lieu of  $Gly^5$  of AL-40 led to the discovery of inhibitor IVDE77 (Figure 1) that shows remarkable efficiency in terms of potency for IRAP ( $K_i$  = 1.7 nM), IRAP/APN

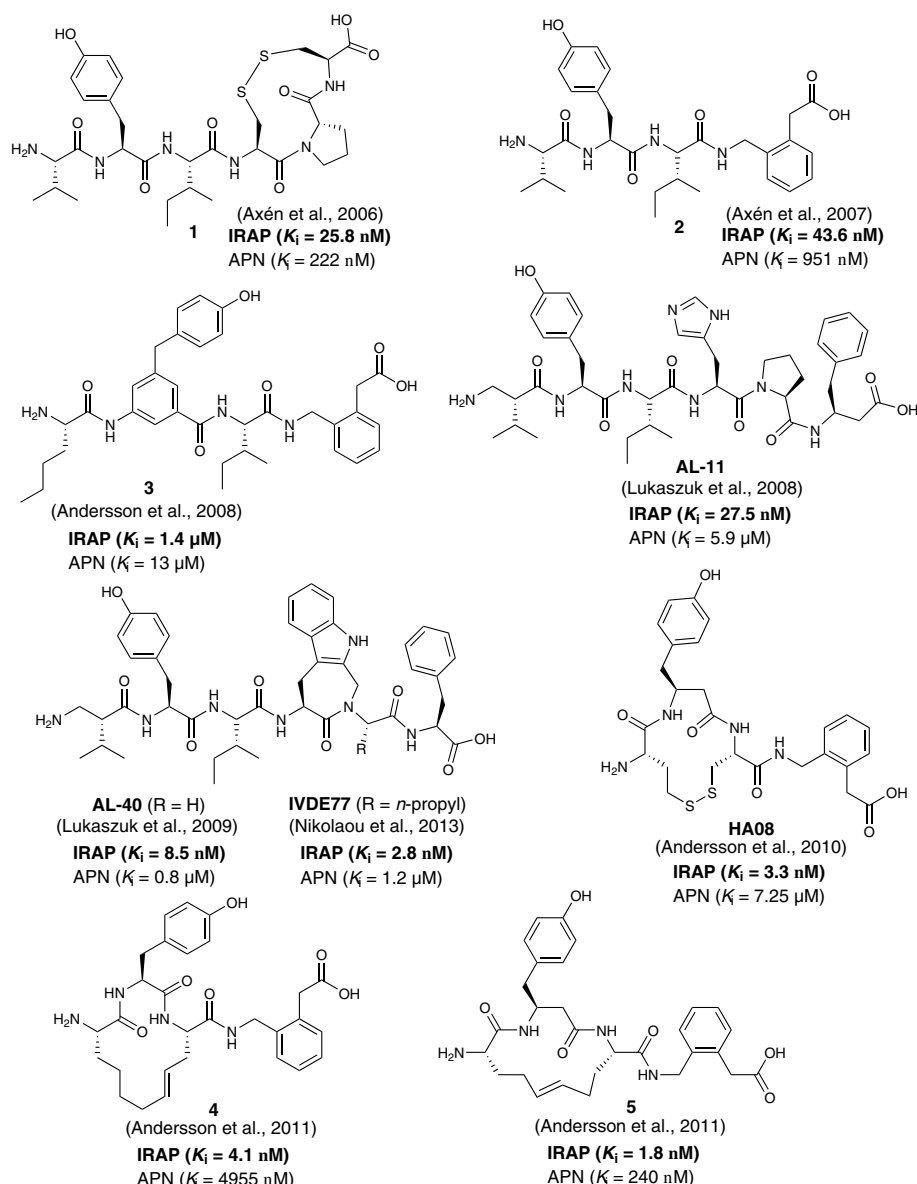


**FIGURE 1 |** Chemical structures of AngIV-based inhibitors of IRAP **1-5**, **AL-11**, **AL-40**, **IVDE77**, and **HA08**.  $K_i$  values for IRAP and APN are given in all cases.

and IRAP/AT1 selectivity and metabolic resistance against proteolytic degradation (Nikolaou et al., 2013). Moreover, by using a tritiated analog of the inhibitor, it was demonstrated that IVDE77 was able to completely eliminate IRAP availability at the cell surface *in vitro*.

Concurrently with the work of Belgian researchers that culminated in the discovery of IVDE77, Hallberg and co-workers refined the structure of previously reported AngIV-based inhibitors bearing a C-terminal AMPAA motif (e.g. compound **2**) by imposing conformational constraints at the N-terminal region (Andersson et al., 2010). Prior work had shown that replacement of Val<sup>1</sup> and Ile<sup>3</sup> of AngIV with Cys residues followed by oxidative cyclization causes a dramatic drop in IRAP

inhibitory activity ( $K_i = 16.9$   $\mu$ M), suggesting that the N-terminal of AngIV is very sensitive to conformational changes (Axén et al., 2006). However, potency was significantly restored ( $K_i = 303$  nM) when hCys instead of Cys residues were employed, thus expanding the initial 11-membered to a 13-membered ring. Interestingly, replacement of the C-terminal His<sup>4</sup>-Pro<sup>5</sup>-Phe<sup>6</sup> with the AMPAA motif, not only resulted to a 13-fold increase in IRAP inhibitory potency but also abolished activity toward APN. Further structural modifications led to optimized inhibitor HA08 (**Figure 1**) which displays excellent IRAP potency and IRAP/APN selectivity and encompasses a  $\beta^3$ -hTyr<sup>2</sup>-Cys<sup>3</sup> sequence, thus retaining the privileged 13-membered

ring size. Very recently, Mpakali et al. solved the crystal structure of IRAP/HA08 complex and identified several key features of the inhibition mechanism (Mpakali et al., 2020). The authors propose that upon binding, HA08 induces an extensive conformational change to IRAP which corresponds to the so-called “closed” state, previously observed also in the case of an IRAP inhibitor of phosphinic type (*vide infra*). This conformational transition establishes tight interactions between the macrocyclic inhibitor and the GAMEN loop of IRAP, a common structural feature of M1 aminopeptidases which in the case of IRAP presents unusual conformational plasticity and unprecedented adaptability. Despite HA08’s peptidic nature, its tolerance to degradation by IRAP relies on the tight spatial juxtaposition with the GAMEN loop that precludes water molecules to be activated by Glu465 and trigger catalysis.

Unfortunately, unlike IRAP, other proteases are able to degrade HA08, rendering this inhibitor metabolically unstable. To this regard, Andersson et al. developed a series of improved macrocyclic analogs by applying a ring-olefin metathesis protocol, in order to replace the labile disulfide bond of HA08 with a carbon-carbon bond (Andersson et al., 2011). Gratifyingly, researchers succeeded in producing proteolytically stable derivatives showing excellent potency for IRAP and IRAP/APN selectivity, as it is exemplified in the most efficient inhibitors of this series, compounds 4 and 5 (**Figure 1**). In contrast to HA08, optimized inhibitors 4 and 5 encompass an one-carbon expanded 14-membered ring, a structural feature that improves binding affinity by one order of magnitude, implying that the size of the macrocycle critically affects the conformational characteristics of the inhibitor. Efforts to bridge positions 1 and 3 of AngIV macrocyclic peptidomimetics by an amide bond had a negative effect in inhibitory potency, as it was described in a recent report (Barlow et al., 2020). According to molecular dynamics analysis, this behavior could be explained by an unfavorable orientation of the AMPAA moiety inside the active-site pocket, due to conformational changes induced by the presence of amide linkage.

## 4H-Benzopyrans

Another milestone discovery in the history of IRAP inhibitors appeared in the literature in 2008 by a group of Australian researchers (Albiston et al., 2008). By performing virtual screening of a database of 1.5 million compounds against an homology model of IRAP, the team identified the 2-amino-4H-benzopyran scaffold as a promising hit for further development. Indeed, after evaluating several benzopyran analogs and applying medicinal chemistry modifications to the most active lead, compounds HFI-419, HFI-435, and HFI-437 (**Figure 2**) were selected as those exhibiting  $K_i$  values lower than 1  $\mu\text{M}$ . These were the first IRAP inhibitors that were not based on AngIV or other peptide scaffolds. All of the inhibitors were selective for IRAP versus other aminopeptidases such as LTA4H, APN, ERAP1, and ERAP2, as it is exemplified in the case HFI-437 in **Figure 2**. All compounds were tested as racemates, however the S-isomer is believed to be more active, as it was suggested by molecular docking that revealed a better fit to the catalytic site of IRAP (based on a LTA4H crystal structure) (Albiston et al., 2010). During these initial docking efforts, two different poses

were predicted as optimal for pyridine and quinoline derivatives. In both cases, interactions with Phe544 appeared to be crucial for binding, as it was further verified by site-directed mutagenesis experiments. However, revisited predictions after the resolution of empty IRAP’s crystal structure showed both scaffolds dock with almost identical poses, with the hydroxyl group on the benzopyran ring interacting with  $\text{Zn}^{2+}$  and the benzopyran ring juxtaposing against the GAMEN loop (Hermans et al., 2015). This binding pose accurately explains SAR data showing the complete loss of activity after replacement of the hydroxyl group at 7-position of 4H-benzopyrans that was initially erroneously attributed to disruption of critical hydrogen bonding interactions with active site residues (Mountford et al., 2014). Moreover, according to revisited predictions, the aromatic system of pyridine or quinoline interacts with Phe544 to a different degree, which could explain the greater sensitivity of quinoline derivatives to mutations at residue Phe544. HFI-419 exhibited better aqueous solubility and allowed the improvement of spatial working and recognition memory in rodents, possibly by increasing hippocampal dendritic spine density *via* a GLUT4-mediated mechanism (Seyer et al., 2019).

## Phosphinic Pseudopeptides

Among its several biological functions, IRAP has been implicated in an intracellular pathway that generates antigenic peptides for cross-presentation by dendritic cells (Saveanu et al., 2009; Saveanu and Van Endert, 2012). IRAP is highly homologous to ERAP1 and ERAP2, two other intracellular M1 aminopeptidases that are also key players in the trimming of antigenic peptide precursors to optimal length for loading onto MHC class I molecules. In 2003, in the quest of ERAPs inhibitors that could potentially regulate immune responses, with possible applications ranging from cancer immunotherapy to treatment of inflammatory autoimmune diseases, phosphinic pseudotripeptide DG013A (**Figure 2**) was developed being a potent inhibitor of all three enzymes, with a  $K_i$  value for IRAP of 57 nM (Zervoudi et al., 2013). The mechanism of inhibition by this rationally designed inhibitor was further investigated by solving the crystal structure of ERAP2/DG013A complex which revealed that the hydroxyphosphinyl moiety interacts with  $\text{Zn}^{2+}$  through the two oxygen atoms of tetrahedral phosphorous, forming also hydrogen bonds with Glu371 and Tyr455, two residues critical for catalysis. Based on the analogy of DG013A binding pose with the conformation of a substrate during the transition state of hydrolytic reaction, a typical property of phosphinic pseudopeptide protease inhibitors (Georgiadis and Dive, 2015), a subsequent SAR study was performed aiming to unveil those structural determinants that confer selectivity between ERAPs and IRAP (Kokkala et al., 2016). Two inhibitors derived from this study displayed distinct properties in terms of IRAP inhibition: DG026 and DG046 (**Figure 2**).

DG026, which includes a bulky benzydryl group in its  $\text{P}_1'$  position, showed high potency and selectivity for IRAP vs ERAPs (115-fold for ERAP1 and 23-fold for ERAP2) and succeeds in reducing IRAP-dependent but not ERAP1-dependent cross-presentation by dendritic cells with nanomolar efficacy. Aiming at understanding the reasons behind this inhibition profile,



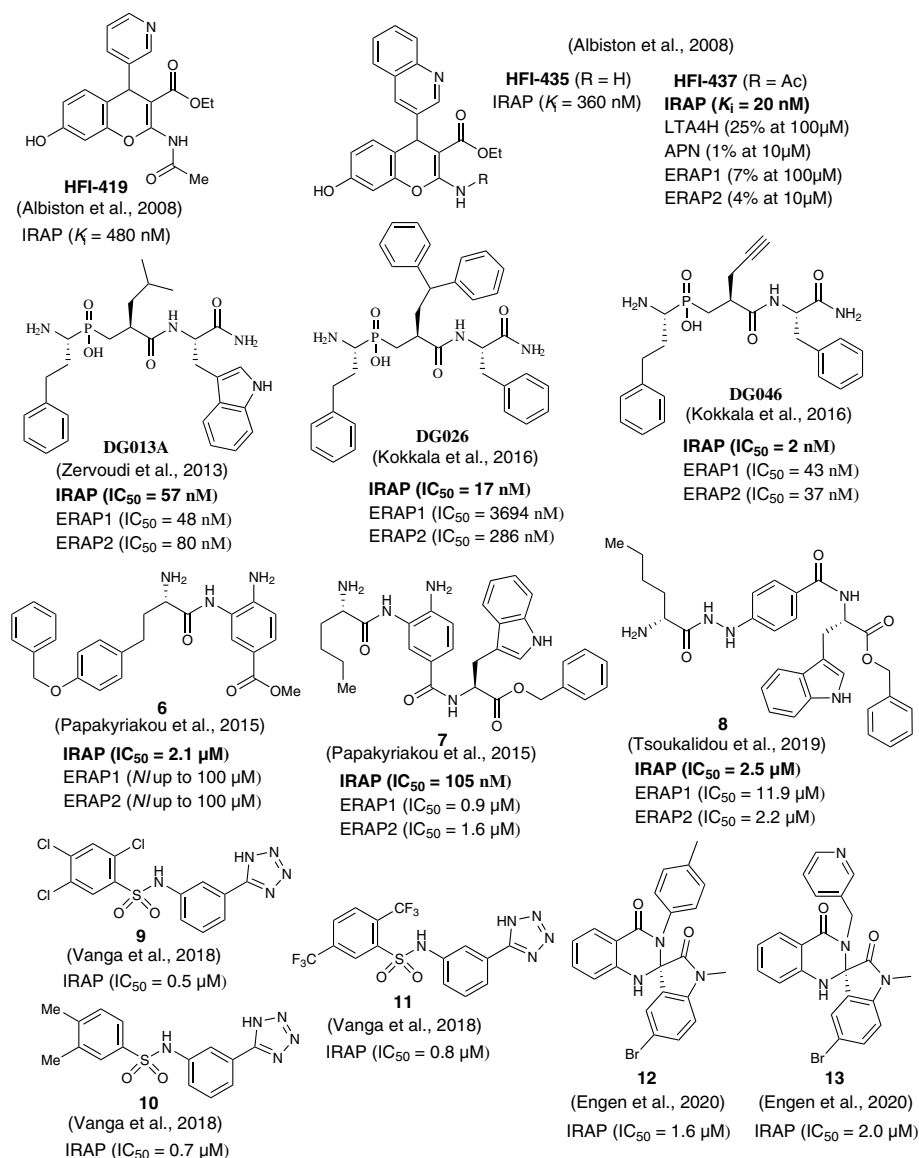


**FIGURE 2 |** Chemical structures of non-AngIV based inhibitors of IRAP **6-13**, **HFI-410**, **HFI-435**, **DG013A**, **DG026**, and **DG046**.  $K_i$  or  $IC_{50}$  values for IRAP are given in all cases.  $K_i$  or  $IC_{50}$  values for other aminopeptidases are also provided, if available.

Mpakali et al. solved the crystal structure of IRAP/DG026 complex which revealed for the first time a “closed” conformational state for IRAP that is believed to be induced upon ligand binding (Mpakali et al., 2017b). This conformation was known for ERAPs but it had never been observed for IRAP. Indeed, both IRAP structures available at that time, one ligand-free and one bound with an antigenic epitope-based phosphinic pseudopeptide, were found in an open or semi-closed conformation, respectively (Hermans et al., 2015; Mpakali et al., 2015). In the transition from empty IRAP to the closed conformation of IRAP/DG026, a large rearrangement of GAMEN loop takes place [as it was later observed in the IRAP/HA08 crystal structure (Mpakali et al., 2020)] that is not

common in other aminopeptidases and may account for the wider substrate specificity of IRAP. The selectivity of DG026 could probably be attributed to unfavorable repulsive interactions of bulky hydrophobic benzhydryl group with the overall more polar environment of ERAPs, compared to IRAP. Furthermore, it was proposed based on structural analysis that the high potency and selectivity of DG026 is a direct result of its near-optimal complementarity for IRAP, creating a network of interactions that probably drive the conformational change from the open to the closed state.

Interestingly, DG046 bearing a small, linear propargylic side chain at  $P_1'$  position is one of the most potent IRAP inhibitors ever reported ( $K_i$  = 2 nM) with a fairly good selectivity versus

ERAP1 and ERAP2 by a factor of ~20 for both. Probably, the proposed plasticity of IRAP's active site leads to potent inhibitors with either small or bulky groups at P<sub>1</sub>' position. Recently, the ERAP1/DG046 structure became available which provides important insights on the selectivity determinants of DG046 (Giastas et al., 2019). In particular, stacking interactions of Tyr residues in the case of ERAP2 and IRAP with the phenyl ring of P<sub>2</sub>' position of DG046 cannot take place in ERAP1 that has a Ser at the same position. Finally, the side chain of Ile461 in the case of IRAP could properly orientate propargyl group toward a zinc coordinating histidine and favor the formation of critical  $\pi$ - $\pi$  interactions.

### 3,4-Diaminobenzoic Acid Derivatives

Another class of compounds that have been extensively evaluated as inhibitors of IRAP and ERAPs by Vourloumis group are 3,4-diaminobenzoic acid (DABA) derivatives bearing natural and/or unnatural aminoacids (Papakyriakou et al., 2013; Papakyriakou et al., 2015). Selectivity for IRAP was feasible in the expense of potency, as it is exemplified in the case of compound 6 (**Figure 2**), an IRAP inhibitor of IC<sub>50</sub> = 2.1  $\mu$ M which was inactive against ERAPs up to 100  $\mu$ M (Papakyriakou et al., 2015). Improvement of binding affinity led to reduced selectivity, as depicted in **Figure 2** for compound 7. In fact, compound 7 (IC<sub>50</sub> = 105 nM) was the most potent inhibitor of all 77 compounds tested in this study for all three enzymes, which emphasizes the overall moderate efficacy of DABA-based inhibitors. Indeed, structural analysis of a DABA derivative with ERAP2 revealed a rather weak interaction between the carbonyl oxygen of DABA core with the zinc ion (Mpakali et al., 2017a). Further, variations of the same structural theme led to only moderate, non-selective IRAP inhibitors with compound 8 being the most representative example (Tsoukalidou et al., 2019).

### Aryl Sulfonamides

In 2014, Swedish researchers recognized the ability of aryl sulfonamides to inhibit IRAP after screening a library of 10,500 drug-like compounds (Borhade et al., 2014; Engen et al., 2016). After a hit-to-lead process, several compounds of moderate potency were selected, such as 9 and 10 which were shown to alter dendritic spine morphology and increase spine density in primary cultures of hippocampal neurons (Diwakarla et al., 2016). Recently, further lead optimization furnished several fluorinated analogs (e.g. compound 11) that presented higher metabolic stability by human or mouse liver microsomes (Vanga et al., 2018). In the absence of any IRAP structure, initial attempts to rationalize inhibitor binding and interpret SAR data by molecular docking concluded that the tetrazole ring may be involved in stabilizing interactions with Zn<sup>2+</sup> and Ty549 (Borhade et al., 2014). However, guided by the IRAP/DG026 structure published in 2015 by Stratikos group (Mpakali et al., 2017b), subsequent extensive computational analysis qualified an alternative binding pose where it is an oxygen atom of sulfonamide that coordinates with Zn<sup>2+</sup>. Moreover, the amide NH is stabilized by interactions with the Glu residue of the GAMEN loop and tetrazole ring develops polar interactions with Arg439.

### Spiro-oxindole Dihydroquinazolinones

During the screening process that led to the discovery of aryl sulfonamide inhibitors, one of the most potent hits was compound 12 (**Figure 2**) based on the spiro-oxindole dihydroquinazolinone scaffold (Engen et al., 2016). Efforts to improve the poor solubility of hit compound 12 (e.g. compound 13, **Figure 2**) led in all cases to derivatives with reduced metabolic stability *in vitro* (Engen et al., 2020). Nevertheless, this class of compounds presents high specificity for IRAP vs APN. According to docking calculations, a unique feature of spiro-oxindole derivatives is that the inhibitor in its preferred binding pose is positioned in close proximity with the GAMEN loop without interacting with Zn<sup>2+</sup>, leading to uncompetitive inhibitors as it was further supported by kinetic experiments.

## CONCLUSIONS

After two decades of intense efforts toward the discovery of IRAP inhibitors, it would not be an exaggeration to say that the field is still in its infancy. Recent crystal structures of IRAP with bound small-molecule inhibitors are expected to rationalize binding preferences of known inhibitors and facilitate the discovery of new ones, either by accelerating the hit-to-lead optimization process during screening endeavours or by guiding efforts toward structure-based rational design or scaffold hopping. Of course, a question that needs to be addressed is whether the "closed" conformational state of the enzyme and the GAMEN loop re-orientation observed in recent structures of IRAP with DG026 and HA08 (Mpakali et al., 2017b; Mpakali et al., 2020), constitute a prerequisite for efficient binding of small-molecule inhibitors or not. Recently, Vanga et al. predicted structural determinants for IRAP inhibition by aryl sulfonamides using IRAP's "open" structure, however attempts to re-examine their predictions by using the "closed" structure of IRAP were unsuccessful due to the inability of inhibitors to access the catalytic site of the enzyme (Vanga et al., 2018). The authors formulate the assumption that in this specific case stabilization of an "open" enzyme conformation would probably be more favourable. Similarly, Mpakali et al. observed substantial differences between preferred binding modes of benzopyran inhibitor HFI-437 when docked to the empty IRAP "open" structure, as compared to the IRAP/DG025 "closed" one (Mpakali et al., 2017b). Taking into account the unique, ligand-induced active-site plasticity of IRAP, possible identification of additional conformational states of IRAP induced by inhibitors of other types will complicate even more the already perplexed mechanism of IRAP inhibition. Inspiration for the design of novel inhibitors can be drawn by scaffolds that have been successfully evaluated against other M1 aminopeptidases but not for IRAP (e.g. boronic acids, aminothiols, bestatin derivatives etc) (Mucha et al., 2010). However, extreme caution is required when such inhibitors are evaluated in order to avoid possible cross-reactivity which may trigger off-

target side-effects (Drinkwater et al., 2017). Undoubtedly, delineation of binding particularities associated with different inhibitor scaffolds is expected to reveal those specific interactions that enhance inhibitor selectivity and eventually lead to next-generation inhibitors with safer inhibition profiles and improved pharmacological properties.

## AUTHOR'S NOTE

Dedicated to the memory of our dear colleague Dr. Dionisios Vourloumis.

## REFERENCES

- Albiston, A. L., McDowall, S. G., Matsacos, D., Sim, P., Clune, E., Mustafa, T., et al. (2001). Evidence that the angiotensin IV (AT(4)) receptor is the enzyme insulin-regulated aminopeptidase. *J. Biol. Chem.* 276, 48623–48626. doi: 10.1074/jbc.C100512200
- Albiston, A. L., Morton, C. J., Ng, H. L., Pham, V., Yeatman, H. R., Ye, S., et al. (2008). Identification and characterization of a new cognitive enhancer based on inhibition of insulin-regulated aminopeptidase. *FASEB J.* 22, 4209–4217. doi: 10.1096/fj.08-112227
- Albiston, A. L., Pham, V., Ye, S., Ng, L., Lew, R. A., Thompson, P. E., et al. (2010). Phenylalanine-544 plays a key role in substrate and inhibitor binding by providing a hydrophobic packing point at the active site of insulin-regulated aminopeptidase. *Mol. Pharmacol.* 78, 600–607. doi: 10.1124/mol.110.065458
- Albiston, A. L., Diwakarla, S., Fernando, R. N., Mountford, S. J., Yeatman, H. R., Morgan, B., et al. (2011). Identification and development of specific inhibitors for insulin-regulated aminopeptidase as a new class of cognitive enhancers. *Br. J. Pharmacol.* 164, 37–47. doi: 10.1111/j.1476-5381.2011.01402.x
- Andersson, H., and Hallberg, M. (2012). Discovery of inhibitors of insulin-regulated aminopeptidase as cognitive enhancers. *Int. J. Hypertens.* 2012, 789671. doi: 10.1155/2012/789671
- Andersson, H., Demaegdt, H., Vauquelin, G., Lindeberg, G., Karlén, A., and Hallberg, M. (2008). Ligands to the (IRAP)/AT4 receptor encompassing a 4-hydroxydiphenylmethane scaffold replacing Tyr2. *Bioorg. Med. Chem.* 16, 6924–6935. doi: 10.1016/j.bmc.2008.05.046
- Andersson, H., Demaegdt, H., Vauquelin, G., Lindeberg, G., Karlén, A., Hallberg, M., et al. (2010). Disulfide cyclized tripeptide analogues of angiotensin IV as potent and selective inhibitors of insulin-regulated aminopeptidase (IRAP). *J. Med. Chem.* 53, 8059–8071. doi: 10.1021/jm100793t
- Andersson, H., Demaegdt, H., Johnsson, A., Vauquelin, G., Lindeberg, G., Hallberg, M., et al. (2011). Potent macrocyclic inhibitors of insulin-regulated aminopeptidase (IRAP) by olefin ring-closing metathesis. *J. Med. Chem.* 54, 3779–3792. doi: 10.1021/jm200036n
- Axén, A., Lindeberg, G., Demaegdt, H., Vauquelin, G., Karlén, A., and Hallberg, M. (2006). Cyclic insulin-regulated aminopeptidase (IRAP)/AT4 receptor ligands. *J. Pept. Sci.* 12, 705–713. doi: 10.1002/psc.782
- Axén, A., Andersson, H., Lindeberg, G., Rönnholm, H., Kortesmaa, J., Demaegdt, H., et al. (2007). Small potent ligands to the insulin-regulated aminopeptidase (IRAP)/AT4 receptor. *J. Pept. Sci.* 13, 434–444. doi: 10.1002/psc.859
- Barlow, N., Vanga, S. R., Sävmarker, J., Sandström, A., Burns, P., Hallberg, A., et al. (2020). Macrocyclic peptidomimetics as inhibitors of insulin-regulated aminopeptidase (IRAP). *RSC Med. Chem.* 11, 234–244. doi: 10.1039/C9MD00485H
- Borhade, S. R., Rosenstrom, U., Savmarker, J., Lundback, T., Jenmalm-Jensen, A., Sigmundsson, K., et al. (2014). Inhibition of Insulin-Regulated Aminopeptidase (IRAP) by Arylsulfonamides. *ChemistryOpen* 3, 256–263. doi: 10.1002/open.201402027
- Diwakarla, S., Nylander, E., Gronbladh, A., Vanga, S. R., Khan, Y. S., Gutierrez-De-Teran, H., et al. (2016). Aryl Sulfonamide Inhibitors of Insulin-Regulated

## AUTHOR CONTRIBUTIONS

EK, AZ, AP, and AL conducted the review of literature, analyzed and organized bibliography, prepared the figures and drafted part of the manuscript. DG conceived the project, drafted part of the manuscript, revised and finalized the manuscript. All authors contributed to the article and approved the submitted version.

## FUNDING

This work was supported by funds from the Special Account for Research Grants of NKUA.

- Aminopeptidase Enhance Spine Density in Primary Hippocampal Neuron Cultures. *ACS Chem. Neurosci.* 7, 1383–1392. doi: 10.1016/j.nlm.2016.09.017
- Drinkwater, N., Lee, J., Yang, W., Malcolm, T. R., and McGowan, S. (2017). M1 aminopeptidases as drug targets: broad applications or therapeutic niche? *FEBS J.* 284, 1473–1488. doi: 10.1111/febs.14009
- Engen, K., Rosenstrom, U., Axelsson, H., Konda, V., Dahllund, L., Otrocka, M., et al. (2016). Identification of Drug-Like Inhibitors of Insulin-Regulated Aminopeptidase Through Small-Molecule Screening. *Assay Drug Dev. Technol.* 14, 180–193. doi: 10.1089/adt.2016.708
- Engen, K., Vanga, S. R., Lundback, T., Agalo, F., Konda, V., Jensen, A. J., et al. (2020). Synthesis, Evaluation and Proposed Binding Pose of Substituted Spiro-Oxindole Dihydroquinazolinones as IRAP Inhibitors. *ChemistryOpen* 9, 325–337. doi: 10.1002/open.201900344
- Evnochidou, I., Chappert, P., Benadda, S., Zucchetti, A., Weimershaus, M., Bens, M., et al. (2020). IRAP-dependent endosomal T cell receptor signalling is essential for T cell responses. *Nat. Commun.* 11, 2779. doi: 10.1038/s41467-020-16471-7
- Fernando, R. N., Larm, J., Albiston, A. L., and Chai, S. Y. (2005). Distribution and cellular localization of insulin-regulated aminopeptidase in the rat central nervous system. *J. Comp. Neurol.* 487, 372–390. doi: 10.1002/cne.20585
- Gaspari, T., Lee, H. W., Fan, K., Salimova, E., Spizzo, I., Samuel, C., et al. (2018a). A9871 Insulin regulated aminopeptidase (irap) inhibition completely reverses age-induced cardiac fibrosis and improves cardiac function. *J. Hypertens.* 36, e57. doi: 10.1097/01.hjh.0000548219.38141.63
- Gaspari, T., Shen, M., Wang, Y., Shastri, A., Chai, S. Y., Samuel, C., et al. (2018b). A9684 Comparing anti-fibrotic effects of the irap inhibitor, hfi-419 to an angiotensin receptor blocker and ace inhibitor in a high salt-induced mouse model of kidney disease. *J. Hypertens.* 36, e56–e57. doi: 10.1097/01.hjh.0000548218.38141.2a
- Georgiadis, D., and Dive, V. (2015). Phosphinic Peptides as Potent Inhibitors of Zinc-Metalloproteases. *Top. Curr. Chem.* 360, 1–38. doi: 10.1007/128\_2014\_571
- Giasas, P., Neu, M., Rowland, P., and Stratikos, E. (2019). High-Resolution Crystal Structure of Endoplasmic Reticulum Aminopeptidase 1 with Bound Phosphinic Transition-State Analogue Inhibitor. *ACS Med. Chem. Lett.* 10, 708–713. doi: 10.1021/acsmchemlett.9b00002
- Gulpinar, M. A., and Yegen, B. C. (2004). The Physiology of Learning and Memory: Role of Peptides and Stress. *Curr. Protein Pept. Sci.* 5, 457–473. doi: 10.2174/1389203043379341
- Hermans, S. J., Ascher, D. B., Hancock, N. C., Holien, J. K., Michell, B. J., Chai, S. Y., et al. (2015). Crystal structure of human insulin-regulated aminopeptidase with specificity for cyclic peptides. *Protein Sci.* 24, 190–199. doi: 10.1002/pro.2604
- Keller, S. R., Scott, H. M., Mastick, C. C., Aebersold, R., and Lienhard, G. E. (1995). Cloning and Characterization of a Novel Insulin-regulated Membrane Aminopeptidase from Glut4 Vesicles. *J. Biol. Chem.* 270, 23612–23618. doi: 10.1074/jbc.270.40.23612
- Kokkala, P., Mpakali, A., Mauvais, F. X., Papakyriakou, A., Daskalaki, I., Petropoulou, I., et al. (2016). Optimization and Structure-Activity Relationships of Phosphinic Pseudotripeptide Inhibitors of Aminopeptidases

- That Generate Antigenic Peptides. *J. Med. Chem.* 59, 9107–9123. doi: 10.1021/acs.jmedchem.6b01031
- Krishnan, R., Hanesworth, J. M., Wright, J. W., and Harding, J. W. (1999). Structure-binding studies of the adrenal AT4 receptor: analysis of position two- and three-modified angiotensin IV analogs. *Peptides* 20, 915–920. doi: 10.1016/S0196-9781(99)00081-9
- Laustsen, P. G., Rasmussen, T. E., Petersen, K., Pedraza-Diaz, S., Moestrup, S. K., Gliemann, J., et al. (1997). The complete amino acid sequence of human placental oxytocinase. The sequences have been submitted to the Genbank database with the accession codes: u62768 and u62769.1. *Biochim. Biophys. Acta Gene Struct. Expression* 1352, 1–7. doi: 10.1016/S0167-4781(97)00036-5
- Lee, J., Mustafa, T., McDowall, S. G., Mendelsohn, F. A., Brennan, M., Lew, R. A., et al. (2003). Structure-activity study of LVV-hemorphin-7: angiotensin AT4 receptor ligand and inhibitor of insulin-regulated aminopeptidase. *J. Pharmacol. Exp. Ther.* 305, 205–211. doi: 10.1124/jpet.102.045492
- Lew, R. A., Mustafa, T., Ye, S., McDowall, S. G., Chai, S. Y., and Albiston, A. L. (2003). Angiotensin AT4 ligands are potent, competitive inhibitors of insulin regulated aminopeptidase (IRAP). *J. Neurochem.* 86, 344–350. doi: 10.1046/j.1471-4159.2003.01852.x
- Lukaszkuk, A., Demaegd, H., Szemenyei, E., Toth, G., Tymecka, D., Misicka, A., et al. (2008). Beta-homo-amino acid scan of angiotensin IV. *J. Med. Chem.* 51, 2291–2296. doi: 10.1021/jm701490g
- Lukaszkuk, A., Demaegd, H., Feytens, D., Vanderheyden, P., Vauquelin, G., and Tourwé, D. (2009). The Replacement of His(4) in Angiotensin IV by Conformationally Constrained Residues Provides Highly Potent and Selective Analogues. *J. Med. Chem.* 52, 5612–5618. doi: 10.1021/jm900651p
- Lukaszkuk, A., Demaegd, H., Van Den Eynde, I., Vanderheyden, P., Vauquelin, G., and Tourwé, D. (2011). Conformational constraints in angiotensin IV to probe the role of Tyr2, Pro5 and Phe6. *J. Pept. Sci.* 17, 545–553. doi: 10.1002/psc.1365
- Mountford, S. J., Albiston, A. L., Charman, W. N., Ng, L., Holien, J. K., Parker, M. W., et al. (2014). Synthesis, structure-activity relationships and brain uptake of a novel series of benzopyran inhibitors of insulin-regulated aminopeptidase. *J. Med. Chem.* 57, 1368–1377. doi: 10.1021/jm401540f
- Mpakali, A., Saridakis, E., Harlos, K., Zhao, Y., Papakyriakou, A., Kokkala, P., et al. (2015). Crystal Structure of Insulin-Regulated Aminopeptidase with Bound Substrate Analogue Provides Insight on Antigenic Epitope Precursor Recognition and Processing. *J. Immunol.* 195, 2842. doi: 10.4049/jimmunol.1501103
- Mpakali, A., Giastas, P., Deprez-Poulain, R., Papakyriakou, A., Koumantou, D., Gealageas, R., et al. (2017a). Crystal Structures of ERAP2 Complexed with Inhibitors Reveal Pharmacophore Requirements for Optimizing Inhibitor Potency. *ACS Med. Chem. Lett.* 8, 333–337. doi: 10.1021/acsmchemlett.6b00505
- Mpakali, A., Saridakis, E., Harlos, K., Zhao, Y., Kokkala, P., Georgiadis, D., et al. (2017b). Ligand-Induced Conformational Change of Insulin-Regulated Aminopeptidase: Insights on Catalytic Mechanism and Active Site Plasticity. *J. Med. Chem.* 60, 2963–2972. doi: 10.1021/acs.jmedchem.6b01890
- Mpakali, A., Saridakis, E., Giastas, P., Maben, Z., Stern, L. J., Larhed, M., et al. (2020). Structural Basis of Inhibition of Insulin-Regulated Aminopeptidase by a Macrocyclic Peptidic Inhibitor. *ACS Med. Chem. Lett.* 11, 1429–1434. doi: 10.1021/acsmchemlett.0c00172
- Mucha, A., Drag, M., Dalton, J. P., and Kafarski, P. (2010). Metallo-aminopeptidase inhibitors. *Biochimie* 92, 1509–1529. doi: 10.1016/j.biochi.2010.04.026
- Nikolaou, A., Van Den Eynde, I., Tourwé, D., Vauquelin, G., Toth, G., Mallareddy, J. R., et al. (2013). [3H]IVDE77, a novel radioligand with high affinity and selectivity for the insulin-regulated aminopeptidase. *Eur. J. Pharmacol.* 702, 93–102. doi: 10.1016/j.ejphar.2013.01.026
- Nomura, S., Tsujimoto, M., and Mizutani, S. (2013). “Chapter 84 - Cystinyl Aminopeptidase/Oxytocinase,” in *Handbook of Proteolytic Enzymes (Third Edition)*. Eds. N. D. Rawlings and G. Salvesen (USA: Academic Press), 419–425. doi: 10.1016/B978-0-12-382219-2.00084-3
- Papakyriakou, A., Zervoudi, E., Theodorakis, E. A., Saveanu, L., Stratikos, E., and Vourloumis, D. (2013). Novel selective inhibitors of aminopeptidases that generate antigenic peptides. *Bioorg. Med. Chem. Lett.* 23, 4832–4836. doi: 10.1016/j.bmcl.2013.07.024
- Papakyriakou, A., Zervoudi, E., Tsoukalidou, S., Mauvais, F. X., Sfyroera, G., Mastellos, D. C., et al. (2015). 3,4-diaminobenzoic acid derivatives as inhibitors of the oxytocinase subfamily of M1 aminopeptidases with immune-regulating properties. *J. Med. Chem.* 58, 1524–1543. doi: 10.1021/jm501867s
- Rimmele, U., Hediger, K., Heinrichs, M., and Klaver, P. (2009). Oxytocin Makes a Face in Memory Familiar. *J. Neurosci.* 29, 38–42. doi: 10.1523/jneurosci.4260-08.2009
- Rogi, T., Tsujimoto, M., Nakazato, H., Mizutani, S., and Tomoda, Y. (1996). Human Placental Leucine Aminopeptidase/Oxytocinase: A NEW MEMBER OF TYPE II MEMBRANE-SPANNING ZINC METALLOPEPTIDASE FAMILY. *J. Biol. Chem.* 271, 56–61. doi: 10.1074/jbc.271.1.56
- Sardinia, M. F., Hanesworth, J. M., Krebs, L. T., and Harding, J. W. (1993). AT4 receptor binding characteristics: d-Amino acid- and glycine-substituted peptides. *Peptides* 14, 949–954. doi: 10.1016/0196-9781(93)90071-N
- Sardinia, M. F., Hanesworth, J. M., Krishnan, F., and Harding, J. W. (1994). AT4 receptor structure-binding relationship: N-terminal-modified angiotensin IV analogues. *Peptides* 15, 1399–1406. doi: 10.1016/0196-9781(94)90115-5
- Saveanu, L., and Van Endert, P. (2012). The role of insulin-regulated aminopeptidase in MHC class I antigen presentation. *Front. Immunol.* 3:57. doi: 10.3389/fimmu.2012.00057
- Saveanu, L., Carroll, O., Weimershaus, M., Guernonprez, P., Firat, E., Lindo, V., et al. (2009). IRAP identifies an endosomal compartment required for MHC class I cross-presentation. *Science* 325, 213–217. doi: 10.1126/science.1172845
- Seyer, B., Diwakarla, S., Burns, P., Hallberg, A., Grönbladh, A., Hallberg, M., et al. (2019). Insulin-regulated aminopeptidase inhibitor-mediated increases in dendritic spine density are facilitated by glucose uptake. *J. Neurochem.* 153, 485–494. doi: 10.1111/jnc.14745
- Tsoukalidou, S., Kakou, M., Mavridis, I., Koumantou, D., Calderone, V., Fragai, M., et al. (2019). Exploration of zinc-binding groups for the design of inhibitors for the oxytocinase subfamily of M1 aminopeptidases. *Bioorg. Med. Chem.* 27:115177. doi: 10.1016/j.bmc.2019.115177
- Vanga, S. R., Savmarker, J., Ng, L., Larhed, M., Hallberg, M., Aqvist, J., et al. (2018). Structural Basis of Inhibition of Human Insulin-Regulated Aminopeptidase (IRAP) by Aryl Sulfonamides. *ACS Omega* 3, 4509–4521. doi: 10.1021/acsomega.8b00595
- Wallis, M. G., Lankford, M. F., and Keller, S. R. (2007). Vasopressin is a physiological substrate for the insulin-regulated aminopeptidase IRAP. *Am. J. Physiol. Endocrinol. Metab.* 293, E1092–E1102. doi: 10.1152/ajpendo.00440.2007
- Zervoudi, E., Saridakis, E., Birtley, J. R., Seregín, S. S., Reeves, E., Kokkala, P., et al. (2013). Rationally designed inhibitor targeting antigen-trimming aminopeptidases enhances antigen presentation and cytotoxic T-cell responses. *Proc. Natl. Acad. Sci. U. S. A.* 110, 19890–19895. doi: 10.1073/pnas.1309781110

**Conflict of Interest:** The authors declare that the research was conducted in the absence of any commercial or financial relationships that could be construed as a potential conflict of interest.

Copyright © 2020 Georgiadis, Ziotopoulou, Kaloumenou, Lelis and Papasava. This is an open-access article distributed under the terms of the Creative Commons Attribution License (CC BY). The use, distribution or reproduction in other forums is permitted, provided the original author(s) and the copyright owner(s) are credited and that the original publication in this journal is cited, in accordance with accepted academic practice. No use, distribution or reproduction is permitted which does not comply with these terms.





# IRAP Inhibitors: M1-Aminopeptidase Family Inspiration

Nicholas Barlow and Philip E. Thompson\*

Medicinal Chemistry, Monash Institute of Pharmaceutical Sciences, Monash University, Parkville, VIC, Australia

The insulin regulated aminopeptidase (IRAP) has been proposed as an important therapeutic target for indications including Alzheimer's disease and immune disorders. To date, a number of IRAP inhibitor designs have been investigated but the total number of molecules investigated remains quite small. As a member the M1 aminopeptidase family, IRAP shares numerous structural features with the other M1 aminopeptidases. The study of those enzymes and the development of inhibitors provide key learnings and new approaches and are potential sources of inspiration for future IRAP inhibitors.

**Keywords:** insulin regulated aminopeptidase, aminopeptidase, enzyme inhibitor design, transition state analog, small molecule inhibitor, peptidomimetic

## OPEN ACCESS

### Edited by:

Hugo Gutiérrez De Teran,  
Uppsala University, Sweden

### Reviewed by:

Claudiana Lameu,  
University of São Paulo, Brazil  
Mats Lars-Erik Larhed,  
Uppsala University, Sweden

### \*Correspondence:

Philip E. Thompson  
philip.thompson@monash.edu

### Specialty section:

This article was submitted to  
Experimental Pharmacology  
and Drug Discovery,  
a section of the journal  
Frontiers in Pharmacology

**Received:** 22 July 2020

**Accepted:** 04 September 2020

**Published:** 25 September 2020

### Citation:

Barlow N and Thompson PE (2020)  
IRAP Inhibitors: M1-Aminopeptidase  
Family Inspiration.  
Front. Pharmacol. 11:585930.  
doi: 10.3389/fphar.2020.585930

## INTRODUCTION

The insulin regulated aminopeptidase (IRAP) is a zinc-dependent M1 aminopeptidase and a type II transmembrane protein with a cytoplasmic N-terminal domain and an extracellular/intra-endosomal C-terminal domain containing the catalytic zinc domain (Keller et al., 1995; Keller et al., 2002). IRAP is found in almost all human tissues (Keller et al., 1995; Tsujimoto and Hattori, 2005) and is known to be expressed in a range of neuronal cells (Fernando et al., 2005), placental cells (Nomura et al., 2005), and leukocytes (Saveanu et al., 2009). IRAP appears to play three distinct physiological roles. Firstly, IRAP degrades a number of extracellular signaling peptides through the removal of the N-terminal amino acid. Proposed substrates include oxytocin, vasopressin, angiotensin III, Met-enkephalin, dynorphin A, neurokinin A, neuromedin B, somatostatin, and CCK-8 (Rogi et al., 1996; Herbst et al., 1997; Matsumoto et al., 2001; Lew et al., 2003; Tsujimoto and Hattori, 2005), although the physiological relevance of these remains controversial. Secondly, IRAP participates in MHC class I antigen presentation through amino terminal trimming of exogenous cross-presenting peptides (Saveanu et al., 2009; Saveanu and van Endert, 2012). Thirdly, IRAP is co-located with Glut4 in insulin-responsive membrane vesicles and is thought to play a role in the insulin-induced translocation of these vesicles to the plasma membrane thus regulating cellular glucose uptake (Waters et al., 1997; Bryant et al., 2002; Pan et al., 2019). Interestingly, genetic deletion of IRAP in mice has not been associated with any major health defects, but rather provides protection against damage due to cerebral ischemia (Pham et al., 2012), thrombosis (Numaguchi et al., 2009; Gaspari et al., 2018) in models of those respective injuries, as well as diet-induced obesity (Niwa et al., 2015).

Commensurate with this pleiotropic character, IRAP is a potential therapeutic target for a range of therapeutic applications. In particular, IRAP is a potential therapeutic target for the treatment of Alzheimer's disease and other cognitive impairments. Rodents treated with the IRAP inhibitors such as Angiotensin IV (AngIV, 1) (**Figure 1**) *via* intracranial injection or subcutaneous administration, show improved performance in learning and memory (Wright et al., 1999;

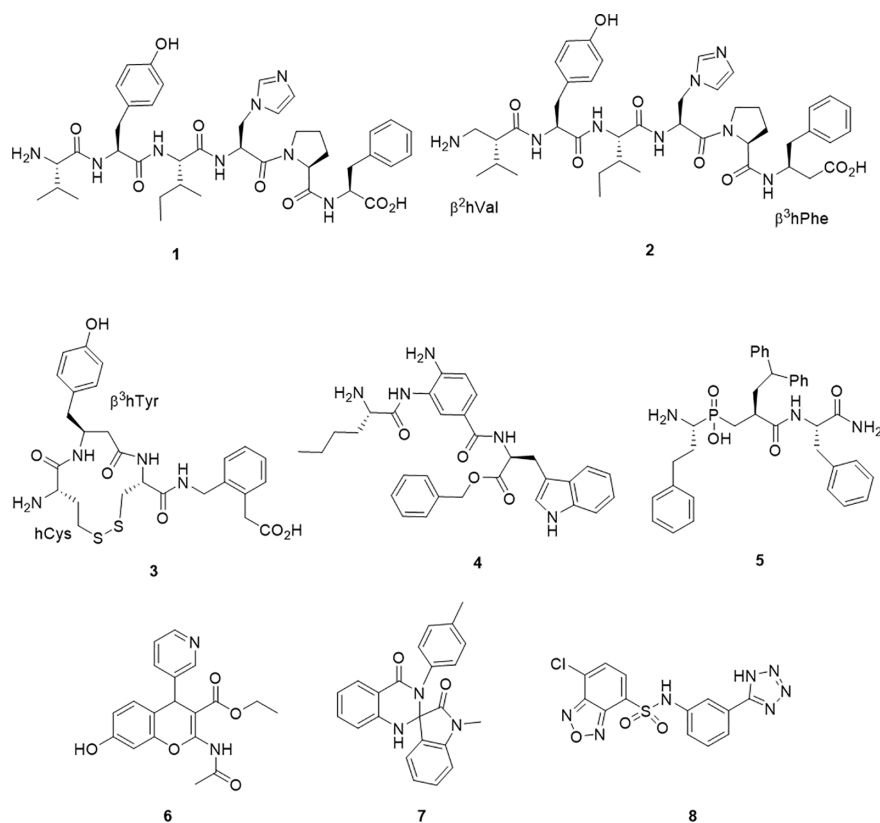


**FIGURE 1** | Chemical structures of IRAP inhibitors.

Albiston et al., 2001; Pederson et al., 2001; Lee et al., 2004; Gard, 2008; Golding et al., 2010). The cellular mechanism for this increased learning is unclear and may be attributable to modulation of glucose uptake *via* GLUT4 containing vesicles or reduced degradation of oxytocin and vasopressin, which have both been shown to improve learning and memory (Vanderheyden, 2009; Fidalgo et al., 2019). A second emerging therapeutic application is the potential of IRAP inhibitors to protect against stroke, thrombosis, and obesity-related disorders in comparable fashion to the knockout phenotypes. A third therapeutic potential for IRAP inhibitors is drawn from their role in preparing peptides for cross-presentation. Disruption of this function by inhibitors has been demonstrated *in vitro* and underscores their potential application in cancer immunotherapy or control of autoimmunity (Stratikos, 2014; Papakyriakou et al., 2015; Kokkala et al., 2016). Together, this pool of research suggests that there may be a number of indications for IRAP inhibitors.

## A QUICK SNAPSHOT OF IRAP INHIBITOR DEVELOPMENT

The search for inhibitors of IRAP dates back to its discovery as oxytocinase in 1959 (Hooper, 1959). In this first study of serum

aminopeptidase activity from human placenta,  $\text{Cu}^{2+}$ , diisopropylphosphorofluoridate (DFP), tetraethylpyrophosphate (TEPP), and ethylenediamine tetra acetic acid (EDTA) were shown to block the enzyme activity, signaling the metalloprotease nature of the enzyme. The first attempts to block this with competing ligands is described soon after using modified oxytocin peptides (Berankova et al., 1960; Berankova and Sorm, 1961). However, further progress appears to have been hampered by the challenges of the complex protease mixtures, including other M1 family members, in the tissue sources being studied.

A major step forward was the identification of the hexapeptide, AngIV, 1 (1) as an IRAP inhibitor. The memory enhancing effects of Ang IV administration and as well as its inhibitory effect on oxytocin metabolism were both reported and investigated separately prior to the appreciation that these effects were modulated through the action of a single target – IRAP (Braszko et al., 1988; Albiston et al., 2001). Ang IV is a component of the renin-angiotensin system as a degradation product from the proteolytic truncation of the vasoconstricting peptide, angiotensin II. With good affinity but poor plasma stability, successful structural modifications of 1 have led to the  $\beta$ -amino acid containing peptide mimetic 2 ( $K_i = 27$  nM), which contains both N and C terminal  $\beta$ -amino acids and is less susceptible to degradation by IRAP (Lukaszuk et al., 2008) and the analogue IVDE77 (Nikolaou et al., 2013). In an alternate but

comparable peptidomimetic approach, cyclic compounds, HA-08, 3 ( $K_i = 3.3$  nM) and analogs were developed (Andersson et al., 2010). The design of these compounds had in mind IRAP's unique ability to process cyclic peptides like oxytocin and vasopressin as part of the design. HA-08 was recently co-crystallised with IRAP (Mpakali et al., 2020), and a considerable body of SAR data pertaining to the cyclic structure has been accumulated (Andersson et al., 2011; Barlow et al., 2020).

Other IRAP inhibitors have been developed from investigations into the S1 subsite using fluorogenic substrates. Non-natural amino acids such as homoPhe and Nle were identified as S1 residues that conferred some substrate selectivity over other M1 aminopeptidases, ERAP1 and ERAP2 (Zervoudi et al., 2011). The selectivity of these probes inspired the development of the aminobenzamide inhibitor 4, which has good potency ( $IC_{50} = 110$  nM) and selectivity against ERAP1 and ERAP2 (Papakyriakou et al., 2015). Transition state mimetics which build on the growing understanding of P1 and P1' SAR have also been effective. In particular, a number of phosphinic acids including 5 have exhibited good potency ( $K_d = 18$  nM) (Kokkala et al., 2016). Compound 5 was also the first inhibitor to be co-crystallised in complex with IRAP (Mpakali et al., 2017a).

The first the small molecule inhibitor series to be described were benzopyrans discovered by a virtual screening approach, including HFI-419, 6 (Albiston et al., 2008; Mountford et al., 2014). This molecule also displays good potency ( $K_i = 0.48$   $\mu$ M). More recently, high throughput screening approaches have led to the discovery of 7 ( $IC_{50} = 6.1$   $\mu$ M) and 8 ( $IC_{50} = 0.4$   $\mu$ M) (Engen et al., 2016; Vanga et al., 2018).

While this represents a diverse series of compounds that have played their roles in defining the pharmacology of IRAP inhibitors, none have emerged as *bone fide* drug candidates as yet. In part, the challenges of delivery to the CNS for indications such as Alzheimer's disease have hampered the progression of peptide-like molecules and have also proved challenging for small molecules. Similarly, for immunological antigen processing, intracellular delivery will be a requirement. Advancing these, or future series of IRAP inhibitors, will therefore require close attention to the specific requirements related to each indication.

## INSPIRATIONAL INHIBITORS WITHIN THE M1 AMINOPEPTIDASE FAMILY

The human M1 aminopeptidase family, which includes IRAP, contains 12 members (Table 1) (Rawlings et al., 2014). All members utilize a single catalytic zinc atom in a conserved HExxHx18E motif and contain a substrate binding domain comprised of a conserved GxMEN motif. Structural similarities between M1 aminopeptidases result in a number of common substrates that are degraded by more than one family member. Indeed, the N-terminal specificity of M1 aminopeptidases is known to be broad and overlapping, and inhibitors are usually required to engage several subsites in order to achieve selectivity (Rawlings and Barrett, 2013).

The collected crystallographic data (Table 1) supports the common structural features of the M1 family as well as various archetypes that distinguish them. A conserved tyrosine residue typically binds the distal C-terminal, and interdomain movement may allow binding of diverse substrates (Cadel et al., 2015; Drinkwater et al., 2017). In particular, both closed and open conformations of the catalytic domains are observed. A dynamic model has been proposed whereby the domains II and IV close around extended substrates to support binding and hydrolysis (Mpakali et al., 2020). This mode of binding may be mimicked by inhibitors, but the dynamic nature provides a challenge to structure-based inhibitor design.

Other members of the M1 aminopeptidase family have also been identified as targets for therapy, most notably APN, APA, LTA4H, and ERAP1. Given the similarities of the family members, it seems that the study of other inhibitor designs within the M1 aminopeptidase family may provide interesting insights into inhibition mechanisms that are pertinent for inhibitor design and could be exploited to provide new IRAP inhibitors.

## ISOFORM HOPPING—ENDOPLASMIC RETICULUM AMINOPEPTIDASE 1

As alluded to above, inhibitors of one aminopeptidase class can be expected to inhibit other classes. In a pessimistic sense, this

TABLE 1 | M1 aminopeptidases.

M1 Aminopeptidases	Abbreviation	S1 substrates	Publications*	X-ray structures <sup>#</sup>
Insulin Regulated Aminopeptidase	IRAP	C, L, K, R, M	170	5MJ6 (Mpakali et al., 2017a), 4PJ6 (Hermans et al., 2015)
Aminopeptidase N	APN	A, F, Y, L, P	1700	4FYS (Wong et al., 2012), 6BV3 (Joshi et al., 2017)
Aminopeptidase A	APA	E, D	515	4KXB (Yang et al., 2013)
Leukotriene A <sub>4</sub> Hydrolase	LA4H	A, R, L	486	6ENB (Numao et al., 2017), 605H (Lee K. H. et al., 2019)
Thyrotropin-releasing hormone-degrading ectoenzyme	TRHDE	pGlu	9	
Puromycin-sensitive aminopeptidase	PSA	A, L, K	109	
Arginyl aminopeptidase N	APB	R, K	111	
Endoplasmic reticulum aminopeptidase 1	ERAP1	L, M, C, F	128	6T6R (Liddle et al., 2020), 6RYF (Giastas et al., 2019)
Endoplasmic reticulum aminopeptidase 2	ERAP2	R, K, M	31	5K1V (Mpakali et al., 2017b)
Arginyl aminopeptidase like 1	RNPL1	A, L, S, L, M	20	
Aminopeptidase Q	APQ	L, R, K, M	13	
Aminopeptidase O	APO	R, N	4	

\*Publications in PubMed that contain the M1 aminopeptidases name in the title, abstract or text.

<sup>#</sup>Recent examples of crystal structures deposited in the Protein Data Bank (PDB).



characterizes the challenge of achieving selectivity, while in a positive sense, redesigns can be used to tune selectivity between family members without major changes to the core molecular scaffold. This selectivity transitioning often manifests within derivative libraries. For example, Zervoudi et al. identified the phosphinic acid inhibitors DG002 (9) and DG013 (10) to target antigenic processing enzymes, ERAP1, ERAP2, and IRAP (**Figure 2**) (Zervoudi et al., 2013). These compounds and, in particular, the *R,S,S*-diastereomer, DG013A, showed good potency across the three isoforms. The same team showed replacement of the central leucine yielded the IRAP selective compound 5 (DG026A) (Mpakali et al., 2017a).

Note that phosphinic acids have an even broader general history. As far back as 1989, such compounds were described as

transition state analogs for metalloproteases (Grobelny et al., 1989; Yiotakis et al., 1994) and are represented in the M-17 Leucine amino peptidase inhibitors described in 2003 by Grembecka et al. (2003). The broader activity and/or selectivity of these ligands needs to be considered (Talma et al., 2019). It is an interesting feature that these peptidomimetic transition state analogs possess intracellular activity also (Koumantou et al., 2019).

## SUCCESS IS HARD TO ACHIEVE—AMINOPEPTIDASE N

As the archetype of the M1-aminopeptidase family, APN has been much studied and numerous attempts to develop inhibitors

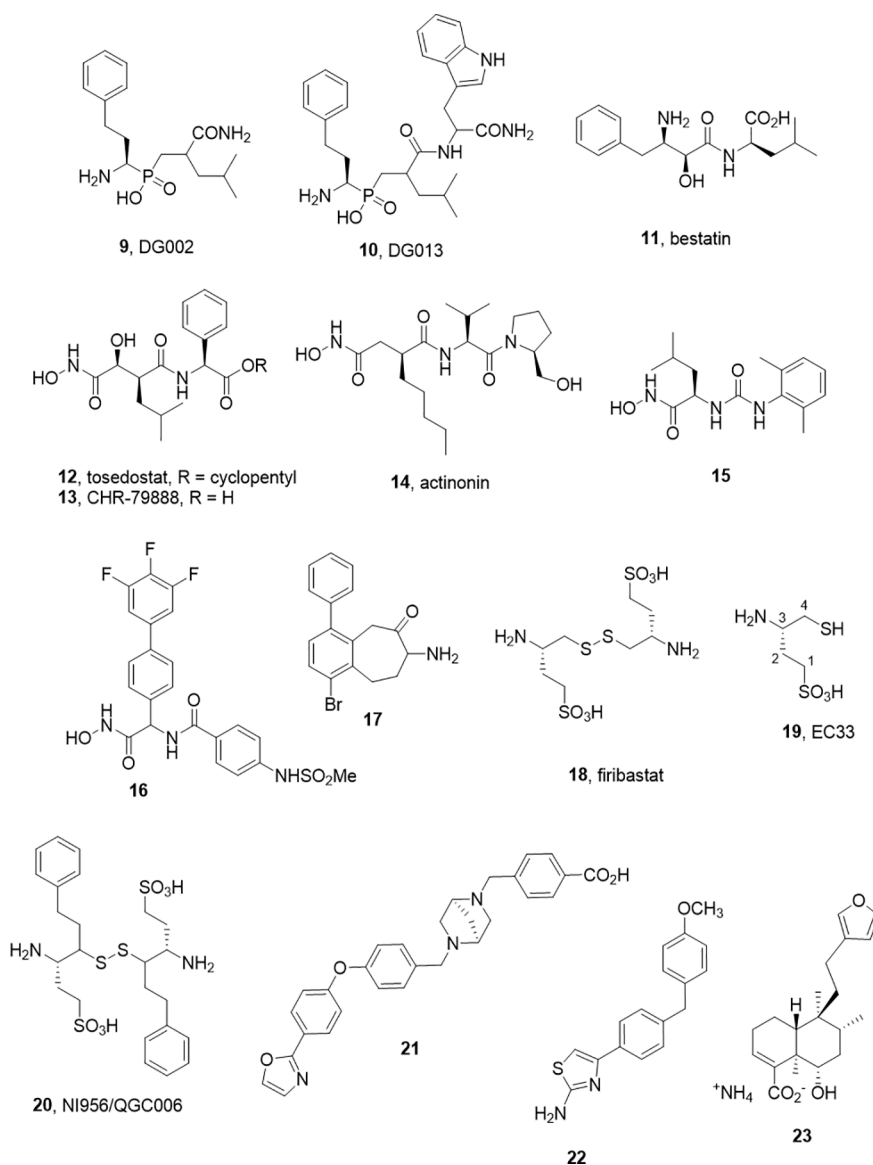


**FIGURE 2** | M1 aminopeptidase inhibitors from other families.

have been described. These have been extensively reviewed recently by Amin et al. (2018). As a protein, APN shares some features also characteristic of IRAP. They include the facts that APN is recognized to be involved in multiple functions (enzyme for peptide cleavage, and signalling molecule in signal transduction), it exhibits broad substrate specificity (although distinct from IRAP) and that it has been shown by crystallography to exist in an open and closed form (Joshi et al., 2017). It has been by far the most studied with respect to inhibitor development, although the results of those efforts are yet to yield an unambiguous drug candidate.

While a large body of work has accumulated in the development of APN inhibitors, the best known examples that have advanced to clinical studies, bestatin (11) and tosedostat (12), are potent but non-selective. Bestatin, bearing the pharmacophoric  $\beta$ -amino  $\alpha$ -hydroxy amide motif was discovered as a natural product inhibitor. Tosedostat, is a synthetic product but shares the hydroxamic acid motif of the natural product actinonin (14) (Figure 2). While both bestatin and tosedostat's acid metabolite, CHR-79888 (13), show good APN inhibition ( $IC_{50} \sim 200$ nM), the activity *in vivo* is not thought to derive simply from APN inhibition. Indeed, CHR-79888 is a potent LTA4 hydrolase inhibitor. A useful lesson to note regarding metabolism is that the circulating bioactive may have a much-altered selectivity profile compared to the administered drug.

Otherwise, these two compounds signal the generalised challenges of developing selective small aminopeptidase inhibitors. For active site binding aminopeptidases, the likely pharmacophore is built around S1 and S1' binding and non-scissile interactions with the catalytic zinc atom. The compounds that achieve this typically will not be impeded from comparable interactions in other zinc metallopeptidase sites, rendering them non-selective. In developing substrate mimetic inhibitors the ongoing challenge has been to tune down the generic zinc binding moiety (which can drive affinity) to exploit the subsite differences of across the metalloprotease families (Tsoukalidou et al., 2019).

The challenges associated with peptide-based analogs can imply replacement of backbone peptide bonds and the use of non-proteinogenic side chain motifs to enhance selectivity. For the former, the replacement of peptide bonds with ureido equivalents in the hydroxamic acid series led to some potent APN inhibitors such as 15. In the latter case, another series of hydroxamate based inhibitors exemplified by 16 ( $K_i$  4.5 nM) were described by Lee J. et al. (2019). These molecules have no obvious peptide character and may offer improved opportunity for achieving selectivity.

Another small molecule series of interest are aminobenzosuberones, which have been identified as a scaffold that selectively inhibits mono-metallic aminopeptidases with 17 showing sub-nanomolar affinity against human APN ( $K_i = 350$  pM) (Peng et al., 2017; Salomon et al., 2018). The origin of this series dates back to corresponding tetralones (Schalk et al., 1994) and the class appears to provide the advantages of small molecule inhibitors (low MW, potential oral availability, potentially BBB penetrating). Co-crystallization of a phenyl substituted

benzosuberone with *EcPepN* showed the binding poExxHx<sub>18</sub>E motifs with the ketone function present in an  $sp^3$  hydrated form, acting as transition state mimetic not dissimilar from the  $\beta$ -amino  $\alpha$ -hydroxy motif of bestatin (Peng et al., 2017). The implications for IRAP inhibitor design in this class are evident with one example showing strong inhibition of IRAP also ( $K_i = 34$  nM). One cautionary note is that these compounds, like many small molecules, are predicted to have challenging metabolism and toxicity profiles although this should be tested experimentally (Salomon et al., 2018).

## DESIGNING FOR SELECTIVITY AND IN VIVO ACTIVITY—AMINOPEPTIDASE A

In contrast, the development of the aminopeptidase A inhibitor, Firibastat (18) presents an optimistic picture of what is possible in the aminopeptidase class (Ferdinand et al., 2019). Firibastat has entered phase III clinical studies for therapy of treatment-resistant hypertension; yet at first view, it would seem an unlikely therapeutic. Firstly, the active species of Firibastat, (S)-3-amino-4-mercaptobutane-1-sulfonic acid (19, EC33) is a thiol. Thiols are known to be effective chelators of zinc and have been employed in a range of zinc enzyme inhibitors, most notably captopril. However, the capacity for numerous off-target chelating or covalent disulfide forming interactions would typically argue against pursuit of such compounds.

The discovery of Firibastat has a long history. Early work by Fournié-Zaluski et al. employed  $\beta$ -amino thiols as substrate mimetics targeting the S' subsite of APN (Fournie-Zaluski et al., 1992). An interesting comparison of zinc chelating groups within this report suggested that  $\beta$ -amino thiols are more effective inhibitors of APN than corresponding hydroxamic acid, phosphate, and carboxylate inhibitors. A compound from the series was found to have significant CNS activity when administered by iv injection as its disulfide prodrug form.

Turning their focus to APA, which cleaves N-terminal Glu or Asp residues and in particular cleaves the N-terminal Asp from angiotensin II, blocking angiotensin III formation. They found the acidic sulfonic acid derivative, EC33 was a potent and selective inhibitor (APA  $K_i = 0.37$   $\mu$ M, APN  $K_i = 25$   $\mu$ M) (Chauvel et al., 1994a; Chauvel et al., 1994b). Intracerebroventricular injection of EC33 was found to prevent APA production of the hypertensive agent angiotensin III, lowering central arterial blood pressure (Zini et al., 1996). By developing the corresponding disulfide prodrug 18, it has been possible to move to oral administration. The oral bioavailability is modest (10–15%), and the drug half-life is short (40 min) but with a somewhat heroic dose of 500 mg, twice daily Firibastat effectively reduced blood pressure in the cohort (Ferdinand et al., 2019). While these clinical studies continue, a second generation oral inhibitor NI956/QGC006 (20) with improved pharmaceutical properties is progressing (Keck et al., 2019).

## NON-CANONICAL BINDING SITE LIGANDS—LEUKOTRIENE A4 HYDROLASE

Leukotriene A<sub>4</sub> hydrolase has been another M1 aminopeptidase that has attracted attention as a potential therapeutic target, particularly in inflammatory disease. As suggested by its name, the best studied feature of the enzyme is not its ability to cleave N-terminal amino acids from substrate peptides, but rather to hydrolyse the epoxide ring of Leukotriene A<sub>4</sub> to Leukotriene B<sub>4</sub> (Haeggstrom et al., 2007). LTB<sub>4</sub> is an inflammatory lipid and thus blocking its formation would be considered a therapeutic option. However, the enzyme has also been shown to process a variety of peptides, most notably Pro-Gly-Pro a collagen degradation product which is a pro-inflammatory chemotactic peptide (Snelgrove et al., 2010). This implies that the action of LTA<sub>4</sub>H has opposing actions, which may be context dependent, and the opposing activities of LTA<sub>4</sub>H reside within distinct yet overlapping active sites, with specific amino acid residues required for each. Several inhibitors including Bestatin (11) and Tosedostat (12) have advanced to the clinics as well as Acebilustat (21) which is in phase 2 studies for treatment of cystic fibrosis (Bhatt et al., 2017). Clinical trial results to date have been disappointing which has led to the postulate that the inhibiting Pro-Gly-Pro degradation was countering the desired therapeutic effects. In response, the concept of biased inhibitors that spare the aminopeptidase activity has emerged including allosteric ligands (22) that activate Pro-Gly-Pro hydrolysis only (Lee K. H. et al., 2019) or those that block LTA<sub>4</sub> hydrolysis and activate Pro-Gly-Pro hydrolysis.

By analogy, Liddle et al. recently described an allosteric ligand for ERAP1 (23) that activates hydrolysis of small substrates (such as Leu-AMC) while inhibiting cleavage of longer substrates by competing with the extended peptide binding site such as the antigen precursor, YTAFTIPSI. It is postulated to achieve this by stabilizing the dynamics of active site residues and/or facilitating conformational change to a partially closed, more active conformation (Liddle et al., 2020).

The actual benefit of these concepts remains controversial, especially in the case of the Pro-Gly-Pro-sparing LTA<sub>4</sub>H inhibitors (Numao et al., 2017), but the dual activity raises

interesting questions for IRAP research. Firstly, have the full gamut of substrates for IRAP been examined? The physiologically relevant peptide substrates are still not confirmed for IRAP and it may also be that there are small peptides or other non-peptide substrates (e.g., lipids) that can be processed by this hydrolytic enzyme. Secondly, what signals might be associated with IRAP cleavage of peptide substrates? It could be the down-regulation of a bioactive substrate (such as vasopressin) or maybe the effects derive from the generation of a bioactive product.

## CONCLUSIONS

IRAP is emerging as a therapeutic target against a host of disease states. As well as long identified connection to indications such as cognition disorders due to the effects of AngIV, extended studies of gene deletion or modification are showing potential applications in stroke, thrombosis, and obesity-related disorders. The localization of IRAP in various tissues and cell types will also present other hypotheses proposing IRAP inhibitors as drug targets such as in immunotherapy and/or combatting autoimmunity.

As a member of the M1 aminopeptidase family, IRAP shares many structural and functional similarities with other family members that have been the subject of parallel drug discovery efforts. Much can be learned from these analogous drug discovery efforts that might be applied to IRAP inhibitor development and guide future drug discovery efforts. We have highlighted some of these efforts with in the M1 aminopeptidase family and outlined some of the success stories, insights, and interesting observations from these campaigns. We have also highlighted particular chemical scaffolds, which we feel may be adapted to serve IRAP focused drug discovery efforts. Hopefully, this information can foster progress in the development of candidate drugs that realize the therapeutic potential of IRAP inhibition.

## AUTHOR CONTRIBUTIONS

NB and PT contributed equally to the research and authorship of the manuscript.

## REFERENCES

- Albiston, A. L., McDowall, S. G., Matsacos, D., Sim, P., Clune, E., Mustafa, T., et al. (2001). Evidence that the angiotensin IV (AT(4)) receptor is the enzyme insulin-regulated aminopeptidase. *J. Biol. Chem.* 276, 48623–48626. doi: 10.1074/jbc.C100512200
- Albiston, A. L., Morton, C. J., Ng, H. L., Pham, V., Yeatman, H. R., Ye, S., et al. (2008). Identification and characterization of a new cognitive enhancer based on inhibition of insulin-regulated aminopeptidase. *FASEB J.* 22, 4209–4217. doi: 10.1096/fj.08-112227
- Amin, S. A., Adhikari, N., and Jha, T. (2018). Design of Aminopeptidase N Inhibitors as Anti-cancer Agents. *J. Med. Chem.* 61, 6468–6490. doi: 10.1021/acs.jmedchem.7b00782
- Andersson, H., Demaegdt, H., Vauquelin, G., Lindeberg, G., Karlen, A., Hallberg, M., et al. (2010). Disulfide cyclized tripeptide analogues of angiotensin IV as potent and selective inhibitors of insulin-regulated aminopeptidase (IRAP). *J. Med. Chem.* 53, 8059–8071. doi: 10.1021/jm100793t
- Andersson, H., Demaegdt, H., Johnsson, A., Vauquelin, G., Lindeberg, G., Hallberg, M., et al. (2011). Potent macrocyclic inhibitors of insulin-regulated aminopeptidase (IRAP) by olefin ring-closing metathesis. *J. Med. Chem.* 54, 3779–3792. doi: 10.1021/jm200036n
- Barlow, N., Vanga, S. R., Sävmarker, J., Sandström, A., Burns, P., Hallberg, A., et al. (2020). Macrocyclic peptidomimetics as inhibitors of insulin-regulated aminopeptidase (IRAP). *RSC Med. Chem.* 11, 234–244. doi: 10.1039/C9MD00485H
- Berankova, Z., and Sorm, F. (1961). Enzymic Inactivation of Oxytocin .3. Dethiooxytocin and S,S'-Dibenzylidihydroxytocin as Oxytocinase Inhibitors and Substrates. *Collect Czech Chem. C.* 26, 2557–2561. doi: 10.1135/cccc19612557
- Berankova, Z., Rychlik, I., and Sorm, F. (1960). Enzymic Inactivation of Oxytocin .1. Selective Inhibitors of Oxytocin Inactivation. *Collect Czech Chem. C.* 25, 2575–2580. doi: 10.1135/cccc19602575

- Bhatt, L., Roinestad, K., Van, T., and Springman, E. B. (2017). Recent advances in clinical development of leukotriene B<sub>4</sub> pathway drugs. *Semin. Immunol.* 33, 65–73. doi: 10.1016/j.smim.2017.08.007
- Braszkowski, J. J., Kupryszewski, G., Witczuk, B., and Wisniewski, K. (1988). Angiotensin II-(3–8)-hexapeptide affects motor activity, performance of passive avoidance and a conditioned avoidance response in rats. *Neuroscience* 27, 777–783. doi: 10.1016/0306-4522(88)90182-0
- Bryant, N. J., Govers, R., and James, D. E. (2002). Regulated transport of the glucose transporter GLUT4. *Nat. Rev. Mol. Cell Biol.* 3, 267–277. doi: 10.1038/nrm782
- Cadel, S., Darmon, C., Pernier, J., Herve, G., and Foulon, T. (2015). The M1 family of vertebrate aminopeptidases: role of evolutionarily conserved tyrosines in the enzymatic mechanism of aminopeptidase B. *Biochimie* 109, 67–77. doi: 10.1016/j.biochi.2014.12.009
- Chauvel, E. N., Coric, P., Llorens-Cortes, C., Wilk, S., Roques, B. P., and Fournie-Zaluski, M. C. (1994a). Investigation of the active site of aminopeptidase A using a series of new thiol-containing inhibitors. *J. Med. Chem.* 37, 1339–1346. doi: 10.1021/jm00035a014
- Chauvel, E. N., Llorens-Cortes, C., Coric, P., Wilk, S., Roques, B. P., and Fournie-Zaluski, M. C. (1994b). Differential inhibition of aminopeptidase A and aminopeptidase N by new beta-amino thiols. *J. Med. Chem.* 37, 2950–2957. doi: 10.1021/jm00044a016
- Drinkwater, N., Lee, J., Yang, W., Malcolm, T. R., and McGowan, S. (2017). M1 aminopeptidases as drug targets: broad applications or therapeutic niche? *FEBS J.* 284, 1473–1488. doi: 10.1111/febs.14009
- Engen, K., Rosenstrom, U., Axelsson, H., Konda, V., Dahllund, L., Otrocka, M., et al. (2016). Identification of Drug-Like Inhibitors of Insulin-Regulated Aminopeptidase Through Small-Molecule Screening. *Assay Drug Dev. Technol.* 14, 180–193. doi: 10.1089/adt.2016.708
- Ferdinand, K. C., Balavoine, F., Besse, B., Black, H. R., Desbrandes, S., Dittrich, H. C., et al. (2019). Efficacy and Safety of Firibastat, A First-in-Class Brain Aminopeptidase A Inhibitor, in Hypertensive Overweight Patients of Multiple Ethnic Origins. *Circulation* 140, 138–146. doi: 10.1161/CIRCULATIONAHA.119.040070
- Fernando, R. N., Larm, J., Albiston, A. L., and Chai, S. Y. (2005). Distribution and cellular localization of insulin-regulated aminopeptidase in the rat central nervous system. *J. Comp. Neurol.* 487, 372–390. doi: 10.1002/cne.20585
- Fidalgo, S., Patel, M., Quadir, A., Sadiq, W., and Gard, P. R. (2019). Decreased behavioural and neurochemical effects of angiotensin IV following prenatal alcohol exposure in the mouse. *Neuropeptides* 77, 101931. doi: 10.1016/j.npep.2019.05.002
- Fournie-Zaluski, M. C., Coric, P., Turcaud, S., Bruetsch, L., Lucas, E., Noble, F., et al. (1992). Potent and systemically active aminopeptidase N inhibitors designed from active-site investigation. *J. Med. Chem.* 35, 1259–1266. doi: 10.1021/jm00085a013
- Gard, P. R. (2008). Cognitive-enhancing effects of angiotensin IV. *BMC Neurosci.* 9 (Suppl 2), S15. doi: 10.1186/1471-2202-9-S2-S15
- Gaspari, T., Lee, H. W., Fan, K., Salimova, E., Spizzo, I., Samuel, C., et al. (2018). A9871 Insulin regulated aminopeptidase (irap) inhibition completely reverses age-induced cardiac fibrosis and improves cardiac function. *J. Hypertens.* 36, e57. doi: 10.1097/01.hjh.0000548219.38141.63
- Giastas, P., Neu, M., Rowland, P., and Stratikos, E. (2019). High-Resolution Crystal Structure of Endoplasmic Reticulum Aminopeptidase 1 with Bound Phosphinic Transition-State Analogue Inhibitor. *ACS Med. Chem. Lett.* 10, 708–713. doi: 10.1021/acsmedchemlett.9b00002
- Golding, B. J., Overall, A. D., Brown, G., and Gard, P. R. (2010). Strain differences in the effects of angiotensin IV on mouse cognition. *Eur. J. Pharmacol.* 641, 154–159. doi: 10.1016/j.ejphar.2010.05.041
- Grembecka, J., Mucha, A., Cierpicky, T., and Kafarski, P. (2003). The most potent organophosphorus inhibitors of leucine aminopeptidase. Structure-based design, chemistry, and activity. *J. Med. Chem.* 46, 2641–2655. doi: 10.1021/jm030795v
- Grobelyns, D., Goli, U. B., and Galarzy, R. E. (1989). Binding energetics of phosphorus-containing inhibitors of thermolysin. *Biochemistry* 28, 4948–4951. doi: 10.1021/bi00438a006
- Haegstrom, J. Z., Tholander, F., and Wetterholm, A. (2007). Structure and catalytic mechanisms of leukotriene A<sub>4</sub> hydrolase. *Prostaglandins Other Lipid Mediat.* 83, 198–202. doi: 10.1016/j.prostaglandins.2007.01.006
- Herbst, J. J., Ross, S. A., Scott, H. M., Bobin, S. A., Morris, N. J., Lienhard, G. E., et al. (1997). Insulin stimulates cell surface aminopeptidase activity toward vasopressin in adipocytes. *Am. J. Physiol.* 272, E600–E606. doi: 10.1152/ajpendo.1997.272.4.E600
- Hermans, S. J., Ascher, D. B., Hancock, N. C., Holien, J. K., Michell, B. J., Chai, S. Y., et al. (2015). Crystal structure of human insulin-regulated aminopeptidase with specificity for cyclic peptides. *Protein Sci.* 24, 190–199. doi: 10.1002/pro.2604
- Hooper, K. C. (1959). The action of inhibitors on enzymes from human placenta. *J. Physiol.* 148, 283–290. doi: 10.1113/jphysiol.1959.sp006288
- Joshi, S., Chen, L., Winter, M. B., Lin, Y. L., Yang, Y., Shapovalova, M., et al. (2017). The Rational Design of Therapeutic Peptides for Aminopeptidase N using a Substrate-Based Approach. *Sci. Rep.* 7, 1424. doi: 10.1038/s41598-017-01542-5
- Keck, M., De Almeida, H., Compere, D., Inguibert, N., Flahault, A., Balavoine, F., et al. (2019). N1956/QGC006, a Potent Orally Active, Brain-Penetrating Aminopeptidase A Inhibitor for Treating Hypertension. *Hypertension* 73, 1300–1307. doi: 10.1161/HYPERTENSIONAHA.118.12499
- Keller, S. R., Scott, H. M., Mastick, C. C., Aebersold, R., and Lienhard, G. E. (1995). Cloning and characterization of a novel insulin-regulated membrane aminopeptidase from Glut4 vesicles. *J. Biol. Chem.* 270, 23612–23618. doi: 10.1074/jbc.270.40.23612
- Keller, S. R., Davis, A. C., and Clairmont, K. B. (2002). Mice deficient in the insulin-regulated membrane aminopeptidase show substantial decreases in glucose transporter GLUT4 levels but maintain normal glucose homeostasis. *J. Biol. Chem.* 277, 17677–17686. doi: 10.1074/jbc.M202037200
- Kokkala, P., Mpakali, A., Mauvais, F. X., Papakyriakou, A., Daskalaki, I., Petropoulou, I., et al. (2016). Optimization and Structure-Activity Relationships of Phosphinic Pseudotriptide Inhibitors of Aminopeptidases That Generate Antigenic Peptides. *J. Med. Chem.* 59, 9107–9123. doi: 10.1021/acs.jmedchem.6b01031
- Koumantou, D., Barnea, E., Martin-Esteban, A., Maben, Z., Papakyriakou, A., Mpakali, A., et al. (2019). Editing the immunopeptidome of melanoma cells using a potent inhibitor of endoplasmic reticulum aminopeptidase 1 (ERAP1). *Cancer Immunol. Immunother.* 68, 1245–1261. doi: 10.1007/s00262-019-02358-0
- Lee, J., Albiston, A. L., Allen, A. M., Mendelsohn, F. A., Ping, S. E., Barrett, G. L., et al. (2004). Effect of I.C.V. injection of AT<sub>4</sub> receptor ligands, NLE1-angiotensin IV and LVV-hemorphin 7, on spatial learning in rats. *Neuroscience* 124, 341–349. doi: 10.1016/j.neuroscience.2003.12.006
- Lee, K. H., Petruncio, G., Shim, A., Burdick, M., Zhang, Z., Shim, Y. M., et al. (2019). Effect of Modifier Structure on the Activation of Leukotriene A<sub>4</sub> Hydrolase Aminopeptidase Activity. *J. Med. Chem.* 62, 10605–10616. doi: 10.1021/acs.jmedchem.9b00663
- Lee, J., Vinh, N. B., Drinkwater, N., Yang, W., Kannan Sivaraman, K., Schembri, L. S., et al. (2019). Novel Human Aminopeptidase N Inhibitors: Discovery and Optimization of Subsite Binding Interactions. *J. Med. Chem.* 62, 7185–7209. doi: 10.1021/acs.jmedchem.9b00757
- Lew, R. A., Mustafa, T., Ye, S., McDowall, S. G., Chai, S. Y., and Albiston, A. L. (2003). Angiotensin AT<sub>4</sub> ligands are potent, competitive inhibitors of insulin regulated aminopeptidase (IRAP). *J. Neurochem.* 86, 344–350. doi: 10.1046/j.1471-4159.2003.01852.x
- Liddle, J., Hutchinson, J. P., Kitchen, S., Rowland, P., Neu, M., Cecconie, T., et al. (2020). Targeting the Regulatory Site of ER Aminopeptidase 1 Leads to the Discovery of a Natural Product Modulator of Antigen Presentation. *J. Med. Chem.* 63, 3348–3358. doi: 10.1021/acs.jmedchem.9b02123
- Lukaszuk, A., Demaegd, H., Szemenyei, E., Toth, G., Tymek, D., Misicka, A., et al. (2008). Beta-homo-amino acid scan of angiotensin IV. *J. Med. Chem.* 51, 2291–2296. doi: 10.1021/jm701490g
- Matsumoto, H., Nagasaka, T., Hattori, A., Rogi, T., Tsuruoka, N., Mizutani, S., et al. (2001). Expression of placental leucine aminopeptidase/oxytocinase in neuronal cells and its action on neuronal peptides. *Eur. J. Biochem.* 268, 3259–3266. doi: 10.1046/j.1432-1327.2001.02221.x
- Mountford, S. J., Albiston, A. L., Charman, W. N., Ng, L., Holien, J. K., Parker, M. W., et al. (2014). Synthesis, structure-activity relationships and brain uptake of a novel series of benzopyran inhibitors of insulin-regulated aminopeptidase. *J. Med. Chem.* 57, 1368–1377. doi: 10.1021/jm401540f
- Mpakali, A., Saridakis, E., Harlos, K., Zhao, Y., Kokkala, P., Georgiadis, D., et al. (2017a). Ligand-Induced Conformational Change of Insulin-Regulated Aminopeptidase: Insights on Catalytic Mechanism and Active Site Plasticity. *J. Med. Chem.* 60, 2963–2972. doi: 10.1021/acs.jmedchem.6b01890
- Mpakali, A., Giastas, P., Deprez-Poulain, R., Papakyriakou, A., Koumantou, D., Gealageas, R., et al. (2017b). Crystal Structures of ERAP2 Complexed with



- Inhibitors Reveal Pharmacophore Requirements for Optimizing Inhibitor Potency. *ACS Med. Chem. Lett.* 8, 333–337. doi: 10.1021/acsmchemlett.6b00505
- Mpakali, A., Saridakis, E., Giasas, P., Maben, Z., Stern, L. J., Larhed, M., et al. (2020). Structural Basis of Inhibition of Insulin-Regulated Aminopeptidase by a Macrocyclic Peptidic Inhibitor. *ACS Med. Chem. Lett.* 11, 1429–1434. doi: 10.1021/acsmchemlett.0c00172
- Nikolaou, A., Van den Eynde, I., Tourwe, D., Vauquelin, G., Toth, G., Mallareddy, J. R., et al. (2013). [3H]IVDE77, a novel radioligand with high affinity and selectivity for the insulin-regulated aminopeptidase. *Eur. J. Pharmacol.* 702, 93–102. doi: 10.1016/j.ejphar.2013.01.026
- Niwa, M., Numaguchi, Y., Ishii, M., Kuwahata, T., Kondo, M., Shibata, R., et al. (2015). IRAP deficiency attenuates diet-induced obesity in mice through increased energy expenditure. *Biochem. Biophys. Res. Commun.* 457, 12–18. doi: 10.1016/j.bbrc.2014.12.071
- Nomura, S., Ito, T., Yamamoto, E., Sumigama, S., Iwase, A., Okada, M., et al. (2005). Gene regulation and physiological function of placental leucine aminopeptidase/oxytocinase during pregnancy. *Biochim. Biophys. Acta* 1751, 19–25. doi: 10.1016/j.bbapap.2005.04.006
- Numaguchi, Y., Ishii, M., Kubota, R., Morita, Y., Yamamoto, K., Matsushita, T., et al. (2009). Ablation of angiotensin IV receptor attenuates hypofibrinolysis via PAI-1 downregulation and reduces occlusive arterial thrombosis. *Arterioscler. Thromb. Vasc. Biol.* 29, 2102–2108. doi: 10.1161/ATVBAHA.109.195057
- Numao, S., Hasler, F., Laguerre, C., Srinivas, H., Wack, N., Jager, P., et al. (2017). Feasibility and physiological relevance of designing highly potent aminopeptidase-sparing leukotriene A4 hydrolase inhibitors. *Sci. Rep.* 7, 13591. doi: 10.1038/s41598-017-13490-1
- Pan, X., Meriin, A., Huang, G., and Kandror, K. V. (2019). Insulin-responsive amino peptidase follows the Glut4 pathway but is dispensable for the formation and translocation of insulin-responsive vesicles. *Mol. Biol. Cell* 30, 1536–1543. doi: 10.1091/mbc.E18-12-0792
- Papakyriakou, A., Zervoudi, E., Tsoukalidou, S., Mauvais, F. X., Sfyroera, G., Mastellos, D. C., et al. (2015). 3,4-diaminobenzoic acid derivatives as inhibitors of the oxytocinase subfamily of M1 aminopeptidases with immune-regulating properties. *J. Med. Chem.* 58, 1524–1543. doi: 10.1021/jm501867s
- Pederson, E. S., Krishnan, R., Harding, J. W., and Wright, J. W. (2001). A role for the angiotensin AT4 receptor subtype in overcoming scopolamine-induced spatial memory deficits. *Regul. Pept.* 102, 147–156. doi: 10.1016/S0167-0115(01)00312-3
- Peng, G., McEwen, A. G., Olieric, V., Schmitt, C., Albrecht, S., Cavarelli, J., et al. (2017). Insight into the remarkable affinity and selectivity of the aminobenzosuberone scaffold for the M1 aminopeptidases family based on structure analysis. *Proteins* 85, 1413–1421. doi: 10.1002/prot.25301
- Pham, V., Albiston, A. L., Downes, C. E., Wong, C. H., Diwakarla, S., Ng, L., et al. (2012). Insulin-regulated aminopeptidase deficiency provides protection against ischemic stroke in mice. *J. Neurotr.* 29, 1243–1248. doi: 10.1089/neu.2011.1824
- Rawlings, N. D., and Barrett, A. J. (2013). “Metallopeptidases and their clans,” in *Handbook of Proteolytic Enzymes*, vol. 1. Eds. N. D. Rawlings and G. S. Salvesen (New York, NY, USA: Academic Press), 325–370.
- Rawlings, N. D., Waller, M., Barrett, A. J., and Bateman, A. (2014). MEROPS: the database of proteolytic enzymes, their substrates and inhibitors. *Nucleic Acids Res.* 42, D503–D509. doi: 10.1093/nar/gkt953
- Rogi, T., Tsujimoto, M., Nakazato, H., Mizutani, S., and Tomoda, Y. (1996). Human placental leucine aminopeptidase/oxytocinase. A new member of type II membrane-spanning zinc metallopeptidase family. *J. Biol. Chem.* 271, 56–61. doi: 10.1074/jbc.271.1.56
- Salomon, E., Schmitt, M., Marapaka, A. K., Stamogiannos, A., Revelant, G., Schmitt, C., et al. (2018). Aminobenzosuberone Scaffold as a Modular Chemical Tool for the Inhibition of Therapeutically Relevant M1 Aminopeptidases. *Molecules* 23, 2607. doi: 10.3390/molecules23102607
- Saveanu, L., and van Endert, P. (2012). The role of insulin-regulated aminopeptidase in MHC class I antigen presentation. *Front. Immunol.* 3, 57. doi: 10.3389/fimmu.2012.00057
- Saveanu, L., Carroll, O., Weimershaus, M., Guernonprez, P., Firat, E., Lindo, V., et al. (2009). IRAP identifies an endosomal compartment required for MHC class I cross-presentation. *Science* 325, 213–217. doi: 10.1126/science.1172845
- Schalk, C., d'Orchymont, H., Jauch, M. F., and Tarnus, C. (1994). 3-Amino-2-tetralone derivatives: novel potent and selective inhibitors of aminopeptidase-M (EC 3.4.11.2). *Arch. Biochem. Biophys.* 311, 42–46. doi: 10.1006/abbi.1994.1206
- Snelgrove, R. J., Jackson, P. L., Hardison, M. T., Noerager, B. D., Kinloch, A., Gaggari, A., et al. (2010). A critical role for LTA4H in limiting chronic pulmonary neutrophilic inflammation. *Science* 330, 90–94. doi: 10.1126/science.1190594
- Stratikos, E. (2014). Regulating adaptive immune responses using small molecule modulators of aminopeptidases that process antigenic peptides. *Curr. Opin. Chem. Biol.* 23, 1–7. doi: 10.1016/j.cbpa.2014.08.007
- Talma, M., Maslanka, M., and Mucha, A. (2019). Recent developments in the synthesis and applications of phosphinic peptide analogs. *Bioorg. Med. Chem. Lett.* 29, 1031–1042. doi: 10.1016/j.bmc.2019.02.034
- Tsoukalidou, S., Kakou, M., Mavridis, I., Koumantou, D., Calderone, V., Fragai, M., et al. (2019). Exploration of zinc-binding groups for the design of inhibitors for the oxytocinase subfamily of M1 aminopeptidases. *Bioorg. Med. Chem.* 27, 115177. doi: 10.1016/j.bmc.2019.115177
- Tsujimoto, M., and Hattori, A. (2005). The oxytocinase subfamily of M1 aminopeptidases. *Biochim. Biophys. Acta* 1751, 9–18. doi: 10.1016/j.bbapap.2004.09.011
- Vanderheyden, P. M. (2009). From angiotensin IV binding site to AT4 receptor. *Mol. Cell Endocrinol.* 302, 159–166. doi: 10.1016/j.mce.2008.11.015
- Vanga, S. R., Savmarker, J., Ng, L., Larhed, M., Hallberg, M., Aqvist, J., et al. (2018). Structural Basis of Inhibition of Human Insulin-Regulated Aminopeptidase (IRAP) by Aryl Sulfonamides. *ACS Omega* 3, 4509–4521. doi: 10.1021/acsomega.8b00595
- Waters, S. B., D'Auria, M., Martin, S. S., Nguyen, C., Kozma, L. M., and Luskey, K. L. (1997). The amino terminus of insulin-responsive aminopeptidase causes Glut4 translocation in 3T3-L1 adipocytes. *J. Biol. Chem.* 272, 23323–23327. doi: 10.1074/jbc.272.37.23323
- Wong, A. H., Zhou, D., and Rini, J. M. (2012). The X-ray crystal structure of human aminopeptidase N reveals a novel dimer and the basis for peptide processing. *J. Biol. Chem.* 287, 36804–36813. doi: 10.1074/jbc.M112.398842
- Wright, J. W., Stubley, L., Pederson, E. S., Kramar, E. A., Hanesworth, J. M., and Harding, J. W. (1999). Contributions of the brain angiotensin IV-AT4 receptor subtype system to spatial learning. *J. Neurosci.* 19, 3952–3961. doi: 10.1523/JNEUROSCI.19-10-03952.1999
- Yang, Y., Liu, C., Lin, Y. L., and Li, F. (2013). Structural insights into central hypertension regulation by human aminopeptidase A. *J. Biol. Chem.* 288, 25638–25645. doi: 10.1074/jbc.M113.494955
- Yiotakis, A., Lecoq, A., Vassiliou, S., Raynal, I., Cuniasse, P., and Dive, V. (1994). Cyclic peptides with a phosphinic bond as potent inhibitors of a zinc bacterial collagenase. *J. Med. Chem.* 37, 2713–2720. doi: 10.1021/jm00043a011
- Zervoudi, E., Papakyriakou, A., Georgiadou, D., Evnouchidou, I., Gajda, A., Poreba, M., et al. (2011). Probing the S1 specificity pocket of the aminopeptidases that generate antigenic peptides. *Biochem. J.* 435, 411–420. doi: 10.1042/BJ20102049
- Zervoudi, E., Saridakis, E., Birtley, J. R., Sereg, S. S., Reeves, E., Kokkala, P., et al. (2013). Rationally designed inhibitor targeting antigen-trimming aminopeptidases enhances antigen presentation and cytotoxic T-cell responses. *Proc. Natl. Acad. Sci. U. S. A.* 110, 19890–19895. doi: 10.1073/pnas.1309781110
- Zini, S., Fournie-Zaluski, M. C., Chauvel, E., Roques, B. P., Corvol, P., and Llorens-Cortes, C. (1996). Identification of metabolic pathways of brain angiotensin II and III using specific aminopeptidase inhibitors: predominant role of angiotensin III in the control of vasopressin release. *Proc. Natl. Acad. Sci. U. S. A.* 93, 11968–11973. doi: 10.1073/pnas.93.21.11968

**Conflict of Interest:** The authors declare that the research was conducted in the absence of any commercial or financial relationships that could be construed as a potential conflict of interest.

Copyright © 2020 Barlow and Thompson. This is an open-access article distributed under the terms of the Creative Commons Attribution License (CC BY). The use, distribution or reproduction in other forums is permitted, provided the original author(s) and the copyright owner(s) are credited and that the original publication in this journal is cited, in accordance with accepted academic practice. No use, distribution or reproduction is permitted which does not comply with these terms.



# Is There an Interplay Between the Functional Domains of IRAP?

Anika Vear<sup>1</sup>, Tracey Gaspari<sup>2</sup>, Philip Thompson<sup>3</sup> and Siew Yeen Chai<sup>1\*</sup>

<sup>1</sup> Department of Physiology, Monash Biomedicine Discovery Institute, Monash University, Clayton, VIC, Australia,

<sup>2</sup> Department of Pharmacology, Monash Biomedicine Discovery Institute, Monash University, Clayton, VIC, Australia,

<sup>3</sup> Department of Medicinal Chemistry, Monash Institute of Pharmaceutical Sciences, Monash University, Parkville, VIC, Australia

## OPEN ACCESS

### Edited by:

Andrei Surguchov,  
University of Kansas Medical Center,  
United States

### Reviewed by:

Peter M. Van Endert,  
Institut National de la Santé et de la  
Recherche Médicale (INSERM),  
France  
Athanasios Papakyriakou,  
National Centre of Scientific Research  
Demokritos, Greece

### \*Correspondence:

Siew Yeen Chai  
Siew.Chai@monash.edu

### Specialty section:

This article was submitted to  
Cellular Biochemistry,  
a section of the journal  
Frontiers in Cell and Developmental  
Biology

**Received:** 20 July 2020

**Accepted:** 08 September 2020

**Published:** 29 September 2020

### Citation:

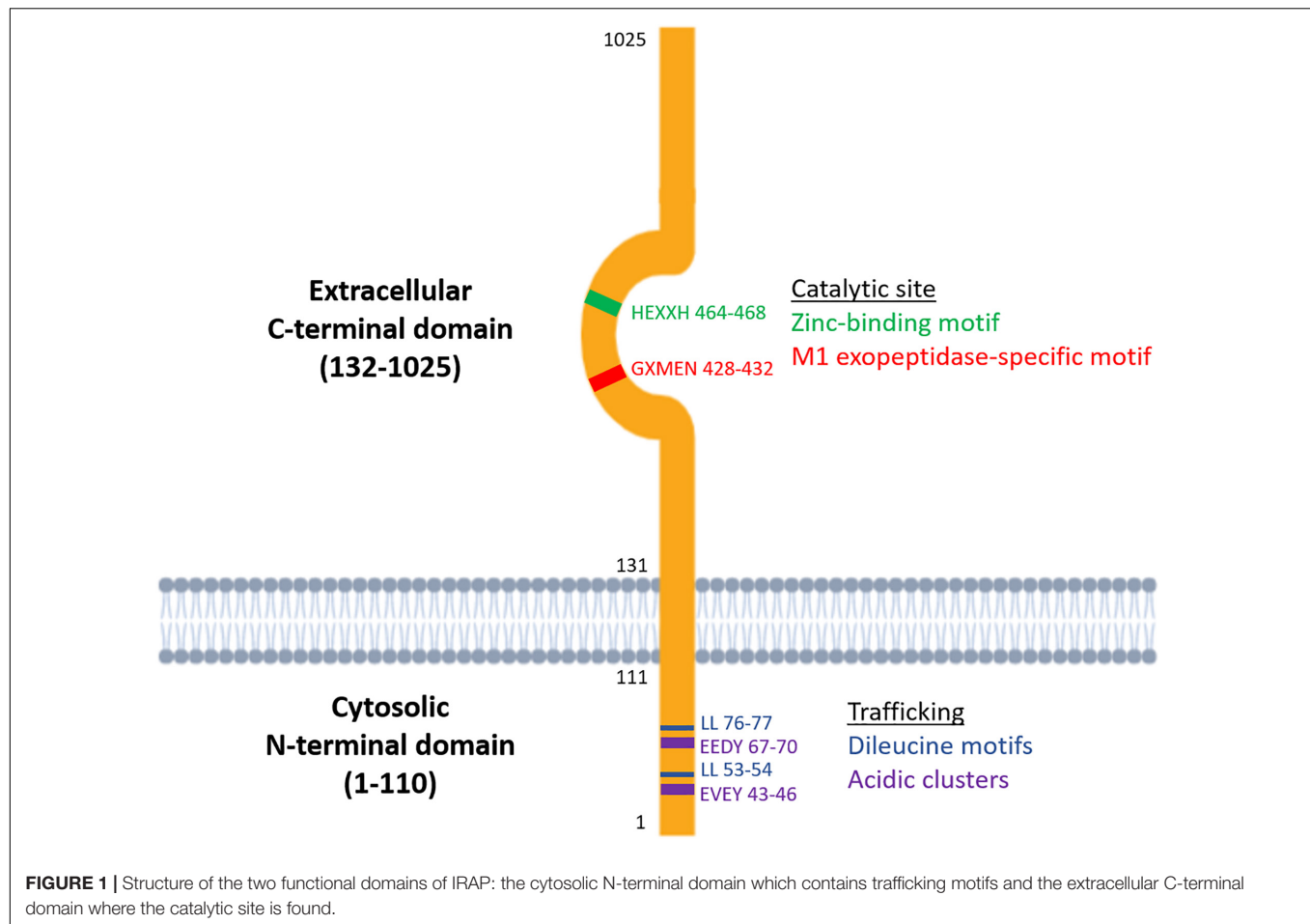
Vear A, Gaspari T, Thompson P  
and Chai SY (2020) Is There an  
Interplay Between the Functional  
Domains of IRAP?  
Front. Cell Dev. Biol. 8:585237.  
doi: 10.3389/fcell.2020.585237

As a member of the M1 family of aminopeptidases, insulin regulated aminopeptidase (IRAP) is characterized by distinct binding motifs at the active site in the C-terminal domain that mediate the catalysis of peptide substrates. However, what makes IRAP unique in this family of enzymes is that it also possesses trafficking motifs at the N-terminal domain which regulate the movement of IRAP within different intracellular compartments. Research on the role of IRAP has focused predominantly on the C-terminus catalytic domain in different physiological and pathophysiological states ranging from pregnancy to memory loss. Many of these studies have utilized IRAP inhibitors, that bind competitively to the active site of IRAP, to explore the functional significance of its catalytic activity. However, it is unknown whether these inhibitors are able to access intracellular sites where IRAP is predominantly located in a basal state as the enzyme may need to be at the cell surface for the inhibitors to mediate their effects. This property of IRAP has often been overlooked. Interestingly, in some pathophysiological states, the distribution of IRAP is altered. This, together with the fact that IRAP possesses trafficking motifs, suggest the localization of IRAP may play an important role in defining its physiological or pathological functions and provide insights into the interplay between the two functional domains of the protein.

**Keywords:** IRAP, Angiotensin IV, M1 aminopeptidase, pathophysiology, trafficking, IRAP inhibitors

## INTRODUCTION

Metallopeptidases are a diverse family of proteolytic enzymes which are involved in regulating the activity of peptide hormones that play crucial roles in maintaining homeostatic balance in physiology (Cerdeira-Costa and Gomis-Ruth, 2014). Failure of these regulatory mechanisms has been shown to result in pathologies such as inflammation, tissue/organ dysfunction, neurological diseases and cardiovascular disorders (Lorenzl et al., 2003; Libby, 2006). A sub-family of metallopeptidases, the metallo-type 1 (M1) aminopeptidases, have important functions in cell maintenance, defense, and growth and development (Drinkwater et al., 2017). Structurally, the M1-aminopeptidases are characterized by two distinct binding motifs, the HEXXH zinc-binding motif which is involved in catalysis and the GXMEN exopeptidase motif which is an N-terminal recognition site that confers selectivity for peptide substrates (Figure 1; Cerdeira-Costa and Gomis-Ruth, 2014). These highly conserved motifs are found at the active site in the C-terminal domain and mediate the catalysis of a range of peptide substrates. This family consists of nine enzymes in



humans, six of which are integral membrane proteins and three of which are found in the cytoplasm (Table 1). Interestingly, only one of these M1 aminopeptidases has a large cytosolic N-terminus which possesses motifs that regulate trafficking events (Figure 1; Keller et al., 1995). This enzyme, known as insulin regulated aminopeptidase (IRAP), is the focus of the current review.

Much of the earlier work on elucidating the enzymatic role of IRAP have involved the use of angiotensin IV (Ang IV), a peptide inhibitor. Treatment with Ang IV or other IRAP inhibitors elicited effects on facilitation of memory (Braszkowski et al., 1988; Wright et al., 1993; Albiston et al., 2008; De Bundel et al., 2009; Royea et al., 2019) and protection against ischemic damage (Coleman et al., 1998; Faure et al., 2006a; Park et al., 2016). It can be reasonably asserted that these peptide inhibitors bind to IRAP at the cell surface, as like many M1 aminopeptidases, IRAP is an integral membrane protein with its catalytic domain on the cell exterior. This enables the regulation of the levels of circulating or extracellular peptide substrates that are secreted to exert autocrine, paracrine and endocrine activities. Given the unique role of the N-terminus of IRAP in the regulation of vesicular trafficking and tethering, the subcellular location of the protein is also an important consideration when investigating its function. Additionally, the mobilization of IRAP to the plasma

membrane is observed in various disease settings suggesting there is an increased demand for its catalytic activity at the cell surface in these states. These properties of IRAP suggest that there is an interplay between the two functional domains of the enzyme and that its spatial location in the cell has important implications in the temporal determination of its aminopeptidase activity. This review will examine our current understanding of the physiological roles of the C- and N-terminus of IRAP and discuss potential evidence of an interplay between these domains.

## TARGETING THE C-TERMINAL DOMAIN OF IRAP

### Peptide Substrates of IRAP Inform on Its Function

The most extensively studied function of IRAP is the ability of its catalytic C-terminus to cleave a range of substrates albeit *in vitro*. These substrates include oxytocin, vasopressin, lys-bradykinin, angiotensin III, met-enkephalin, dynorphin A 1–8, neurokinin A, neuromedin B, somatostatin, and cholecystokinin 8 (Matsumoto et al., 2001a). There is great diversity in the structure of these substrates, from large cyclic peptides such

**TABLE 1** | Enzymes in the M1 aminopeptidase family.

M1 aminopeptidases	Size of protein in humans (number of amino acids)	Size of cytosolic N-terminal domain in humans (number of amino acids)	UniProt ID
<b>Membrane-bound enzymes</b>			
Aminopeptidase A	957	18	Q07075
Thyrotropin-releasing hormone-degrading ectoenzyme	1,024	40	Q9UKU6
Aminopeptidase N	967	7	P15144
Endoplasmic-reticulum aminopeptidase 1 (ERAP1)	941	1	Q9NZ08
Endoplasmic-reticulum aminopeptidase 2 (ERAP2)	960	20	Q6P179
Insulin regulated aminopeptidase (IRAP)	1,025	110	Q9UIQ6
<b>Cytoplasmic enzymes</b>			
Aminopeptidase B	650	–	Q9H4A4
Puromycin-sensitive aminopeptidase	919	–	P55786
Leukotriene A4 hydrolase	611	–	P09960

as oxytocin and vasopressin to small linear peptides like met-enkephalin. This diversity can be attributed to the plasticity of the active site of IRAP. For example, remodeling of the GXMEN exopeptidase loop and reorientation of the key aromatic residue, Tyr549, results in an increased active site volume of  $\sim 5,300 \text{ \AA}^3$  compared with ERAP1's closed state volume of  $2,920 \text{ \AA}^3$  and provides a potential explanation for IRAP's ability to bind large cyclic substrates such as oxytocin and vasopressin (Hermans et al., 2015). This broad substrate specificity suggests IRAP is a relatively promiscuous enzyme and that potentially its conformation and subcellular localization may inform on substrate selectivity.

The diverse physiological roles of the substrates of IRAP range from blood pressure control to the pain response to digestion, reflecting the importance of the enzyme in regulating peptide hormone levels across multiple endocrine and paracrine systems. Notably, only vasopressin has been identified as a physiological substrate of IRAP *in vivo*. This was done by comparing the clearance of radiolabeled vasopressin from the circulation of wildtype and IRAP knockout mice. At 5 min after injection of [ $^{125}\text{I}$ ]-vasopressin, there was a  $\sim 4$ -fold decrease in the intact substrate in the plasma of wildtype mice compared with IRAP knockout mice, with no intact substrate detected in wildtype mice after 20 min (Wallis et al., 2007). These findings were validated with the N-terminal cleavage product, 3-iodo-[ $^{125}\text{I}$ ]tyrosine, detectable only in plasma from wildtype and not knockout mice. In conjunction with the observations that IRAP knockout mice compensate for increased circulating vasopressin levels by decreasing vasopressin synthesis, it was concluded that IRAP plays a role in the cleavage and clearance of vasopressin from the circulation (Wallis et al., 2007).

It has also been proposed that one of the physiological roles of IRAP is regulating levels of circulating oxytocin, a peptide hormone important for initiating contractions during labor (Uvnas-Moberg et al., 2019). Interestingly, oxytocin was suggested to be degraded by secreted soluble IRAP rather than its membrane bound form (Rogi et al., 1996). Northern blot analysis revealed increasing levels of IRAP mRNA in human placental tissue with gestation, peaking at 38 weeks, which correlates

with the increases in circulating oxytocin in the latter stages of pregnancy (Yamahara et al., 2000). Thus, it was proposed that oxytocin degradation by IRAP regulates the onset of labor in humans. However, there is conflicting evidence when we look at the reproductive profiles of IRAP KO mice. In support of the role of IRAP in regulating pregnancy, a significant shortening of gestational term was observed in IRAP KO mice compared with wildtype controls which was further shortened following administration of oxytocin (Ishii et al., 2009). In contrast, Pham et al. (2009) found IRAP deficient mice had no apparent differences in gestational length compared with wildtype controls. It was acknowledged by these authors that the Phe154-Ala155 cleavage site is absent in mice and many other species. Therefore, the role of circulating IRAP during pregnancy is likely restricted to humans. It is also possible that other serum enzymes inactivate oxytocin, with oxytocin cleared from circulation *in vivo* in the absence of IRAP (Wallis et al., 2007). Given there is ample evidence on this area in humans and that soluble IRAP has not been extensively characterized, it is too early to conclude that one of the physiological roles of IRAP is in oxytocin regulation during pregnancy.

Another physiological role of IRAP focuses on its aminopeptidase activity in dendritic cells where IRAP and its close family members, ERAP1 and 2, participate in antigen trimming, a process which is crucial in regulating the presentation of antigen epitopes onto MHC class I molecules in the adaptive immune response. This process was clearly demonstrated in a study by Saveanu et al., 2009, where IRAP-deficiency in bone-marrow derived dendritic cells resulted in a reduction of antigen presentation by 50–70% compared with wild type controls. Unlike ERAP1/2, IRAP is involved in the alternative endosomal pathway, in which exogenous antigens are directly loaded onto MHC class I molecules in endosomes as opposed to the endoplasmic reticulum (Joffre et al., 2012). Thus, IRAP as the principal trimming aminopeptidase in endosomes, is postulated to play a crucial role in cross presentation. Notably, this is the only known example in which IRAP is catalytically active intracellularly and suggests the spatial demand for its aminopeptidase activity may be cell- and tissue-dependent.



Various studies have also probed for IRAP's substrate preference in terms of amino acid length and sequence, by measuring its ability to trim antigenic peptide precursors. Similar to ERAP1, IRAP was able to efficiently trim a variety of long peptide sequences and accumulate mature antigenic epitopes of 8 or 9 amino acids (Georgiadou et al., 2010). However, in contrast to ERAP1, IRAP was more efficient in accumulating smaller products by further trimming of the mature antigenic epitopes (Georgiadou et al., 2010). These findings suggest IRAP has a broad substrate selectivity compared with ERAP1 and is able to process peptide substrates of varying lengths and amino acid side chains.

## Angiotensin IV, a Competitive Inhibitor of IRAP

IRAP has been identified as the angiotensin type 4 receptor (AT<sub>4</sub>R), the specific and high affinity binding site for Ang IV, a hexapeptide corresponding to residues 3–8 of angiotensin II (Ang II) (Albiston et al., 2001). This conclusion was supported by evidence that membranes from cells transfected with the full-length cDNA for human IRAP crosslinked with a photoactivable analog of Ang IV, [<sup>125</sup>I]Nle<sup>1</sup>-BzPhe<sup>6</sup>-Gly<sup>7</sup>-Ang IV. SDS-PAGE revealed the crosslinked IRAP was resolved as a major band of 165 kDa which was displaceable by 10 μM Ang IV, observations consistent with the previously characterized AT<sub>4</sub>R (Albiston et al., 2001). Additionally, *in vitro* receptor autoradiography confirmed the localization of both IRAP mRNA and protein in mouse brain sections correlated with the distribution of the AT<sub>4</sub>R (Albiston et al., 2001). These findings, along with a loss of Ang IV binding to the AT<sub>4</sub>R in the brain of the IRAP knockout mouse, provided compelling evidence that IRAP is the AT<sub>4</sub>R.

Ang IV was first shown to bind to IRAP in bovine adrenal cortex membranes (Swanson et al., 1992). Additionally, IRAP also binds LVV-hemorphin-7 (LVV-H7) (Moeller et al., 1997), which is structurally distinct and shares little sequence homology with Ang IV (Moeller et al., 1999a). Unlike substrates of the enzyme, both Ang IV and LVV-H7 are resistant to proteolytic degradation by IRAP and instead were found to be competitive inhibitors of IRAP. This was shown by Lew, Mustafa (28) where the inhibitory effects of the IRAP ligands Ang IV, Nle<sup>1</sup>-Ang IV, divalinal-Ang IV, and LVV-H7 was assessed following cleavage of leu-β-naphthylamide (Leu-β-NA), a synthetic substrate of the enzyme. All four of the tested IRAP ligands were seen to inhibit IRAP activity, with Ang IV displaying the highest potency ( $K_i = 113$  nM) (Lew et al., 2003). Lineweaver Burk analysis also revealed a 14-fold increase in the  $K_m$  for Leu-β-NA with increasing inhibitor concentrations and only minor changes in  $V_{max}$ . Thus, it was concluded that IRAP inhibitors display competitive kinetics, indicating they bind directly to the catalytic site of the enzyme (Lew et al., 2003).

Despite Ang IV and LVV-H7 binding with high affinity to IRAP to inhibit its catalytic activity, a number of factors have hindered their potential for therapeutic use and as research tools to examine IRAP function. These include their limited stability in the circulation and lack of specificity for IRAP over other aminopeptidases and receptors such as the AT<sub>1</sub>R for Ang IV and

μ-opioid receptor for LVV-H7 (Lew et al., 2003). Thus, a range of novel peptidomimetic (Axen et al., 2007; Lukaszuk et al., 2008; Andersson et al., 2010; Kokkala et al., 2016) and small molecule inhibitors (Albiston et al., 2008; Borhade et al., 2014) have been developed to address these limitations with some of these compounds showing promise as potential therapeutic agents.

## IRAP Inhibition Facilitates Learning and Memory

Whilst Ang IV was initially thought to just be an inactive metabolic fragment of Ang II, it was demonstrated to have memory-enhancing properties in rats and mice in a range of memory and cognitive tasks. This facilitation of learning and memory occurs following acute central administration of Ang IV (Braszko et al., 1988; Wright et al., 1993), LVV-H7 (De Bundel et al., 2009), as well as with the small molecular weight IRAP inhibitor, HFI-419 (Albiston et al., 2008), further strengthening the proposal that inhibition of IRAP leads to enhancement of memory. IRAP therefore presents as a promising target for neurodegenerative diseases such as Alzheimer's Disease (AD), in which there is progressive cognitive decline and memory loss. This was validated in a recent study by Royea et al. (2019) in which 4 weeks of centrally administered Ang IV (1.3 nmol/day) restored short-term memory, spatial learning and spatial memory in a transgenic mouse model of AD with alternatively spliced amyloid precursor protein.

Evidence of changes in the brain with IRAP inhibitor treatment include normalization of hippocampal subgranular zone cellular proliferation, enhanced dendritic branching, and reduced oxidative stress (Royea et al., 2019). Furthermore, treatment of primary rat hippocampal cultures with a number of different classes of IRAP inhibitors has been shown to significantly alter dendritic spine morphology and increase spine density (Diwakarla et al., 2016a,b; Seyer et al., 2019). Similarly, enhancement of long-term potentiation was observed in rats in the dentate gyrus *in vivo* following Ang IV treatment (Wayner et al., 2001) and within the hippocampus *in vitro* following treatment with Ang IV analogs (Kramar et al., 2001). The changes in spine morphology are thought to correlate with the strength and activity of the synapse, which coupled with enhanced long-term potentiation, provides strong supporting evidence of the memory enhancing role of IRAP inhibitors.

Despite these effects of IRAP inhibitors on memory enhancement, Albiston et al. (2010) found that global deletion of the IRAP gene resulted in mice with an accelerated, age-related decline in spatial memory as seen in the Y maze task. Similarly, conditional forebrain neuron specific-IRAP knockout led to deficits in spatial reference and novel object recognition memory (Yeatan et al., 2016). These unexpected observations were thought to potentially be due to altered brain development of the knockout mice, given there is high IRAP expression in the highly neurogenic ventricular and subventricular zone of the embryonic mouse brain, possibly implicating IRAP as having a role in neuronal development. Regardless of this finding, there is comprehensive evidence supporting the cognitive enhancing

effect of IRAP inhibition (Albiston et al., 2004; Lee et al., 2004; De Bundel et al., 2009; Fidalgo et al., 2019; Royea et al., 2019).

Ang IV has also been shown to have positive effects on other central nervous system functions. For example, centrally administered Ang IV (0.1–1 µg/mouse) provides protection against pentylenetetrazol (PTZ)-induced seizures in mice, by dose-dependently increasing PTZ-seizure threshold and decreasing PTZ-seizure intensity (Tchekalarova et al., 2001). Additionally, inhibition of IRAP by Ang IV has an anxiolytic (Beyer et al., 2010) and anti-hyperalgesia (Chow et al., 2013) effect in rats and an anti-allodynia effect in male mice (Chow et al., 2018), all proposed to be due to elevated levels of oxytocin in the brain or spinal cord.

## IRAP Inhibitor Treatment Protects Against Ischemic Damage

IRAP also presents as a promising target for the treatment of ischemic damage in the brain and heart. For example, IRAP inhibition with Ang IV (1 nmol) in a rat model of embolic stroke has been shown to significantly reduce cerebral infarct volume compared with untreated controls (Faure et al., 2006a). Importantly, this reduction corresponded with improvements in neurological performance and decreased mortality at 24 h post-stroke and is likely attributed to redistribution of blood flow to the ischemic areas (Faure et al., 2006a). However, these initial findings on the vasodilatory effect of Ang IV was contradicted by a more recent study by Faure et al. (2006b) who suggested low concentrations of Ang IV (0.001–3 µM) had a vasoconstrictive effect on isolated rat basilar arteries that is mediated by binding to IRAP. Given that increases in blood flow to damaged brain areas with subsequent neurological improvement have been consistently reported in a number of studies, it is likely that Ang IV acts as a vasodilator in the brain.

There are conflicting reports on the effects of Ang IV on the renal vasculature as well. Interestingly, this effect appears to be dependent on the concentration and route of administration of the inhibitor, with infusion of low doses of Ang IV (0.1–100 pmol) directly into renal arteries increasing renal blood flow (Coleman et al., 1998), compared with systemic administration of high concentrations of Ang IV (100 nmol/kg) which results in renal vasoconstriction (Fitzgerald et al., 1999; Yang et al., 2008). At higher concentrations, Ang IV also binds to the AT<sub>1</sub>R which may mediate this vasoconstrictory effect. Therefore, lower concentrations of Ang IV (<1 µM) should be used to investigate the effect of IRAP inhibition to avoid off-target binding. Similarly in the heart, 3 days of pre-treatment with Ang IV (1 mg/kg/day) in rats was found to blunt the ischemia/reperfusion (I/R)-induced increases in pro-fibrotic factors such as TNF-α, MMP-9, and VCAM-1 (Park et al., 2016). This led to an overall improvement in I/R-induced myocardial dysfunction in these rats. In combination, these studies suggest that loss of function of the catalytic activity of IRAP provides protection against ischemic events in multiple organs, which may potentially also prevent downstream consequences of this ischemic damage such as tissue fibrosis.

## IRAP Inhibition Is Cardio- and Vaso-Protective

Ang IV treatment has also been observed to be cardio-protective, displaying opposing effects to Ang II. Yang et al. (2011) demonstrated that Ang II-induced cardiac dysfunction and injury were improved following Ang IV administration (100 nM) in isolated rat heart. Ang IV was also seen to inhibit Ang-II induced cell apoptosis, cardiomyocyte hypertrophy, and collagen synthesis of cardiac fibroblasts (Yang et al., 2011). Following IRAP siRNA knockdown, it was concluded that these effects were mediated by IRAP (Yang et al., 2011). The vaso-protective actions of Ang IV have also been observed, with increased aortic nitric oxide bioavailability following chronic Ang IV treatment (1.44 mg/kg/day) of high-fat diet fed apolipoprotein E-deficient mice (Vinh et al., 2008b). This improvement was associated with decreased superoxide levels and increased endothelial nitric oxide synthase-3 expression. Similarly, treatment with the small molecule IRAP inhibitor, HFI-419, prevents against acetylcholine-mediated vasoconstriction *in vitro*, in abdominal aorta from a rabbit model of coronary artery vasospasm (El-Hawli et al., 2017). These studies, in conjunction with those mentioned earlier on IRAP in I/R injury, suggest that IRAP inhibition is cardio- and vaso-protective.

## Knowledge Gaps

In summary, the catalytic activity of the C-terminal domain of IRAP has been shown to have important functions in many body systems, ranging from reproduction to the cardiovascular system. Interestingly, whilst it is required for maintaining normal physiological processes in some of these systems, its upregulation is seen in many pathophysiological states such as atherosclerosis (Vinh et al., 2008a), following balloon injury of the carotid arteries (Moeller et al., 1999b) and in response to hypoxia in the carotid body (Fung et al., 2007), suggesting the consequences of its functions are cell/tissue- and state-dependent. Generally, inhibition of IRAP appears to provide protection against many of these diseases, encouraging researchers to further validate IRAP as a promising therapeutic target. However, many questions remain regarding the specific mechanisms underlying IRAP's role in disease, and whether it is a cause or consequence of disease pathogenesis. Better understanding of these mechanisms would also provide important insights to guide the design of novel IRAP inhibitors as therapeutic agents. Notably, the subcellular localization of IRAP, regulated by its other functional domain at the N-terminus, has not been investigated in many of these contexts, nor has the trafficking of IRAP following inhibitor binding. It is also not known if the current classes of IRAP inhibitors have access to the catalytic site of IRAP in its location in intracellular vesicles. Interestingly, it has been demonstrated that the distribution of IRAP is altered in various disease states. Collectively, these findings suggest the efficacy of IRAP inhibitors may be influenced by the location of the enzyme. The trafficking of IRAP may reflect or regulate its function at a given point in time and location. Therefore, future research recognizing the role of the N-terminal domain and its potential influence on

IRAP's catalytic activity may help us to better understand IRAP function in disease.

## RECOGNISING THE N-TERMINAL DOMAIN OF IRAP

### Trafficking Motifs at the N-Terminus of IRAP Regulate Its Movement in the Cell

The cytosolic N-terminus is unique to IRAP compared with other M1 aminopeptidases and contains two dileucine motifs, each with a preceding acidic cluster (Keller et al., 1995). This domain is postulated to have two key functions both of which influence the subcellular distribution of IRAP. One of these involves regulating the trafficking of IRAP in vesicles in turn, modulating the subcellular distribution of associated vesicular proteins. The key studies exploring the trafficking of IRAP have been conducted in 3T3-L1 adipocytes, following observations that IRAP colocalized with the insulin responsive glucose transporter, glucose transporter isoform 4 (GLUT4), in these cells (Keller et al., 1995). This was clearly demonstrated

by Waters et al. (1997), where microinjection of a fusion protein containing the cytosolic domain of IRAP into 3T3-L1 adipocytes resulted in translocation of GLUT4-containing vesicles to the plasma membrane. Interestingly, this increase in cell surface GLUT4 was equivalent to that seen following stimulation with insulin and was not blocked by wortmannin, an inhibitor of the PI3K signaling pathway downstream of insulin receptor activation (Waters et al., 1997). This suggests the translocation of GLUT4 was regulated by the N-terminus of IRAP. The fact that IRAP, unlike its close family members, has these trafficking motifs suggests that tight regulation of its localization must be important to, or even regulate, its function.

In the basal state, newly synthesized IRAP is targeted to the trans-Golgi network (TGN), evidenced by colocalization with a TGN-specific marker (TGN38) (De Bundel et al., 2015). It is subsequently transported for storage to specialized endosomal vesicles in the perinuclear region of the cell, with slow recycling of these endosomes to the plasma membrane (Figure 2; Shi et al., 2008; Jordens et al., 2010). The dileucine motif at position 76 and 77 of IRAP's cytoplasmic N-terminal domain was found to be required for this sorting to specialized endosomes in adipocytes, with alanine substitution of these residues resulting in a dramatic

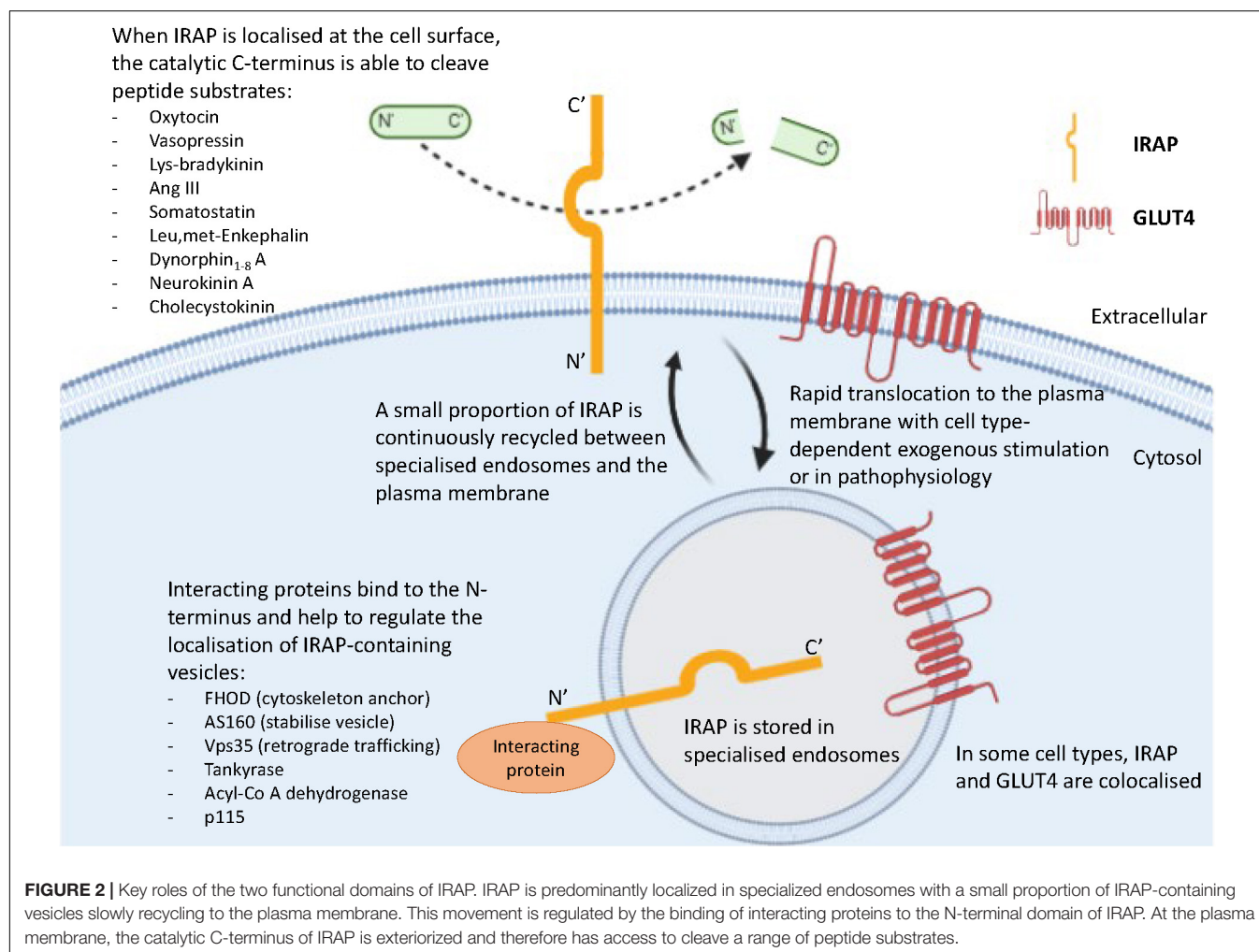


**FIGURE 2 |** Key roles of the two functional domains of IRAP. IRAP is predominantly localized in specialized endosomes with a small proportion of IRAP-containing vesicles slowly recycling to the plasma membrane. This movement is regulated by the binding of interacting proteins to the N-terminal domain of IRAP. At the plasma membrane, the catalytic C-terminus of IRAP is exteriorized and therefore has access to cleave a range of peptide substrates.



increase in the cell surface localization of IRAP (Hou et al., 2006). Notably, an electron microscopy study in hippocampal neurons found IRAP specific immunoreactivity predominantly associated with 100–200 nm vesicles (Fernando et al., 2007). This finding, along with those from sub-cellular fractionation and dual-label immunofluorescence experiments, led the authors to propose the subcellular distribution of IRAP in these neurons is very similar to that seen in insulin-responsive cells (Fernando et al., 2007). Thus, the trafficking of IRAP observed in adipocytes can likely be generalized to other cell types such as neurons and cardiac fibroblasts, in which there is a distinct perinuclear IRAP distribution in a basal state.

## IRAP Has a Role in Tethering Vesicles

The N-terminus of IRAP is also believed to be important for tethering specialized endosomes to the cytoskeleton via binding of interacting proteins including tankyrase (Chi and Lodish, 2000), acyl-coenzyme A dehydrogenase (Katagiri et al., 2002), formin homology domain (FHOD) (Babdor et al., 2017), p115 (Hosaka et al., 2005), Vps35 (Pan et al., 2019), and Akt substrate of 160 kDa (AS160) (Figure 2; Peck et al., 2006). This has been clearly demonstrated in dendritic cells, in which the role of the N-terminal domain of IRAP has only recently been implicated in immune function. A comprehensive study by Babdor et al. (2017) revealed that anchorage of endosomes containing toll-like receptor 9 (TLR9) to the actin cytoskeleton by the N-terminus of IRAP via the interacting protein, FHOD4, prevents TLR9 activation. Thus, in the absence of IRAP, the trafficking of TLR9 to lysosomes and subsequent activation was enhanced in cultured dendritic cells and in mice following bacterial infection, leading to an increased secretion of pro-inflammatory cytokines (Babdor et al., 2017). This study is crucial as it not only suggests another intracellular trafficking mechanism regulated by IRAP, but also has potential implications for understanding the mechanisms underlying certain autoimmune disorders such as arthritis, where there is inappropriate activation of endosomal TLRs (Rifkin et al., 2005). Furthermore, the importance of IRAP in immune functioning is supported by the identification of a deleterious missense mutation in IRAP's gene associated with psoriasis, an autoimmune disorder linked to activation of TLR9 (Cheng et al., 2014).

The role of IRAP in tethering vesicles is also seen in adipocytes in which it is thought to regulate GLUT4 translocation. For example, Peck et al. (2006) proposes that a GTP-ase activating protein (GAP), AS160, is tethered with the cytosolic tail of IRAP in the basal state thus preventing the translocation of GLUT4 storage vesicles (GSVs). Subsequent stimulation by insulin is suggested to inactivate AS160, resulting in translocation of the GSV to the plasma membrane, thus facilitating glucose uptake by the cell. Notably, immunostaining revealed IRAP, GLUT4 and AS160 all have a punctate-like expression in the cytoplasm in a basal state, with areas of concentration adjacent to the nucleus, whilst insulin stimulation caused a marked redistribution of IRAP and GLUT4 to the plasma membrane (Peck et al., 2006). A recent study also found retrograde trafficking of IRAP from endosomes to the TGN was dependent on binding of the retromers Vps35 and Vps26 to the cytoplasmic tail of IRAP (Pan

et al., 2019). Not only did these retromers strongly colocalize with IRAP in unstimulated 3T3-L1 adipocytes, but knockout of Vps35 in particular, increased the targeting of IRAP to lysosomes due to the lack of retromer-dependent endosomal retrieval to the TGN (Pan et al., 2019).

Studies exploring the functions of the N-terminus of IRAP in trafficking and tethering specialized vesicles have shed new light on its potential roles in these cells. However, the physiological relevance of these functions is not well-understood. Despite this, the fact that IRAP possesses a cytosolic N-terminus which has the ability to not only regulate its trafficking but that of other vesicular proteins, suggests the subcellular localization of IRAP must be significant in regulating its function. This logic provides the first hint of an interplay between IRAP's functional domains.

## AN INTERPLAY BETWEEN THE FUNCTIONAL DOMAINS OF IRAP?

### Subcellular Localization of IRAP Is Altered in Pathophysiology

In a basal state IRAP is predominantly located intracellularly in specialized endosomes, with slow recycling of these vesicles to the plasma membrane (Shi et al., 2008; Jordens et al., 2010). However, this recycling appears to be altered in pathophysiology. For example, following exogenous stimulation, IRAP is seen to rapidly translocate to the cell surface. Measurement of cell surface IRAP using a cell surface biotinylation method revealed that following treatment of 3T3-L1 adipocytes with insulin, there was an 8-fold increase in the proportion of IRAP at the plasma membrane (Ross et al., 1998). Similar results were seen in the same cell line using an alternative technique; immunofluorescence with an IRAP specific antibody (Liu et al., 2005). Redistribution of IRAP to the cell surface was also observed following stimulation with endothelin-1 in 3T3-L1 adipocytes (Wu-Wong et al., 1999), oxytocin in human vascular endothelial cells (Nakamura et al., 2000), immunoglobulin E in mast cells (Liao et al., 2006) and forskolin in PC12 cells (Matsumoto et al., 2001b). This translocation of IRAP is potentially indicative of an increased cellular demand for the C-terminus of IRAP to be expressed at the cell surface in these stimulated states to subserve a particular protective or pathophysiological role. Importantly, some of these stimulants mimic what is seen in various pathophysiological settings in which IRAP has a predominantly cell surface localization. For example, an increase in cell surface IRAP, measured by binding of the radiolabeled IRAP inhibitor, [ $H^3$ ]IVDE77, was observed in mouse pro-inflammatory M1-activated macrophages following stimulation with interferon- $\gamma$  or lipopolysaccharide (Nikolaou et al., 2014).

Furthermore, an alteration to the characteristic recycling of IRAP is seen in type 2 diabetes. Maianu et al. (2001) examined the subcellular localization of both GLUT4 and IRAP in adipocytes isolated from healthy controls and type 2 diabetics and found that despite no detectable difference in IRAP protein expression between groups, IRAP and GLUT4 trafficking in diabetic patients



appeared to be altered with redistribution to high-density microsomes and plasma membrane fractions in basal cells and impaired translocation following insulin stimulation. This results in impaired insulin action and a decrease in insulin-responsive vesicular trafficking (Maianu et al., 2001). Importantly, the accumulation of IRAP at the plasma membrane in type 2 diabetics correlates with the redistribution of IRAP to the cell surface in other disease states.

Overall, these studies suggest that the slow recycling of IRAP-containing vesicles to the plasma membrane seen in a basal state, is altered in pathophysiology, and mimics what is reported following exogenous stimulation. This potentially provides a mechanism by which the cell is able to regulate IRAP function by altering its localization. It is also worth considering whether this change in IRAP distribution contributes to the disease phenotype, with both a loss of IRAP in one location and a gain of IRAP in another having positive or negative consequences on the cell.

## Physiological Example of IRAP Trafficking Regulating Its Catalytic Activity

Most studies to date have explored the functions of either the C- or N-terminus of IRAP independently. However, there is one reported physiological example in which a clear relationship between these domains was demonstrated. In the study by Wallis, Lankford (16), fasted wildtype or IRAP knockout mice were injected with saline or insulin, and then 5 min later, with radiolabeled vasopressin. Blood samples taken at 1, 2, and 3 min after injection, revealed significantly less intact substrate in the plasma of insulin-treated wildtype mice compared with saline treated wildtype mice. This suggests that insulin increased the clearance of circulating vasopressin, most likely due to a higher proportion of IRAP found at the cell surface following insulin stimulation. Importantly, there was no difference in the clearance of radiolabeled vasopressin from the circulation of saline- or insulin-treated IRAP knockout mice, validating that the vasopressin cleavage in wildtype animals can most likely be attributed to IRAP's aminopeptidase activity (Wallis et al., 2007).

Additionally, these results were not due to insulin-induced changes in total distribution volume or excretion, with similar plasma concentrations of radiolabeled inulin in saline- and insulin-treated wildtype and IRAP knockout mice (Wallis et al., 2007). Taken together, these findings show that increased translocation of IRAP to the cell surface following insulin stimulation, mediated the increase in vasopressin cleavage in wildtype animals. This highlights the physiological role of the N-terminus of IRAP in potentially regulating its aminopeptidase activity at the C-terminus.

## CONCLUSION

Whilst the catalytic activity of IRAP as well as the mechanisms underlying the trafficking of IRAP-containing vesicles have been independently studied, the influence of one functional domain on the other remains poorly understood. The fact that IRAP alone in the M1 aminopeptidase family possesses trafficking motifs in its N-terminal domain suggests that tight regulation of its localization must be important in determining its functional significance. Additionally, mobilization of IRAP to the cell surface in various pathophysiological states further supports the idea that its localization may reflect the cellular demand for its catalytic activity in a given location and time and may provide a means by which the cell can regulate the degradation of extracellular substrates. These observations provide insights into the interplay between the catalytic activity of IRAP and its trafficking, highlighting the importance of addressing these functions together in future studies.

## AUTHOR CONTRIBUTIONS

AV wrote the manuscript with input on ideas and writing from SC. TG and PT provided important feedback on the final manuscript. All authors contributed to the article and approved the submitted version.

## REFERENCES

- Albiston, A. L., Fernando, R. N., Yeatman, H. R., Burns, P., Ng, L., Daswani, D., et al. (2010). Gene knockout of insulin-regulated aminopeptidase: loss of the specific binding site for angiotensin IV and age-related deficit in spatial memory. *Neurobiol. Learn. Mem.* 93, 19–30. doi: 10.1016/j.nlm.2009.07.011
- Albiston, A. L., McDowall, S. G., Matsacos, D., Sim, P., Clune, E., Mustafa, T., et al. (2001). Evidence that the angiotensin IV (AT(4)) receptor is the enzyme insulin-regulated aminopeptidase. *J. Biol. Chem.* 276, 48623–48626. doi: 10.1074/jbc.c100512200
- Albiston, A. L., Morton, C. J., Ng, H. L., Pham, V., Yeatman, H. R., Ye, S., et al. (2008). Identification and characterization of a new cognitive enhancer based on inhibition of insulin-regulated aminopeptidase. *FASEB J.* 22, 4209–4217. doi: 10.1096/fj.08-112227
- Albiston, A. L., Pederson, E. S., Burns, P., Purcell, B., Wright, J. W., Harding, J. W., et al. (2004). Attenuation of scopolamine-induced learning deficits by LVV-hemorphin-7 in rats in the passive avoidance and water maze paradigms. *Behav. Brain Res.* 154, 239–243. doi: 10.1016/j.bbr.2004.02.012
- Andersson, H., Demaegdt, H., Vauquelin, G., Lindeberg, G., Karlen, A., Hallberg, M., et al. (2010). Disulfide cyclized tripeptide analogues of angiotensin IV as potent and selective inhibitors of insulin-regulated aminopeptidase (IRAP). *J. Med. Chem.* 53, 8059–8071. doi: 10.1021/jm100793t
- Axen, A., Andersson, H., Lindeberg, G., Ronnholm, H., Kortessmaa, J., Demaegdt, H., et al. (2007). Small potent ligands to the insulin-regulated aminopeptidase (IRAP)/AT(4) receptor. *J. Pept. Sci.* 13, 434–444. doi: 10.1002/psc.859
- Babdor, J., Descamps, D., Adiko, A. C., Tohme, M., Maschalidi, S., Evnouchidou, I., et al. (2017). IRAP(+) endosomes restrict TLR9 activation and signaling. *Nat. Immunol.* 18, 509–518. doi: 10.1038/ni.3711
- Beyer, C. E., Dwyer, J. M., Platt, B. J., Neal, S., Luo, B., Ling, H. P., et al. (2010). Angiotensin IV elevates oxytocin levels in the rat amygdala and produces anxiolytic-like activity through subsequent oxytocin receptor activation. *Psychopharmacology* 209, 303–311. doi: 10.1007/s00213-010-1791-1
- Borhade, S. R., Rosenstrom, U., Savmarker, J., Lundback, T., Jenmalm-Jensen, A., Sigmundsson, K., et al. (2014). Inhibition of insulin-regulated aminopeptidase (IRAP) by Arylsulfonamides. *Chem. Open* 3, 256–263. doi: 10.1002/open.201402027

- Braszkowski, J. J., Kupryszewski, G., Witczuk, B., and Wisniewski, K. (1988). Angiotensin II-(3-8)-hexapeptide affects motor activity, performance of passive avoidance and a conditioned avoidance response in rats. *Neuroscience* 27, 777–783. doi: 10.1016/0306-4522(88)90182-0
- Cerda-Costa, N., and Gomis-Ruth, F. X. (2014). Architecture and function of metalloproteinase catalytic domains. *Protein Sci.* 23, 123–144. doi: 10.1002/pro.2400
- Cheng, H., Li, Y., Zuo, X. B., Tang, H. Y., Tang, X. F., Gao, J. P., et al. (2014). Identification of a missense variant in LNPEP that confers psoriasis risk. *J. Invest. Dermatol.* 134, 359–365. doi: 10.1038/jid.2013.317
- Chi, N. W., and Lodish, H. F. (2000). Tankyrase is a golgi-associated mitogen-activated protein kinase substrate that interacts with IRAP in GLUT4 vesicles. *J. Biol. Chem.* 275, 38437–38444. doi: 10.1074/jbc.m007635200
- Chow, L. H., Chen, Y. H., Lai, C. F., Lin, T. Y., Chen, Y. J., Kao, J. H., et al. (2018). Sex Difference of Angiotensin IV-, LVV-Hemorphin 7-, and oxytocin-induced antiallodynia at the spinal level in mice with neuropathic pain. *Anesth. Analg.* 126, 2093–2101. doi: 10.1213/ane.0000000000002795
- Chow, L. H., Tao, P. L., Chen, J. C., Liao, R. M., Chang, E. P., and Huang, E. Y. (2013). A possible correlation between oxytocin-induced and angiotensin IV-induced anti-hyperalgesia at the spinal level in rats. *Peptides* 39, 21–28. doi: 10.1016/j.peptides.2012.10.012
- Coleman, J. K., Krebs, L. T., Hamilton, T. A., Ong, B., Lawrence, K. A., Sardinia, M. F., et al. (1998). Autoradiographic identification of kidney angiotensin IV binding sites and angiotensin IV-induced renal cortical blood flow changes in rats. *Peptides* 19, 269–277. doi: 10.1016/s0196-9781(97)00291-x
- De Bundel, D., Fafouri, A., Csaba, Z., Loyens, E., Lebon, S., El Ghouzzi, V., et al. (2015). Trans-modulation of the somatostatin Type 2A receptor trafficking by insulin-regulated aminopeptidase decreases limbic seizures. *J. Neurosci.* 35, 11960–11975. doi: 10.1523/jneurosci.0476-15.2015
- De Bundel, D., Smolders, I., Yang, R., Albiston, A. L., Michotte, Y., and Chai, S. Y. (2009). Angiotensin IV and LVV-haemorphin 7 enhance spatial working memory in rats: effects on hippocampal glucose levels and blood flow. *Neurobiol. Learn. Mem.* 92, 19–26. doi: 10.1016/j.nlm.2009.02.004
- Diwakarla, S., Nylander, E., Gronbladh, A., Vanga, S. R., Khan, Y. S., Gutierrez-de-Teran, H., et al. (2016a). Aryl sulfonamide inhibitors of insulin-regulated aminopeptidase enhance spine density in primary hippocampal neuron cultures. *ACS Chem. Neurosci.* 7, 1383–1392. doi: 10.1021/acschemneuro.6b00146
- Diwakarla, S., Nylander, E., Gronbladh, A., Vanga, S. R., Khan, Y. S., Gutierrez-de-Teran, H., et al. (2016b). Binding to and inhibition of insulin-regulated aminopeptidase by macrocyclic disulfides enhances spine density. *Mol. Pharmacol.* 89, 413–424. doi: 10.1124/mol.115.102533
- Drinkwater, N., Lee, J., Yang, W., Malcolm, T. R., and McGowan, S. (2017). M1 aminopeptidases as drug targets: broad applications or therapeutic niche? *FEBS J.* 284, 1473–1488. doi: 10.1111/febs.14009
- El-Hawli, A., Qaradakh, T., Hayes, A., Rybalka, E., Smith, R., Caprnda, M., et al. (2017). IRAP inhibition using HFI419 prevents moderate to severe acetylcholine mediated vasoconstriction in a rabbit model. *Biomed. Pharmacother.* 86, 23–26. doi: 10.1016/j.biopha.2016.11.142
- Faure, S., Chapot, R., Tallet, D., Javellaud, J., Achard, J. M., and Oudart, N. (2006a). Cerebroprotective effect of angiotensin IV in experimental ischemic stroke in the rat mediated by AT(4) receptors. *J. Physiol. Pharmacol.* 57, 329–342.
- Faure, S., Javellaud, J., Achard, J. M., and Oudart, N. (2006b). Vasoconstrictive effect of angiotensin IV in isolated rat basilar artery independent of AT1 and AT2 receptors. *J. Vasc. Res.* 43, 19–26. doi: 10.1159/000089186
- Fernando, R. N., Luff, S. E., Albiston, A. L., and Chai, S. Y. (2007). Sub-cellular localization of insulin-regulated membrane aminopeptidase, IRAP to vesicles in neurons. *J. Neurochem.* 102, 967–976. doi: 10.1111/j.1471-4159.2007.04659.x
- Fidalgo, S., Patel, M., Quadri, A., Sadiq, W., and Gard, P. R. (2019). Decreased behavioural and neurochemical effects of angiotensin IV following prenatal alcohol exposure in the mouse. *Neuropeptides* 77:101931. doi: 10.1016/j.npep.2019.05.002
- Fitzgerald, S. M., Evans, R. G., Bergstrom, G., and Anderson, W. P. (1999). Renal hemodynamic responses to intrarenal infusion of ligands for the putative angiotensin IV receptor in anesthetized rats. *J. Cardiovasc. Pharmacol.* 34, 206–211. doi: 10.1097/00005344-199908000-00005
- Fung, M. L., Lam, S. Y., Wong, T. P., Tjong, Y. W., and Leung, P. S. (2007). Carotid body AT(4) receptor expression and its upregulation in chronic hypoxia. *Open Cardiovasc. Med. J.* 1, 1–7. doi: 10.2174/1874192400701010001
- Georgiadou, D., Hearn, A., Evnouchidou, I., Chroni, A., Leondiadis, L., York, I. A., et al. (2010). Placental leucine aminopeptidase efficiently generates mature antigenic peptides in vitro but in patterns distinct from endoplasmic reticulum aminopeptidase 1. *J. Immunol.* 185, 1584–1592. doi: 10.4049/jimmunol.0902502
- Hermans, S. J., Ascher, D. B., Hancock, N. C., Holien, J. K., Michell, B. J., Chai, S. Y., et al. (2015). Crystal structure of human insulin-regulated aminopeptidase with specificity for cyclic peptides. *Protein Sci.* 24, 190–199. doi: 10.1002/pro.2604
- Hosaka, T., Brooks, C. C., Presman, E., Kim, S. K., Zhang, Z., Breen, M., et al. (2005). p115 Interacts with the GLUT4 vesicle protein, IRAP, and plays a critical role in insulin-stimulated GLUT4 translocation. *Mol. Biol. Cell.* 16, 2882–2890. doi: 10.1091/mbc.e05-01-0072
- Hou, J. C., Suzuki, N., Pessin, J. E., and Watson, R. T. (2006). A specific dileucine motif is required for the GGA-dependent entry of newly synthesized insulin-responsive aminopeptidase into the insulin-responsive compartment. *J. Biol. Chem.* 281, 33457–33466. doi: 10.1074/jbc.m601583200
- Ishii, M., Naruse, K., Hattori, A., Tsujimoto, M., Ishiura, S., Numaguchi, Y., et al. (2009). Oxytocin hypersensitivity in pregnant P-LAP deficient mice. *Life Sci.* 84, 668–672. doi: 10.1016/j.lfs.2009.02.018
- Joffre, O. P., Segura, E., Savina, A., and Amigorena, S. (2012). Cross-presentation by dendritic cells. *Nat. Rev. Immunol.* 12, 557–569.
- Jordens, I., Molle, D., Xiong, W., Keller, S. R., and McGraw, T. E. (2010). Insulin-regulated aminopeptidase is a key regulator of GLUT4 trafficking by controlling the sorting of GLUT4 from endosomes to specialized insulin-regulated vesicles. *Mol. Biol. Cell.* 21, 2034–2044. doi: 10.1091/mbc.e10-02-0158
- Katagiri, H., Asano, T., Yamada, T., Aoyama, T., Fukushima, Y., Kikuchi, M., et al. (2002). Acyl-coenzyme A dehydrogenases are localized on GLUT4-containing vesicles via association with insulin-regulated aminopeptidase in a manner dependent on its dileucine motif. *Mol. Endocrinol.* 16, 1049–1059. doi: 10.1210/mend.16.5.0831
- Keller, S. R., Scott, H. M., Mastick, C. C., Aebersold, R., and Lienhard, G. E. (1995). Cloning and characterization of a novel insulin-regulated membrane aminopeptidase from Glut4 vesicles. *J. Biol. Chem.* 270, 23612–23618. doi: 10.1074/jbc.270.40.23612
- Kokkala, P., Mpakali, A., Mauvais, F. X., Papakyriakou, A., Daskalaki, I., Petropoulou, I., et al. (2016). Optimization and structure-activity relationships of phosphinic pseudotripeptide inhibitors of aminopeptidases that generate antigenic peptides. *J. Med. Chem.* 59, 9107–9123. doi: 10.1021/acs.jmedchem.6b01031
- Kramer, E. A., Armstrong, D. L., Ikeda, S., Wayner, M. J., Harding, J. W., and Wright, J. W. (2001). The effects of angiotensin IV analogs on long-term potentiation within the CA1 region of the hippocampus in vitro. *Brain Res.* 897, 114–121. doi: 10.1016/s0006-8993(01)02100-x
- Lee, J., Albiston, A. L., Allen, A. M., Mendelsohn, F. A., Ping, S. E., Barrett, G. L., et al. (2004). Effect of I.C.V. injection of AT4 receptor ligands, NLE1-angiotensin IV and LVV-hemorphin 7, on spatial learning in rats. *Neuroscience* 124, 341–349. doi: 10.1016/j.neuroscience.2003.12.006
- Lew, R. A., Mustafa, T., Ye, S., McDowell, S. G., Chai, S. Y., and Albiston, A. L. (2003). Angiotensin AT4 ligands are potent, competitive inhibitors of insulin regulated aminopeptidase (IRAP). *J. Neurochem.* 86, 344–350. doi: 10.1046/j.1471-4159.2003.01852.x
- Liao, H., Keller, S. R., and Castle, J. D. (2006). Insulin-regulated aminopeptidase marks an antigen-stimulated recycling compartment in mast cells. *Traffic* 7, 155–167. doi: 10.1111/j.1600-0854.2006.00373.x
- Libby, P. (2006). Atherosclerosis: disease biology affecting the coronary vasculature. *Am. J. Cardiol.* 98, 3Q–9Q.
- Liu, G., Hou, J. C., Watson, R. T., and Pessin, J. E. (2005). Initial entry of IRAP into the insulin-responsive storage compartment occurs prior to basal or insulin-stimulated plasma membrane recycling. *Am. J. Physiol. Endocrinol. Metab.* 289, E746–E752.
- Lorenzl, S., Albers, D. S., Relkin, N., Ngyuen, T., Hilgenberg, S. L., Chirichigno, J., et al. (2003). Increased plasma levels of matrix metalloproteinase-9 in patients with Alzheimer's disease. *Neurochem. Int.* 43, 191–196. doi: 10.1016/s0197-0186(03)00004-4
- Lukaszuk, A., Demagdt, H., Szemenyei, E., Toth, G., Tymecka, D., Misicka, A., et al. (2008). Beta-homo-amino acid scan of angiotensin IV. *J. Med. Chem.* 51, 2291–2296. doi: 10.1021/jm701490g
- Maianu, L., Keller, S. R., and Garvey, W. T. (2001). Adipocytes exhibit abnormal subcellular distribution and translocation of vesicles containing glucose

- transporter 4 and insulin-regulated aminopeptidase in type 2 diabetes mellitus: implications regarding defects in vesicle trafficking. *J. Clin. Endocrinol. Metab.* 86, 5450–5456. doi: 10.1210/jcem.86.11.8053
- Matsumoto, H., Hattori, A., Mitzutani, S., and Tsujimoto, M. (2001a). "Cleavage of peptide hormones by placental leucine aminopeptidase/oxytocinase," in *Cell Surface Aminopeptidases: Basic and Clinical Aspects*, ed. S. Mitzutani (Nagoya: Elsevier Science BV), 295–299.
- Matsumoto, H., Nagasaka, T., Hattori, A., Rogi, T., Tsuruoka, N., Mizutani, S., et al. (2001b). Expression of placental leucine aminopeptidase/oxytocinase in neuronal cells and its action on neuronal peptides. *Eur. J. Biochem.* 268, 3259–3266. doi: 10.1046/j.1432-1327.2001.02221.x
- Moeller, I., Albiston, A. L., Lew, R. A., Mendelsohn, F. A., and Chai, S. Y. (1999a). A globin fragment, LVV-hemorphin-7, induces [3H]thymidine incorporation in a neuronal cell line via the AT4 receptor. *J. Neurochem.* 73, 301–308. doi: 10.1046/j.1471-4159.1999.0730301.x
- Moeller, I., Clune, E. F., Fennessy, P. A., Bingley, J. A., Albiston, A. L., Mendelsohn, F. A., et al. (1999b). Up regulation of AT4 receptor levels in carotid arteries following balloon injury. *Regul. Pept.* 83, 25–30. doi: 10.1016/s0167-0115(99)00047-6
- Moeller, I., Lew, R. A., Mendelsohn, F. A., Smith, A. I., Brennan, M. E., Tetaz, T. J., et al. (1997). The globin fragment LVV-hemorphin-7 is an endogenous ligand for the AT4 receptor in the brain. *J. Neurochem.* 68, 2530–2537. doi: 10.1046/j.1471-4159.1997.68062530.x
- Nakamura, H., Itakura, A., Okamura, M., Ito, M., Iwase, A., Nakanishi, Y., et al. (2000). Oxytocin stimulates the translocation of oxytocinase of human vascular endothelial cells via activation of oxytocin receptors. *Endocrinology* 141, 4481–4485. doi: 10.1210/endo.141.12.7832
- Nikolaou, A., Stijlemans, B., Laoui, D., Schoupe, E., Tran, H. T., Tourwe, D., et al. (2014). Presence and regulation of insulin-regulated aminopeptidase in mouse macrophages. *J. Renin. Angiotensin. Aldosterone Syst.* 15, 466–479. doi: 10.1177/1470320313507621
- Pan, X., Meriin, A., Huang, G., and Kandror, K. V. (2019). Insulin-responsive amino peptidase follows the Glut4 pathway but is dispensable for the formation and translocation of insulin-responsive vesicles. *Mol. Biol. Cell* 30, 1536–1543. doi: 10.1091/mbc.e18-12-0792
- Park, B. M., Cha, S. A., Lee, S. H., and Kim, S. H. (2016). Angiotensin IV protects cardiac reperfusion injury by inhibiting apoptosis and inflammation via AT4R in rats. *Peptides* 79, 66–74. doi: 10.1016/j.peptides.2016.03.017
- Peck, G. R., Ye, S., Pham, V., Fernando, R. N., Macaulay, S. L., Chai, S. Y., et al. (2006). Interaction of the Akt substrate, AS160, with the glucose transporter 4 vesicle marker protein, insulin-regulated aminopeptidase. *Mol. Endocrinol.* 20, 2576–2583. doi: 10.1210/me.2005-0476
- Pham, V., Burns, P., Albiston, A. L., Yeatman, H. R., Ng, L., Diwakarla, S., et al. (2009). Reproduction and maternal behavior in insulin-regulated aminopeptidase (IRAP) knockout mice. *Peptides* 30, 1861–1865. doi: 10.1016/j.peptides.2009.07.019
- Rifkin, I. R., Leadbetter, E. A., Busconi, L., Viglianti, G., and Marshak-Rothstein, A. (2005). Toll-like receptors, endogenous ligands, and systemic autoimmune disease. *Immunol. Rev.* 204, 27–42. doi: 10.1111/j.0105-2896.2005.00239.x
- Rogi, T., Tsujimoto, M., Nakazato, H., Mizutani, S., and Tomoda, Y. (1996). Human placental leucine aminopeptidase/oxytocinase. A new member of type II membrane-spanning zinc metallopeptidase family. *J. Biol. Chem.* 271, 56–61. doi: 10.1074/jbc.271.1.56
- Ross, S. A., Keller, S. R., and Lienhard, G. E. (1998). Increased intracellular sequestration of the insulin-regulated aminopeptidase upon differentiation of 3T3-L1 cells. *Biochem. J.* 330(Pt 2), 1003–1008. doi: 10.1042/bj3301003
- Royea, J., Martinot, P., and Hamel, E. (2019). Memory and cerebrovascular deficits recovered following angiotensin IV intervention in a mouse model of Alzheimer's disease. *Neurobiol. Dis.* 134:104644. doi: 10.1016/j.nbd.2019.104644
- Saveanu, L., Carroll, O., Weimershaus, M., Guernonprez, P., Firat, E., Lindo, V., et al. (2009). IRAP identifies an endosomal compartment required for MHC class I cross-presentation. *Science* 325, 213–217. doi: 10.1126/science.1172845
- Seyer, B., Diwakarla, S., Burns, P., Hallberg, A., Grnbladh, A., Hallberg, M., et al. (2019). Insulin-regulated aminopeptidase inhibitor-mediated increases in dendritic spine density are facilitated by glucose uptake. *J. Neurochem.* 153, 485–494. doi: 10.1111/jnc.14880
- Shi, J., Huang, G., and Kandror, K. V. (2008). Self-assembly of Glut4 storage vesicles during differentiation of 3T3-L1 adipocytes. *J. Biol. Chem.* 283, 30311–30321. doi: 10.1074/jbc.m805182200
- Swanson, G. N., Hanesworth, J. M., Sardinia, M. F., Coleman, J. K., Wright, J. W., Hall, K. L., et al. (1992). Discovery of a distinct binding site for angiotensin II (3-8), a putative angiotensin IV receptor. *Regul. Pept.* 40, 409–419. doi: 10.1016/0167-0115(92)90527-2
- Tchekalarova, J., Kambourova, T., and Georgiev, V. (2001). Effects of angiotensin III and angiotensin IV on pentylenetetrazol seizure susceptibility (threshold and kindling): interaction with adenosine A(1) receptors. *Brain Res. Bull.* 56, 87–91. doi: 10.1016/s0361-9230(01)00568-8
- Uvnas-Moberg, K., Ekstrom-Bergstrom, A., Berg, M., Buckley, S., Pajalic, Z., Hadjigeorgiou, E., et al. (2019). Maternal plasma levels of oxytocin during physiological childbirth - a systematic review with implications for uterine contractions and central actions of oxytocin. *BMC Pregn. Childbirth* 19:285. doi: 10.1186/s12884-019-2365-9
- Vinh, A., Widdop, R. E., Chai, S. Y., and Gaspari, T. A. (2008a). Angiotensin IV-evoked vasoprotection is conserved in advanced atheroma. *Atherosclerosis* 200, 37–44. doi: 10.1016/j.atherosclerosis.2007.12.042
- Vinh, A., Widdop, R. E., Drummond, G. R., and Gaspari, T. A. (2008b). Chronic angiotensin IV treatment reverses endothelial dysfunction in ApoE-deficient mice. *Cardiovasc. Res.* 77, 178–187. doi: 10.1093/cvr/cvm021
- Wallis, M. G., Lankford, M. F., and Keller, S. R. (2007). Vasopressin is a physiological substrate for the insulin-regulated aminopeptidase IRAP. *Am. J. Physiol. Endocrinol. Metab.* 293, E1092–E1102.
- Waters, S. B., D'Auria, M., Martin, S. S., Nguyen, C., Kozma, L. M., and Luskey, K. L. (1997). The amino terminus of insulin-responsive aminopeptidase causes Glut4 translocation in 3T3-L1 adipocytes. *J. Biol. Chem.* 272, 23323–23327. doi: 10.1074/jbc.272.37.23323
- Wayner, M. J., Armstrong, D. L., Phelix, C. F., Wright, J. W., and Harding, J. W. (2001). Angiotensin IV enhances LTP in rat dentate gyrus in vivo. *Peptides* 22, 1403–1414. doi: 10.1016/s0196-9781(01)00475-2
- Wright, J. W., Miller-Wing, A. V., Shaffer, M. J., Higginson, C., Wright, D. E., Hanesworth, J. M., et al. (1993). Angiotensin II(3-8) (ANG IV) hippocampal binding: potential role in the facilitation of memory. *Brain Res. Bull.* 32, 497–502. doi: 10.1016/0361-9230(93)90297-o
- Wu-Wong, J. R., Berg, C. E., Wang, J., Chiou, W. J., and Fissel, B. (1999). Endothelin stimulates glucose uptake and GLUT4 translocation via activation of endothelin ETA receptor in 3T3-L1 adipocytes. *J. Biol. Chem.* 274, 8103–8110. doi: 10.1074/jbc.274.12.8103
- Yamahara, N., Nomura, S., Suzuki, T., Itakura, A., Ito, M., Okamoto, T., et al. (2000). Placental leucine aminopeptidase/oxytocinase in maternal serum and placenta during normal pregnancy. *Life Sci.* 66, 1401–1410. doi: 10.1016/s0024-3205(00)00451-3
- Yang, H., Zeng, X. J., Wang, H. X., Zhang, L. K., Dong, X. L., Guo, S., et al. (2011). Angiotensin IV protects against angiotensin II-induced cardiac injury via AT4 receptor. *Peptides* 32, 2108–2115. doi: 10.1016/j.peptides.2011.09.015
- Yang, R., Smolders, I., De Bundel, D., Fouyn, R., Halberg, M., Demaegd, H., et al. (2008). Brain and peripheral angiotensin II type 1 receptors mediate renal vasoconstrictor and blood pressure responses to angiotensin IV in the rat. *J. Hypertens.* 26, 998–1007. doi: 10.1097/hjh.0b013e3282f5ed58
- Yeatman, H. R., Albiston, A. L., Burns, P., and Chai, S. Y. (2016). Forebrain neurone-specific deletion of insulin-regulated aminopeptidase causes age related deficits in memory. *Neurobiol. Learn. Mem.* 136, 174–182. doi: 10.1016/j.nlm.2016.09.017

**Conflict of Interest:** The authors declare that the research was conducted in the absence of any commercial or financial relationships that could be construed as a potential conflict of interest.

Copyright © 2020 Vear, Gaspari, Thompson and Chai. This is an open-access article distributed under the terms of the Creative Commons Attribution License (CC BY). The use, distribution or reproduction in other forums is permitted, provided the original author(s) and the copyright owner(s) are credited and that the original publication in this journal is cited, in accordance with accepted academic practice. No use, distribution or reproduction is permitted which does not comply with these terms.



# From Angiotensin IV to Small Peptidemimetics Inhibiting Insulin-Regulated Aminopeptidase

Mathias Hallberg<sup>1\*</sup> and Mats Larhed<sup>2</sup>

<sup>1</sup>The Beijer Laboratory, Division of Biological Research on Drug Dependence, Department of Pharmaceutical Biosciences, BMC, Uppsala University, Uppsala, Sweden, <sup>2</sup>Department of Medicinal Chemistry, Science for Life Laboratory, BMC, Uppsala University, Uppsala, Sweden

## OPEN ACCESS

### Edited by:

Efstratios Stratikos,  
National Centre of Scientific Research  
Demokritos, Greece

### Reviewed by:

Marcin Poreba,  
Wrocław University of Science and  
Technology, Poland  
Akira Hattori,  
Kyoto University, Japan

### \*Correspondence:

Mathias Hallberg  
Mathias.Hallberg@farmbio.uu.se

### Specialty section:

This article was submitted to  
Experimental Pharmacology  
and Drug Discovery,  
a section of the journal  
Frontiers in Pharmacology

**Received:** 03 August 2020

**Accepted:** 18 September 2020

**Published:** 15 October 2020

### Citation:

Hallberg M and Larhed M (2020) From  
Angiotensin IV to Small  
Peptidemimetics Inhibiting Insulin-  
Regulated Aminopeptidase.  
Front. Pharmacol. 11:590855.  
doi: 10.3389/fphar.2020.590855

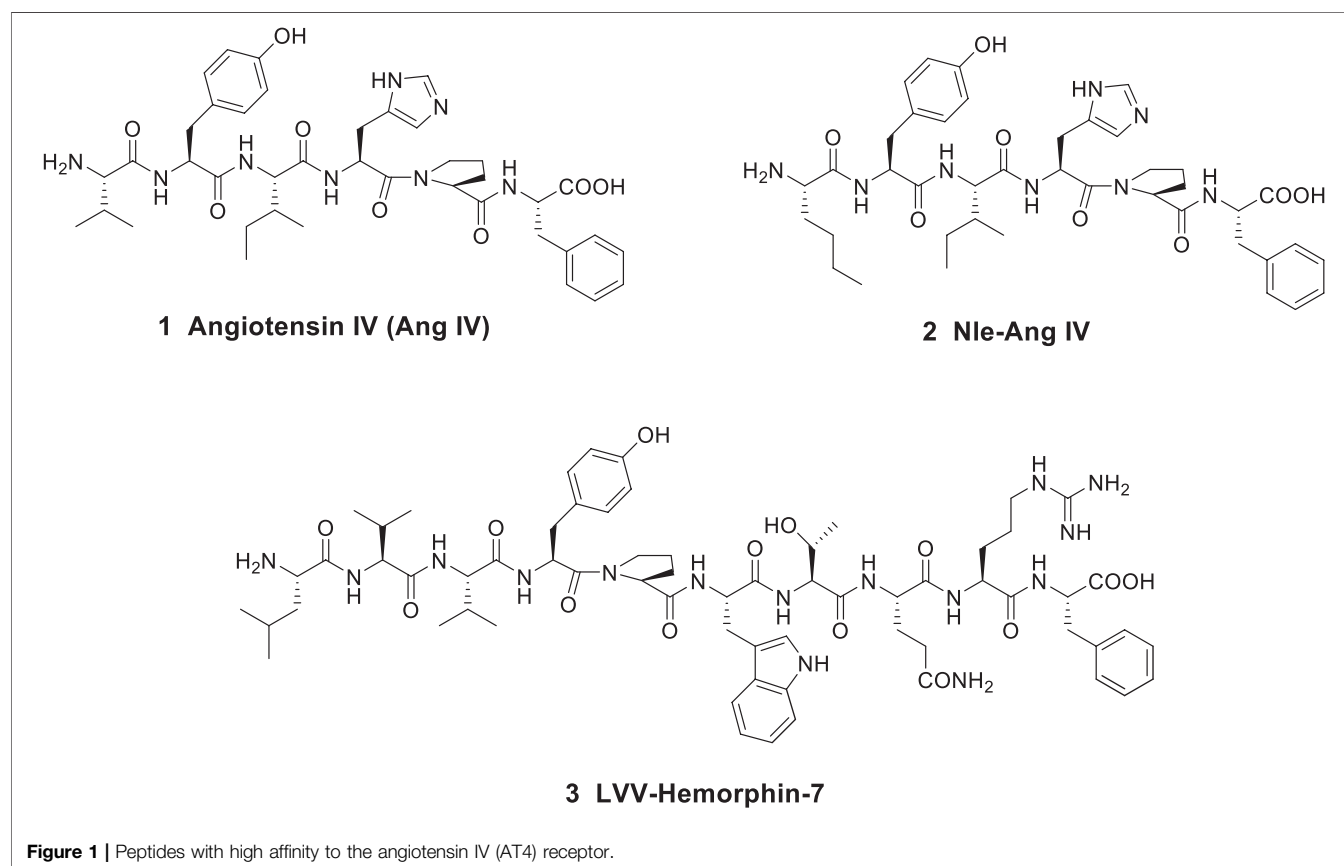
It was reported three decades ago that intracerebroventricular injection of angiotensin IV (Ang IV, Val-Tyr-Ile-His-Pro-Phe) improved memory and learning in the rat. There are several explanations for these positive effects of the hexapeptide and related analogues on cognition available in the literature. In 2001, it was proposed that the insulin-regulated aminopeptidase (IRAP) is a main target for Ang IV and that Ang IV serves as an inhibitor of the enzyme. The focus of this review is the efforts to stepwise transform the hexapeptide into more drug-like Ang IV peptidemimetics serving as IRAP inhibitors. Moreover, the discovery of IRAP inhibitors by virtual and substance library screening and direct design applying knowledge of the structure of IRAP and of related enzymes is briefly presented.

**Keywords:** angiotensin IV, peptidemimetics, aminopeptidase N, cystinyl aminopeptidase, insulin-regulated aminopeptidase

## INTRODUCTION

Angiotensin IV (Ang IV) is a small bioactive peptide in the renin-angiotensin system (RAS) formed after proteolytic degradation of angiotensin II (Ang II). In 1988, Braszko et al. (1988), at the Medical University of Białystok, Poland demonstrated that intracerebroventricular injection of Ang IV (Val-Tyr-Ile-His-Pro-Phe), **1** in rat (1 nmol dose) improved memory and learning (**Figure 1**). Furthermore, it was reported that Ang IV affects both passive and conditioned avoidance response as well as motor activity. The impact of the hexapeptide in various experimental models, e.g., for Barnes maze, swim mazes as well as radial arm mazes were subsequently explored (Wright et al., 1993; Wright et al., 1996; Wright et al., 1999; Lee et al., 2003; Braszko et al., 2008; De Bundel et al., 2009). Related Ang IV analogues were studied as well, such as Nle-Ang IV **2** (Nle-Tyr-Ile-His-Pro-Phe) and the endogenous LVV-hemorphin-7 **3** (Leu-Val-Val-Tyr-Pro-Trp-Thr-Gln-Arg-Phe), both with structural similarities to Ang IV at the N-terminal part of the peptides (**Figure 1**). Nle-Ang IV **2** and LVV-hemorphin-7 **3**, the latter formed after degradation of  $\beta$ -globin, were demonstrated to be strong promoters of memory retention and retrieval in rats (Lee et al., 2003; Lee et al., 2004; De Bundel et al., 2009). In 1992, Wright and Harding identified binding sites for the hexapeptide Ang IV in several brain areas associated with cognition, motor and sensory physiological functions (Swanson et al., 1992), e.g., in hippocampus (Harding et al., 1992). The encouraging data obtained after administration of Ang IV in the experimental models and the impact of Ang IV on parameters anticipated to be linked to cognition promoted an interest in more detailed studies of the hexapeptide.





Excellent reviews on Ang IV and its contribution to cognition are available (Gard, 2008; Albiston et al., 2011; Ho and Nation, 2018; Jackson et al., 2018; Wright and Harding, 2019). Herein we summarize the efforts the last three decades to transform the hexapeptide into more drug-like peptidemimetics acting at its receptor(s). We discuss from a medicinal chemistry perspective, starting points in the design processes and the very different approaches applied. The incorporation of various unnatural amino acid residues into peptides was proven to be a very productive methodology. The iterative stepwise modifications of the parent ligand Ang IV is first presented.

## LINEAR ANGIOTENSIN IV ANALOGUES AND INCORPORATION OF UNNATURAL AMINO ACIDS

After systematic structure activity studies (SAR) of Ang IV analogues, involving glycine and D-amino acid scans in combination with displacement and incorporation of various alternative amino acid residues it became clear that the N-terminal Val-Tyr-Ile residues of the peptide ligands were important for high affinity to the specific binding site identified (Sardinia et al., 1993), named the AT4 receptor (de

Gasparo et al., 1995). Furthermore, amino acid residues with hydrophobic side chains in the 1-position of the Ang IV analogues, e.g., a norleucine residue (cf. 2) combined with an unsubstituted amino group in the N-terminal seemed optimal. On the contrary, alterations in the C-terminal seemed less critical for activity and for instance a deletion of the C-terminal phenylalanine residue of 1 had only a minor impact and the binding affinity was essentially maintained (Sardinia et al., 1993; Sardinia et al., 1994; Krishnan et al., 1999).

Ang IV and related analogues are susceptible to proteolytic cleavage of the peptide bond between the Val<sup>1</sup> and Tyr<sup>2</sup> amino acid residues. Thus, a reduction of this N-terminal peptide bond rendered peptides significantly less prone to hydrolysis. Notably, most of the affinity to the binding site was still maintained. The Ang IV analogue peptide 4 and the Nle-Ang IV analogue 5 provide examples comprising two basic amino groups accessible for protonation in the N-terminal of the peptides and flanking hydrophobic 2-isopropyl and n-butyl side chains, respectively (Figure 2) (Sardinia et al., 1994). A reduced peptide bond between the amino acid residues Ile<sup>3</sup> (or Val<sup>3</sup>) and His<sup>4</sup> is the characteristic feature of divalinal-Ang IV 6 and norleual 7, two pseudopeptides that both for a long time served as important research tools (Krebs et al., 1996; Kramár et al., 2001).

In the late 1990s Taisho Pharmaceuticals filed patent applications covering compounds that according to

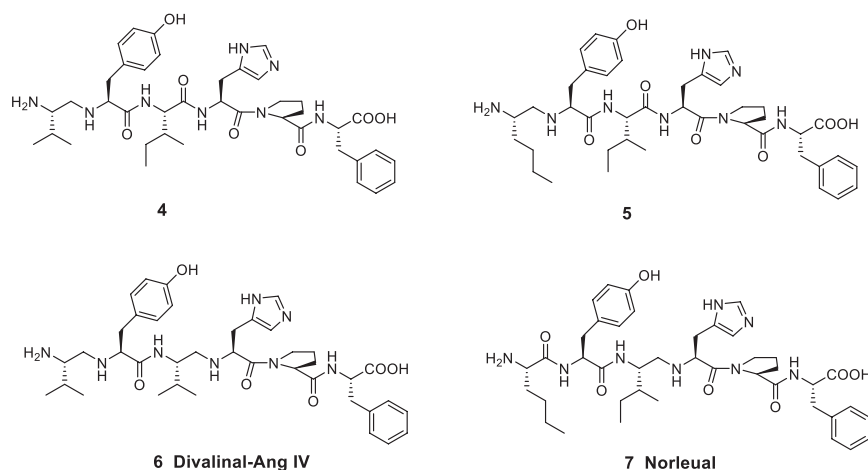


**Figure 2 |** Linear peptides with high affinity to the angiotensin IV (AT4) receptor and that are less prone to proteolytic degradation.

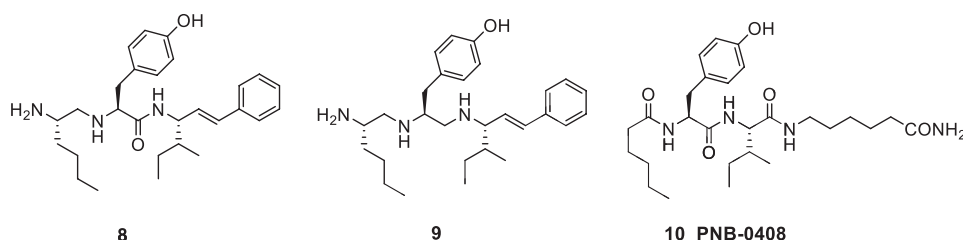


**Figure 3 |** The low molecular weight high-affinity angiotensin IV (AT4) receptor binding analogues **8** and **9** incorporate one or two reduced peptide bonds. PNB-0408 (**10**), devoid of an N-terminal amino group crosses the blood-brain barrier, enhances cognition and is interfering with the hepatocyte growth factor/c-Met receptor system.

competitive experiments with radiolabeled [ $^{125}$ I]Ang IV exhibited high affinity to hippocampus membranes from guinea pig (Kobori et al., 1997; Kobori et al., 1998). Kobori et al. (1997), Kobori et al. (1998) characterized the compounds as Ang IV receptor agonists and some of them, e.g., **8** with the straight four-carbon chain of the Nle residue at position one, exhibited very high affinity to the binding site ( $IC_{50}$  values < 1 nM) (**Figure 3**). The drug-like **8** encompasses a styrene moiety replacing His-Pro-Phe residues in the C-terminal of Ang IV. Furthermore, it was demonstrated that saturation of the *trans* styrene double bond of **8** was deleterious for activity. Reduction of the remaining peptide bond of **8** furnished **9**, a compound that still bind to the binding site although with 40 times lower affinity. From the series of compounds that were disclosed it appears that the binding site favors two amine functions in the N-terminal part of the ligands in order to achieve an efficient binding to the receptor (cf. **4**, **5**, **6**). Hence, a compound with an intact peptide bond between the Nle<sup>1</sup> and Tyr<sup>2</sup> residues but with a reduced peptide bond between the Tyr<sup>2</sup> and Ile<sup>3</sup> residues was essentially inactive (Kobori et al., 1997; Kobori et al., 1998).

In 2001, Albiston and Chai suggested that Ang IV exerts its procognitive actions by inhibition of a peptidase, insulin-regulated aminopeptidase (IRAP) (Albiston et al., 2001) and not through binding to a G-protein-coupled receptor as is the

case of its major precursor angiotensin II (Ang II, Asp-Arg-Val-Tyr-Ile-His-Pro-Phe), that mediates its effects mainly through the Ang II receptor type 1 (AT1R) and the angiotensin receptor type 2 (AT2R). Thus, while the octapeptide Ang II exerts a powerful hypertensive effect and acts as a receptor agonist, it is degraded by proteolysis to a bioactive hexapeptide metabolite with a very different pharmacological profile that acts as an enzyme inhibitor. Notably, there are several other examples known demonstrating that small neuropeptides can be converted into fragments with significantly different biological effects, e.g., the nociceptive substance P is degraded to the antinociceptive substance P (1–7) (Fransson et al., 2008; Hallberg, 2015). Ang IV binds to both AT1R and AT2R but only at micromolar concentrations (Bosnyak et al., 2011; Hallberg et al., 2017). Furthermore, the IRAP inhibitors Ang IV (**1**) and LVV-hemorphin-7 (**3**) (Lee et al., 2003; Lew et al., 2003) inhibit also aminopeptidase N (AP-N, EC 3.4.11.2) activity (Garreau et al., 1998; Fruitier-Arnaudin et al., 2002) and LVV-hemorphin-7 (**3**), in addition, binds to the  $\mu$ -opioid receptor (Nyberg et al., 1996).

IRAP (EC 3.4.11.3) is a single-spanning transmembrane zinc-metallopeptidase that belongs to the M1 family of aminopeptidases. The enzyme was cloned and characterized in adipocytes in vesicles containing the insulin-regulated glucose

transporter GLUT4 (Keller et al., 1995; Keller, 2003), was identified as placental leucine aminopeptidase, oxytocinase, gp160 and vp165 and is a cystinyl aminopeptidase (Tsujimoto et al., 1992; Kandror and Pilch, 1994; Rogi et al., 1996; Rasmussen et al., 2000; De Bundel et al., 2008). IRAP is able to cleave the peptide bond between the N-terminal amino acid residues from several bioactive peptides *in vitro*, e.g., met-enkephalin and leu-enkephalin, dynorphin A, lysine-bradykinin, neurokinin A1, cholecystokinin-8, somatostatin, oxytocin and vasopressin (Lew et al., 2003) although the key substrates seem to be the macrocyclic oxytocin and arginine-vasopressin (Albiston et al., 2010a). Studies on the IRAP knockout (KO) mice suggest that vasopressin, oxytocin and somatostatin are physiologically important substrates (Wallis et al., 2007; De Bundel et al., 2015). Hence, the N-terminal peptide bonds of macrocyclic peptidic regulators of cognition, as vasopressin and oxytocin can be cleaved (Alescio-Lautier et al., 2000; Matsumoto et al., 2000; Matsumoto et al., 2001; Wallis et al., 2007). The aminopeptidase is expressed in areas of the brain associated with cognition (Fernando et al., 2005; Albiston et al., 2007; Albiston et al., 2011), and the observation that Ang IV improves memory and learning has attracted attention to the aminopeptidase IRAP as a potential macromolecular target for drugs for treatment of cognitive disorders (Wolfe, 2002; Gard, 2008; Wright and Harding, 2008; Hallberg, 2009). Moreover, the enzyme mediates a series of other important physiological activities that are related to immunology (Stratikos, 2014), e.g., antigen processing and trafficking of T-cells receptors and of glucose transporters (Waters et al., 1997; Bryant et al., 2002). The catalytic site of IRAP is located in the extracellular region and is highly homologous to two other important members of the M1 aminopeptidase family, endoplasmic reticulum aminopeptidase 1 (ERAP1) and 2 (ERAP2) (Evnouchidou et al., 2009). IRAP, ERAP1, and ERAP2 are the three so-called antigen processing aminopeptidases responsible for the processing of the N-terminus of antigenic peptides and the activity of the three enzymes constitutes an important regulatory node in antigen processing, *vide infra* (Stratikos, 2014).

It should be emphasized that macromolecular targets other than IRAP have been proposed to account for the positive physiological effects on cognition observed *in vivo* after administration of Ang IV and related analogues (Vanderheyden, 2009; Kawas et al., 2012; Benoist et al., 2014). The tyrosine kinase receptor c-Met that binds hepatocyte growth factor (HGF) and that is associated with memory and learning consolidation is one candidate (Wright et al., 2008; Yamamoto et al., 2010) being implicated in Alzheimer's disease (AD) (Wright and Harding, 2011). Consequently, it is suggested that Ang IV exerts its action through the c-Met signaling pathway (Wright and Harding, 2019) and an overexpression HGF in the nervous system enhances learning and memory performance in mice (Kato et al., 2012). The Ang IV analogue Norleual 7 inhibits HGF-mediated effects at picomolar concentrations and blocks [ $^{125}$ I]HGF binding to c-Met (Yamamoto et al., 2010). The drug-like PNB-0408 (N-hexanoyl-Tyr-Ile-N'-(5-carbamoylpentyl) amide **10**, synthesized in the laboratories of Wright and Harding is of particular interest and penetrates the blood-

brain barrier and improves cognitive activity. (**Figure 3**) (Wright and Harding, 2008; Wright and Harding, 2009; McCoy, 2010). PNB-0408 (dihexa) with a primary amid function in the C-terminal attached via a lipophilic tether to the Ile residue is devoid of the N-terminal amino group found in most Ang IV analogues, *vide supra*. The compound **10**, derived from Nle-Ang IV **2** facilitates formation of new functional synaptic connections, facilitates LTP in hippocampal slices and amplifies memory consolidation in animal models of AD (Wright and Harding, 2015; Wright and Harding, 2019). Even though the brain hepatocyte growth factor/c-Met receptor system has attracted considerable attention (Wright and Harding, 2019), with regard to synthesis of small molecules and medicinal chemistry, it seems that most efforts so far have been devoted to identify new selective inhibitors of IRAP. To the best of our knowledge, no data on inhibition of IRAP by compounds **8** and **9** and related ligands from the Kobori laboratory nor by PNB-0408 (**10**) are yet available in literature.

After the pioneering work by Wright and Harding at Washington State University and by Kobori et al. (1997), Kobori et al. (1998). at Taisho Pharmaceuticals in Japan who identified low molecule strong binders to the Ang IV receptor in the 1990s, several groups have been engaged in the search for improved compounds interacting with the Ang IV receptor. The fundamental discovery by Albiston and Chai that IRAP is a molecular target for Ang IV and that IRAP seems to play an important physiological role and is associated with cognition encouraged focused research aimed at identifying new efficient IRAP inhibitors that could serve as pharmaceutical agents. Several complementary approaches were applied; 1) iterative modifications of the endogenous Ang IV, 2) virtual and substance library screening, and 3) direct design applying knowledge of the structure of IRAP. To make orally bioavailable IRAP inhibitors that reach the brain and that are metabolically relatively stable is a tremendous challenge.

Previously metal chelators (e.g., EDTA and phenantroline) were normally added in the experimental settings for determination of binding affinity. Although many of the ligands that in the 1990 ties had been identified as high-affinity binders inhibit IRAP (Lee et al., 2003; Lew et al., 2003), the ligands often demonstrated differences in potencies and rank orders in the IRAP assay in experiments where chelators were absent. It was postulated that the differences observed were attributed to the absence of zinc in the active site in presence of metal chelators (Lew et al., 2003; Demaegdt et al., 2004; Laeremans et al., 2005; Demaegdt et al., 2006). It became apparent that chelators must be omitted to obtain physiologically relevant data (Demaegdt et al., 2009).

Introduction of unnatural amino acids into peptide structures was demonstrated to provide a successful concept in the search for potent and metabolically stable inhibitors of IRAP. Hence, a  $\beta$ -homoamino acid scan of Ang IV performed at Vrije University in Brussels resulted in the identification of the metabolically stable derivative **11** (AL-11) with five-fold higher affinity to IRAP than Ang IV ( $K_i = 7.6$  vs. 62 nM for Ang IV) and exhibiting a high selectivity for IRAP over AP-N (**Figure 4**) (Lukaszuk et al., 2008). Thus, insertion of methylene groups in

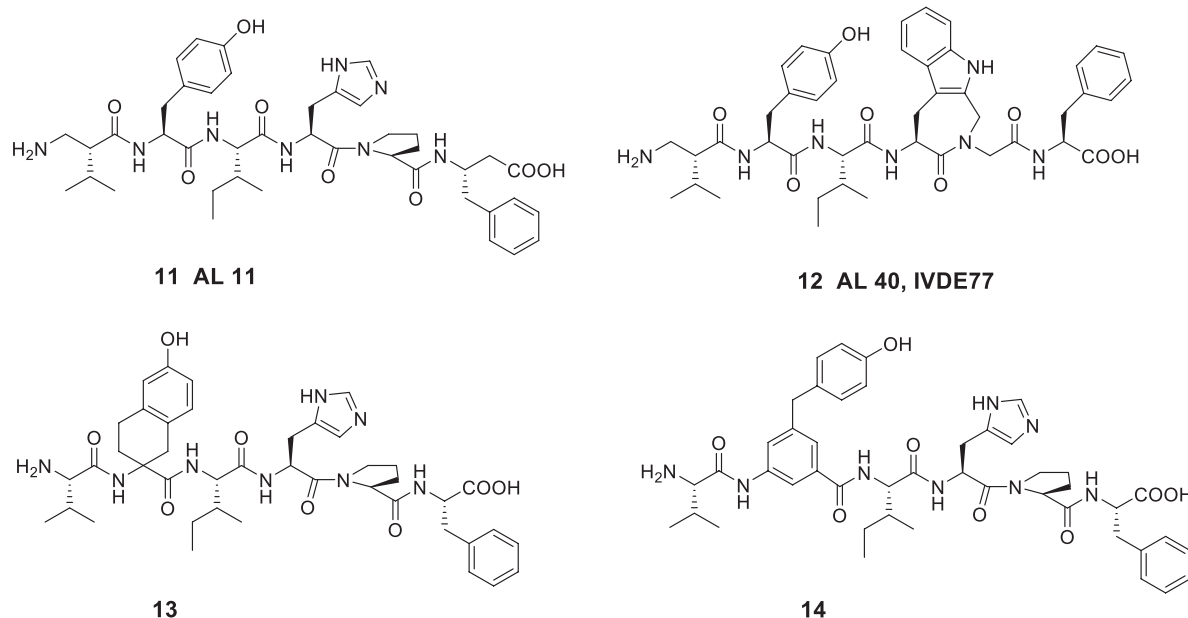


**Figure 4 |** The high affinity and metabolically stable IRAP inhibitors **11** (AL-11) and **12** (AL-40) both comprising  $\beta$  amino acid residues. The compounds **13** and **14** where the Tyr<sup>2</sup> residue is replaced are inactive as IRAP inhibitors.

both in the N- and C-terminals of Ang IV improved the inhibitors. The His<sup>4</sup> and Pro<sup>5</sup> residues of Ang IV were subsequently replaced by conformationally constrained residues and the highly selective and stable IRAP inhibitor **12** (AL-40, IVDE77) was identified, with >30-fold higher affinity ( $K_i = 1.7$  nM) than Ang IV and improved both selectivity and metabolic stability (Lukaszuk et al., 2008; Lukaszuk et al., 2009; Nikolaou et al., 2013). In addition, the Belgium group assessed the roles of Tyr<sup>2</sup>, Pro<sup>5</sup>, and Phe<sup>6</sup> in Ang IV by systematic incorporation of constrained residues. The replacements of Tyr<sup>2</sup> by residues with restricted flexibility were deleterious for activity. For example, the compound **13** (racemic) is a very weak IRAP inhibitor (Lukaszuk et al., 2011) and compound **14** with a 4-hydroxydiphenylmethane scaffold as a substitute for Tyr<sup>2</sup> is essentially inactive (**Figure 4**) (Andersson et al., 2008). Thus, in summary the lipophilic character of the side chain in position **1** is essential and the proper orientation of the Tyr<sup>2</sup> side chain in space is critical for activity and IRAP inhibition while various alternations and topography at the C-terminal are more acceptable.

## MACROCYCLIC ANGIOTENSIN IV ANALOGUES

The capability of IRAP to degrade physiologically important cyclic peptides has inspired the development of macrocyclic analogues of Ang IV. Our group synthesized a series of macrocyclic peptides with the aim to determine bioactive conformations and better understand the mode of binding and structural requirements for efficient binding of Ang IV to IRAP (Axén et al., 2006; Axén et al., 2007; Andersson et al., 2010;

Andersson et al., 2011). Steric constraints were introduced. Attempts to obtain high affinity binding inhibitors by cyclization in the C-terminal was productive as expected from previously obtained data. Hence, the macrocyclic disulphide **15** encompassing an 11-membered macrocycle was more potent as an IRAP inhibitor than the native Ang IV and exhibited a  $K_i$  value of 26 nM (**Figure 5**). Since the macrocyclic system of **15**, as deduced from modeling tends to adopt a  $\gamma$ -turn (Schmidt et al., 1997; Lindman et al., 2001), the entire C-terminal tripeptide fragment His-Pro-Phe was replaced by a 2-(aminomethyl) phenylacetic acid moiety anticipated to serve as a proper  $\gamma$ -turn mimic. The structurally simplified Ang IV peptidomimetic **16** was almost as active as Ang IV as an IRAP inhibitor while **17** was five-fold and **18** and the open chain **19** were 20-fold less active (**Figure 5**). Furthermore, compound **16** is degraded considerably more slowly in membrane preparations than Ang IV and stimulates proliferation of mouse neural stem cells at low concentrations, supporting a role of IRAP in neurogenesis (Axén et al., 2007).

Contrary to the results obtained after modification in the C-terminal of Ang IV where essentially all compounds examined exhibited some activity, oxidative cyclization of the side chains of Cys<sup>1</sup> and Cys<sup>3</sup> and consequently creation of an 11-membered disulfide macrocycle in the N-terminal rendered the inactive compound **20** (**Figure 6**). However, a widening of the ring system was productive and the Ang IV analogue **21** with a 13-membered macrocycle exhibited a moderate IRAP inhibitory capacity. Compound **22**, a hybrid with the N-terminal from **21** and the C-terminal from **16** demonstrated a further enhanced potency ( $K_i = 23$  nM) and a high selectivity for IRAP over AP-N (Andersson et al., 2010). Notably **16**, devoid of a macrocyclic ring



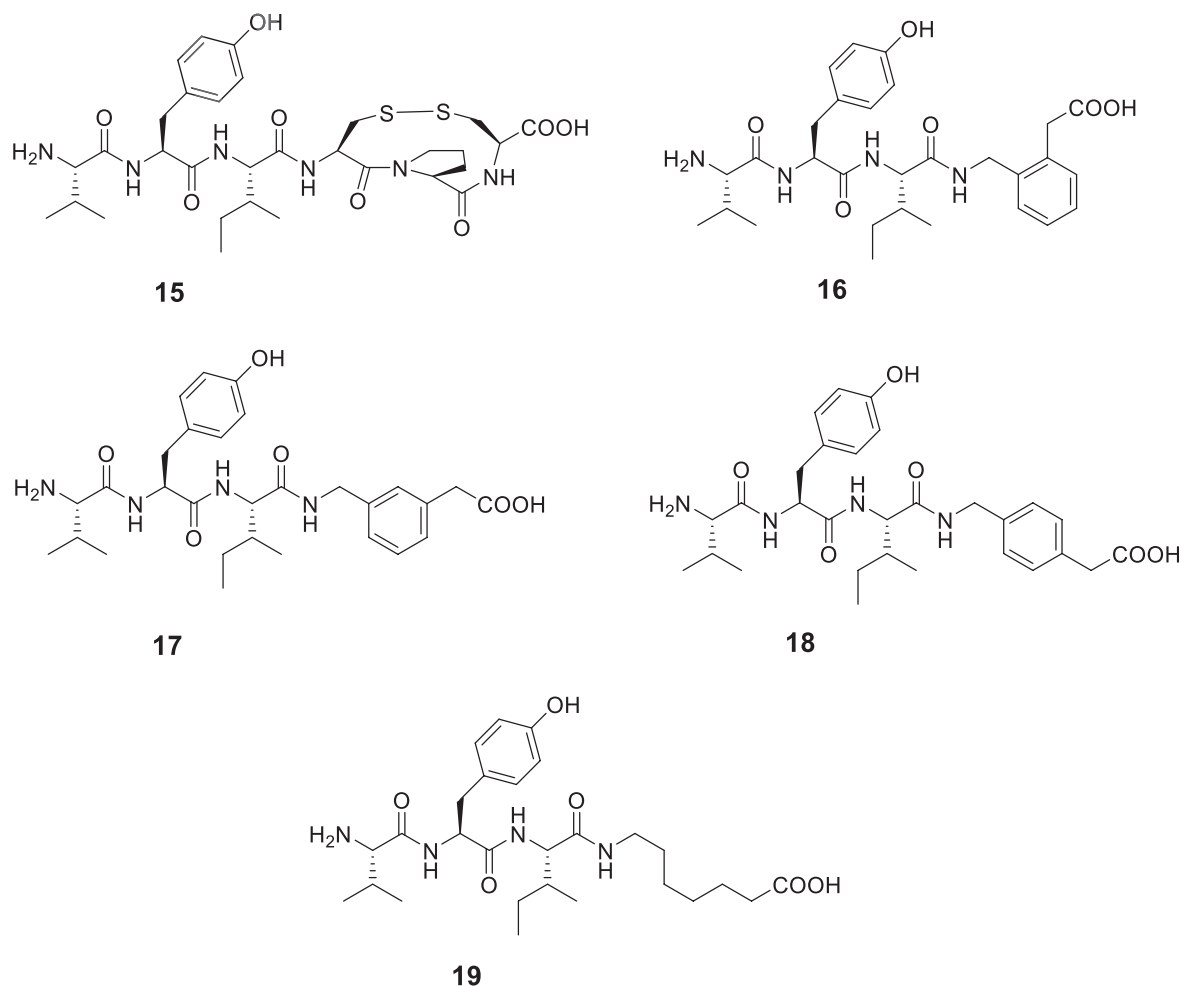


**Figure 5 |** Modifications in the C-terminal. Compound **15** with an 11-membered macrocyclic ring adopting a  $\gamma$ -turn in the C-terminal binds better than Ang IV to IRAP and **16** with a scaffold serving as a  $\gamma$ -turn mimetic incorporated in the C-terminal is essentially as active as Ang IV. Compounds **17**, **18**, and **19** bind to IRAP but are more than five-fold less potent.

system in the N-terminal is not selective and inhibits both IRAP and AP-N activity, suggesting that introduction of proper conformational constraints in the N-terminal by macrocyclization improves selectivity (Axén et al., 2007). As deduced from molecular modeling, **15** and Ang IV seem to adopt a  $\gamma$ -turn at the C-terminal when binding to IRAP, while in the case of **21**, a less well-defined turn conformation is adopted at the N-terminal. Further structural optimization delivered a large number of macrocyclic disulfides and among them **23** (HA08) encompassing a  $\beta$ 3-homotyrosine residue in a 13-membered ring system and exhibiting the lowest  $K_i$  value in the series ( $K_i = 3.3$  nM). HA08 is formed after an Hcy<sup>1</sup>/Cys<sup>3</sup> side chain cyclization and is a competitive inhibitor and 20 times more potent than Ang IV and less prone to proteolytic degradation (Figure 6). The compound was designed to provide both high IRAP inhibitory capacity and an improved metabolic stability attributed to the introduction of an  $\beta$ -amino acid residue adjacent to the predicted scissile peptide bond. Enlargement of the ring system of **23**, by oxidative cyclization of Hcy<sup>1</sup>/Hcy<sup>3</sup> side chains

rather than the Hcy<sup>1</sup>/Cys<sup>3</sup> side chains of **23** resulted in a compound comprising a 14-membered macrocycle but with a somewhat lower affinity to IRAP ( $K_i = 5.1$  nM), *vide infra*. Furthermore, one important characteristic of **23** (HA08) is its high 2,000-fold selectivity for IRAP over AP-N and high selectivity vs. the homologous enzymes ER aminopeptidase 1 (ERAP1) and ER aminopeptidase 2 (ERAP2). Replacement of the L-amino acids of **23** with D-amino acids were not productive (Andersson et al., 2010). Deletion of the N-terminal amino group of **23** had a dramatic effect. Hence, **24** is inactive as an IRAP inhibitor, cf. the potent cognitive enhancer **10** (PNB-0408, dihexa), derived from Ang IV, *vide supra*. Furthermore, removal of the methylene carboxy group at the C-terminal of **23** resulted in a less efficient IRAP inhibitor. Introduction of a primary carboxamide in the C-terminal (cf. PNB-0408, **10**) to replace the carboxy group of **23** provided **25** that inhibits IRAP but exhibits a two-fold lower activity (Figure 6). A reduction of the N-terminal peptide bond of **25**, with the ambition to achieve a compound even more resistant to proteolytic cleavage, provided

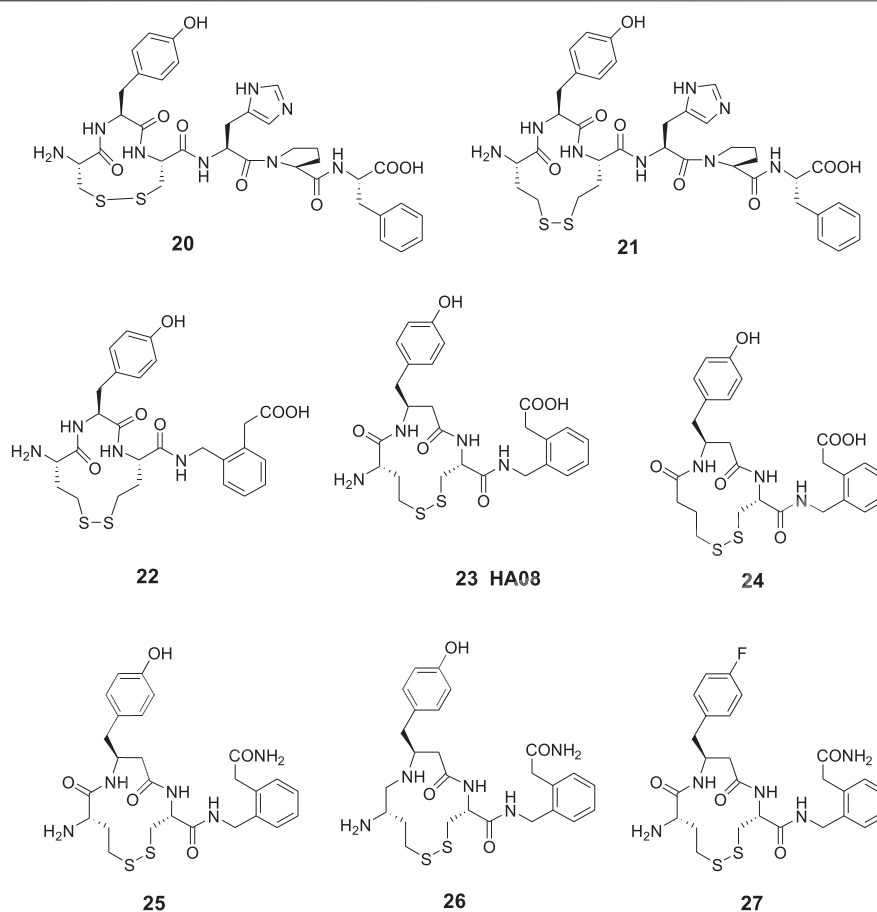


**Figure 6 |** Macrocyclizations in the N-terminal. The Ang IV analogue **20** encompassing an 11-membered macrocycle is inactive while **21** with a 13-membered ring system inhibits IRAP efficiently. The selective compound **23** (HA08) is the most potent IRAP inhibitor in the series and deletion of the N-terminal amino group of **23** makes the ligand (**24**) inactive. The carboxamide **25** is two-fold and the fluoro compound **27** is 10-fold less potent than **23** as IRAP inhibitors. Compound **26** comprising a reduced peptide bond in the N-terminal is a weak IRAP inhibitor.

**26** (Barlow et al., 2020). This maneuver was not fruitful and compound **26** displays a  $K_i$  value in the micromolar range in sharp contrast to what could be expected considering the results obtained after reduction of Ang IV or Nle-Ang IV, cf. **1** vs. **4** and **2** vs. **5** where the bioactivities were essentially retained after reduction of the carbonyl group of the peptide bond, *vide supra*. Moreover, in attempts to replace the hydroxyl group of the tyrosine moiety to avoid potential problems with phase II metabolism compound **27** was prepared (Barlow et al., 2020). This fluoro compound (**27**) is 10-fold less potent than **25** demonstrating that interactions with the hydroxyl group is important, although not critical for activity.

Crystal structures of IRAP were recently solved (Hermans et al., 2015; Mpakali et al., 2015). Based on analyses of available crystal structures a tentative model for **23** (HA08) binding to IRAP was created in 2016 by applying MD simulations and calculating associated binding free energies by the linear interaction energy (LIE) method. According to the model, the carbonyl group of the N-terminal peptide bond of **23** is coordinated to the  $Zn^{2+}$  ion, whereas the terminal amine is fixed by three glutamate carboxylates (Glu431, Glu487, and

Glu295) (Diwakarla et al., 2016b). Regarding the affinity of the fluoro compound **27**, it was anticipated that the hydroxyl group of the tyrosine side chain of **25** makes a hydrogen-bond with Glu494 of IRAP, an interaction that is lost in the case of **27** according to the free energy perturbation (FEP) analysis (Jespers et al., 2019), explaining the reduction in binding affinity of compound **27** as compared to the analogous compound **25**. Moreover, it was postulated that the aromatic ring of the  $\beta$ 3-homotyrosine side chain and the C-terminal phenyl ring interact and Phe550 in IRAP further stabilizes aromatic/hydrophobic packing (Barlow et al., 2020).

More recently, a crystal structure of IRAP with the macrocyclic peptide inhibitor **23** (HA08) was reported (Mpakali et al., 2020). After a comparison with the known IRAP structures and a combination with small angle X-ray scattering experiments it was proposed that IRAP is an open dimer in solution and assumes a more compact conformation upon HA08 binding. Thus, **23** (HA08) stabilizes the closed conformation of IRAP. Compound **23** is combining the structural elements from Ang IV and the physiological substrates vasopressin and oxytocin. The cleavage of the

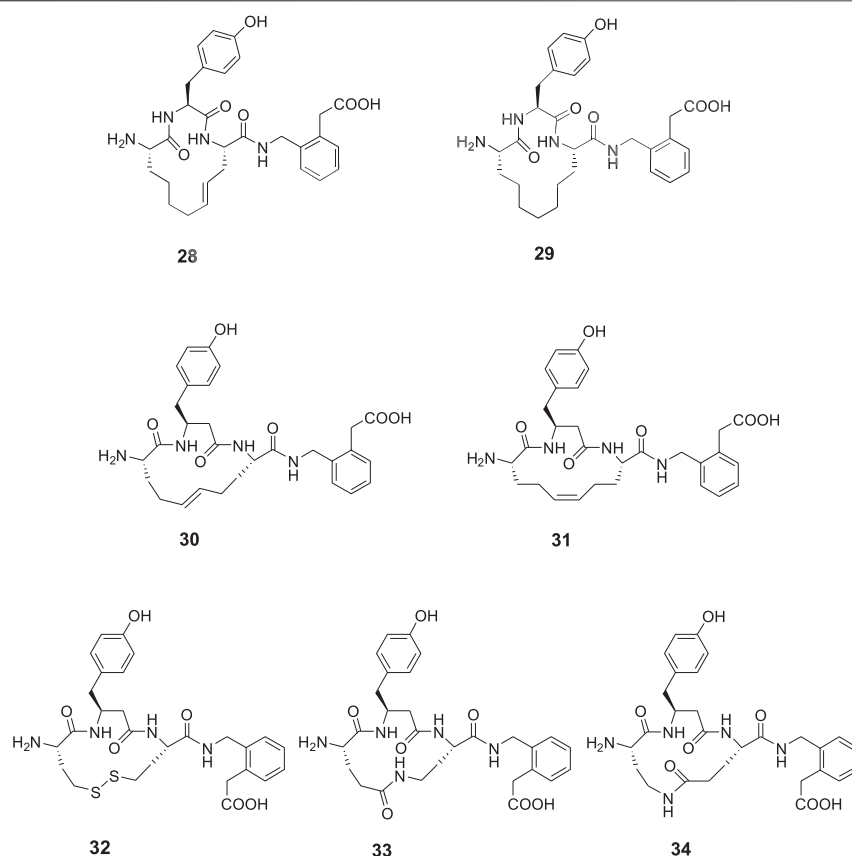


**Figure 7 |** Macrocyclizations in the N-terminal. A comparison of the activity of a series of cyclized Ang IV analogues encompassing 14-membered ring systems. The macrocyclic **28** and **30**, made by metathesis reactions are the most potent IRAP inhibitors in the series and somewhat more potent than the disulfide analogue **32**. Compound **29** with a saturated carbon bridge and the *cis* isomer **31** are 10-fold less potent and the amides **33** and **34** more than 100-fold less potent than the most effective IRAP inhibitor compound **30**.

scissile bond of substrates as oxytocin and vasopressin is anticipated to take place after a nucleophilic attack by water assisted by the carboxylate function of Glu465 in the active site of IRAP. Importantly, the corresponding cleavage of the scissile bond of the 13-membered **23** (HA08) in the closed conformation of IRAP is less prone to occur since there is not enough space for motion of water molecules to interact with the carboxylate group of Glu465. In fact, no ordered water molecule is found in the crystal structure at that location. The structure reveals that the side-chain of the  $\beta$ -tyrosine amino acid residue is situated in the S1 pocket of the enzyme and that the disulfide bond abuts to the S1' pocket. The phenylacetic acid group of HA08 was found in two different orientations; *a*) the carboxyl group makes electrostatic interactions with Arg439 and Arg929 of IRAP and *b*) phenyl ring of the phenylacetic acid group makes pi-stacking interactions with Tyr961. Moreover, it was suggested from inhibition data that **23** (HA08) acting through a competitive mechanism and Ang IV may occupy the same binding site and operate by the same mode of action. The structure of the IRAP (Mpakali et al., 2020) was found very similar to that reported previously with a phosphinic pseudotripeptide transition-state analogue binding to the enzyme, *vide infra* (Mpakali et al., 2017).

It was concluded that HA08 binds to IRAP in a very similar conformation to what was proposed by the MD simulations (Diwakarla et al., 2016b; Barlow et al., 2020).

The metathesis reaction was applied to obtain a series of macrocyclic compounds, devoid of the reactive disulfide function and with the potential to become oral bioavailable and more metabolically stable (Driggers et al., 2008; Marsault and Peterson, 2011). Several carba analogues comprising a 13- or 14-membered heterocycle were synthesized and assessed (Andersson et al., 2011). Among those, the tyrosine derivative **28** exhibited a  $K_i$  value of 4.1 nM and the corresponding analogue with a saturated double bond, compound **29**, a  $K_i$  value of 25 nM, demonstrating that a proper constrain of flexibility of the ring system, alternatively an electron density in the center of the lipophilic bridge between amino acid residues in positions 1 and 3 is favorable for affinity to IRAP (Figure 7). Compound **30** encompassing a homo tyrosine in a 14-membered macrocycle and with a *trans* double bond provided the lowest  $K_i$  value in the series, 1.8 nM, while the corresponding tyrosine analogues with the 13-membered ring system exhibited a  $K_i$  value of 50 nM. Compound **31**, the *cis* isomer of **30**, demonstrated a lower affinity to the enzyme ( $K_i$  = 30.4 nM). The high activity of **30** prompted a

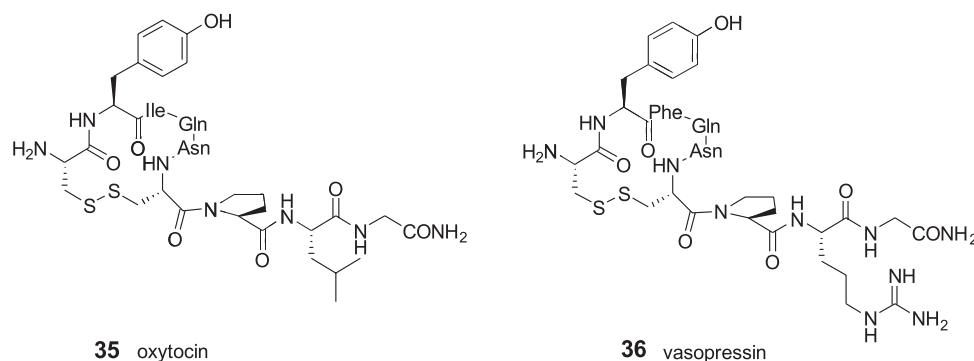


**Figure 8 |** The macrocyclic disulfides oxytocin (**35**) and vasopressin (**36**) are IRAP substrates.

synthesis of the corresponding disulfide **32** with a 14-membered ring system anticipated be able to adopt a similar “trans conformation” as **30**. A high activity was encountered,  $K_i = 5.1$  nM, to be compared with **23** (HA08) with a  $K_i$  of 3.3 nM, the latter comprising a 13-membered macrocyclic system. Insertion of amide bonds at various locations in the carbon chain was not productive. The lactams **33** and **34** comprising 14-membered ring systems were most active in the series but nonetheless 100-fold less potent than the best disulfide and carba analogues (Barlow et al., 2020).

The disulfide and carba analogues examined demonstrated a relative high stability against proteolysis by metallopeptidases, despite the similarities in the N-terminal to oxytocin **35** and vasopressin **36** that both serve as substrates to IRAP (Alescio-Lautier et al., 2000; Matsumoto et al., 2000; Matsumoto et al., 2001; Wallis et al., 2007; Hermans et al., 2015). This is most likely attributed to the inability of the constrained 13- and 14-membered macrocycles to adopt the proper transition states required for cleavage of the N-terminal peptide bond (Andersson et al., 2011) (**Figure 8**).

To conclude, macrocyclizations by oxidative disulfide formations in the N-terminal of Ang IV analogues or alternatively displacement of the disulfide unite with a *trans* double bond can provide very potent inhibitors of IRAP, as exemplified with **23** (HA08) comprising a 13-membered ring system and **28**, **30**, and **32** comprising 14-membered ring systems. Macrocyclization can convey drug-like properties of larger molecules (Driggers et al., 2008; Brandt et al., 2010; Marsault and Peterson, 2011; Mallinson and Collins, 2012; Giordanetto and Kihlberg, 2014) that includes improved membrane permeability compared to acyclic matched pairs and oral bioavailability but also often improved affinity for the target, improved selectivity and reduced metabolism (Hess et al., 2008; Bogdan et al., 2011; Yap et al., 2016).

The macrocycle **23** was selected as a proper research tool for more detailed studies since the molecule is convenient to prepare and due to its structural similarity to the IRAP substrates oxytocin and vasopressin in its N-terminal. A decline in the dendritic spine density (DSD) is an early characteristic feature of many neurodegenerative diseases (Fiala et al., 2002; Bourne and Harris, 2008; van Spronsen and Hoogenraad, 2010; Penzes et al.,

2011) and drugs able to enhance DSD are suggested as potential candidates for future treatment of memory disorders (Lynch et al., 2008). Dendritic spines, small protrusions from the dendrites that acts as contacts with neighboring axons and contain all of the molecular machinery required for synaptic plasticity and storage of memories. Hence, the procognitive activity of a molecule *in vivo* correlates well with its *in vitro* ability to alter dendritic spine structure and DSD (Moser et al., 1994; O'Malley et al., 1998; O'Malley et al., 2000; Benoist et al., 2011; Fu et al., 2012; Lai et al., 2012; McCoy et al., 2013). The specific loss of stubby/mushroom spines, which morphologically are characterized by a larger spine head and functionally have stronger synapses (Nusser et al., 1998; Matsuzaki et al., 2001; Murthy et al., 2001) is assumed to have a more pronounced impact on cognitive decline (Kasai et al., 2003). The competitive IRAP inhibitor **23** (HA08) enhances the numbers of dendritic spines in hippocampal cell cultures and HA08 treatment resulted in an increasing number of stubby and mushroom-like spines, a morphology typically associated with mature spines, which are believed to have strengthened synaptic connectivity. The dendritic spines were also vesicular glutamate transporter 1 (vGLUT1) positive, indicating that spines were receptive to glutamatergic signaling. Notably, in contrast to **23** (HA08), a structurally very similar epimer (HA09) which differs only with regard to one stereogenic center and exhibiting a 100-fold lower affinity to IRAP did not affect spine morphology, indicating a correlation between the capacity to inhibit IRAP and a positive impact on DSD and spine morphology. HA09 comprises a Cys<sup>3</sup> residue with *R* rather than *S*-configuration. The effect of **23** (HA08) was similar to that of brain-derived neurotrophic factor (BDNF) that is a known inducer of spine development (Diwakarla et al., 2016b).

## SMALL MOLECULE INSULIN-REGULATED AMINOPEPTIDASE INHIBITORS FROM *IN SILICO* SCREENING

In 2008, Siew Chai and her group in Australia disclosed the first generation of drug-like small molecular weight inhibitors of IRAP (Albiston et al., 2008). An *in silico* screening of a homology model



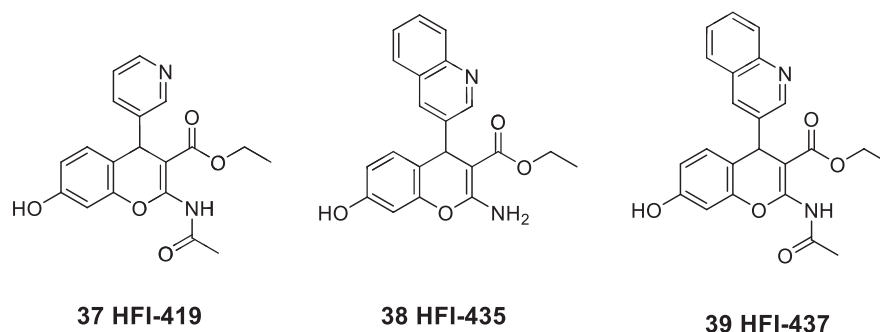


**Figure 9 |** The first drug-like small molecule IRAP inhibitors reported. The benzopyran derivatives **37**, **38**, and **39** were discovered after *in silico* screening.

of IRAP based on the crystal structure of LTA4H (Leukotriene-A4 hydrolase) was applied (Thunnissen et al., 2001). The virtual screening of a library of approximately two million compounds resulted in a lead series of inhibitors encompassing a benzopyran scaffold. Among the more potent compounds were the racemic pyridine derivative **37** (HFI-419), and the quinoline derivatives **38** (HFI-435) and **39** (HFI-437) exhibiting  $K_i$  values of 420, 360, and 20 nM, respectively (Figure 9). The benzopyran-based IRAP inhibitor **37**, with high selectivity vs. aminopeptidases such as APN, ERAP1, ERAP2, and LTA4H, exerted a cognitive-enhancing effect in rodents after *icv* administration similar to that of Ang IV 1 and LVV-H7 3 (Albiston et al., 2008; De Bundel et al., 2009).

As deduced from computational docking the *S*-isomer is the preferred binding mode of the inhibitors although alternative binding conformations were suggested (Albiston et al., 2010b). However, after determination of the crystal structure of IRAP, computational docking of, e.g., **37**, **38**, and **39** into the IRAP structure demonstrated that these inhibitors all bind in the same orientation relative to the active site (Hermans et al., 2015), in contrast to conclusions drawn in previous modeling studies. Moreover, a rationale for the unique specificity of IRAP to process endogenous macrocyclic peptides such as oxytocin (**35**) and vasopressin (**36**) was presented (Hermans et al., 2015). Structure-activity relationship of a large series of benzopyran analogues has been established and the structural elements most important for binding have been determined. The lead candidate **37** (HFI-419) exhibits brain exposure following intravenous administration in rats but was found to be rapidly degraded to the corresponding deacetylated and less active IRAP inhibitor (Mountford et al., 2014).

An increase in the activity of matrix-metalloproteases (MMPs) or an increase in neuronal glucose uptake are two likely mechanisms by which inhibition of IRAP can provide an enhancement of memory. Modulation of either of the two systems is known to improve memory and learning as well as affect DSD. The benzopyran **37** (HFI-419) enhances spatial working memory in rats and the inhibition of IRAP by **37** increased DSD prior to peak dendritic growth in hippocampal neurons (Seyer et al., 2020). Moreover, it was concluded that this enhancement was likely to be driven by GLUT<sub>4</sub>-mediated changes to DSD. In particular, the inhibition of IRAP led to an enhancement of the proportion of mushroom/stubby-like

spines. Furthermore, the spines were estimated to be functional based on their expression of the pre-synaptic markers vesicular glutamate transporter 1 and synapsin. The spine formation was inhibited in the case when the GLUT<sub>4</sub>-mediated glucose uptake was blocked. Thus, these results strongly suggest that IRAP inhibitors may facilitate memory by increasing hippocampal DSD via a GLUT<sub>4</sub>-mediated mechanism (Seyer et al., 2020).

## SMALL MOLECULE INSULIN-REGULATED AMINOPEPTIDASE INHIBITORS FROM SUBSTANCE LIBRARY SCREENING

Our laboratory screened a substance library screen of 10 500 low-molecular-weight compounds in an enzyme inhibition assay with IRAP originating from Chinese hamster ovary (CHO). Three structurally different classes of compounds considered to be of particular interest as starting points for the development of small-molecule IRAP inhibitors were identified. The arylsulfonamide **40** with no structural similarities to Ang IV was one of them (Engen et al., 2016) (Figure 10). Compound **40** comprises a tetrazole ring in the meta position of an aromatic ring of an arylsulfonamide which is the characteristic feature of the sulfonamide class of compounds. Subsequently a large series of tetrazole derivatives were prepared and examined (Borhade et al., 2014) and a few of them were studied in detail. For example **41**, that is a competitive inhibitor of IRAP and exhibits an IC<sub>50</sub> of 540 nM in a recombinant human IRAP assay. This sulfonamide (**41**) demonstrates a high metabolic stability and alters dendritic spine morphology and increases spine density in primary cultures of hippocampal neurons (Diwakarla et al., 2016a; Vanga et al., 2018). Molecular dynamics simulations and binding affinity estimations with the linear interaction energy method were performed for a large series of the arylsulfonamides. The significant agreement with experimental affinities suggested one of several tentatively proposed binding modes. Thus, the side chain of Arg439 of IRAP was estimated to interact with the tetrazole ring of the inhibitors while one of the oxygens of the sulfonamide function binds to the zinc ion of the enzyme. The NH of the sulfonamide binds to Glu 431 and Glu 295 via a water molecule bridge. This proposal was supported by the essentially perfect correlation for binding affinity differences between the selected pair of

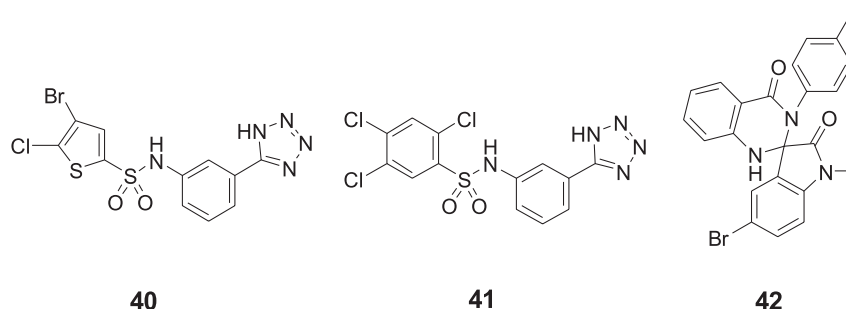


**Figure 10 |** The sulfonamides **40** and **41** and the spiro-oxindole dihydroquinazolinone **42** were identified after screening a substance library of 10,500 low-molecular-weight compounds.

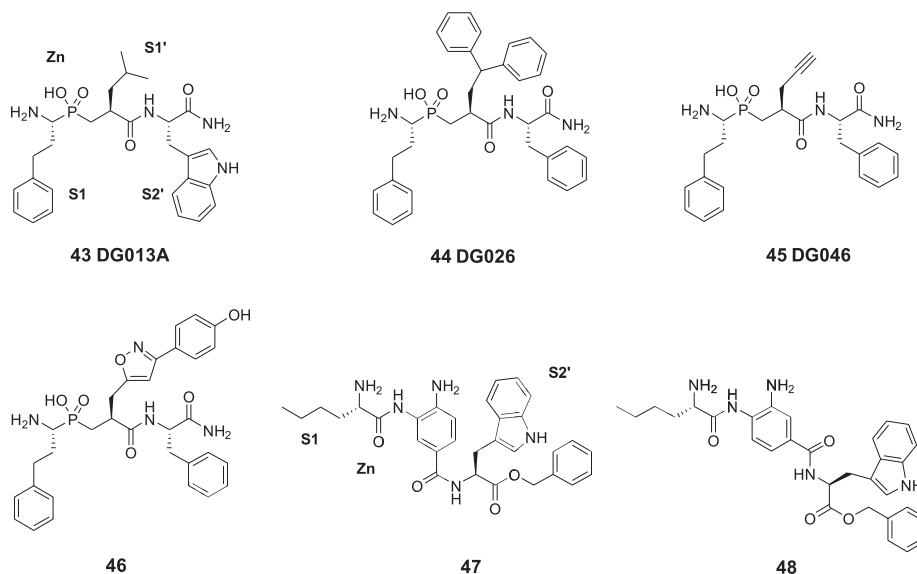


**Figure 11 |** The phosphinic pseudotripeptide **43** (DG013A) is a potent IRAP inhibitor but is not selective and is equally effective inhibiting both ERAP1 and ERAP2. Compound **44** (DG026) comprising a bulky P1' substituent is more IRAP selective than **43**. Compounds **45** (DG046) and **46** that are further modified in the P1' position are the most potent IRAP inhibitors in the series and approximately 10-fold selective vs. ERAP1 and ERAP2. The IRAP inhibitors **47** and **48** encompassing a 3,4-diaminobenzoic acid (DABA) scaffold are significantly less efficient than **43–46** as IRAP inhibitors.

compounds obtained by rigorous free energy perturbation calculations by Gutierrez-de-Teran's group (Vanga et al., 2018).

In addition to the sulfonamides, e.g., **40** and **41**, the spiro-oxindole dihydroquinazolinone derivative **42** was identified in the screening campaign and subsequently a large series of related analogues were made, e.g., by applying rapid MW-assisted reactions and thereafter examined as IRAP inhibitors in bioassays (Engen et al., 2020) (Figure 10). Compounds that were selective toward the closely related APN and that exhibited sub- $\mu$ M affinity were identified. Enantiomers were separated and according to computational modeling the inhibitory capacity of the compounds were attributed to the *S*-configuration of the spiro-oxindole dihydroquinazolinones. The derivatives with corresponding *R*-configuration were postulated to be essentially inactive in all cases. Notably, the

proposed binding mode is compatible with the simultaneous binding of the substrate L-Leu-pNA, in agreement with the uncompetitive IRAP inhibition determined for a representative compound. Unfortunately, the compounds suffer from poor *in vitro* metabolic stability (Engen et al., 2020).

## DIRECT DESIGN FROM THE STRUCTURE OF INSULIN-REGULATED AMINOPEPTIDASE

In 2013, laboratories in Greece and Stratikos' and Georgiadis' groups reported that the phosphinic pseudotripeptide **43** (DG013A) is a potent inhibitor of IRAP with an IC<sub>50</sub> of 57 nM (Figure 11). In contrast to **23** (HA08), the

pseudotriptide **43** was not selective and the related ERAP1 and ERAP2 were inhibited as well showing IC<sub>50</sub> values of 48 and 80 nM, respectively (Zervoudi et al., 2013). As deduced from an X-ray crystallographic analysis of **43** in complex with ERAP2 it was concluded that the three first specificity pockets of the enzyme was of particular importance for binding to the enzyme (Zervoudi et al., 2013). The two oxygen atoms of the hydroxyphosphinyl group of **43** are interacting with the zinc ion whilst hydrogen bonds with Glu371 and Tyr455 essential for catalysis are created. Phosphinic peptides often share structural similarities with the transition-state of peptide substrate upon hydrolysis (Georgiadis and Dive, 2015).

The phosphinic group is, as compared to, e.g., thiols and hydroxamic acids more weakly binding to zinc ions in metalloproteases and a significantly improved selectivity could be achieved by systematic variations of the side chains at P1' and P2' positions of **43**. Thus, the affinity to IRAP was improved after an enlargement of the P1' as exemplified by **44** (DG026) exhibiting an IC<sub>50</sub> of 32 nM while the affinity to ERAP1 dropped 100-fold. The crystal structure of IRAP in complex with **44** reveals that the enzyme undergoes structural reconfiguration that allows the accommodation of bulky side chains of the inhibitor. A closed conformational state of IRAP is created that is believed to be induced upon ligand binding. A hollow structure is formed excluding access of external solvent to the catalytic center (Mpakali et al., 2017). Notably, a propargyl group at P1' or alternatively an extended P1' side chain resulted both in very potent and fairly selective IRAP inhibitors, **45** (DG046) with IC<sub>50</sub> values of 2 nM and **46** with a IC<sub>50</sub> value of 4 nM (Figure 11). Thus, the potent IRAP inhibitor **45** demonstrated for ERAP1 an IC<sub>50</sub> of 43 nM and for ERAP2 an IC<sub>50</sub> value of 37 nM. The corresponding IC<sub>50</sub> values for the oxazole derivative **46** with the extended P1' side chain were 35 and 57 nM, respectively (Kokkala et al., 2016). Recently, a high-resolution crystal structure of phosphinic pseudopeptide inhibitor **45** (DG046) in the closed-conformation of ERAP1 was disclosed (Giastas et al., 2019b) and a mechanism for antigen peptide selection by ERAP1 presented (Giastas et al., 2019a). A review on inhibitors ERAP1 and ERAP2 was recently published (Georgiadis et al., 2019).

In 2015, Papakyriakou et al. reported a large series of inhibitors of ERAP1, ERAP2, and IRAP. This set of compounds comprises a 3,4-diaminobenzoic acid (DABA) scaffold (Papakyriakou et al., 2015). Compound **47** exhibited the best IRAP inhibitory capacity (IC<sub>50</sub> = 105 nM) and demonstrated an almost 10-fold selectivity vs. ERAP1 (IC<sub>50</sub> = 900 nM) and 15-fold improved selectivity vs. ERAP2 (IC<sub>50</sub> = 1,600 nM) (Figure 11). L-Nle was preferred in the N-terminal for optimal inhibition and zinc coordination to the oxygen of the benzamide function is estimated to allow the lipophilic P1 substituent to be easily accommodated in the S1 pocket. In such conformation, the terminal amine group can form salt bridge interactions with two conserved glutamates, Glu295 and Glu431. Furthermore, the free aniline group could form a hydrogen bond with the catalytic E465 residue of IRAP. Deprotection of **47** to furnish an inhibitor with a carboxylate in the C-terminal exhibited a somewhat lower binding affinity for

IRAP (IC<sub>50</sub> = 296 nM). L-Val-OBn rather than L-Trp-OBn in the C-terminal led to a ten times less potent inhibitor of IRAP. The IRAP inhibitor **48** was the best inhibitor in a second series of bioisosteric diaminobenzoic acid inhibitors but was both less potent and selective as compared **47** (Papakyriakou et al., 2015).

Most small molecule binders of the oxytocinase subfamily of M1 aminopeptidases, e.g., the phosphinic pseudotriptides **43–46** address the active site and establish strong interactions with the catalytic zinc ion. Highly potent enzyme inhibitors can be achieved but the selectivity obtained is often insufficient. Vourloumis' group explored a large series of weaker zinc binding groups as potential alternatives to, e.g., the zinc binding amide function found in the 3,4-diaminobenzoic acid derivatives **47** and **48** (Tsoukalidou et al., 2019). Functionalized pyridinone- and pyridinethione-scaffolds, nicotinic-, isonicotinic-, aminobenzoic- and hydrazinobenzoic acids were prepared and examined as bioisosters, but no significant improvement of affinity was encountered by this maneuver. It was concluded that the potency of the compounds in the oxytocinase subfamily is mainly attributed to the occupation of the active site specificity pockets and their orientation in the enzymes (Tsoukalidou et al., 2019).

## CONCLUSION

A series linear Ang IV analogues demonstrating improved metabolic stability and very high affinity to IRAP have been reported, e.g., the potent hexapeptides **11** (AL-11) and **12** (IVDE77) with K<sub>i</sub> values of 7.6 and 1.7 nM, respectively, data to be compared with the K<sub>i</sub> value of Ang IV of 62 nM in the same binding assay. These pseudopeptides that have been studied in some detail are encompassing  $\beta$ -amino acid residues and **12**, in addition a conformationally constrained residue close to the C-terminal of the peptide. Furthermore, various macrocyclizations of Ang IV and subsequent simplifications of the structures delivered a series of selective high affinity ligands mimicking the substrates oxytocin and vasopressin in the N-terminal. For example, the disulfide **23** (HA08) that comprises a 13-membered ring system, a  $\gamma$ -turn mimetic in the C-terminal and a  $\beta$ -amino acid residue in the N-terminal ring system exhibits a K<sub>i</sub> of 3.3 nM. The density of dendritic spines is closely associated with memory enhancement and **23** was found to increase the density of spines in the hippocampus significantly. To summarize, although very potent IRAP inhibitors have been discovered after systematic alterations starting from Ang IV none of the compounds are expected to reach the brain, at least not after oral administration.

Furthermore, ligands derived from the hexapeptide Ang IV but that are not proven to act as IRAP inhibitors have been reported. Thus, according to patent literature the drug-like **8** and **9** exhibit a very high affinity to the Ang IV binding site named the AT<sub>4</sub> receptor. Moreover **10** (PNB-0408), a low-molecular weight molecule lacking the N-terminal amino group found in Ang IV analogues enhances cognition and is reported to crosses the blood-brain barrier and subsequently exert its action by interacting with the hepatocyte growth factor/c-Met receptor

system. The compound has been studied in detail and promising pharmacological data have been reported. We believe that the positive effects of **10** on cognition are not attributed to inhibition of IRAP.

The HFI series of compounds, e.g., **37** (HFI 419) identified in 2008 after the virtual screening are much more drug-like than the hexapeptides **11** (AL-11), **12** (IVDE77), and the potent macrocyclic Ang IV analogue **23** (HA08) and can hopefully after further systematic optimization be converted into bioactive small molecules with capacity to cross the blood-brain barrier. However, while HFI 419 exerts a proven cognitive-enhancing effect in rodents after *icv* administration similar to that of Ang IV **1** and LVV-H7 **3**, the  $K_i$  value of 420 nM seems not optimal. The high throughput screening campaign of the substance library provided several hit compounds one of those the drug-like aryl sulfonamide **40** that was subsequently optimized into **41** that is a metabolically stable and reversible IRAP inhibitor. The sulfonamide **41**, like **23** (HA08) and **37** (HFI 419) increases spine density in primary cultures of hippocampal neurons but is unfortunately a too poor inhibitor of IRAP and is demonstrating a  $K_i$  value of 540 nM. Similarly, compounds from the spiro-oxindole dihydroquinazolinone series identified in the screening, e.g., **42** are weak inhibitors and besides that not stable in *in vitro* assays.

The phosphinic pseudotriptide series of compounds designed from structural and mechanistic knowledge of IRAP and the related ERAP1 and ERAP2 are promising and some of them exert powerful IRAP inhibitory effects. Thus, pseudotriptides **45** and **46** exhibit  $K_i$  values of 2 and 4 nM, respectively and an approximately 10-fold selectivity vs. ERAP1 and ERAP2. This class of inhibitors holds promise for the future. The 3,4-diaminobenzoic acid series of compounds, e.g., **47** with a  $K_i$  value of 105 nM are less efficient IRAP inhibitors.

## REFERENCES

- Albiston, A. L., Diwakarla, S., Fernando, R. N., Mountford, S. J., Yeatman, H. R., Morgan, B., et al. (2011). Identification and development of specific inhibitors for insulin-regulated aminopeptidase as a new class of cognitive enhancers. *Br. J. Pharmacol.* 164, 37–47. doi:10.1111/j.1476-5381.2011.01402.x
- Albiston, A. L., Fernando, R. N., Yeatman, H. R., Burns, P., Ng, L., Daswani, D., et al. (2010a). Gene knockout of insulin-regulated aminopeptidase: loss of the specific binding site for angiotensin IV and age-related deficit in spatial memory. *Neurobiol. Learn. Mem.* 93, 19–30. doi:10.1016/j.nlm.2009.07.011
- Albiston, A. L., Pham, V., Ye, S., Ng, L., Lew, R. A., Thompson, P. E., et al. (2010b). Phenylalanine-544 plays a key role in substrate and inhibitor binding by providing a hydrophobic packing point at the active site of insulin-regulated aminopeptidase. *Mol. Pharmacol.* 78, 600–607. doi:10.1124/mol.110.065458
- Albiston, A. L., McDowall, S. G., Matsacos, D., Sim, P., Clune, E., Mustafa, T., et al. (2001). Evidence that the Angiotensin IV (AT4) receptor is the enzyme insulin-regulated aminopeptidase. *J. Biol. Chem.* 276, 48623–48626. doi:10.1074/jbc.c100512200
- Albiston, A. L., Morton, C. J., Ng, H. L., Pham, V., Yeatman, H. R., Ye, S., et al. (2008). Identification and characterization of a new cognitive enhancer based on inhibition of insulin-regulated aminopeptidase. *Faseb. J.* 22, 4209–4217. doi:10.1096/fj.08-112227
- Albiston, A. L., Peck, G. R., Yeatman, H. R., Fernando, R., Ye, S., and Chai, S. Y. (2007). Therapeutic targeting of insulin-regulated aminopeptidase: heads and tails? *Pharmacol. Ther.* 116, 417–427. doi:10.1016/j.pharmthera.2007.07.006
- In summary, both direct design relying on mechanistic knowledge and available structural data from the oxytocinase subfamily of M1 aminopeptidases as well as iterative manipulations of the parent peptide Ang IV, involving insertion of unnatural amino acids as  $\beta$ -amino acids, macrocyclizations and various structural simplifications have provided highly potent selective Ang IV peptidemimetics inhibiting IRAP. Nevertheless, no inhibitor has yet reached phase I clinical trials and further efforts are needed to circumvent all obstacles related to absorption, metabolism and various issues on pharmacokinetics in order to eventually achieve orally bioavailable drug candidates acting as cognitive enhancers *in vivo*.

## AUTHOR CONTRIBUTIONS

MH and ML contributed equally in the preparation of the manuscript.

## FUNDING

We thank the Kjell and Märta Beijer Foundation, the Swedish Brain Foundation and King Gustaf V and Queen Victoria's Foundation of Freemasons for economic support.

## ACKNOWLEDGMENTS

We are very grateful for valuable discussions and constructive comments on the manuscript from Professor Anders Hallberg.

- Alescio-Lautier, B., Paban, V., and Soumireu-Mourat, B. (2000). Neuromodulation of memory in the hippocampus by vasopressin. *Eur. J. Pharmacol.* 405, 63–72. doi:10.1016/S0014-2999(00)00542-2
- Andersson, H., Demaegdt, H., Johnsson, A., Vauquelin, G., Lindeberg, G., Hallberg, M., et al. (2011). Potent macrocyclic inhibitors of insulin-regulated aminopeptidase (IRAP) by olefin ring-closing metathesis. *J. Med. Chem.* 54, 3779–3792. doi:10.1021/jm200036n
- Andersson, H., Demaegdt, H., Vauquelin, G., Lindeberg, G., Karlén, A., and Hallberg, M. (2008). Ligands to the (IRAP)/AT4 receptor encompassing a 4-hydroxydiphenylmethane scaffold replacing Tyr2. *Bioorg. Med. Chem.* 16, 6924–6935. doi:10.1016/j.bmc.2008.05.046
- Andersson, H., Demaegdt, H., Vauquelin, G., Lindeberg, G., Karlén, A., Hallberg, M., et al. (2010). Disulfide cyclized tripeptide analogues of angiotensin IV as potent and selective inhibitors of insulin-regulated aminopeptidase (IRAP). *J. Med. Chem.* 53, 8059–8071. doi:10.1021/jm100793t
- Axén, A., Andersson, H., Lindeberg, G., Rönnholm, H., Kortessmaa, J., Demaegdt, H., et al. (2007). Small potent ligands to the insulin-regulated aminopeptidase (IRAP)/AT4 receptor. *J. Pept. Sci.* 13, 434–444. doi:10.1002/psc.859
- Axén, A., Lindeberg, G., Demaegdt, H., Vauquelin, G., Karlén, A., and Hallberg, M. (2006). Cyclic insulin-regulated aminopeptidase (IRAP)/AT4 receptor ligands. *J. Pept. Sci.* 12, 705–713. doi:10.1002/psc.782
- Barlow, N., Vanga, S. R., Sävmarker, J., Sandström, A., Burns, P., Hallberg, A., et al. (2020). Macrocyclic peptidomimetics as inhibitors of insulin-regulated aminopeptidase (IRAP). *RSC Med. Chem.* 11, 234–244. doi:10.1039/c9md00485h
- Benoist, C. C., Kawas, L. H., Zhu, M., Tyson, K. A., Stillmaker, L., Appleyard, S. M., et al. (2014). The procognitive and synaptogenic effects of angiotensin IV-derived peptides are dependent on activation of the hepatocyte growth factor/



- c-met system. *J. Pharmacol. Exp. Therapeut.* 351, 390–402. doi:10.1124/jpet.114.218735
- Benoist, C. C., Wright, J. W., Zhu, M., Appleyard, S. M., Wayman, G. A., and Harding, J. W. (2011). Facilitation of hippocampal synaptogenesis and spatial memory by C-terminal truncated Nle1-angiotensin IV analogs. *J. Pharmacol. Exp. Therapeut.* 339, 35–44. doi:10.1124/jpet.111.182220
- Bogdan, A. R., Davies, N. L., and James, K. (2011). Comparison of diffusion coefficients for matched pairs of macrocyclic and linear molecules over a drug-like molecular weight range. *Org. Biomol. Chem.* 9, 7727–7733. doi:10.1039/c1ob05996c
- Borhade, S. R., Rosenström, U., Sävmarker, J., Lundbäck, T., Jenmalm-Jensen, A., Sigmundsson, K., et al. (2014). Inhibition of insulin-regulated aminopeptidase (IRAP) by arylsulfonamides. *ChemistryOpen* 3, 256–263. doi:10.1002/open.201402027
- Bosnyak, S., Jones, E. S., Christopoulos, A., Aguilar, M.-I., Thomas, W. G., and Widdop, R. E. (2011). Relative affinity of angiotensin peptides and novel ligands at AT1 and AT2 receptors. *Clin. Sci. (Lond.)* 121, 297–303. doi:10.1042/cs20110036
- Bourne, J. N., and Harris, K. M. (2008). Balancing structure and function at hippocampal dendritic spines. *Annu. Rev. Neurosci.* 31, 47–67. doi:10.1146/annurev.neuro.31.060407.125646
- Brandt, W., Joachim Haupt, V., and Wessjohann, L. A. (2010). Chemoinformatic analysis of biologically active macrocycles. *Curr. Top. Med. Chem.* 10, 1361–1379. doi:10.2174/156802610792232060
- Braszkowski, J. J., Kupryszewski, G., Witczuk, B., and Wiśniewski, K. (1988). Angiotensin II-(3-8)-hexapeptide affects motor activity, performance of passive avoidance and a conditioned avoidance response in rats. *Neuroscience* 27, 777–783. doi:10.1016/0306-4522(88)90182-0
- Braszkowski, J. J., Wielgat, P., and Walesiuk, A. (2008). Effect of D3 dopamine receptors blockade on the cognitive effects of angiotensin IV in rats. *Neuropeptides* 42, 301–309. doi:10.1016/j.npep.2008.02.001
- Bryant, N. J., Govers, R., and James, D. E. (2002). Regulated transport of the glucose transporter GLUT4. *Nat. Rev. Mol. Cell Biol.* 3, 267–277. doi:10.1038/nrm782
- De Bundel, D., Fafouri, A., Csaba, Z., Loyens, E., Lebon, S., El Ghouzzi, V., et al. (2015). Trans-modulation of the somatostatin type 2A receptor trafficking by insulin-regulated aminopeptidase decreases limbic seizures. *J. Neurosci.* 35, 11960–11975. doi:10.1523/jneurosci.0476-15.2015
- De Bundel, D., Smolders, I., Vanderheyden, P., and Michotte, Y. (2008). Ang II and Ang IV: unraveling the mechanism of action on synaptic plasticity, memory, and epilepsy. *CNS Neurosci. Ther.* 14, 315–339. doi:10.1111/j.1755-5949.2008.00057.x
- De Bundel, D., Smolders, I., Yang, R., Albiston, A. L., Michotte, Y., and Chai, S. Y. (2009). Angiotensin IV and LVV-haemorphin 7 enhance spatial working memory in rats: effects on hippocampal glucose levels and blood flow. *Neurobiol. Learn. Mem.* 92, 19–26. doi:10.1016/j.nlm.2009.02.004
- De Gasparo, M., Husain, A., Alexander, W., Catt, K. J., Chiu, A. T., Drew, M., et al. (1995). Proposed update of angiotensin receptor nomenclature. *Hypertension* 25, 924–927. doi:10.1161/01.hyp.25.5.924
- Demaegdt, H., Laeremans, H., De Backer, J.-P., Mosselmans, S., Le, M. T., Kersemans, V., et al. (2004). Synergistic modulation of cystinyl aminopeptidase by divalent cation chelators. *Biochem. Pharmacol.* 68, 893–900. doi:10.1016/j.bcp.2004.05.046
- Demaegdt, H., Lenaerts, P.-J., Swales, J., De Backer, J.-P., Laeremans, H., Le, M. T., et al. (2006). Angiotensin AT4 receptor ligand interaction with cystinyl aminopeptidase and aminopeptidase N: [<sup>125</sup>I]Angiotensin IV only binds to the cystinyl aminopeptidase apo-enzyme. *Eur. J. Pharmacol.* 546, 19–27. doi:10.1016/j.ejphar.2006.07.005
- Demaegdt, H., Lukaszuk, A., De Buyser, E., De Backer, J.-P., Szemenyei, E., Tóth, G., et al. (2009). Selective labeling of IRAP by the tritiated AT4 receptor ligand [<sup>3</sup>H]Angiotensin IV and its stable analog [<sup>3</sup>H]AL-11. *Mol. Cell. Endocrinol.* 311, 77–86. doi:10.1016/j.mce.2009.07.020
- Diwakarla, S., Nylander, E., Grönbladh, A., Vanga, S. R., Khan, Y. S., Gutiérrez-de-Terán, H., et al. (2016a). Aryl sulfonamide inhibitors of insulin-regulated aminopeptidase enhance spine density in primary hippocampal neuron cultures. *ACS Chem. Neurosci.* 7, 1383–1392. doi:10.1021/acscchemneuro.6b00146
- Diwakarla, S., Nylander, E., Grönbladh, A., Vanga, S. R., Khan, Y. S., Gutiérrez-de-Terán, H., et al. (2016b). Binding to and inhibition of insulin-regulated aminopeptidase by macrocyclic disulfides enhances spine density. *Mol. Pharmacol.* 89, 413–424. doi:10.1124/mol.115.102533
- Driggers, E. M., Hale, S. P., Lee, J., and Terrett, N. K. (2008). The exploration of macrocycles for drug discovery—an underexploited structural class. *Nat. Rev. Drug Discov.* 7, 608–624. doi:10.1038/nrd2590
- Engen, K., Rosenström, U., Axelsson, H., Konda, V., Dahllund, L., Otrocka, M., et al. (2016). Identification of drug-like inhibitors of insulin-regulated aminopeptidase through small-molecule screening. *Assay Drug Dev. Technol.* 14, 180–193. doi:10.1089/adt.2016.708
- Engen, K., Vanga, S. R., Lundbäck, T., Agalo, F., Konda, V., Jensen, A. J., et al. (2020). Synthesis, evaluation and proposed binding pose of substituted spiro-indole dihydroquinazolinones as IRAP inhibitors. *ChemistryOpen* 9, 325–337. doi:10.1002/open.201900344
- Evnochidou, I., Papakyriakou, A., and Stratikos, E. (2009). A new role for Zn(II) aminopeptidases: antigenic peptide generation and destruction. *Curr. Pharmaceut. Des.* 15, 3656–3670. doi:10.2174/138161209789271816
- Fernando, R. N., Larm, J., Albiston, A. L., and Chai, S. Y. (2005). Distribution and cellular localization of insulin-regulated aminopeptidase in the rat central nervous system. *J. Comp. Neurol.* 487, 372–390. doi:10.1002/cne.20585
- Fiala, J. C., Spacek, J., and Harris, K. M. (2002). Dendritic spine pathology: cause or consequence of neurological disorders? *Brain Res. Brain Res. Rev.* 39, 29–54. doi:10.1016/s0165-0173(02)00158-3
- Fransson, R., Botros, M., Nyberg, F., Lindeberg, G., Sandström, A., and Hallberg, M. (2008). Small peptides mimicking substance P (1–7) and encompassing a C-terminal amide functionality. *Neuropeptides* 42, 31–37. doi:10.1016/j.npep.2007.11.002
- Fruitier-Arnaudin, I., Cohen, M., Bordenave, S., Sannier, F., and Piot, J.-M. (2002). Comparative effects of angiotensin IV and two hemorphins on angiotensin-converting enzyme activity. *Peptides* 23, 1465–1470. doi:10.1016/s0196-9781(02)00083-9
- Fu, M., Yu, X., Lu, J., and Zuo, Y. (2012). Repetitive motor learning induces coordinated formation of clustered dendritic spines *in vivo*. *Nature* 483, 92–95. doi:10.1038/nature10844
- Gard, P. R. (2008). Cognitive-enhancing effects of angiotensin IV. *BMC Neurosci.* 9 (Suppl. 2), S15. doi:10.1186/1471-2202-9-s2-s15
- Garreau, I., Chansel, D., Vandermeersch, S., Fruitier, I., Piot, J. M., and Ardaillou, R. (1998). Hemorphins inhibit angiotensin IV binding and interact with aminopeptidase N. *Peptides* 19, 1339–1348. doi:10.1016/s0196-9781(98)00075-8
- Georgiadis, D., and Dive, V. (2015). Phosphinic peptides as potent inhibitors of zinc-metalloproteases. *Top. Curr. Chem.* 360, 1–38. doi:10.1007/128\_2014\_571
- Georgiadis, D., Mpakali, A., Koumantou, D., and Stratikos, E. (2019). Inhibitors of ER aminopeptidase 1 and 2: from design to clinical application. *Curr. Med. Chem.* 26, 2715–2729. doi:10.2174/0929867325666180214111849
- Giasas, P., Mpakali, A., Papakyriakou, A., Lelis, A., Kokkala, P., Neu, M., et al. (2019a). Mechanism for antigenic peptide selection by endoplasmic reticulum aminopeptidase 1. *Proc. Natl. Acad. Sci. U.S.A.* 116, 26709–26716. doi:10.1073/pnas.1912070116
- Giasas, P., Neu, M., Rowland, P., and Stratikos, E. (2019b). High-resolution crystal structure of endoplasmic reticulum aminopeptidase 1 with bound phosphinic transition-state analogue inhibitor. *ACS Med. Chem. Lett.* 10, 708–713. doi:10.1021/acsmchemlett.9b00002
- Giordanetto, F., and Kihlberg, J. (2014). Macrocyclic drugs and clinical candidates: what can medicinal chemists learn from their properties? *J. Med. Chem.* 57, 278–295. doi:10.1021/jm400887j
- Hallberg, M. (2009). Targeting the insulin-regulated aminopeptidase/AT4 receptor for cognitive disorders. *Drug News Perspect.* 22, 133–139. doi:10.1358/dnp.2009.22.3.1325032
- Hallberg, M. (2015). Neuropeptides: metabolism to bioactive fragments and the pharmacology of their receptors. *Med. Res. Rev.* 35, 464–519. doi:10.1002/med.21323
- Hallberg, M., Sävmarker, J., and Hallberg, A. (2017). Angiotensin peptides as AT2 receptor agonists. *Curr. Protein Pept. Sci.* 18, 809–818. doi:10.2174/1389203718666170203150344
- Harding, J. W., Cook, V. I., Miller-Wing, A. V., Hanesworth, J. M., Sardinia, M. F., Hall, K. L., et al. (1992). Identification of an AII(3–8) [AIV] binding site in guinea pig hippocampus. *Brain Res.* 583, 340–343. doi:10.1016/s0006-8993(10)80047-2
- Hermans, S. J., Ascher, D. B., Hancock, N. C., Holien, J. K., Michell, B. J., Chai, S. Y., et al. (2015). Crystal structure of human insulin-regulated aminopeptidase with specificity for cyclic peptides. *Protein Sci.* 24, 190–199. doi:10.1002/pro.2604

- Hess, S., Linde, Y., Ovadia, O., Safrai, E., Shalev, D. E., Swed, A., et al. (2008). Backbone cyclic peptidomimetic melanocortin-4 receptor agonist as a novel orally administrated drug lead for treating obesity. *J. Med. Chem.* 51, 1026–1034. doi:10.1021/jm701093y
- Ho, J. K., and Nation, D. A. (2018). Cognitive benefits of angiotensin IV and angiotensin-(1-7): a systematic review of experimental studies. *Neurosci. Biobehav. Rev.* 92, 209–225. doi:10.1016/j.neubiorev.2018.05.005
- Jackson, L., Eldahshan, W., Fagan, S. C., and Ergul, A. (2018). Within the brain: the renin angiotensin system. *Int. J. Mol. Sci.* 19, 876. doi:10.3390/ijms19030876
- Jespers, W., Esguerra, M., Aqvist, J., and Gutierrez-De-Teran, H. (2019). QligFEP: an automated workflow for small molecule free energy calculations in Q. *J. Cheminf.* 11, 26. doi:10.1186/s13321-019-0348-5
- Kandror, K. V., and Pilch, P. F. (1994). gp160, a tissue-specific marker for insulin-activated glucose transport. *Proc. Natl. Acad. Sci. U.S.A.* 91, 8017–8021. doi:10.1073/pnas.91.17.8017
- Kasai, H., Matsuzaki, M., Noguchi, J., Yasumatsu, N., and Nakahara, H. (2003). Structure-stability-function relationships of dendritic spines. *Trends Neurosci.* 26, 360–368. doi:10.1016/s0166-2236(03)00162-0
- Kato, T., Funakoshi, H., Kadoyama, K., Noma, S., Kanai, M., Ohya-Shimada, W., et al. (2012). Hepatocyte growth factor overexpression in the nervous system enhances learning and memory performance in mice. *J. Neurosci. Res.* 90, 1743–1755. doi:10.1002/jnr.23065
- Kawas, L. H., McCoy, A. T., Yamamoto, B. J., Wright, J. W., and Harding, J. W. (2012). Development of angiotensin IV analogs as hepatocyte growth factor/Met modifiers. *J. Pharmacol. Exp. Therapeut.* 340, 539–548. doi:10.1124/jpet.111.188136
- Keller, S. R. (2003). The insulin-regulated aminopeptidase a companion and regulator of GLUT4. *Front. Biosci.* 8, s410–s420. doi:10.2741/1078
- Keller, S. R., Scott, H. M., Mastick, C. C., Aebersold, R., and Lienhard, G. E. (1995). Cloning and characterization of a novel insulin-regulated membrane aminopeptidase from Glut4 vesicles. *J. Biol. Chem.* 270, 23612–23618. doi:10.1074/jbc.270.40.23612
- Kobori, T., Goda, K., Sugimoto, K., Ota, T., and Tomisawa, K. (1997). Preparation of peptide derivatives as angiotensin IV receptor agonists. WO 97/03093 A1.
- Kobori, T., Goda, K., Sugimoto, K., Ota, T., and Tomisawa, K. (1998). Preparation of amino acid derivatives as angiotensin IV receptor agonists. WO 98/05624 A1.
- Kokkala, P., Mpakali, A., Mauvais, F.-X., Papakyriakou, A., Daskalaki, I., Petropoulou, I., et al. (2016). Optimization and structure-activity relationships of phosphinic pseudotriptide inhibitors of aminopeptidases that generate antigenic peptides. *J. Med. Chem.* 59, 9107–9123. doi:10.1021/acs.jmedchem.6b01031
- Kramár, E. A., Armstrong, D. L., Ikeda, S., Wayner, M. J., Harding, J. W., and Wright, J. W. (2001). The effects of angiotensin IV analogs on long-term potentiation within the CA1 region of the hippocampus *in vitro*. *Brain Res.* 897, 114–121. doi:10.1016/s0006-8993(01)02100-x
- Krebs, L. T., Kramár, E., Hanesworth, J. M., Sardinia, M. F., Ball, A. E., Wright, J. W., et al. (1996). Characterization of the binding properties and physiological action of divalinal-angiotensin IV, a putative AT4 receptor antagonist. *Regul. Pept.* 67, 123–130. doi:10.1016/s0167-0115(96)00121-8
- Krishnan, R., Hanesworth, J. M., Wright, J. W., and Harding, J. W. (1999). Structure-binding studies of the adrenal AT4 receptor: analysis of position two- and three-modified angiotensin IV analogs. *Peptides* 20, 915–920. doi:10.1016/s0196-9781(99)00081-9
- Laeremans, H., Demaegd, H., De Backer, J.-P., Le, M. T., Kersemans, V., Michotte, Y., et al. (2005). Metal ion modulation of cystinyl aminopeptidase. *Biochem. J.* 390, 351–357. doi:10.1042/bj20050349
- Lai, C. S. W., Franke, T. F., and Gan, W.-B. (2012). Opposite effects of fear conditioning and extinction on dendritic spine remodelling. *Nature* 483, 87–91. doi:10.1038/nature10792
- Lee, J., Albiston, A. L., Allen, A. M., Mendelsohn, F. A. O., Ping, S. E., Barrett, G. L., et al. (2004). Effect of I.C.V. injection of AT4 receptor ligands, NLE1-angiotensin IV and LVV-hemorphin 7, on spatial learning in rats. *Neuroscience* 124, 341–349. doi:10.1016/j.neuroscience.2003.12.006
- Lee, J., Mustafa, T., McDowall, S. G., Mendelsohn, F. A. O., Brennan, M., Lew, R. A., et al. (2003). Structure-activity study of LVV-hemorphin-7: angiotensin AT4 receptor ligand and inhibitor of insulin-regulated aminopeptidase. *J. Pharmacol. Exp. Therapeut.* 305, 205–211. doi:10.1124/jpet.102.045492
- Lew, R. A., Mustafa, T., Ye, S., McDowall, S. G., Chai, S. Y., and Albiston, A. L. (2003). Angiotensin AT4 ligands are potent, competitive inhibitors of insulin regulated aminopeptidase (IRAP). *J. Neurochem.* 86, 344–350. doi:10.1046/j.1471-4159.2003.01852.x
- Lindman, S., Lindeberg, G., Gogoll, A., Nyberg, F., Karlén, A., and Hallberg, A. (2001). Synthesis, receptor binding affinities and conformational properties of cyclic methylenedioether analogues of angiotensin II. *Bioorg. Med. Chem.* 9, 763–772. doi:10.1016/s0968-0896(00)00294-7
- Lukaszuk, A., Demaegd, H., Feytens, D., Vanderheyden, P., Vauquelin, G., and Tourwé, D. (2009). The replacement of His(4) in angiotensin IV by conformationally constrained residues provides highly potent and selective analogues. *J. Med. Chem.* 52, 5612–5618. doi:10.1021/jm900651p
- Lukaszuk, A., Demaegd, H., Szemenyei, E., Tóth, G., Tymecka, D., Misicka, A., et al. (2008).  $\beta$ -Homo-amino acid scan of angiotensin IV. *J. Med. Chem.* 51, 2291–2296. doi:10.1021/jm701490g
- Lukaszuk, A., Demaegd, H., Van Den Eynde, I., Vanderheyden, P., Vauquelin, G., and Tourwé, D. (2011). Conformational constraints in angiotensin IV to probe the role of Tyr2, Pro5 and Phe6. *J. Pept. Sci.* 17, 545–553. doi:10.1002/psc.1365
- Lynch, G., Rex, C. S., Chen, L. Y., and Gall, C. M. (2008). The substrates of memory: defects, treatments, and enhancement. *Eur. J. Pharmacol.* 585, 2–13. doi:10.1016/j.ejphar.2007.11.082
- Mallinson, J., and Collins, I. (2012). Macrocycles in new drug discovery. *Future Med. Chem.* 4, 1409–1438. doi:10.4155/fmc.12.93
- Marsault, E., and Peterson, M. L. (2011). Macrocycles are great cycles: applications, opportunities, and challenges of synthetic macrocycles in drug discovery. *J. Med. Chem.* 54, 1961–2004. doi:10.1021/jm1012374
- Matsumoto, H., Nagasaka, T., Hattori, A., Rogi, T., Tsuruoka, N., Mizutani, S., et al. (2001). Expression of placental leucine aminopeptidase/oxytocinase in neuronal cells and its action on neuronal peptides. *Eur. J. Biochem.* 268, 3259–3266. doi:10.1046/j.1432-1327.2001.02221.x
- Matsumoto, H., Rogi, T., Yamashiro, K., Kodama, S., Tsuruoka, N., Hattori, A., et al. (2000). Characterization of a recombinant soluble form of human placental leucine aminopeptidase/oxytocinase expressed in Chinese hamster ovary cells. *Eur. J. Biochem.* 267, 46–52. doi:10.1046/j.1432-1327.2000.00949.x
- Matsuzaki, M., Ellis-Davies, G. C. R., Nemoto, T., Miyashita, Y., Iino, M., and Kasai, H. (2001). Dendritic spine geometry is critical for AMPA receptor expression in hippocampal CA1 pyramidal neurons. *Nat. Neurosci.* 4, 1086–1092. doi:10.1038/nn736
- McCoy, A. (2010). Pharmacokinetic characterization of angiotensin IV analogs with therapeutic potential for cancer and dementia. PhD thesis. Pullman, WA: Washington State University.
- McCoy, A. T., Benoist, C. C., Wright, J. W., Kawas, L. H., Bule-Ghogare, J. M., Zhu, M., et al. (2013). Evaluation of metabolically stabilized angiotensin IV analogs as procognitive/antidementia agents. *J. Pharmacol. Exp. Therapeut.* 344, 141–154. doi:10.1124/jpet.112.199497
- Moser, M. B., Trommald, M., and Andersen, P. (1994). An increase in dendritic spine density on hippocampal CA1 pyramidal cells following spatial learning in adult rats suggests the formation of new synapses. *Proc. Natl. Acad. Sci. U.S.A.* 91, 12673–12675. doi:10.1073/pnas.91.26.12673
- Mountford, S. J., Albiston, A. L., Charman, W. N., Ng, L., Holien, J. K., Parker, M. W., et al. (2014). Synthesis, structure-activity relationships and brain uptake of a novel series of benzopyran inhibitors of insulin-regulated aminopeptidase. *J. Med. Chem.* 57, 1368–1377. doi:10.1021/jm401540f
- Mpakali, A., Saridakis, E., Giastas, P., Maben, Z., Stern, L. J., Larhed, M., et al. (2020). Structural basis of inhibition of insulin-regulated aminopeptidase by a macrocyclic peptidic inhibitor. *ACS Med. Chem. Lett.* 11, 1429–1434. doi:10.1021/acsmchemlett.0c00172
- Mpakali, A., Saridakis, E., Harlos, K., Zhao, Y., Kokkala, P., Georgiadis, D., et al. (2017). Ligand-induced conformational change of insulin-regulated aminopeptidase: insights on catalytic mechanism and active site plasticity. *J. Med. Chem.* 60, 2963–2972. doi:10.1021/acs.jmedchem.6b01890
- Mpakali, A., Saridakis, E., Harlos, K., Zhao, Y., Papakyriakou, A., Kokkala, P., et al. (2015). Crystal structure of insulin-regulated aminopeptidase with bound substrate analogue provides insight on antigenic epitope precursor recognition and processing. *J. Immunol.* 195, 2842–2851. doi:10.4049/jimmunol.1501103
- Murthy, V. N., Schikorski, T., Stevens, C. F., and Zhu, Y. (2001). Inactivity produces increases in neurotransmitter release and synapse size. *Neuron* 32, 673–682. doi:10.1016/s0896-6273(01)00500-1
- Nikolaou, A., Eynde, I. V. D., Tourwé, D., Vauquelin, G., Tóth, G., Mallareddy, J. R., et al. (2013). [ $^3$ H]IVDE77, a novel radioligand with high affinity and

- selectivity for the insulin-regulated aminopeptidase. *Eur. J. Pharmacol.* 702, 93–102. doi:10.1016/j.ejphar.2013.01.026
- Nusser, Z., Lujan, R., Laube, G., Roberts, J. D. B., Molnar, E., and Somogyi, P. (1998). Cell type and pathway dependence of synaptic AMPA receptor number and variability in the hippocampus. *Neuron* 21, 545–559. doi:10.1016/s0896-6273(00)80565-6
- Nyberg, G., Sanderson, K., Andrén, P., Thörnwall, M., Einarsson, M., Danielson, B., et al. (1996). Isolation of haemorphin-related peptides from filter membranes collected in connection with haemofiltration of human subjects. *J. Chromatogr. A* 723, 43–49. doi:10.1016/0021-9673(95)00811-x
- O'Malley, A., O'Connell, C., Murphy, K. J., and Regan, C. M. (2000). Transient spine density increases in the mid-molecular layer of hippocampal dentate gyrus accompany consolidation of a spatial learning task in the rodent. *Neuroscience* 99, 229–232. doi:10.1016/s0306-4522(00)00182-2
- O'Malley, A., O'Connell, C., and Regan, C. M. (1998). Ultrastructural analysis reveals avoidance conditioning to induce a transient increase in hippocampal dentate spine density in the 6 hour post-training period of consolidation. *Neuroscience* 87, 607–613. doi:10.1016/s0306-4522(98)00178-x
- Papakyriakou, A., Zervoudi, E., Tsoukalidou, S., Mauvais, F.-X., Sfyroera, G., Mastellos, D. C., et al. (2015). 3,4-diaminobenzoic acid derivatives as inhibitors of the oxytocinase subfamily of M1 aminopeptidases with immune-regulating properties. *J. Med. Chem.* 58, 1524–1543. doi:10.1021/jm501867s
- Penzes, P., Cahill, M. E., Jones, K. A., Vanleeuwen, J.-E., and Woolfrey, K. M. (2011). Dendritic spine pathology in neuropsychiatric disorders. *Nat. Neurosci.* 14, 285–293. doi:10.1038/nn.2741
- Rasmussen, T. E., Pedraza-Díaz, S., Hardré, R., Laustsen, P. G., Carrion, A. G., and Kristensen, T. (2000). Structure of the human oxytocinase/insulin-regulated aminopeptidase gene and localization to chromosome 5q21. *Eur. J. Biochem.* 267, 2297–2306. doi:10.1046/j.1432-1327.2000.01234.x
- Rogi, T., Tsujimoto, M., Nakazato, H., Mizutani, S., and Tomoda, Y. (1996). Human placental leucine aminopeptidase/oxytocinase. *J. Biol. Chem.* 271, 56–61. doi:10.1074/jbc.271.1.56
- Sardinia, M. F., Hanesworth, J. M., Krebs, L. T., and Harding, J. W. (1993). AT4 receptor binding characteristics: D-amino acid- and glycine-substituted peptides. *Peptides* 14, 949–954. doi:10.1016/0196-9781(93)90071-n
- Sardinia, M. F., Hanesworth, J. M., Krishnan, F., and Harding, J. W. (1994). AT4 receptor structure-binding relationship: angiotensin IV analogues. *Peptides* 15, 1399–1406. doi:10.1016/0196-9781(94)90115-5
- Schmidt, B., Lindman, S., Tong, W., Lindeberg, G., Gogoll, A., Lai, Z., et al. (1997). Design, synthesis, and biological activities of four angiotensin II receptor ligands with  $\gamma$ -turn mimetics replacing amino acid residues 3–5. *J. Med. Chem.* 40, 903–919. doi:10.1021/jm960553d
- Seyer, B., Diwakarla, S., Burns, P., Hallberg, A., Grönbladh, A., Hallberg, M., et al. (2020). Insulin-regulated aminopeptidase inhibitor-mediated increases in dendritic spine density are facilitated by glucose uptake. *J. Neurochem.* 153, 485–494. doi:10.1111/jnc.14880
- Stratikos, E. (2014). Regulating adaptive immune responses using small molecule modulators of aminopeptidases that process antigenic peptides. *Curr. Opin. Chem. Biol.* 23, 1–7. doi:10.1016/j.cbpa.2014.08.007
- Swanson, G. N., Hanesworth, J. M., Sardinia, M. F., Coleman, J. K. M., Wright, J. W., Hall, K. L., et al. (1992). Discovery of a distinct binding site for angiotensin II (3–8), a putative angiotensin IV receptor. *Regul. Pept.* 40, 409–419. doi:10.1016/0167-0115(92)90527-2
- Thunnissen, M. M., Nordlund, P., and Haeggström, J. Z. (2001). Crystal structure of human leukotriene A(4) hydrolase, a bifunctional enzyme in inflammation. *Nat. Struct. Biol.* 8, 131–135. doi:10.1038/84117
- Tsoukalidou, S., Kakou, M., Mavridis, I., Koumantou, D., Calderone, V., Fragai, M., et al. (2019). Exploration of zinc-binding groups for the design of inhibitors for the oxytocinase subfamily of M1 aminopeptidases. *Bioorg. Med. Chem.* 27, 115177. doi:10.1016/j.bmc.2019.115177
- Tsujimoto, M., Mizutani, S., Adachi, H., Kimura, M., Nakazato, H., and Tomoda, Y. (1992). Identification of human placental leucine aminopeptidase as oxytocinase. *Arch. Biochem. Biophys.* 292, 388–392. doi:10.1016/0003-9861(92)90007-j
- Vanderheyden, P. M. L. (2009). From angiotensin IV binding site to AT4 receptor. *Mol. Cell. Endocrinol.* 302, 159–166. doi:10.1016/j.mce.2008.11.015
- Vanga, S. R., Sävmarker, J., Ng, L., Larhed, M., Hallberg, M., Åqvist, J., et al. (2018). Structural basis of inhibition of human Insulin-Regulated Aminopeptidase (IRAP) by aryl sulfonamides. *ACS Omega*. 3, 4509–4521. doi:10.1021/acsomega.8b00595
- Van Spronsen, M., and Hoogenraad, C. C. (2010). Synapse pathology in psychiatric and neurologic disease. *Curr. Neurol. Neurosci. Rep.* 10, 207–214. doi:10.1007/s11910-010-0104-8
- Wallis, M. G., Lankford, M. F., and Keller, S. R. (2007). Vasopressin is a physiological substrate for the insulin-regulated aminopeptidase IRAP. *Am. J. Physiol. Endocrinol. Metab.* 293, E1092–E1102. doi:10.1152/ajpendo.00440.2007
- Waters, S. B., D'Auria, M., Martin, S. S., Nguyen, C., Kozma, L. M., and Luskey, K. L. (1997). The amino terminus of insulin-responsive aminopeptidase causes Glut4 translocation in 3T3-L1 adipocytes. *J. Biol. Chem.* 272, 23323–23327. doi:10.1074/jbc.272.37.23323
- Wolfe, M. S. (2002). Therapeutic strategies for Alzheimer's disease. *Nat. Rev. Drug Discov.* 1, 859–866. doi:10.1038/nrd938
- Wright, J. W., Clemens, J. A., Panetta, J. A., Smalstig, E. B., Weatherly, L. S., Kramár, E., et al. (1996). Effects of LY231617 and angiotensin IV on ischemia-induced deficits in circular water maze and passive avoidance performance in rats. *Brain Res.* 717, 1–11. doi:10.1016/0006-8993(95)01454-3
- Wright, J. W., and Harding, J. W. (2008). The angiotensin AT4 receptor subtype as a target for the treatment of memory dysfunction associated with Alzheimer's disease. *J. Renin Angiotensin Aldosterone Syst.* 9, 226–237. doi:10.1177/1470320308099084
- Wright, J. W., and Harding, J. W. (2009). The brain angiotensin IV/AT4receptor system as a new target for the treatment of Alzheimer's disease. *Drug Dev. Res.* 70, 472–480. doi:10.1002/ddr.20328
- Wright, J. W., and Harding, J. W. (2011). Brain renin-angiotensin-A new look at an old system. *Prog. Neurobiol.* 95, 49–67. doi:10.1016/j.pneurobio.2011.07.001
- Wright, J. W., and Harding, J. W. (2015). The brain hepatocyte growth factor/c-met receptor system: a new target for the treatment of Alzheimer's disease. *J. Alzheimers Dis.* 45, 985–1000. doi:10.3233/jad-142814
- Wright, J. W., and Harding, J. W. (2019). Contributions by the brain renin-angiotensin system to memory, cognition, and Alzheimer's disease. *J. Alzheimers Dis.* 67, 469–480. doi:10.3233/jad-181035
- Wright, J. W., Miller-Wing, A. V., Shaffer, M. J., Higginson, C., Wright, D. E., Hanesworth, J. M., et al. (1993). Angiotensin II(3–8) (ANG IV) hippocampal binding: potential role in the facilitation of memory. *Brain Res. Bull.* 32, 497–502. doi:10.1016/0361-9230(93)90297-o
- Wright, J. W., Stubley, L., Pederson, E. S., Kramár, E. A., Hanesworth, J. M., and Harding, J. W. (1999). Contributions of the brain angiotensin IV-AT4Receptor subtype system to spatial learning. *J. Neurosci.* 19, 3952–3961. doi:10.1523/jneurosci.19-10-03952.1999
- Wright, J., Yamamoto, B., and Harding, J. (2008). Angiotensin receptor subtype mediated physiologies and behaviors: new discoveries and clinical targets. *Prog. Neurobiol.* 84, 157–181. doi:10.1016/j.pneurobio.2007.10.009
- Yamamoto, B. J., Elias, P. D., Masino, J. A., Hudson, B. D., McCoy, A. T., Anderson, Z. J., et al. (2010). The angiotensin IV analog Nle-Tyr-Leu-ψ-(CH<sub>2</sub>-NH<sub>2</sub>)3-4-His-Pro-Phe (Norleual) can act as a hepatocyte growth factor/c-Met inhibitor. *J. Pharmacol. Exp. Therapeut.* 333, 161–173. doi:10.1124/jpet.109.161711
- Yap, B. K., Harjani, J. R., Leung, E. W. W., Nicholson, S. E., Scanlon, M. J., Chalmers, D. K., et al. (2016). Redox-stable cyclic peptide inhibitors of the SPSB2-iNOS interaction. *FEBS Lett.* 590, 696–704. doi:10.1002/1873-3468.12115
- Zervoudi, E., Saridakis, E., Birtley, J. R., Seregin, S. S., Reeves, E., Kokkala, P., et al. (2013). Rationally designed inhibitor targeting antigen-trimming aminopeptidases enhances antigen presentation and cytotoxic T-cell responses. *Proc. Natl. Acad. Sci. U.S.A.* 110, 19890–19895. doi:10.1073/pnas.1309781110

**Conflict of Interest:** The authors declare that the research was conducted in the absence of any commercial or financial relationships that could be construed as a potential conflict of interest.

The handling editor declared a past co-authorship with the authors.

Copyright © 2020 Hallberg and Larhed. This is an open-access article distributed under the terms of the Creative Commons Attribution License (CC BY). The use, distribution or reproduction in other forums is permitted, provided the original author(s) and the copyright owner(s) are credited and that the original publication in this journal is cited, in accordance with accepted academic practice. No use, distribution or reproduction is permitted which does not comply with these terms.



# The Role of Insulin Regulated Aminopeptidase in Endocytic Trafficking and Receptor Signaling in Immune Cells

**Delphyne Descamps<sup>1\*</sup>, Irini Evnouchidou<sup>2,3</sup>, Vivien Caillens<sup>2</sup>, Carole Drjac<sup>1</sup>, Sabine Riffault<sup>1</sup>, Peter van Endert<sup>2,4,5</sup> and Loredana Saveanu<sup>2\*</sup>**

<sup>1</sup> Université Paris-Saclay, INRAE, UVSQ, VIM, Jou-en-Josas, France, <sup>2</sup> Université de Paris, Centre de recherche sur l'inflammation, INSERM U1149, CNRS ERL8252, Paris, France, <sup>3</sup> Inovation, Paris, France, <sup>4</sup> Université de Paris, INSERM Unité 1151, CNRS UMR 8253, Paris, France, <sup>5</sup> Service d'immunologie biologique, AP-HP, Hôpital Necker, Paris, France

## OPEN ACCESS

### Edited by:

Efstathios Stratikos,  
National Centre of Scientific Research  
Demokritos, Greece

### Reviewed by:

Angeliki Chroni,  
National Centre of Scientific Research  
Demokritos, Greece  
Susanna R. Keller,  
University of Virginia, United States

### \*Correspondence:

Delphyne Descamps  
delphyne.descamps@inrae.fr  
Loredana Saveanu  
loredana.saveanu@inserm.fr

### Specialty section:

This article was submitted to  
Cellular Biochemistry,  
a section of the journal  
Frontiers in Molecular Biosciences

**Received:** 15 July 2020

**Accepted:** 25 September 2020

**Published:** 20 October 2020

### Citation:

Descamps D, Evnouchidou I,  
Caillens V, Drjac C, Riffault S,  
van Endert P and Saveanu L (2020)  
The Role of Insulin Regulated  
Aminopeptidase in Endocytic  
Trafficking and Receptor Signaling  
in Immune Cells.  
Front. Mol. Biosci. 7:583556.  
doi: 10.3389/fmolb.2020.583556

Insulin regulated aminopeptidase (IRAP) is a type II transmembrane protein with broad tissue distribution initially identified as a major component of Glut4 storage vesicles (GSV) in adipocytes. Despite its almost ubiquitous expression, IRAP had been extensively studied mainly in insulin responsive cells, such as adipocytes and muscle cells. In these cells, the enzyme displays a complex intracellular trafficking pattern regulated by insulin. Early studies using fusion proteins joining the IRAP cytosolic domain to various reporter proteins, such as GFP or the transferrin receptor (TfR), showed that the complex and regulated trafficking of the protein depends on its cytosolic domain. This domain contains several motifs involved in IRAP trafficking, as demonstrated by mutagenesis studies. Also, proteomic studies and yeast two-hybrid experiments showed that the IRAP cytosolic domain engages in multiple protein interactions with cytoskeleton components and vesicular trafficking adaptors. These findings led to the hypothesis that IRAP is not only a cargo of GSV but might be a part of the sorting machinery that controls GSV dynamics. Recent work in adipocytes, immune cells, and neurons confirmed this hypothesis and demonstrated that IRAP has a dual function. Its carboxy-terminal domain located inside endosomes is responsible for the aminopeptidase activity of the enzyme, while its amino-terminal domain located in the cytosol functions as an endosomal trafficking adaptor. In this review, we recapitulate the published protein interactions of IRAP and summarize the increasing body of evidence indicating that IRAP plays a role in intracellular trafficking of several proteins. We describe the impact of IRAP deletion or depletion on endocytic trafficking and the consequences on immune cell functions. These include the ability of dendritic cells to cross-present antigens and prime adaptive immune responses, as well as the control of innate and adaptive immune receptor signaling and modulation of inflammatory responses.

**Keywords:** IRAP, endosome trafficking, immune cell responses, receptor signaling, formin, vacuolar protein sorting, TLR9, TCR



## IRAP IDENTIFICATION AND TISSUE EXPRESSION

The IRAP (insulin regulated or responsive aminopeptidase) protein is encoded by the human gene *LNPEP*. Although IRAP is the most commonly used name for this protein, other names related to the various substrates cleaved by the enzyme are also used, such as oxytocinase, OTASE, leucyl and cystinyl aminopeptidase, placental leucine aminopeptidase (P-LAP), cystinyl aminopeptidase (CAP), and vasopressinase.

While placental leucine aminopeptidase activities were described more than 50 years ago (Beckman et al., 1966, 1969), DNA sequences coding for IRAP were first identified in 1995 from a rat adipose tissue cDNA library (Keller et al., 1995) and 1 year later from a human placental cDNA library (Rogi et al., 1996). Soon after its identification, IRAP intracellular distribution was analyzed in adipocytes, where in basal conditions the enzyme colocalizes with the regulated glucose transporter, Glut4, in intracellular vesicles called Glut4 storage vesicles (GSV) (Ross et al., 1996). Upon adipocyte stimulation by insulin, IRAP, like Glut4, rapidly translocates to the cell surface from where it is rapidly endocytosed with a half-life of about 3 to 5 min, probably *via* a clathrin-mediated endocytic pathway (Summers et al., 1999). Even though the vast majority of studies on IRAP had been performed in adipocytes, already Keller et al. (1995) detected the protein by immunoblot in several tissues, such as heart, brain, spleen, lung, muscles, and kidney. The wide tissue distribution of IRAP has been confirmed by Mizutani's group which detected IRAP at mRNA and protein level in placental syncytiotrophoblasts, endothelial cells, gastrointestinal tract, several epithelial cell types from the liver, pancreas, lung, and kidney, as well as neuronal cells (Nagasaka et al., 1997). They concluded that the broad tissue distribution of IRAP is suggestive for a much more complex and varied function of the protein beyond the regulation of oxytocin and vasopressin levels in the blood.

Further studies confirmed the almost ubiquitous IRAP expression and its involvement in a variety of physiological processes, such as antigen cross-presentation by major histocompatibility class I (MHC-I) molecules (Saveanu et al., 2009; Segura et al., 2009; Weimershaus et al., 2012), endosomal Toll-like receptor (TLR) signaling (Babdor et al., 2017), lactation (Tobin et al., 2014), cognition (Banegas et al., 2010; Elkins et al., 2017), and stress responses (Hernández et al., 2015). During the investigation of these various functions, it became evident that in all cell types analyzed, IRAP is localized in intracellular vesicles reminiscent of adipocyte GSV that we proposed to call "cell-specific storage endosomes" (Saveanu and van Endert, 2012).

## IRAP PROTEIN STRUCTURE AND POST-TRANSLATIONAL MODIFICATIONS

IRAP belongs to the M1 aminopeptidase family and has more than 40% sequence identity with the endoplasmic reticulum

aminopeptidases ERAP1 (synonyms A-LAP, PILSAP) and ERAP2 (synonym L-RAP). Based on phylogenetic analyses, IRAP, ERAP1, and ERAP2 were classified in a distinct group of M1 aminopeptidases named "oxytocinase subfamily of M1 aminopeptidases" (Tsujimoto and Hattori, 2005). Even though all three enzymes are able to trim the N-terminus of antigenic peptides, they do so in different patterns consistent with the need to produce epitopes in different antigen presentation pathways: ERAP1 and ERAP2 mainly contributing to direct MHC-I presentation (Saveanu et al., 2005; Weimershaus et al., 2013) and IRAP to cross-presentation (Saveanu et al., 2009; Segura et al., 2009; Weimershaus et al., 2012). The elucidation of the crystal structures of IRAP, ERAP1, and ERAP2 in combination with biochemical studies revealed differences in substrate specificity and mechanism of action (Nguyen et al., 2011; Evnouchidou et al., 2012, 2014; Mpakali et al., 2015a,b, 2017a) that could also explain different antigen processing by different cell types (Segura et al., 2009; Weimershaus et al., 2012; Dinter et al., 2014; Mpakali et al., 2017b). IRAP was the last member of this subfamily to have its crystal structure resolved (Mpakali et al., 2015b). This delay was mainly due to the presence of a cytoplasmic and transmembrane domain, which make the expression and purification of the full-length protein very difficult, as well as its high degree of glycosylation, which is a major hurdle for the acquisition of high-quality crystals suitable for crystallography. Therefore, much information on the enzyme structure came earlier from biochemical studies.

IRAP is a type-II membrane-spanning protein that has a cytoplasmic domain composed of 109 amino acids, followed by a 23-amino acid transmembrane domain and an extracellular or intraluminal (depending on its localization inside the cell) 893-amino acid domain. The extracellular domain bears the Zn<sup>2+</sup> binding and GAMEN motifs that are essential for the enzyme's aminopeptidase activity (Keller et al., 1995). Unlike murine IRAP, the human protein bears a putative cleavage site for ADAM12 (F154/A155) that after proteolysis allows the release of a soluble form detectable in the serum during pregnancy (Iwase et al., 2001; Ofner and Hooper, 2002; Ito et al., 2004). The targeting motifs in the IRAP cytosolic tail responsible for intracellular distribution and trafficking were identified to be the di-Leucine motifs LL53,54 and LL76,77 (Keller et al., 1995). Contrary to a mutant for LL53,54 that was found to have no effect on trafficking, a mutant for LL76,77 had a very strong impact on trafficking, indicating this di-leucine motif as the one essential for this function. More specifically, this motif was essential for the initial entry of IRAP in the insulin-responsive compartment during biosynthesis but not for its recycling back to this compartment after endocytosis (Hou et al., 2006; Watson et al., 2008). Moreover, a study by Jordens et al. (2010) demonstrated that the IRAP cytosolic domain alone is able to reconstitute the normal intracellular distribution of Glut4 in adipocytes and that its role is specific for trafficking of storage endosomes, since the constitutive TfR<sup>+</sup> recycling endosomes were not affected.

A later study where recombinant IRAP fragments were expressed in, and purified from, insect cells provided important information on IRAP structure (Ascher et al., 2011). Using size-exclusion chromatography and dynamic light scattering,

the authors observed that the full-length soluble protein was completely dimerized, even after mutation of two key cysteine residues that could form disulfide bonds, suggesting an extended dimer interface. Dimerization could be important for the optimization of the enzyme's aminopeptidase activity, similar to findings for heterodimers formed by its sister enzymes ERAP1 and ERAP2 (Evnouchidou et al., 2014). The study by Ascher et al. (2011) also proposed an interaction between the domain containing the catalytic site and the C-terminal domain, since a construct lacking the latter showed reduced activity indicating an activating or regulatory role for the C-terminal domain. Recombinant IRAP exhibited enhanced substrate affinity in the presence of DTT suggesting a potential better access to the active site upon disruption of internal disulfide bonds. Moreover, the authors found evidence for a second non-catalytic  $\text{Zn}^{2+}$  binding site whose role still remains to be investigated.

The first IRAP crystal structure was obtained by the group of Parker (Hermans et al., 2015) at a 3.02 Å resolution for soluble recombinant human IRAP expressed in insect cells. The IRAP structure has four domains. Domain I forms an extended  $\beta$ -sandwich and domain II adopts a thermolysin-like  $\alpha/\beta$  fold. Domain III forms a  $\beta$ -sandwich fold and makes a bridge between domains II and IV, while domain IV is completely  $\alpha$ -helical and shows extensive interactions with domain II. IRAP was found as a dimer both in solution and in the crystal, with a conformation intermediate between the open and closed state of ERAP1 (Kochan et al., 2011; Nguyen et al., 2011). Similar to aminopeptidases A and N, IRAP uses its C-terminal domain to dimerize. Since the hydroxyl group of Tyr549, which is crucial for the formation of the catalytic intermediate, was not in a position allowing it to form a hydrogen bond, the authors proposed that the obtained structure is a snapshot of an inactive state of the enzyme. They suggested that this structure corresponds to an enzyme-product complex, where the C-terminal domain swings out from the active site in order to allow product release. The S1 pocket could fit well all amino acids except for tryptophan, which explains the wider specificity spectrum of IRAP compared to ERAP1 or ERAP2. More importantly, the GAMEN loop adopted a completely different position compared to other M1 aminopeptidases, which explains the unique ability of IRAP to cleave cyclic peptides such as oxytocin and vasopressin. Another structure (3.3 Å) obtained by the group of Stratikos (Mpakali et al., 2015b) superposed completely with the first one. In this case, the authors used a mammalian expression system with permanently transfected glycosylation-deficient cells, since use of cells with normal glycosylation did not provide crystals of good quality. The group provided also a second structure with a substrate analog (3.4 Å) containing a phosphinic group in the place of the first peptide bond, which allowed the formation of crystals corresponding to a transition state analog. The peptide N-terminus was anchored at the catalytic site while IRAP remained in the same semi-closed state, suggesting a domain organization unaffected by ligand binding, contrary to what has been observed for ERAP1. Though there were no deep specificity pockets interacting with the substrate, most interacting residues belonged to domain II. The C-terminus of the peptide was found to interact with residues from domain IV (C-terminal

domain), but molecular dynamics simulations showed that it has a high degree of plasticity, suggesting that there is no specific recognition of the C-terminus by IRAP, again contrary to ERAP1. The GAMEN loop showed no direct interactions with the substrate, therefore it seems not to be crucial for binding of linear peptides. Mapping of the A609T single nucleotide polymorphism (SNP) that has been associated with psoriasis and ankylosing spondylitis revealed an interaction with the hinge domain III of IRAP. Similar to the ERAP1 SNP K528R also associated with various autoimmune diseases, the IRAP SNP A609T reduced enzyme activity almost by half. The same group obtained more recently the first structure of IRAP with an inhibitor at 2.53 Å that displayed important differences compared to the previous ones (Mpakali et al., 2017b). This structure is closed, with domain IV juxtaposed against domains I and II, being very similar to the active closed ERAP1 structure and to the only structure available for ERAP2 (Evnouchidou et al., 2012). The internal cavity containing the catalytic site has no access to the solvent and a new specificity pocket is formed. The GAMEN loop adopts in this case a unique configuration depicting an active site with structural plasticity that could allow accommodation of a wide range of substrates, including cyclic peptides suited to the various biological functions of IRAP. The active site shows a capacity to bind a greater variety of antigenic precursors and its structural adaptability could explain why most ERAP1 inhibitors are also IRAP inhibitors but not vice versa.

IRAP can undergo many post-translational modifications including *N*-glycosylation, *S*-acylation, phosphorylation, ubiquitination, acetylation, and mono-methylation and of course the soluble form produced by proteolytic processing in pregnant women (Table 1). Apart from being highly glycosylated already at steady state, IRAP glycosylation is modulated under inflammatory conditions since it contains glycans regulated by  $\text{TNF}\alpha$ , as shown in adipocytes treated with  $\text{TNF}\alpha$ . These altered glycans may modulate the role of IRAP in GSV trafficking (Parker et al., 2016). IRAP could be phosphorylated *in vitro* by PKC- $\zeta$  both in insulin-stimulated rat adipocytes and in purified Glut4 vesicles. Phosphorylation occurred on two major sites, Ser80 and Ser91, with the former accounting for 80–90% of total phosphorylation, and was partially inhibited in the presence of a PKC- $\zeta$  pseudo-substrate. The fact that intracellular trafficking of certain recycling membrane proteins has been shown to be regulated by phosphorylation and that PKC- $\zeta$  inhibitors abolish Glut4 recruitment to the plasma membrane, suggests that IRAP phosphorylation could be important for GSV trafficking (Ryu et al., 2002). More recently, IRAP was also found to be phosphorylated on Ser91 after activation of human  $\text{CD8}^+$  T lymphocytes bearing a chimeric antigen receptor (Salter et al., 2018), which indicates a potential role of IRAP in the trafficking of these receptors used in immunotherapy.

IRAP was found to be *S*-acylated at 60% in 3T3-L1 adipocytes. The two *S*-acylated residues were identified to be Cys103, just upstream of the transmembrane domain, and Cys114 that lies in the cytoplasmic side of the transmembrane domain. This attachment of palmitate and other fatty acids to a cysteine could mediate membrane attachment of soluble proteins, regulate intracellular trafficking and also affect protein–protein

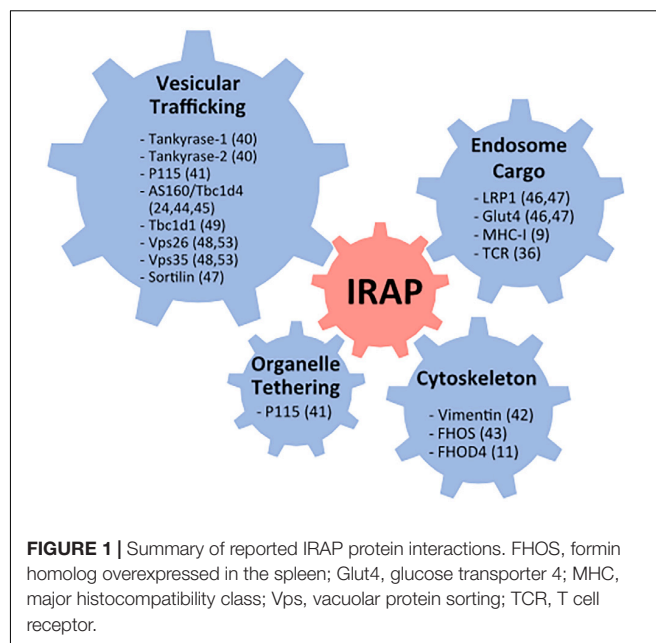
**TABLE 1 |** Post-translational modifications found in human IRAP and their known or potential effect on IRAP function.

Post-translational modification	Regulation of modification	Known or potential effect on function
N-Glycosylation (Wollscheid et al., 2009; Parker et al., 2016)	At steady state/ inflammation: TNF $\alpha$ regulation	Adipocytes: modulation of GSV trafficking?
Phosphorylation (Ryu et al., 2002; Salter et al., 2018)	Ser80 and Ser91/PKC- $\zeta$ phosphatase	Adipocytes: important for GSV trafficking? CAR CD8 <sup>+</sup> T cells-role in CAR trafficking?
S-Acylation (Werno and Chamberlain, 2015; Evnouchidou et al., 2020)	Cys103 and Cys114	HEK 293T cells: normal localization T cells: interaction with TCR, unaltered intracellular localization
Soluble form (Ofner and Hooper, 2002)	Proteolytic processing	Human serum during pregnancy: oxytocin and vasopressin degradation
Mono-methylation (Larsen et al., 2016)	Arg904	Protein-protein interaction
Ubiquitination (Udeshi et al., 2013)	Several sites	Protein degradation
Acetylation (phosphosite.org)	Lys691	Regulation of chromatin structure, gene expression and protein function

interactions and protein stability. A triple IRAP mutant that cannot be S-acylated was found to have a normal localization in HEK 293T cells (Werno and Chamberlain, 2015). However, in a recent study (Evnouchidou et al., 2020), we found that in T cells IRAP S-acylation is crucial for its interaction with the T cell receptor (TCR), even though, similar to HEK 293T cells, S-acylation-deficient IRAP mutant showed an unaltered intracellular localization. Therefore, it would be interesting to study the effect of IRAP S-acylation in other cell types, taking into account the specific function of IRAP in each cell type.

## IRAP PROTEIN INTERACTIONS

Soon after its identification IRAP was found to interact with several proteins involved in vesicular trafficking, organelle tethering, and cytoskeleton remodeling (**Figure 1**). These include tankyrase-1, tankyrase-2 (Chi and Lodish, 2000), and p115 (Hosaka et al., 2005), three proteins involved in the regulation of Golgi vesicle trafficking, vimentin, an intermediate cytoskeleton filament (Hirata et al., 2011) and the actin remodeling protein FHOS [formin homolog overexpressed in the spleen (Tojo et al., 2003)]. In addition, IRAP was shown to interact with AS160/Tbc1d4, a Rab GTPase activating protein (GAP) specific for Rab8, 10, and 14, suggesting that IRAP participates in the recruitment of AS160 to endocytic membranes (Larance et al., 2005; Peck et al., 2006). However, further investigations did not confirm the role of the IRAP-AS160 interaction in AS160 recruitment to GSV in adipocytes (Jordens et al., 2010). In addition to these proteins involved in intracellular trafficking, IRAP was found to interact with proteins located in GSVs, such as sortilin, LRP1 and Glut4 in adipocytes (Shi et al., 2008; Kandror and Pilch, 2011), and with MHC-I in dendritic cells (DCs) (Saveanu et al., 2009). These protein interactions have been



previously reviewed in Saveanu and van Endert (2012). The list of IRAP protein interactions has more recently been enriched by the discovery of its interaction with the  $\zeta$  chain of the TCR as well as the Lck kinase in T lymphocytes (Evnouchidou et al., 2020) and by identification of other interactions relevant for IRAP's role in vesicular trafficking, such as interaction with FHOD4, a formin similar to FHOS (Babdor et al., 2017), the retromer subunits Vps35 and Vps26 (Pan et al., 2019) and the Rab GAP Tbc1d1 (Mafakheri et al., 2018b).

FHOD4 is an actin-nucleation factor that assembles actin monomers into filaments (Kühn and Geyer, 2014) and might promote actin assembly on endosomes (Fernandez-Borja et al., 2005). We demonstrated that, in DCs, the interaction between FHOD4 and IRAP is required for anchoring the endosomes containing TLR9 and its ligands to the cell periphery and avoiding their fusion with lysosomes (Babdor et al., 2017).

The retromer is a large protein complex composed of a sorting nexin (SNX) dimer and a vacuolar protein sorting trimer (Vps26, Vps29, Vps35) that recycles diverse cargos from early endosomes to the *trans*-Golgi network or to the plasma membrane, preventing thus their transport to lysosomes (Chen et al., 2019). The SNX dimer is responsible for the retromer complex recruitment to the endosomal membrane, while the Vps trimer binds to various cargo molecules, among which IRAP has been recently identified (Pan et al., 2019). In the absence of the Vps35 subunit of the retromer, IRAP and Glut4 trafficking are perturbed and both proteins are found in lysosomes (Pan et al., 2017, 2019).

Tbc1d1 is a Rab GAP that is highly similar to Tbc1d4 and controls the activity of the same Rab proteins. When recruited to vesicular membranes, both Tbc1d4 and Tbc1d1 reduce the activity of Rab proteins involved in vesicle transport, thus mediating intracellular retention of IRAP vesicles. The interaction of Tbc1d1 with IRAP (Mafakheri et al., 2018a,b)



suggests that IRAP participates in the mechanism of intracellular retention, not only in cells and tissues expressing Tbc1d4, but also in those expressing Tbc1d1. However, considering that in adipocytes depleted for IRAP, AS160 was still recruited to GSV (Jordens et al., 2010), the role of IRAP interactions with both Tbc1d4 and Tbc1d1 needs further investigation, not only in adipocytes, but also in other cell types.

## REGULATION OF IRAP TRAFFICKING BY CELL-SPECIFIC CELL SURFACE RECEPTORS

In all the cells studied, IRAP is localized in intracellular vesicles, whose cargo varies depending on the cell type. In adipocytes, the main cargo is the regulated glucose transporter Glut4 and in neurons, the sst2A somatostatin receptor (De Bundel et al., 2015). In the immune system, where IRAP is expressed in almost all cells except neutrophils, IRAP vesicles contain MHC-I and TLR9 in DCs (Saveanu et al., 2009; Weimershaus et al., 2012; Babdor et al., 2017) or the  $\zeta$  chain of the TCR in T cells (Evnouchidou et al., 2020). All these proteins display constitutive slow recycling and some of them also regulated trafficking, being transported to the cell surface under specific conditions. Thus, Glut4 translocates to the plasma membrane to increase glucose uptake under insulin stimulation (Antonescu et al., 2009) and the TCR  $\zeta$  chain is rapidly transported to the plasma membrane under TCR activation by a cognate peptide/MHC-I complex (Evnouchidou et al., 2020).

The molecular mechanisms driving cell surface translocation of IRAP vesicle cargos are by far best understood for adipocyte GSV (Figure 2). In basal conditions, GSV are retained intracellularly and their recycling to the plasma membrane is much slower than that of TfR (Zeigerer et al., 2004). Insulin binding to its receptor initiates a signaling cascade, in which class I-A PI3K plays a key role by triggering rapid translocation of GLUT4 and IRAP to the cell surface. By producing the PtdIns(3,4,5)P3 lipid at the inner leaflet of the plasma membrane, class I-A PI3K induces membrane recruitment of the kinases of the Akt/PKB family (Hopkins et al., 2020). Although all the members of the Akt family can be recruited to PtdIns(3,4,5)P3-rich membranes, Akt2 is the major kinase recruited to the plasma membrane upon insulin stimulation, as demonstrated by total internal reflection fluorescence (TIRF) microscopy and confirmed by Akt2 depletion or deletion (Gonzalez and McGraw, 2009a,b). Akt activity phosphorylates the GAPs AS160/Tbc1d4 and Tbc1d1, as discussed above (Mafakheri et al., 2018a). Phosphorylation inactivates the GAPs and allows activation of their Rab substrates. In adipocytes, Rab10 seems to be the main GTPase regulating Glut4 trafficking (Brewer et al., 2016), while in muscle cells this role seems to be played by Rab8 (Sun et al., 2014).

Although as yet there is no experimental evidence showing that the PI3K-AKT pathway and its downstream effectors, Tbc1d1/Tbc1d4, regulate IRAP vesicle trafficking in other cell types, recent data from our laboratory support the hypothesis that this may be the case in DCs (Weimershaus et al., 2018). In these

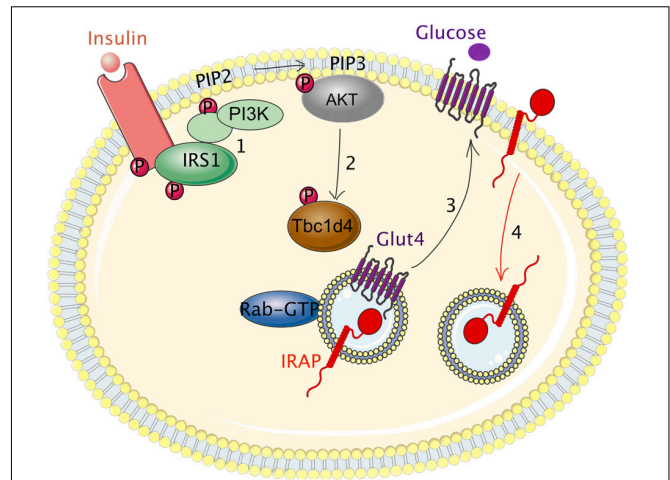


**FIGURE 2 |** Regulation of IRAP trafficking by the insulin receptor in adipocytes. (1) Insulin binding to its receptor initiates a signaling cascade that induces the phosphorylation of insulin receptor substrate 1 (IRS1) on tyrosine residues (p-Tyr). p-Tyr in IRS1 serve as docking sites for class I-A PI3K. The interaction of PI3K with IRS1 activates PI3K leading to increased production of PIP3 at the inner leaflet of the plasma membrane that in turn leads to recruitment and activation of Akt. Akt phosphorylates Tbc1d4, the GAP for Rab14, Rab8, and Rab10 small GTPases. (2) Tbc1d4 phosphorylation inactivates its GAP activity, allows Rabs activation and finally, induces GSV trafficking to the adipocyte cell surface (3). After Glut4 and IRAP translocation to the plasma membrane, Glut4 and IRAP rapidly re-internalize into intracellular vesicles (4). GTP, guanosine triphosphate; Glut4, glucose transporter 4; IRAP, insulin-regulated aminopeptidase; IRS1, insulin receptor substrate 1; GSV, Glut4 storage vesicles; PI3K, phosphoinositide 3-kinase; PIP2, phosphatidylinositol diphosphate; PIP3, phosphatidylinositol triphosphate; P, phosphorylation.

cells, IRAP vesicle trafficking and translocation to the phagocytic cup is regulated by immune receptors, such as TLR4 and the receptors for the Fc fragment of immunoglobulins, FcγRs. Similar to insulin responsive tissues, the regulation of IRAP trafficking in DCs involves the GAP Tbc1d4 and its downstream effector Rab14, but the upstream kinases that phosphorylate Tbc1d4 in these cells remain to be identified.

By analogy with insulin responsive tissues and DCs, IRAP and the TCR  $\zeta$  chain trafficking might also be regulated by class I PI3K, which in T cells is activated downstream of the co-stimulatory receptor CD28 (Esensten et al., 2016). The downstream GAP and Rab effectors could differ between T lymphocytes and DCs, since the microarray data from the Immunological Genome Project<sup>1</sup> predict that T cells express mainly Tbc1d1, Rab8, and Rab10, while DCs express foremost Tbc1d4 and Rab14 (Heng et al., 2008).

## IRAP ENDOSOME TRAFFICKING IN IMMUNE CELLS

Immune cells display complex and highly regulated endocytic trafficking that is essential for triggering a correct immune

<sup>1</sup><http://www.immgen.org/>



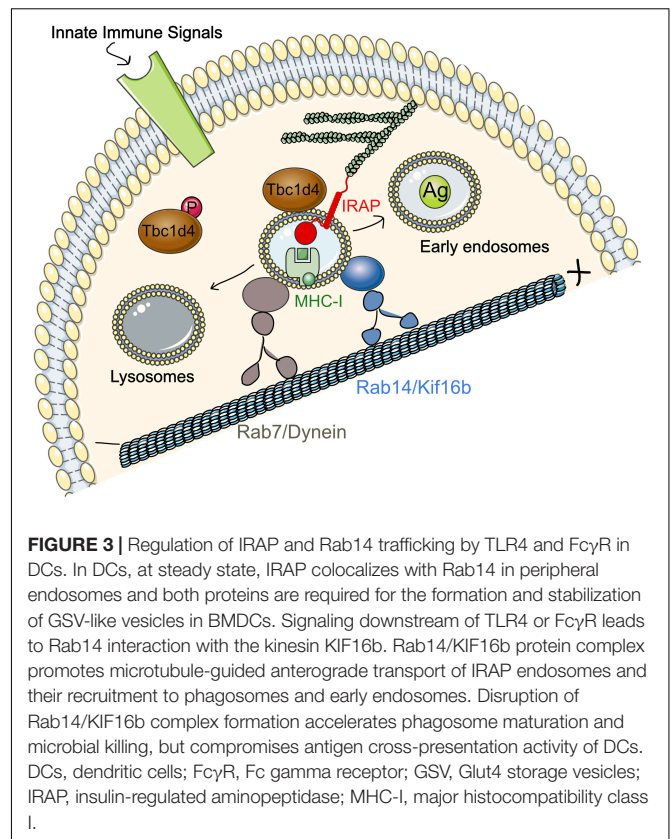
response, avoiding inappropriate reactions that could lead to uncontrolled inflammation or autoimmune disease. Through its localization and protein interactions, IRAP participates in the regulation of diverse immunological processes described below.

## Accelerated Phagosomal Maturation in the Absence of Rab14

In immune cells, endocytosis or phagocytosis of pathogens is followed by maturation of internalized vesicles through fusion and fission with intracellular vesicles (Huotari and Helenius, 2011). Gradual changes in protein composition and pH result in degradation of the internalized material, while delayed or attenuated maturation promotes cross-presentation (Alloatti et al., 2015). Published mechanisms regulating maturation kinetics include incomplete assembly of the proton pump V-ATPase (Delamarre et al., 2005), recruitment of NADPH oxidase 2 (Savina et al., 2006) and LPS-induced Rab34-dependent perinuclear clustering of lysosomes (Alloatti et al., 2015). More recently, we proposed an additional mechanism regulating trafficking of early endosomes and phagosomes, with important consequences for phagosome maturation (Weimershaus et al., 2018). We found that, in bone marrow-derived DCs (BMDCs), IRAP colocalizes with Rab14 in peripheral endosomes and that both proteins are required for the formation and stabilization of GSV-like vesicles in these cells. Moreover, Rab14 knock-down led to accelerated phagosome maturation and enhanced killing of phagocytized *Pseudomonas aeruginosa*. Our data confirmed the previously published reports demonstrating that pathogens recruit Rab14 to slow down phagosome maturation through an unknown mechanism (Kyei et al., 2006; Kuijl et al., 2007; Capmany and Damiani, 2010; Hoffmann et al., 2014) and revealed the involvement of Rab14 in antigen cross-presentation.

In the absence of Rab14, cross-presentation of ova-anti-ova immune complexes by HEK293 cells transfected with FcγR and H2K<sup>b</sup> was significantly decreased, while reconstitution with Rab14 in the same cells led to formation of enlarged GSV-like early endosomes and completely restored cross-presentation. Similar results were obtained in BMDCs, where Rab14 knock-down led to defective cross-presentation of both particulate and a soluble receptor-targeted ovalbumin antigen. Consistent with this, knock-out of Tbc1d4, the GAP for Rab14, resulted in formation of enlarged Rab14<sup>+</sup>Stx6<sup>+</sup> endosomes and promoted cross-presentation. However, both a GTP-locked and a GDP-locked form of Rab14 reduced cross-presentation suggesting that the balance between active and inactive Rab14 and GTP hydrolysis itself are critical for cross-presentation.

We further demonstrated that the mechanism underlying the important role of Rab14 in cross-presentation is its interaction with the kinesin KIF16b (Weimershaus et al., 2018). Using a proximity ligation assay (PLA), we showed that this interaction is strongly enhanced upon immune complex binding to FcγR both in HEK293 expressing FcγR and in BMDCs after LPS stimulation. Our data suggest that IRAP is required for phagosomal recruitment of Rab14 (Figure 3). Thus, in the absence of IRAP, Rab14 failed to get recruited to early phagosomes and, in line with this result, maturation of IRAP-deficient phagosomes



is not affected by Rab14 knock-down. The Rab14<sup>+</sup> vesicles, as well as cross-presentation, could be restored in these cells through microtubule stabilization or dynein knock-down, while these cellular manipulations had little effect on wild type (WT) BMDCs. These results indicate that the dominant retrograde transport along microtubules in IRAP-deficient (IRAP KO) cells is responsible for the destabilization of Rab14<sup>+</sup>Stx6<sup>+</sup> endosomes by favoring their fusion with lysosomes. In contrast, in WT cells, the anterograde motor formed by Rab14 and KIF16b ensures peripheral distribution of the endosomes, as demonstrated by the central distribution of Rab14 upon KIF16b knock-down. Moreover, KIF16b depletion led to reduced recruitment of Rab14 to phagosomes and defective cross-presentation, while it had no effect in IRAP KO BMDCs. In agreement with the results obtained by PLA, we showed that *in vitro* KIF16b interacts exclusively with GTP-locked Rab14.

Based on these results, we proposed a model in which, after receptor-mediated endocytosis or phagocytosis, Rab14<sup>+</sup>Stx6<sup>+</sup>IRAP<sup>+</sup> vesicles are recruited to the internalized material (Figure 3). The signaling cascade engaged after FcγR or TLR4 activation leads to phosphorylation and therefore inactivation of Tbc1d4 that results in Rab14 activation. Rab14 can then bind GTP and allow formation of Rab14/KIF16b complexes that will promote anterograde transport of the vesicles. This will finally result in delayed antigen degradation and enhanced cross-presentation, two interconnected processes that both depend on IRAP and Rab14 (Weimershaus et al., 2018).

## IRAP Restricts TLR9-Driven Inflammatory Responses

Inappropriate activation of innate immune receptors, such as endosomal TLR7 or TLR9, promotes several autoimmune diseases, including psoriasis (Rahmani and Rezaei, 2016), a skin inflammatory disease that has been associated with single nucleotide mutations (A763T, A609T) in the *Lnpep* gene coding for IRAP. The A763T mutation generates a missense variant leading to decreased expression of the IRAP protein in skin lesions (Cheng et al., 2014). However, there is no direct evidence in humans that the IRAP protein regulates endosomal TLR activation in psoriasis. In contrast, in mice, we have demonstrated that IRAP controls the function of TLR9 (Babdor et al., 2017).

TLR9 is an innate immune receptor important for both innate and adaptive immune responses. Its activation directly induces innate immune responses, such as inflammatory cytokine and type I interferon (IFN) production. In parallel, by increasing the capacity of DCs to process and present antigens to lymphocytes, TLR9 indirectly participates in the generation of adaptive immune responses (Iwasaki and Medzhitov, 2004; Kawai and Akira, 2010). These responses are initiated by binding of pathogen-derived single-stranded DNA or self-derived nucleic acids to TLR9. While the recognition of pathogen DNA is crucial for the priming of immune responses, the recognition of self-DNA can generate autoimmune diseases. To prevent this, TLR9 activation is tightly regulated by intracellular receptor trafficking (Majer et al., 2017). At the steady state, TLR9 associated with the chaperon protein UNC93B1 is retained in the endoplasmic reticulum (ER) (Majer et al., 2019) whereas it translocates to endocytic vesicles after stimulation by TLR9 ligands, such as synthetic CpG-oligonucleotides. CpG dinucleotides are internalized *via* clathrin-mediated endocytosis in early endosomes, from where they are targeted to late endosomes containing the LAMP proteins (Latz et al., 2004). In addition, following cellular stimulation by TLR9 ligands, the TLR9-UNC93B1 complex is translocated to the cell surface, from where it is internalized in a clathrin-dependent manner through the interaction of UNC93B1 with the adaptor protein-2 (AP2) (Lee et al., 2013). The TLR9-UNC93B1 complex traffics to EEA1<sup>+</sup>VAMP3<sup>+</sup> endosomes where TLR9 is processed by an array of proteases, such as cathepsins or the asparaginyl endopeptidase. This processing produces a carboxyterminal fragment able to bind the signaling adaptor Myd88 and to activate NF- $\kappa$ B-dependent proinflammatory cytokine production (Asagiri et al., 2008; Park et al., 2008; Sepulveda et al., 2009). Finally, the recruitment of AP-3 to the TLR9-UNC93B1 complex is mandatory for the trafficking of TLR9 to the lysosomal LAMP<sup>+</sup> compartments where the IFN regulatory factor 7 (IRF7)-dependent signaling cascade is activated for type I IFN production (Sasai et al., 2010).

We recently found that IRAP interaction with the formin FHOD4 plays an important role in endosomal TLR9 trafficking and activation (Babdor et al., 2017). In the absence of IRAP and upon CpG activation of the cells, TLR9 signaling was amplified, leading to increased pro-inflammatory cytokine and type I IFN production in several DC subsets, such as BMDCs

and splenic conventional and plasmacytoid DCs. IRAP-deficient mice displayed an exacerbated inflammatory response not only after CpG treatment, but also in the context of a model of respiratory infection (Babdor et al., 2017) with *P. aeruginosa*, a pathogen previously shown to activate TLR9 (Benmohamed et al., 2014). *P. aeruginosa* infection caused the death of IRAP-deficient animals, in experimental settings in which half of the WT animals survived. The death of IRAP-deficient animals was likely due to an uncontrolled inflammatory response since the broncho-alveolar lavage fluids from *P. aeruginosa*-infected IRAP-deficient mice contained higher concentrations of inflammatory cytokines (CXCL1, IL-6, TNF- $\alpha$ , and IL-1 $\beta$ ) than that of WT mice. Moreover, upon *ex vivo* *P. aeruginosa* infection, alveolar macrophages isolated from IRAP-deficient mice secreted more IL-6 and TNF- $\alpha$  than their WT counterparts (Babdor et al., 2017).

By a combination of biochemical and cell biology methods, we demonstrated that TLR9 signaling is accelerated in IRAP-deficient BMDCs (Babdor et al., 2017). Enhanced TLR9 signaling was not due to IRAP's enzymatic activity but was a consequence of aberrant TLR9 trafficking in the absence of IRAP. In WT cells, in basal conditions, TLR9 was localized in the ER and upon cell activation by CpG, TLR9 and CpG were internalized and retained for 2 h in IRAP<sup>+</sup> endosomes. In contrast to WT cells, in IRAP-deficient cells, in basal conditions, TLR9 was found in LAMP<sup>+</sup> lysosomes, in its processed form, ready to bind the signaling adaptors. In addition, upon cell activation, the TLR9 ligand was more rapidly targeted to lysosomes in IRAP-deficient cells compared to wild-type cells.

To understand how IRAP retains TLR9 and its ligand away from lysosomes, we screened the previously published interactions of IRAP with cytoskeleton proteins and demonstrated that the cytosolic tail of IRAP interacts with the formin FHOD4, an actin-polymerization factor involved in anchoring vesicles to the actin cytoskeleton (Goode and Eck, 2007). Similar to IRAP deletion, FHOD4 depletion by RNA interference led to aberrant trafficking of TLR9 and increased production of pro-inflammatory cytokines upon cell stimulation by CpG. These data indicate that IRAP recruits FHOD4 to TLR9-containing endosomes. FHOD4 might drive actin polymerization around the endosomal compartments (Fernandez-Borja et al., 2005; Kühn and Geyer, 2014) which could delay the transport of TLR9-containing endosomes to lysosomes, thereby limiting TLR9 processing and activation. Thus, in DCs, IRAP controls TLR9 activation by delaying targeting of the receptor and its ligand to the acidic lysosomal compartments (Figure 4). Future experiments are required to establish if in addition to the IRAP/FHOD4 interaction, the recently discovered interaction between IRAP and the retromer (Pan et al., 2019) also participates in TLR9 retention away from lysosomes.

## Compromised TCR Signaling in the Absence of IRAP

The TCR complex is composed of the  $\alpha\beta$ ,  $\gamma\epsilon$  and  $\delta\epsilon$  heterodimers and a  $\zeta\zeta$  homodimer. The TCR initiates signaling cascades

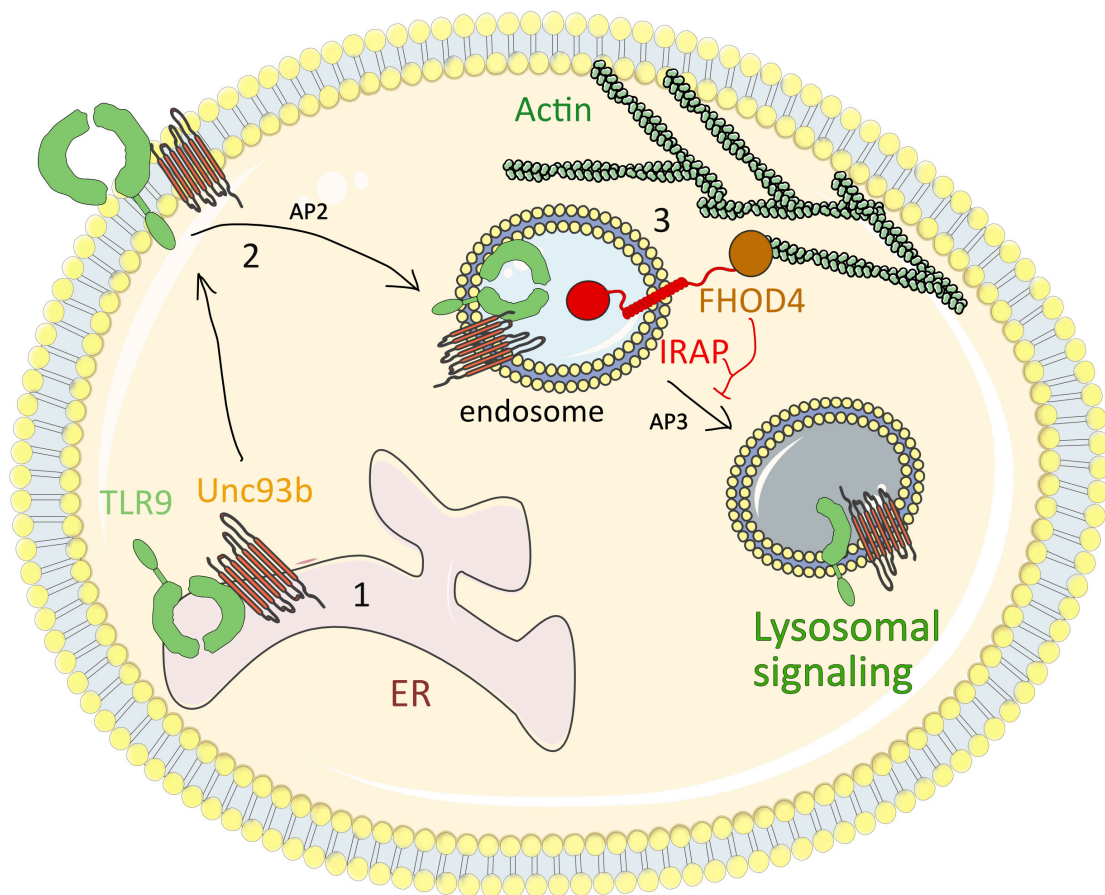


**FIGURE 4 |** IRAP restricts TLR9-driven inflammatory response. (1) At steady state, TLR9 associated with the chaperon protein UNC93B1 is retained in the ER. (2) After cell stimulation by TLR9 ligands, such as synthetic CpG-oligonucleotides, the TLR9-UNC93B1 complex is translocated to the cell surface, from where it is internalized in a clathrin-dependent manner through the interaction of UNC93B1 with AP-2. (3) The internalized TLR9-UNC93B1 complex traffics to IRAP endosomes. IRAP interaction with the formin FHOD4 anchors the endosomes to the actin cytoskeleton and delays TLR9 trafficking to acidic endosomal compartments, where TLR9 undergoes a partial proteolysis and triggers the pro-inflammatory signaling cascades. AP2, adaptor protein-2; ER, endoplasmic reticulum; TLR9, Toll-like receptor 9; IRAP, insulin-regulated aminopeptidase.

after recognition of a peptide-MHC (pMHC) complex, with low affinity recognition taking place in the thymus allowing for export to and survival in the periphery, and with high affinity interactions in initiation of effector T cell responses. The trafficking of TCR components and signaling partners is regulated in separate vesicular pools. While the  $\alpha$ ,  $\beta$ ,  $\gamma$ ,  $\delta$  and  $\epsilon$  chains are localized mainly in the ER, the nature of the  $\zeta$  intracellular pool has been less well characterized (Soares et al., 2013; Alcover et al., 2018). Each of the  $\gamma$ ,  $\delta$  and  $\epsilon$  chains bears one immunoreceptor tyrosine-based activation motif (ITAM), whereas each  $\zeta$  chain contains three. In the absence of the  $\zeta$  chain, TCR expression at the cell surface is almost abolished and there are substantial defects in T cell development (Love and Hayes, 2010; Alcover et al., 2018). Interestingly, signaling induced by the  $\zeta$  chain is not necessary to reverse this situation but rather seems to be crucial for the activation of T cells in the periphery (Shores et al., 1994; Ardouin et al., 1999; Love and Hayes, 2010).

In a recent study (Evnouchidou et al., 2020), we investigated the nature of the intracellular  $\zeta$  pool in Jurkat T cells and

observed by immunofluorescence that it localizes in endosomes characterized by the presence of IRAP and Stx6. Moreover, IRAP could be co-immunoprecipitated with the  $\zeta$  chain as well as with one of the first players in the TCR signaling pathway, the Lck kinase. We showed that at steady state,  $\zeta$  chain endocytosis is controlled by the clathrin adaptor AP-2 and Dnm2, while the absence of IRAP led to  $\zeta$  chain accumulation at the cell surface, accompanied by higher expression of the whole TCR complex. To our surprise, despite higher TCR expression at the cell surface, IRAP-deficient Jurkat T cells presented a severe defect in TCR signaling as seen by diminished phosphorylation of various TCR signaling partners after activation. This result was in agreement with defective recruitment of these molecules to the immune synapse (IS) as seen by TIRF microscopy, and by confocal microscopy of conjugates of Jurkat T cells with Raji B cells loaded with the staphylococcal enterotoxin E (SEE) superantigen. Moreover, the conjugates with IRAP-deficient Jurkat T cells poorly stimulated IL-2 secretion, as measured by ELISA both in the case of the SEE superantigen and of a melanoma antigen.



To investigate whether the observed defect could be attributed not only to a defective polarization of the intracellular pool to the IS but also to a reduced signaling capacity of the intracellular pool itself, we took advantage of a CD3 $\zeta$  FRET-FLIM reporter molecule (Yudushkin and Vale, 2010). We observed a significant FRET reduction in IRAP-deficient Jurkat T cells, which was much more profound in the intracellular pool. Using the same reporter, we were able to visualize IS formation in live cells and observed a dynamic IS in WT cells being continuously supplied with CD3 $\zeta$  from the intracellular pool, whereas the IRAP KO IS was rather static, getting CD3 $\zeta$  mainly from the plasma membrane. In accordance with these results, Lck as well as pCD3 $\zeta$  were also located at the plasma membrane in IRAP KO activated cells and IRAP vesicles were shown to contain various components of the TCR signalosome by PLA. We concluded that apart from TCR plasma membrane signaling, T cell activation necessitates the engagement of endosomal TCR signaling that takes place in IRAP + compartments (Figure 5).

Like in Jurkat T cells, IRAP colocalized with the TCR in mouse primary T cells and IRAP-deficient effector T cells presented increased TCR levels at the cell surface but defective

signaling. Activation of the cells with a low affinity ligand resulted in similar initial cell division, but lower numbers of IRAP KO cells due to subsequent cell death. OT1 IRAP KO, as well as conditional IRAP KO in T cells, led to lymphopenia. In an effort to study whether this was due to a thymic selection defect, we checked IRAP expression and found that IRAP expression gradually increases through the stages of thymic selection and reaches its highest levels in the periphery. Moreover, there were no significant alterations observed in thymus subpopulations, which led us to the conclusion that the lymphopenic phenotype likely can be attributed to a reduced survival capacity in the periphery due to a defective tonic signal (Kirberg et al., 2001; Garbi et al., 2010). We finally showed that IRAP is important for the first wave of low affinity T cells in pathogen-specific T cell responses in the context of a tumor model where IRAP T cell conditional KO mice developed bigger tumors and were unable to initiate effective anti-tumor T cell responses. The results of this study could be used to ameliorate current T cell-based immunotherapies, as well as to investigate intracellular signaling of other immune receptors.

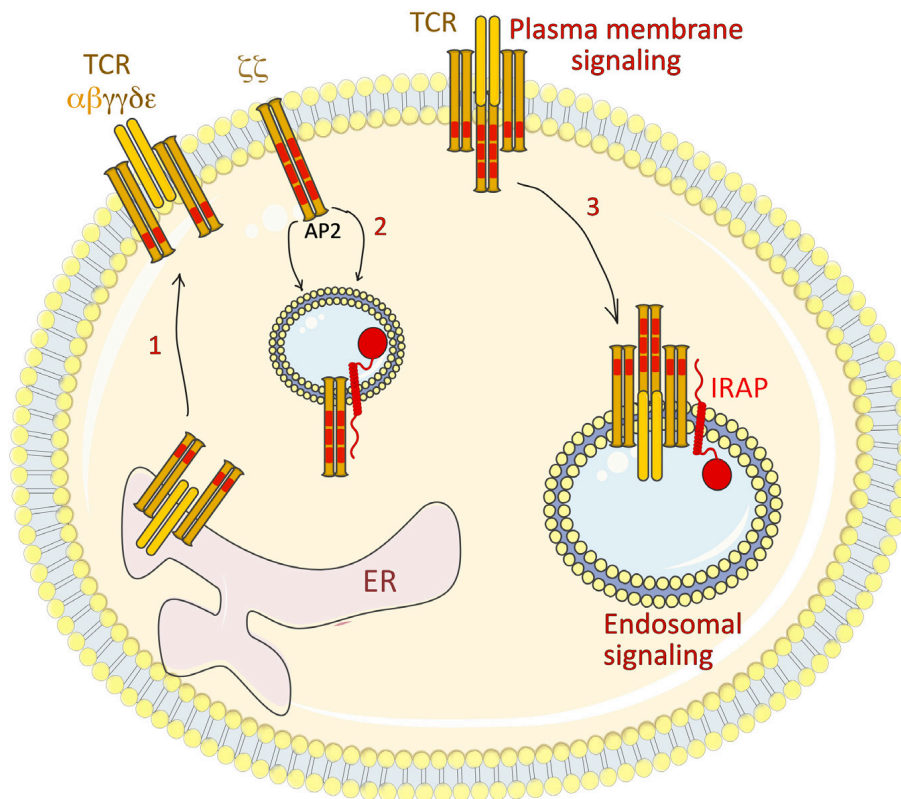


**FIGURE 5 |** IRAP regulates TCR  $\zeta$  chain trafficking and signaling. The full TCR comprises the clonotypic  $\alpha\beta$  chains, the  $\gamma\delta$  and  $\delta\epsilon$  heterodimers and a  $\zeta\zeta$  homodimer. (1) While the  $\alpha\beta$ ,  $\gamma\delta$  and  $\delta\epsilon$  heterodimers assemble in the ER and are transported via the Golgi stacks to the plasma membrane, the majority of the  $\zeta\zeta$  homodimer is stored in IRAP intracellular vesicles. (2) In basal conditions, the  $\zeta$  chain recycles between plasma membrane and the intracellular pool by a recycling pathway involving the clathrin adaptor AP2, the DnM2 and IRAP. Inhibition of this recycling pathway by AP2, DnM2 or IRAP depletion increases the levels of  $\zeta$  chain at plasma membrane. (3) Under T cell activation, the  $\zeta\zeta$  homodimer is internalized in IRAP vesicles, from where it is able to trigger signaling cascades, as demonstrated by its interaction with several signalosome components, such as ZAP-70, Lck and LAT. AP2, adaptor protein-2; DnM2, dynamin-2; ER, endoplasmic reticulum; IRAP, insulin-regulated aminopeptidase; LAP, linker for activation of T cells; TCR, T cell receptor.



## CONSEQUENCE OF IRAP DELETION ON ENDOCYTIC TRAFFICKING IN OTHER CELLS

### IRAP as an Old Partner of Glut4 Transporter Trafficking

Soon after Glut4 discovery (Birnbaum, 1989; James et al., 1989), IRAP was identified as an abundant protein in biochemically isolated GSV (Keller et al., 1995). IRAP-deficient mice were produced for the first time in 2002 (Keller et al., 2002). These mice had normal levels of *Glut4* mRNA but showed reduced levels of Glut4 protein, with a reduction varying between 45% and 85% in different muscles and in adipocytes, indicating a role for IRAP in Glut4 expression. Interestingly, Glut4 deletion also reduced by 35% the amount of IRAP at protein level, but not its mRNA (Carvalho et al., 2004), indicating that both proteins participate in the regulation of GSV trafficking.

Further studies in differentiated 3T3-L1 adipocytes confirmed that IRAP knock-down disturbs Glut4 trafficking by increasing its levels at the plasma membrane in basal conditions, but does not affect Glut4 translocation upon insulin stimulation of the cells (Jordens et al., 2010). However, Glut4 trafficking seems to be slightly different between differentiated 3T3-L1 adipocytes and primary adipocytes, in which IRAP deletion does not increase the cell surface levels of Glut4, but reduces its protein amount (Keller et al., 2002). Differences in Glut4 trafficking between differentiated 3T3-L1 and primary adipocytes are also suggested by a more recent report in which IRAP-depleted differentiated 3T3-L1 adipocytes did not show a strong reduction of Glut4 protein (Pan et al., 2019). However, this study detected a significant shift of Glut4 from the endosomal pool to acidic lysosomal compartments, similar to that observed for TLR9 in IRAP KO DCs (Babdor et al., 2017). The lysosomal localization of Glut4 in the absence of IRAP might be explained by the interaction between IRAP and the retromer (Pan et al., 2019). By interacting with the retromer, IRAP can cooperate with sortilin, another component of GSV that interacts with the retromer (Pan et al., 2017), and rescue Glut4 from degradation in lysosomes. This phenomenon could be particularly relevant in primary cells, where IRAP deletion strongly reduced Glut4 protein levels (Keller et al., 2002), probably due to its degradation in lysosomes.

### Somatostatin Receptors

In neurons, the major somatostatin receptor subtype, sst2A, has been found in IRAP vesicles (De Bundel et al., 2015). Sst2A is an inhibitory receptor that reduces neuron excitability and has anticonvulsant effects (Schonbrunn, 1999). Like the majority of G-protein-coupled receptors, sst2A is rapidly internalized after ligand binding and undergoes slow recycling through the *trans*-Golgi network, avoiding lysosomal degradation. When rat hippocampal neurons were incubated with the sst2A agonist octreotide, the sst2A receptor was rapidly internalized in IRAP

endosomes from where it was recycled back to the plasma membrane and reached the initial expression levels at the plasma membrane between 1 and 2 h after cell stimulation. IRAP depletion by lentiviral shRNA accelerated the recycling of the receptor that recovered its normal expression at the plasma membrane within 45 min. Interestingly, angiotensin IV and the LVV-H7 compound, two previously known IRAP ligands, also increased the speed of sst2A receptor recycling, similar to IRAP depletion. Further experiments are required to investigate if angiotensin IV or LVV-H7 binding to IRAP disturb IRAP intracellular trafficking and by consequence, sst2A receptor recycling.

## CONCLUSION AND PERSPECTIVES

A growing number of experimental data, partially reviewed in this article, show that next to its aminopeptidase activity, IRAP is a regulator of endosomal trafficking. IRAP protein interactions with cytoskeleton components and with the retromer contribute to the regulation of cell specific receptor trafficking and activation. The majority of these receptors are involved in cellular adaptation to the environmental conditions, such as high glucose concentration for Glut4, bacterial infections for TLR9, increased neuronal excitability for sstA2 or anti-tumor activity of T lymphocytes for the TCR. Identification of other cell-specific cargos of IRAP endosomes in the future will complete the list of physiological and pathological conditions in which IRAP might help the organism to maintain its homeostasis. Whether the enzymatic activity of IRAP, next to its undisputed and independent role in processing substrates such as vasopressin, also matters in its role in vesicle trafficking remains to be explored further. Enzymatic activity is not involved in the regulation of TLR9 or TCR trafficking and function, and Glut4 trafficking in IRAP KO cells is restored by the expression of the cytosolic domain of IRAP that lacks aminopeptidase activity (Jordens et al., 2010). However, the example of modulation of sstA2 trafficking by IRAP inhibitors (De Bundel et al., 2015) suggests that IRAP inhibitors might change protein trafficking, a hypothesis that is worth future studies.

Further studies are also required to extend our knowledge on the cell surface receptors and the downstream signaling pathways that regulate IRAP vesicles trafficking in the immune system. For example, our recent results demonstrate that IRAP trafficking is affected by TLR4 and FcRs activation in DCs (Weimershaus et al., 2018), and by TCR activation in T cells (Evnouchidou et al., 2020). Class I PI3K are known to be activated by the signaling cascades downstream of TLR4 and FcRs (Ben Mkaddem et al., 2019; Fitzgerald and Kagan, 2020), as well as through the signaling downstream of T cell costimulatory receptors and the IL-2 receptor (Saravia et al., 2020). Therefore, PI3K/AKT signaling could be a regulator of IRAP trafficking in immune cells, similar to its role in adipocytes (Li et al., 2019). This hypothesis

is compatible with the results available for immune cells and adipocytes but needs further experimental validation.

## AUTHOR CONTRIBUTIONS

DD, IE, VC, CD, SR, PE, and LS wrote the manuscript. All authors contributed to the article and approved the submitted version.

## REFERENCES

- Alcover, A., Alarcón, B., and Di Bartolo, V. (2018). Cell biology of T cell receptor expression and regulation. *Annu. Rev. Immunol.* 36, 103–125. doi: 10.1146/annurev-immunol-042617-053429
- Alloatti, A., Kotsias, F., Pauwels, A.-M., Carpiere, J.-M., Jouve, M., Timmerman, E., et al. (2015). Toll-like receptor 4 engagement on dendritic cells restrains phagolysosome fusion and promotes cross-presentation of antigens. *Immunity* 43, 1087–1100. doi: 10.1016/j.immuni.2015.11.006
- Antonescu, C. N., Foti, M., Sauvonnnet, N., and Klip, A. (2009). Ready, set, internalize: mechanisms and regulation of GLUT4 endocytosis. *Biosci. Rep.* 29, 1–11. doi: 10.1042/BSR20080105
- Ardouin, L., Boyer, C., Gillet, A., Trucy, J., Bernard, A. M., Nunes, J., et al. (1999). Crippling of CD3-zeta ITAMs does not impair T cell receptor signaling. *Immunity* 10, 409–420. doi: 10.1016/s1074-7613(00)80041-2
- Asagiri, M., Hirai, T., Kunigami, T., Kamano, S., Gober, H.-J., Okamoto, K., et al. (2008). Cathepsin K-dependent toll-like receptor 9 signaling revealed in experimental arthritis. *Science* 319, 624–627. doi: 10.1126/science.1150110
- Ascher, D. B., Cromer, B. A., Morton, C. J., Volitakis, I., Cherny, R. A., Albiston, A. L., et al. (2011). Regulation of insulin-regulated membrane aminopeptidase activity by its C-terminal domain. *Biochemistry* 50, 2611–2622. doi: 10.1021/bi101893w
- Babdor, J., Descamps, D., Adiko, A. C., Tohmé, M., Maschalidi, S., Evnouchidou, I., et al. (2017). IRAP+ endosomes restrict TLR9 activation and signaling. *Nat. Immunol.* 18, 509–518. doi: 10.1038/ni.3711
- Banegas, I., Prieto, I., Vives, F., Alba, F., de Gasparo, M., Duran, R., et al. (2010). Lateralized response of oxytocinase activity in the medial prefrontal cortex of a unilateral rat model of Parkinson's disease. *Behav. Brain Res.* 213, 328–331. doi: 10.1016/j.bbr.2010.05.030
- Beckman, L., Beckman, G., Mi, M. P., and de Simone, J. (1969). The human placental amino acid naphthylamidases; their molecular interrelations and correlations with perinatal factors. *Hum. Hered.* 19, 249–257. doi: 10.1159/000152226
- Beckman, L., Björling, G., and Christodoulou, C. (1966). Pregnancy enzymes and placental polymorphism. II. Leucine aminopeptidase. *Acta Genet. Stat. Med.* 16, 122–131. doi: 10.1159/000151957
- Ben Mkaddem, S., Benhamou, M., and Monteiro, R. C. (2019). Understanding Fc receptor involvement in inflammatory diseases: from mechanisms to new therapeutic tools. *Front. Immunol.* 10:811. doi: 10.3389/fimmu.2019.00811
- Benmohamed, F., Medina, M., Wu, Y.-Z., Maschalidi, S., Jouvion, G., Guillemot, L., et al. (2014). Toll-like receptor 9 deficiency protects mice against *Pseudomonas aeruginosa* lung infection. *PLoS One* 9:e90466. doi: 10.1371/journal.pone.0090466
- Birnbaum, M. J. (1989). Identification of a novel gene encoding an insulin-responsive glucose transporter protein. *Cell* 57, 305–315. doi: 10.1016/0092-8674(89)90968-9
- Brewer, P. D., Habtemichael, E. N., Romenskaia, I., Mastick, C. C., and Coster, A. C. F. (2016). Glut4 is sorted from a Rab10 GTPase-independent constitutive recycling pathway into a highly insulin-responsive Rab10 GTPase-dependent sequestration pathway after adipocyte differentiation. *J. Biol. Chem.* 291, 773–789. doi: 10.1074/jbc.M115.694919

## ACKNOWLEDGMENTS

The authors of this review were supported by the French “Agence nationale de la recherche” (ANR) grants Cytoendostor, ECLIPSE and IDEA and by Région Ile-de-France (DIM-Malinf). Vector image parts were used from the Servier medical art web site (<https://smart.servier.com/>) under the Creative Commons Attribution 3.0 Unported License (<https://creativecommons.org/licenses/by/3.0/>).

- Capmany, A., and Damiani, M. T. (2010). Chlamydia trachomatis intercepts Golgi-derived sphingolipids through a Rab14-mediated transport required for bacterial development and replication. *PLoS One* 5:e14084. doi: 10.1371/journal.pone.0014084
- Carvalho, E., Schellhorn, S. E., Zabolotny, J. M., Martin, S., Tozzo, E., Peroni, O. D., et al. (2004). GLUT4 overexpression or deficiency in adipocytes of transgenic mice alters the composition of GLUT4 vesicles and the subcellular localization of GLUT4 and insulin-responsive aminopeptidase. *J. Biol. Chem.* 279, 21598–21605. doi: 10.1074/jbc.M312269200
- Chen, K.-E., Healy, M. D., and Collins, B. M. (2019). Towards a molecular understanding of endosomal trafficking by retromer and retriever. *Traffic* 20, 465–478. doi: 10.1111/tra.12649
- Cheng, H., Li, Y., Zuo, X.-B., Tang, H.-Y., Tang, X.-F., Gao, J.-P., et al. (2014). Identification of a missense variant in LNPEP that confers psoriasis risk. *J. Invest. Dermatol.* 134, 359–365. doi: 10.1038/jid.2013.317
- Chi, N. W., and Lodish, H. F. (2000). Tankyrase is a golgi-associated mitogen-activated protein kinase substrate that interacts with IRAP in GLUT4 vesicles. *J. Biol. Chem.* 275, 38437–38444. doi: 10.1074/jbc.M007635200
- De Bundel, D., Fafouri, A., Csaba, Z., Loyens, E., Lebon, S., El Ghouzzi, V., et al. (2015). Trans-modulation of the somatostatin type 2A receptor trafficking by insulin-regulated aminopeptidase decreases limbic seizures. *J. Neurosci.* 35, 11960–11975. doi: 10.1523/JNEUROSCI.0476-15.2015
- Delamarre, L., Pack, M., Chang, H., Mellman, I., and Trombetta, E. S. (2005). Differential lysosomal proteolysis in antigen-presenting cells determines antigen fate. *Science* 307, 1630–1634. doi: 10.1126/science.1108003
- Dinter, J., Gourdain, P., Lai, N. Y., Duong, E., Bracho-Sanchez, E., Rucevic, M., et al. (2014). Different antigen-processing activities in dendritic cells, macrophages, and monocytes lead to uneven production of HIV epitopes and affect CTL recognition. *J. Immunol.* 193, 4322–4334. doi: 10.4049/jimmunol.1400491
- Elkins, E. A., Walti, K. A., Newberry, K. E., and Lema, S. C. (2017). Identification of an oxytocinase/vasopressinase-like leucyl-cystinyl aminopeptidase (LNPEP) in teleost fish and evidence for hypothalamic mRNA expression linked to behavioral social status. *Gen. Comp. Endocrinol.* 250, 58–69. doi: 10.1016/j.ygcen.2017.06.002
- Esensten, J. H., Helou, Y. A., Chopra, G., Weiss, A., and Bluestone, J. A. (2016). CD28 costimulation: from mechanism to therapy. *Immunity* 44, 973–988. doi: 10.1016/j.immuni.2016.04.020
- Evnouchidou, I., Birtley, J., Seregin, S., Papakyriakou, A., Zervoudi, E., Samiotaki, M., et al. (2012). A common single nucleotide polymorphism in endoplasmic reticulum aminopeptidase 2 induces a specificity switch that leads to altered antigen processing. *J. Immunol.* 189, 2383–2392. doi: 10.4049/jimmunol.1200918
- Evnouchidou, I., Chappert, P., Benadda, S., Zuchetti, A., Weimershaus, M., Bens, M., et al. (2020). IRAP-dependent endosomal T cell receptor signalling is essential for T cell responses. *Nat. Commun.* 11:2779. doi: 10.1038/s41467-020-16471-7
- Evnouchidou, I., Weimershaus, M., Saveanu, L., and van Endert, P. (2014). ERAP1-ERAP2 dimerization increases peptide-trimming efficiency. *J. Immunol.* 193, 901–908. doi: 10.4049/jimmunol.1302855
- Fernandez-Borja, M., Janssen, L., Verwoerd, D., Hordijk, P., and Neefjes, J. (2005). RhoB regulates endosome transport by promoting actin assembly on

- endosomal membranes through Dia1. *J. Cell. Sci.* 118, 2661–2670. doi: 10.1242/jcs.02384
- Fitzgerald, K. A., and Kagan, J. C. (2020). Toll-like receptors and the control of immunity. *Cell* 180, 1044–1066. doi: 10.1016/j.cell.2020.02.041
- Garbi, N., Hämmerling, G. J., Probst, H.-C., and van den Broek, M. (2010). Tonic T cell signalling and T cell tolerance as opposite effects of self-recognition on dendritic cells. *Curr. Opin. Immunol.* 22, 601–608. doi: 10.1016/j.coi.2010.08.007
- Gonzalez, E., and McGraw, T. E. (2009a). Insulin-modulated Akt subcellular localization determines Akt isoform-specific signaling. *Proc. Natl. Acad. Sci. U.S.A.* 106, 7004–7009. doi: 10.1073/pnas.0901933106
- Gonzalez, E., and McGraw, T. E. (2009b). The Akt kinases: isoform specificity in metabolism and cancer. *Cell Cycle* 8, 2502–2508. doi: 10.4161/cc.8.16.9335
- Goode, B. L., and Eck, M. J. (2007). Mechanism and function of formins in the control of actin assembly. *Annu. Rev. Biochem.* 76, 593–627. doi: 10.1146/annurev.biochem.75.103004.142647
- Heng, T. S. P., Painter, M. W., and Immunological genome project Consortium, (2008). The Immunological Genome Project: networks of gene expression in immune cells\*. *Nat. Immunol.* 9, 1091–1094. doi: 10.1038/ni1008-1091
- Hermans, S. J., Ascher, D. B., Hancock, N. C., Holien, J. K., Michell, B. J., Chai, S. Y., et al. (2015). Crystal structure of human insulin-regulated aminopeptidase with specificity for cyclic peptides. *Protein Sci.* 24, 190–199. doi: 10.1002/pro.2604
- Hernández, J., Prieto, I., Segarra, A. B., de Gasparo, M., Wangenstein, R., Villarejo, A. B., et al. (2015). Interaction of neuropeptidase activities in cortico-limbic regions after acute restraint stress. *Behav. Brain Res.* 287, 42–48. doi: 10.1016/j.bbr.2015.03.036
- Hirata, Y., Hosaka, T., Iwata, T., Le, C. T. K., Jambaldorj, B., Teshigawara, K., et al. (2011). Vimentin binds IRAP and is involved in GLUT4 vesicle trafficking. *Biochem. Biophys. Res. Commun.* 405, 96–101. doi: 10.1016/j.bbrc.2010.12.134
- Hoffmann, C., Finsel, I., Otto, A., Pfaffinger, G., Rothmeier, E., Hecker, M., et al. (2014). Functional analysis of novel Rab GTPases identified in the proteome of purified Legionella-containing vacuoles from macrophages. *Cell. Microbiol.* 16, 1034–1052. doi: 10.1111/cmi.12256
- Hopkins, B. D., Goncalves, M. D., and Cantley, L. C. (2020). Insulin-PI3K signalling: an evolutionarily insulated metabolic driver of cancer. *Nat. Rev. Endocrinol.* 16, 276–283. doi: 10.1038/s41574-020-0329-9
- Hosaka, T., Brooks, C. C., Presman, E., Kim, S.-K., Zhang, Z., Breen, M., et al. (2005). p115 Interacts with the GLUT4 vesicle protein, IRAP, and plays a critical role in insulin-stimulated GLUT4 translocation. *Mol. Biol. Cell.* 16, 2882–2890. doi: 10.1091/mbc.e05-01-0072
- Hou, J. C., Suzuki, N., Pessin, J. E., and Watson, R. T. (2006). A specific dileucine motif is required for the GGA-dependent entry of newly synthesized insulin-responsive aminopeptidase into the insulin-responsive compartment. *J. Biol. Chem.* 281, 33457–33466. doi: 10.1074/jbc.M601583200
- Huotari, J., and Helenius, A. (2011). Endosome maturation. *EMBO J.* 30, 3481–3500. doi: 10.1038/emboj.2011.286
- Ito, N., Nomura, S., Iwase, A., Ito, T., Kikkawa, F., Tsujimoto, M., et al. (2004). ADAMs, a disintegrin and metalloproteinases, mediate shedding of oxytocinase. *Biochem. Biophys. Res. Commun.* 314, 1008–1013. doi: 10.1016/j.bbrc.2003.12.183
- Iwasaki, A., and Medzhitov, R. (2004). Toll-like receptor control of the adaptive immune responses. *Nat. Immunol.* 5, 987–995. doi: 10.1038/ni1112
- Iwase, A., Nomura, S., and Mizutani, S. (2001). Characterization of a secretase activity for placental leucine aminopeptidase. *Arch. Biochem. Biophys.* 393, 163–169. doi: 10.1006/abbi.2001.2489
- James, D. E., Strube, M., and Muecdler, M. (1989). Molecular cloning and characterization of an insulin-regulatable glucose transporter. *Nature* 338, 83–87. doi: 10.1038/338083a0
- Jordens, I., Molle, D., Xiong, W., Keller, S. R., and McGraw, T. E. (2010). Insulin-regulated aminopeptidase is a key regulator of GLUT4 trafficking by controlling the sorting of GLUT4 from endosomes to specialized insulin-regulated vesicles. *Mol. Biol. Cell.* 21, 2034–2044. doi: 10.1091/mbc.e10-02-0158
- Kandror, K. V., and Pilch, P. F. (2011). The sugar is sIRVed: sorting Glut4 and its fellow travelers. *Traffic* 12, 665–671. doi: 10.1111/j.1600-0854.2011.01175.x
- Kawai, T., and Akira, S. (2010). The role of pattern-recognition receptors in innate immunity: update on Toll-like receptors. *Nat. Immunol.* 11, 373–384. doi: 10.1038/ni.1863
- Keller, S. R., Davis, A. C., and Clairmont, K. B. (2002). Mice deficient in the insulin-regulated membrane aminopeptidase show substantial decreases in glucose transporter GLUT4 levels but maintain normal glucose homeostasis. *J. Biol. Chem.* 277, 17677–17686. doi: 10.1074/jbc.M202037200
- Keller, S. R., Scott, H. M., Mastick, C. C., Aebersold, R., and Lienhard, G. E. (1995). Cloning and characterization of a novel insulin-regulated membrane aminopeptidase from Glut4 vesicles. *J. Biol. Chem.* 270, 23612–23618. doi: 10.1074/jbc.270.40.23612
- Kirberg, J., von Boehmer, H., Brocker, T., Rodewald, H. R., and Takeda, S. (2001). Class II essential for CD4 survival. *Nat. Immunol.* 2, 136–137. doi: 10.1038/84229
- Kochan, G., Krojer, T., Harvey, D., Fischer, R., Chen, L., Vollmar, M., et al. (2011). Crystal structures of the endoplasmic reticulum aminopeptidase-1 (ERAP1) reveal the molecular basis for N-terminal peptide trimming. *Proc. Natl. Acad. Sci. U.S.A.* 108, 7745–7750. doi: 10.1073/pnas.1101262108
- Kühn, S., and Geyer, M. (2014). Formins as effector proteins of Rho GTPases. *Small GTPases* 5:e29513. doi: 10.4161/sgtp.29513
- Kuijl, C., Savage, N. D. L., Marsman, M., Tuin, A. W., Janssen, L., Egan, D. A., et al. (2007). Intracellular bacterial growth is controlled by a kinase network around PKB/AKT1. *Nature* 450, 725–730. doi: 10.1038/nature06345
- Kyei, G. B., Vergne, I., Chua, J., Roberts, E., Harris, J., Junutula, J. R., et al. (2006). Rab14 is critical for maintenance of Mycobacterium tuberculosis phagosome maturation arrest. *EMBO J.* 25, 5250–5259. doi: 10.1038/sj.emboj.7601407
- Larance, M., Ramm, G., Stöckli, J., van Dam, E. M., Winata, S., Wasinger, V., et al. (2005). Characterization of the role of the Rab GTPase-activating protein AS160 in insulin-regulated GLUT4 trafficking. *J. Biol. Chem.* 280, 37803–37813. doi: 10.1074/jbc.M503897200
- Larsen, S. C., Sylvestersen, K. B., Mund, A., Lyon, D., Mullari, M., Madsen, M. V., et al. (2016). Proteome-wide analysis of arginine monomethylation reveals widespread occurrence in human cells. *Sci. Signal.* 9:rs9. doi: 10.1126/scisignal.aaf7329
- Latz, E., Schoenemeyer, A., Visintin, A., Fitzgerald, K. A., Monks, B. G., Knetter, C. F., et al. (2004). TLR9 signals after translocating from the ER to CpG DNA in the lysosome. *Nat. Immunol.* 5, 190–198. doi: 10.1038/ni1028
- Lee, B. L., Moon, J. E., Shu, J. H., Yuan, L., Newman, Z. R., Schekman, R., et al. (2013). UNC93B1 mediates differential trafficking of endosomal TLRs. *eLife* 2:e00291. doi: 10.7554/eLife.00291
- Li, D. T., Habtemichael, E. N., Julca, O., Sales, C. I., Westergaard, X. O., DeVries, S. G., et al. (2019). GLUT4 storage vesicles: specialized organelles for regulated trafficking. *Yale J. Biol. Med.* 92, 453–470.
- Love, P. E., and Hayes, S. M. (2010). ITAM-mediated signaling by the T-cell antigen receptor. *Cold Spring Harb. Perspect. Biol.* 2:a002485. doi: 10.1101/cshperspect.a002485
- Mafakheri, S., Chad, A., and Al-Hasani, H. (2018a). Regulation of RabGAPs involved in insulin action. *Biochem. Soc. Trans.* 46, 683–690. doi: 10.1042/BST20170479
- Mafakheri, S., Flörke, R. R., Kanngießer, S., Hartwig, S., Espelage, L., De Wendt, C., et al. (2018b). AKT and AMP-activated protein kinase regulate TBC1D1 through phosphorylation and its interaction with the cytosolic tail of insulin-regulated aminopeptidase IRAP. *J. Biol. Chem.* 293, 17853–17862. doi: 10.1074/jbc.RA118.005040
- Majer, O., Liu, B., and Barton, G. M. (2017). Nucleic acid-sensing TLRs: trafficking and regulation. *Curr. Opin. Immunol.* 44, 26–33. doi: 10.1016/j.coi.2016.10.003
- Majer, O., Liu, B., Woo, B. J., Kreuk, L. S. M., Van Dis, E., and Barton, G. M. (2019). Release from UNC93B1 reinforces the compartmentalized activation of select TLRs. *Nature* 575, 371–374. doi: 10.1038/s41586-019-1611-7
- Mpakali, A., Giastas, P., Mathioudakis, N., Mavridis, I. M., Saridakis, E., and Stratikos, E. (2015a). Structural basis for antigenic peptide recognition and processing by endoplasmic reticulum (ER) aminopeptidase 2. *J. Biol. Chem.* 290, 26021–26032. doi: 10.1074/jbc.M115.685909
- Mpakali, A., Giastas, P., Deprez-Poulain, R., Papakyriakou, A., Koumantou, D., Gealageas, R., et al. (2017a). Crystal structures of ERAP2 complexed with inhibitors reveal pharmacophore requirements for optimizing inhibitor potency. *ACS Med. Chem. Lett.* 8, 333–337. doi: 10.1021/acsmchemlett.6b00505
- Mpakali, A., Saridakis, E., Harlos, K., Zhao, Y., Kokkala, P., Georgiadis, D., et al. (2017b). Ligand-induced conformational change of insulin-regulated



- aminopeptidase: insights on catalytic mechanism and active site plasticity. *J. Med. Chem.* 60, 2963–2972. doi: 10.1021/acs.jmedchem.6b01890
- Mpakali, A., Saridakis, E., Harlos, K., Zhao, Y., Papakyriakou, A., Kokkala, P., et al. (2015b). Crystal structure of insulin-regulated aminopeptidase with bound substrate analogue provides insight on antigenic epitope precursor recognition and processing. *J. Immunol.* 195, 2842–2851. doi: 10.4049/jimmunol.1501103
- Nagasaka, T., Nomura, S., Okamura, M., Tsujimoto, M., Nakazato, H., Oiso, Y., et al. (1997). Immunohistochemical localization of placental leucine aminopeptidase/oxytocinase in normal human placental, fetal and adult tissues. *Reprod. Fertil. Dev.* 9, 747–753. doi: 10.1071/r97055
- Nguyen, T. T., Chang, S.-C., Evnouchidou, I., York, I. A., Zikos, C., Rock, K. L., et al. (2011). Structural basis for antigenic peptide precursor processing by the endoplasmic reticulum aminopeptidase ERAP1. *Nat. Struct. Mol. Biol.* 18, 604–613. doi: 10.1038/nsmb.2021
- Ofner, L. D., and Hooper, N. M. (2002). Ectodomain shedding of cystinyl aminopeptidase from human placental membranes. *Placenta* 23, 65–70. doi: 10.1053/plac.2001.0751
- Pan, X., Meriin, A., Huang, G., and Kandror, K. V. (2019). Insulin-responsive amino peptidase follows the Glut4 pathway but is dispensable for the formation and translocation of insulin-responsive vesicles. *Mol. Biol. Cell.* 30, 1536–1543. doi: 10.1091/mbc.E18-12-0792
- Pan, X., Zaarur, N., Singh, M., Morin, P., and Kandror, K. V. (2017). Sortilin and retromer mediate retrograde transport of Glut4 in 3T3-L1 adipocytes. *Mol. Biol. Cell.* 28, 1667–1675. doi: 10.1091/mbc.E16-11-0777
- Park, B., Brinkmann, M. M., Spooner, E., Lee, C. C., Kim, Y.-M., and Ploegh, H. L. (2008). Proteolytic cleavage in an endolysosomal compartment is required for activation of Toll-like receptor 9. *Nat. Immunol.* 9, 1407–1414. doi: 10.1038/ni.1669
- Parker, B. L., Thaysen-Andersen, M., Fazakerley, D. J., Holliday, M., Packer, N. H., and James, D. E. (2016). Terminal galactosylation and sialylation switching on membrane glycoproteins upon TNF- $\alpha$ -induced insulin resistance in adipocytes. *Mol. Cell. Proteomics* 15, 141–153. doi: 10.1074/mcp.M115.054221
- Peck, G. R., Ye, S., Pham, V., Fernando, R. N., Macaulay, S. L., Chai, S. Y., et al. (2006). Interaction of the Akt substrate, AS160, with the glucose transporter 4 vesicle marker protein, insulin-regulated aminopeptidase. *Mol. Endocrinol.* 20, 2576–2583. doi: 10.1210/me.2005-0476
- Rahmani, F., and Rezaei, N. (2016). Therapeutic targeting of Toll-like receptors: a review of Toll-like receptors and their signaling pathways in psoriasis. *Expert Rev. Clin. Immunol.* 12, 1289–1298. doi: 10.1080/1744666X.2016.1204232
- Rogi, T., Tsujimoto, M., Nakazato, H., Mizutani, S., and Tomoda, Y. (1996). Human placental leucine aminopeptidase/oxytocinase. A new member of type II membrane-spanning zinc metallopeptidase family. *J. Biol. Chem.* 271, 56–61. doi: 10.1074/jbc.271.1.56
- Ross, S. A., Scott, H. M., Morris, N. J., Leung, W. Y., Mao, F., Lienhard, G. E., et al. (1996). Characterization of the insulin-regulated membrane aminopeptidase in 3T3-L1 adipocytes. *J. Biol. Chem.* 271, 3328–3332. doi: 10.1074/jbc.271.6.3328
- Ryu, J., Hah, J. S., Park, J. S. S., Lee, W., Rampal, A. L., and Jung, C. Y. (2002). Protein kinase C-zeta phosphorylates insulin-responsive aminopeptidase in vitro at Ser-80 and Ser-91. *Arch. Biochem. Biophys.* 403, 71–82. doi: 10.1016/S0003-9861(02)00261-8
- Salter, A. I., Ivey, R. G., Kennedy, J. J., Voillet, V., Rajan, A., Alderman, E. J., et al. (2018). Phosphoproteomic analysis of chimeric antigen receptor signaling reveals kinetic and quantitative differences that affect cell function. *Sci. Signal.* 11:eat6753. doi: 10.1126/scisignal.aat6753
- Saravia, J., Raynor, J. L., Chapman, N. M., Lim, S. A., and Chi, H. (2020). Signaling networks in immunometabolism. *Cell Res.* 30, 328–342. doi: 10.1038/s41422-020-0301-1
- Sasai, M., Linehan, M. M., and Iwasaki, A. (2010). Bifurcation of Toll-like receptor 9 signaling by adaptor protein 3. *Science* 329, 1530–1534. doi: 10.1126/science.1187029
- Saveanu, L., Carroll, O., Lindo, V., Del Val, M., Lopez, D., Lepelletier, Y., et al. (2005). Concerted peptide trimming by human ERAP1 and ERAP2 aminopeptidase complexes in the endoplasmic reticulum. *Nat. Immunol.* 6, 689–697. doi: 10.1038/ni1208
- Saveanu, L., Carroll, O., Weimershaus, M., Guernonprez, P., Firat, E., Lindo, V., et al. (2009). IRAP identifies an endosomal compartment required for MHC class I cross-presentation. *Science* 325, 213–217. doi: 10.1126/science.1172845
- Saveanu, L., and van Endert, P. (2012). The role of insulin-regulated aminopeptidase in MHC class I antigen presentation. *Front. Immunol.* 3:57. doi: 10.3389/fimmu.2012.00057
- Savina, A., Jancic, C., Hugues, S., Guernonprez, P., Vargas, P., Moura, I. C., et al. (2006). NOX2 controls phagosomal pH to regulate antigen processing during crosspresentation by dendritic cells. *Cell* 126, 205–218. doi: 10.1016/j.cell.2006.05.035
- Schonbrunn, A. (1999). Somatostatin receptors present knowledge and future directions. *Ann. Oncol.* 10(Suppl. 2), S17–S21. doi: 10.1093/annonc/10.suppl\_2.s17
- Segura, E., Albiston, A. L., Wicks, I. P., Chai, S. Y., and Villadangos, J. A. (2009). Different cross-presentation pathways in steady-state and inflammatory dendritic cells. *Proc. Natl. Acad. Sci. U.S.A.* 106, 20377–20381. doi: 10.1073/pnas.0910295106
- Sepulveda, F. E., Maschalidi, S., Colisson, R., Heslop, L., Ghirelli, C., Sakka, E., et al. (2009). Critical role for asparagine endopeptidase in endocytic Toll-like receptor signaling in dendritic cells. *Immunity* 31, 737–748. doi: 10.1016/j.immuni.2009.09.013
- Shi, J., Huang, G., and Kandror, K. V. (2008). Self-assembly of Glut4 storage vesicles during differentiation of 3T3-L1 adipocytes. *J. Biol. Chem.* 283, 30311–30321. doi: 10.1074/jbc.M805182200
- Shores, E. W., Huang, K., Tran, T., Lee, E., Grinberg, A., and Love, P. E. (1994). Role of TCR zeta chain in T cell development and selection. *Science* 266, 1047–1050. doi: 10.1126/science.7526464
- Soares, H., Lasserre, R., and Alcover, A. (2013). Orchestrating cytoskeleton and intracellular vesicle traffic to build functional immunological synapses. *Immunol. Rev.* 256, 118–132. doi: 10.1111/imr.12110
- Summers, S. A., Yin, V. P., Whiteman, E. L., Garza, L. A., Cho, H., Tuttle, R. L., et al. (1999). Signaling pathways mediating insulin-stimulated glucose transport. *Ann. N. Y. Acad. Sci.* 892, 169–186. doi: 10.1111/j.1749-6632.1999.tb07795.x
- Sun, Y., Chiu, T. T., Foley, K. P., Bilan, P. J., and Klip, A. (2014). Myosin Va mediates Rab8A-regulated GLUT4 vesicle exocytosis in insulin-stimulated muscle cells. *Mol. Biol. Cell.* 25, 1159–1170. doi: 10.1091/mbc.E13-08-0493
- Tobin, V. A., Arechaga, G., Brunton, P. J., Russell, J. A., Leng, G., Ludwig, M., et al. (2014). Oxytocinase in the female rat hypothalamus: a novel mechanism controlling oxytocin neurones during lactation. *J. Neuroendocrinol.* 26, 205–216. doi: 10.1111/jne.12141
- Tojo, H., Kaieda, I., Hattori, H., Katayama, N., Yoshimura, K., Kakimoto, S., et al. (2003). The Formin family protein, formin homolog overexpressed in spleen, interacts with the insulin-responsive aminopeptidase and profilin IIa. *Mol. Endocrinol.* 17, 1216–1229. doi: 10.1210/me.2003-0056
- Tsujimoto, M., and Hattori, A. (2005). The oxytocinase subfamily of M1 aminopeptidases. *Biochim. Biophys. Acta* 1751, 9–18. doi: 10.1016/j.bbapap.2004.09.011
- Udeshi, N. D., Svinkina, T., Mertins, P., Kuhn, E., Mani, D. R., Qiao, J. W., et al. (2013). Refined preparation and use of anti-diglycine remnant (K-e-GG) antibody enables routine quantification of 10,000s of ubiquitination sites in single proteomics experiments. *Mol. Cell. Proteomics* 12, 825–831. doi: 10.1074/mcp.O112.027094
- Watson, R. T., Hou, J. C., and Pessin, J. E. (2008). Recycling of IRAP from the plasma membrane back to the insulin-responsive compartment requires the Q-SNARE syntaxin 6 but not the GGA clathrin adaptors. *J. Cell. Sci.* 121, 1243–1251. doi: 10.1242/jcs.017517
- Weimershaus, M., Evnouchidou, I., Saveanu, L., and van Endert, P. (2013). Peptidases trimming MHC class I ligands. *Curr. Opin. Immunol.* 25, 90–96. doi: 10.1016/j.coi.2012.10.001
- Weimershaus, M., Maschalidi, S., Sepulveda, F., Manoury, B., van Endert, P., and Saveanu, L. (2012). Conventional dendritic cells require IRAP-Rab14 endosomes for efficient cross-presentation. *J. Immunol.* 188, 1840–1846. doi: 10.4049/jimmunol.1101504
- Weimershaus, M., Mauvais, F.-X., Saveanu, L., Adiko, C., Babdor, J., Abramova, A., et al. (2018). Innate immune signals induce anterograde endosome transport promoting MHC class I cross-presentation. *Cell. Rep.* 24, 3568–3581. doi: 10.1016/j.celrep.2018.08.041
- Werno, M. W., and Chamberlain, L. H. (2015). S-acylation of the insulin-responsive aminopeptidase (IRAP): quantitative analysis and identification of modified cysteines. *Sci. Rep.* 5:12413. doi: 10.1038/srep12413



- Wollscheid, B., Bausch-Fluck, D., Henderson, C., O'Brien, R., Bibel, M., Schiess, R., et al. (2009). Mass-spectrometric identification and relative quantification of N-linked cell surface glycoproteins. *Nat. Biotechnol.* 27, 378–386. doi: 10.1038/nbt.1532
- Yudushkin, I. A., and Vale, R. D. (2010). Imaging T-cell receptor activation reveals accumulation of tyrosine-phosphorylated CD3 $\zeta$  in the endosomal compartment. *Proc. Natl. Acad. Sci. U.S.A.* 107, 22128–22133. doi: 10.1073/pnas.1016388108
- Zeigerer, A., McBrayer, M. K., and McGraw, T. E. (2004). Insulin stimulation of GLUT4 exocytosis, but not its inhibition of endocytosis, is dependent on RabGAP AS160. *Mol. Biol. Cell.* 15, 4406–4415. doi: 10.1091/mbc.e04-04-0333

**Conflict of Interest:** The authors declare that the research was conducted in the absence of any commercial or financial relationships that could be construed as a potential conflict of interest.

Copyright © 2020 Descamps, Evnouchidou, Caillens, Drjac, Riffault, van Endert and Saveanu. This is an open-access article distributed under the terms of the Creative Commons Attribution License (CC BY). The use, distribution or reproduction in other forums is permitted, provided the original author(s) and the copyright owner(s) are credited and that the original publication in this journal is cited, in accordance with accepted academic practice. No use, distribution or reproduction is permitted which does not comply with these terms.



# Insulin-Regulated Aminopeptidase Inhibition Ameliorates Metabolism in Obese Zucker Rats

Katarina Krskova<sup>1\*</sup>, Lucia Balazova<sup>1</sup>, Viktoria Dobrocsyova<sup>1</sup>, Rafal Olszanecki<sup>2</sup>, Maciej Suski<sup>2</sup>, Siew Yeen Chai<sup>3</sup> and Štefan Zorad<sup>1</sup>

<sup>1</sup> Institute of Experimental Endocrinology, Biomedical Research Center, Department of Endocrine Regulations and Psychopharmacology, Slovak Academy of Sciences, Bratislava, Slovakia, <sup>2</sup> Department of Pharmacology, Jagiellonian University Medical College, Cracow, Poland, <sup>3</sup> Monash Biomedicine Discovery Institute, Department of Physiology, Monash University, Clayton, VIC, Australia

## OPEN ACCESS

### Edited by:

Cesare Indiveri,  
University of Calabria, Italy

### Reviewed by:

Christian Borgo,  
University of Padua, Italy  
Soudamani Singh,  
Marshall University, United States

### \*Correspondence:

Katarina Krskova  
katarina.krskova@savba.sk;  
krskova.katka@gmail.com

### Specialty section:

This article was submitted to  
Cellular Biochemistry,  
a section of the journal  
Frontiers in Molecular Biosciences

**Received:** 22 July 2020

**Accepted:** 06 November 2020

**Published:** 04 December 2020

### Citation:

Krskova K, Balazova L,  
Dobrocsyova V, Olszanecki R,  
Suski M, Chai SY and Zorad Š (2020)  
Insulin-Regulated Aminopeptidase  
Inhibition Ameliorates Metabolism  
in Obese Zucker Rats.  
Front. Mol. Biosci. 7:586225.  
doi: 10.3389/fmolb.2020.586225

The aim of our study was to determine the influence of inhibition of insulin-regulated aminopeptidase/oxytocinase (IRAP) on glucose tolerance and metabolism of skeletal muscle and visceral adipose tissue in obese Zucker rats. Obese Zucker rats administered with IRAP inhibitor-HFI-419 at a dose of 29  $\mu$ g/100 g BW/day by osmotic minipumps implanted subcutaneously for 2 weeks. Two-hour intraperitoneal glucose tolerance test (ipGTT) was performed in fasting rats. Plasma oxytocin levels were measured by enzyme immunoassay after plasma extraction. In the musculus quadriceps and epididymal adipose tissue, the expression of factors affecting tissue oxidative status and metabolism was determined by real-time qPCR and/or Western blot analysis. The plasma and tissue enzymatic activities were determined by colorimetric or fluorometric method. Circulated oxytocin levels in obese animals strongly tended to increase after HFI-419 administration. This was accompanied by significantly improved glucose utilization during ipGTT and decreased area under the curve (AUC) for glucose. In skeletal muscle IRAP inhibitor treatment up-regulated enzymes of antioxidant defense system – superoxide dismutase 1 and 2 and improved insulin signal transduction pathway. HFI-419 increased skeletal muscle aminopeptidase A expression and activity and normalized its plasma levels in obese animals. In epididymal adipose tissue, gene expression of markers of inflammation and adipocyte hypertrophy was down-regulated in obese rats after HFI-419 treatment. Our results demonstrate that IRAP inhibition improves whole-body glucose tolerance in insulin-resistant Zucker fatty rats and that this metabolic effect of HFI-419 involves ameliorated redox balance in skeletal muscle.

**Keywords:** obesity, insulin resistance, insulin-regulated aminopeptidase, IRAP, HFI-419

## INTRODUCTION

Obesity comprises one of the key risk factors for the metabolic syndrome and contributes to the development of insulin resistance and subsequently to type two diabetes mellitus, atherogenic dyslipidemia and cardiovascular disease (Ritchie and Connell, 2007). The high fat intake is associated with oxidative stress and activation of pro-inflammatory transcription factors (Ritchie and Connell, 2007). One of the most deleterious effects of obesity is the deposition of lipids

in non-adipose tissues and hyperlipidemia-induced reactive oxygen species production leading to mitochondrial dysfunction in insulin-responsive tissues which might promote inhibition of insulin action (Di Meo et al., 2017). The Zucker fatty rat represents a well-established model of human obesity and insulin resistance. Obesity in this animal model is a consequence of spontaneous mutation (fa) in the gene encoding the leptin receptor resulting in hyperphagia (Phillips et al., 1996).

Insulin-regulated aminopeptidase (IRAP; leucyl-cystinyl aminopeptidase; oxytocinase), encoded by a *Lnpep* gene, has a broad distribution including skeletal muscle and white adipose tissue (Chai et al., 2004). IRAP is predominantly present in cytosolic vesicles together with the glucose transporter (GLUT4), from where they translocate to the plasma membrane upon insulin stimulation. The IRAP is a membrane bound protein belonging to the M1 family of aminopeptidases and its substrates include vasopressin and oxytocin (Chai et al., 2004). IRAP has been proposed as the surrogate marker of insulin-regulated vesicular traffic along with GLUT4 since the presence of IRAP is required for maintaining normal insulin-dependent translocation as well as forming an insulin-responsive vesicular compartment at the plasma membrane (Gross et al., 2004).

It has been found out that obesity in Zucker rats and also ob/ob mice is associated with a high plasma aminopeptidase A (AP-A) activity, the enzyme responsible for generating angiotensin III, thus contributing to blood pressure control (Morais et al., 2017; Lory et al., 2019). In our previous study we have shown that increased AP-A release from the skeletal muscle in obese Zucker rats significantly contributes to elevated plasma AP-A activity (Lory et al., 2019).

Recently, we have shown that obesity is accompanied by marked reduction of plasma oxytocin level in Zucker fatty rats caused by increased peptide degradation by liver and adipose tissue (Gajdosechova et al., 2014). This study highlighted the importance of the oxytocin system in the pathogenesis of obesity and suggested oxytocinase inhibition to improve obesity-induced metabolic disturbances. Several studies have examined the role of IRAP in obesity and glucose handling using various animal models. Results have revealed that insulin regulated traffic of IRAP toward membrane fraction in adipocytes is disturbed by monosodium glutamate-induced obesity (Alponti et al., 2015) and IRAP deficiency in mice fed high-fat diet lead to prevention of development of obesity (Niwa et al., 2015). On the other hand, acute inhibition of IRAP aminopeptidase activity with specific inhibitor, HFI-419, does not affect glucose homeostasis in the streptozotocin-induced experimental rat model of diabetes mellitus (Albiston et al., 2017). However, the effect of inhibitor of aminopeptidase activity HFI-419 on the physiology of skeletal muscle and adipose tissue in obese pre-diabetic Zucker rats has not been examined yet. The main hypothesis of our study was that prolonged treatment with IRAP inhibitor moderates oxytocin degradation in tissues, normalizes plasma oxytocin level and alleviates the obese phenotype in Zucker rats.

The aim of our study was to investigate the impact of HFI-419 application on the (i) whole-body metabolic parameters, (ii) expression of the markers of oxidative stress in skeletal

muscle and adipose tissue, and (iii) expression of the tissue-specific parameters involved in their (pato) physiology in obese Zucker rats.

## METHODS

### Animals

Male Zucker fatty rats (fa/fa) were purchased from Harlan (Udine, Italy). The animals were housed in a 12-h light/dark cycle with access to water and standard diet *ad libitum*. At the age of 34 weeks, the animals were divided into three groups. The control group of lean ( $n = 6$ ) as well as the control group of obese ( $n = 6$ ) rats received vehicle (30% cyclodextrin solution) and the experimental group of obese rats ( $n = 6$ ) received IRAP inhibitor (HFI-419) (Merck KGaA, Darmstadt, Germany) in a dose 29  $\mu\text{g}/100\text{ g}$  body weight/day dissolved in 30% solution of cyclodextrin for two weeks via osmotic minipumps (ALZET, CA, United States) implanted subcutaneously, as described previously (Eckertova et al., 2011). After the minipumps were implanted, the rats were housed two per cage and were separated by a transparent barrier. On the 12th day, animals were subjected to intraperitoneal glucose tolerance test (ipGTT). After 2 days of recovery, overnight-fasted animals were sacrificed by decapitation at the age of 34 weeks. Experimental procedures involving animals were approved by the Jagiellonian University Ethical Committee on Animal Experiments and conformed to Declaration of Helsinki.

### Intraperitoneal Glucose Tolerance Test

The ipGTT was performed to assess glucose clearance. Overnight-fasted rats were administered an intraperitoneal injection of 50% glucose (w/v) at a dose of 2 g/kg body weight. The blood glucose was measured in the tail vein blood prior to and 30, 60, 90, and 120 min after glucose administration using a glucometer (Accu-Check Active, Roche Diagnostics, Switzerland).

### Measurement of Selected Metabolic Parameters and Hormones

After decapitation the trunk blood was collected in cooled tubes containing EDTA as anticoagulant and centrifuged immediately at 4°C to separate plasma, which was stored in aliquots at -20°C until analysed. Fasting plasma insulin level was measured using commercial radioimmunoassay kit (Millipore, Bedford, MA, United States) following the manufacturer's protocol. Fasting plasma glucose levels were measured using the multianalyser COBAS Integra 800 (Roche Diagnostics Ltd., Rotkreuz, Switzerland). Plasma lipid profile determination was performed using commercially available kits (Roche Molecular Diagnostics, Pleasanton, CA, United States). Quantitative insulin sensitivity check index (QUICKI) was calculated as follows: inverse of the sum of the logarithms of the fasting insulin ( $\mu\text{U}/\text{ml}$ ) and fasting glucose (mg/dl). Plasma oxytocin concentrations were measured by EIA (Phoenix Pharmaceuticals, Burlingame, CA, United States) after extraction of the peptides using C-18

SEP COLUMN, following the manufacturer's instructions. Precision of the assay declared by the manufacturer is: intra-assay variation <10%; inter-assay variation: <15%. Plasma C-peptide 2 concentrations were measured by ELISA (EMD Millipore Corporation, St. Louis, MO, United States) following the manufacturer's protocol.

## RNA Isolation and Real-Time PCR

Prior to sampling for RNA, dissected samples from *musculus quadriceps* and epididymal adipose tissues were removed, frozen in liquid nitrogen and stored at  $-80^{\circ}\text{C}$  until analysis. Total RNA was isolated using RNeasy Plus Universal Mini Kit (Qiagen, Valencia, CA, United States) following the manufacturer's instructions. The reverse transcription of isolated RNA was performed using Maxima First Strand cDNA Synthesis Kit (Thermo Fisher, Waltham, MA, United States) according to the manufacturer's protocol. Real-time PCRs were carried out applying Maxima SYBR Green qPCR Master Mix (Thermo Fisher, Waltham, MA, United States) and run on an ABI 7900HT thermal cycler (Applied Biosystems, Life Technologies, Carlsbad, CA, United States) using rat-specific primer pairs as described previously (Dobrocsyova et al., 2020). Data were normalized to the expression of housekeeping gene ribosomal protein S29 (*Rps29*) which was not altered by the treatment.

## Measurement of Enzyme Activity

Activity of glutamyl aminopeptidase was determined in the membrane fraction. Skeletal muscle and epididymal adipose tissue were homogenized using a glass Teflon homogenizer in lysis buffer (250 mM saccharose, 10 mM Tris, pH 7.4). The homogenates were centrifuged at  $1,000 \times g/10 \text{ min}/4^{\circ}\text{C}$ . The supernatants were collected and centrifuged at  $16,000 \times g/15 \text{ min}/4^{\circ}\text{C}$  to separate the membrane fraction. Protein concentration was measured by the Bicinchoninic Acid Protein Assay (Sigma-Aldrich, St. Louis, MO, United States). Prepared samples were mixed with substrate solution containing 100mM H-Glu- $\beta$ -naphthylamide (Bachem, Bubendorf, Switzerland), 10 mg/100 ml bovine serum albumin, 10 mg/100 ml dithiothreitol, 50 mM CaCl<sub>2</sub> in 50 mM Tris pH 7.4. The 96-well plate was placed in a Synergy H4 Hybrid Reader (BioTek, Winooski, VT, United States) fluorimeter and the enzyme kinetics was measured during 60 min at  $37^{\circ}\text{C}$  with data collection in 5-min intervals as the amount of  $\beta$ -naphthylamide released from the substrate due to the enzyme activity of AP-A at wavelengths 340 nm (excitation) and 410 nm (emission).

Superoxide dismutase activity was measured in skeletal muscle tissue samples by colorimetric SOD Activity Assay Kit (Abcam, Cambridge, United Kingdom). Tissue homogenization and assay procedure were performed in accordance with the manufacturer's protocol.

## Western Blot

Quadriceps muscle was homogenized as described previously (Gajdosechova et al., 2014). After separation of proteins by SDS-PAGE electrophoresis and their transfer to a PVDF membrane (Immobilon-FL, Millipore, Bedford, MA, United States) the blots were incubated with primary antibody overnight at

$4^{\circ}\text{C}$  against insulin receptor substrate 1 (IRS-1) total protein or its phosphorylated form at residue Ser307 and Ser612 (#2382, #2381, and #2386, respectively; all purchased in Cell Signaling Technology, Danvers, MA, United States), insulin receptor  $\beta$  (IR $\beta$ ) total and phosphorylated IR $\beta$  at Tyr1150/1151 residue (#3025 and #3024, Cell Signaling Technology, Danvers, MA, United States), SOD1, SOD2, NAD-dependent protein deacetylase sirtuin-1 (SirT1) and GAPDH (#37385, #13141, #9475, and #5174, respectively; Cell Signaling Technology, Danvers, MA) diluted (1:1000) in blocking buffer containing 0.1% Igepal. After membrane washing, the signal of fluorescently labeled secondary anti-rabbit IgG (#5151; Cell Signaling Technology, Danvers, MA, United States) was detected using the Odyssey infrared imaging system (LI-COR Biosciences, Lincoln, NE, United States) and quantified by Odyssey IR imaging system software version 2.0.

## Statistical Analysis

The results are presented as mean  $\pm$  SEM. Analysis of normally distributed data was performed using the Kolmogorov-Smirnov test. Non-normally distributed data were subjected to natural logarithm transformation prior to statistical analysis. ANOVA with repeated measures was used to analyze glycemia at different time points of glucose tolerance test. Differences in basic metabolic and morphometric parameters, hormone levels and total area under the curve (AUC) for the glucose between experimental groups were analyzed by one-way ANOVA and differences between obese rats treated with vehicle and obese rats treated with HFI-419 aimed at determining skeletal muscle and adipose tissue metabolism were analyzed using Student's *t*-test. Overall level of statistical significance was reached at  $*p < 0.05$ ,  $**p < 0.01$ , and  $***p < 0.001$ .

## RESULTS

We determined the basic characteristics of systemic metabolic and morphometric parameters in lean and obese Zucker rats and obese Zucker rats treated with HFI-419 for two weeks. As expected, obesity in Zucker (*fa/fa*) rats was accompanied by an increase in plasma insulin, C-peptide 2, triglycerides, cholesterol and LDL/HDL ratio, decreased insulin sensitivity index (QUICKI) and plasma oxytocin level without significant changes in fasting glycemia (Table 1). Plasma oxytocin concentration displayed a strong tendency ( $p = 0.058$ ) toward increase after HFI-419 treatment. Two weeks administration of HFI-419 had no statistically significant effect on obesity-induced impaired metabolic and morphometric parameters (Table 1).

In order to determine the systemic effect of HFI-419 on glucose utilization, we performed ipGTT (Figure 1). The ANOVA with repeated measures revealed significant interaction between time and group of rats ( $p < 0.001$ ) and subsequent *post hoc* analysis detected that HFI-419 treatment in obese rats led to decline of blood glucose at 30 ( $p < 0.001$ ), 60 ( $p < 0.001$ ), and 90 ( $p < 0.01$ ) min after the glucose load when compared with obese animals treated with vehicle (Figure 1A). Similar marked tendency for 2-h glycemia to decrease ( $p = 0.065$ ) was



**TABLE 1** | Metabolic parameters in lean and obese Zucker rats treated with vehicle and obese Zucker rats treated with HFI-419.

	leanVEH (n = 6)	obVEH (n = 6)	obHFI-419 (n = 6)	ANOVA p
Body weight (g)	419.2 ± 18.0	608.5 ± 33.3 ***	161.0 ± 9.5 ***	<0.001
Fasting glycemia (mmol/l)	6.30 ± 0.20	6.48 ± 0.10	6.63 ± 0.27	0.523
Fasting insulin (ng/ml)	0.93 ± 0.20	10.91 ± 1.07 ***	11.66 ± 0.79 ***	<0.001
C-peptide (pM)	266 ± 37	1745 ± 121 ***	1734 ± 87 ***	<0.001
QUICKI <sup>#</sup>	0.294 ± 0.010	0.220 ± 0.002 ***	0.218 ± 0.002 ***	<0.001
2-h glycemia (mmol/l)	5.97 ± 0.44	9.75 ± 0.61 ***	8.33 ± 0.30 ***	0.001
Triglycerides (mmol/l)	1.07 ± 0.07	3.54 ± 0.57 ***	4.21 ± 0.69 ***	<0.001
Cholesterol (mmol/l)	2.48 ± 0.09	6.40 ± 0.41 ***	7.18 ± 0.70 ***	<0.001
LDL/HDL	0.205 ± 0.015	0.418 ± 0.037 *	0.510 ± 0.108 *	0.005
Plasma oxytocin (pg/ml)	26.98 ± 8.50	2.88 ± 1.01 **	7.79 ± 1.74	0.013

<sup>#</sup>QUICKI: quantitative insulin sensitivity check index. Data are presented as mean ± SEM and were analyzed using one-way ANOVA with Holm-Sidak post hoc test: \*p < 0.05, \*\*p < 0.01, \*\*\*p < 0.001 vs. leanVEH.

observed after the treatment (Table 1). Calculated AUC for glucose from ipGTT data was significantly reduced after HFI-419 administration (Figure 1B).

Regarding the insulin signaling pathway the protein expression of total insulin receptor  $\beta$  subunit (IR $\beta$ ) and insulin receptor substrate (IRS-1) as well as phosphorylation of IRS-1 at residue Ser307 and Ser612 and IR $\beta$  at residue Tyr1150/1151 were evaluated in skeletal muscle. We did not observe statistically significant differences in total IR $\beta$  content (IR $\beta$ /GAPDH: Vehicle – 1.224 ± 0.092 vs. HFI-419 – 1.215 ± 0.127 a.u.,  $p = 0.589$ ) and total IRS-1 protein level (IRS-1/GAPDH: Vehicle – 0.553 ± 0.084 vs. HFI-419 – 0.499 ± 0.063 a.u.  $p = 0.621$ ) after HFI-419 administration. The ratios of phospho-IR $\beta$  (Tyr1150/1151)/IR $\beta$  was significantly increased by HFI-419 treatment while the phospho-IRS-1 (Ser307)/IRS-1 ratio was significantly reduced by IRAP inhibitor application (Figures 1C,D). The ratio of phospho-IRS-1 (Ser612)/IRS-1 was unaffected by the treatment (Ser612)/IRS-1: Vehicle – 0.238 ± 0.039 vs. HFI-419 – 0.252 ± 0.030 a.u.  $p = 0.780$ ).

The observed changes led us to an extensive investigation of impact of HFI-419 treatment on insulin-responsive tissues metabolism in obese Zucker rats. Regarding skeletal muscle glutamyl aminopeptidase (AP-A), which is dysregulated in obesity, both *Enpep* mRNA level (Figure 1A) and AP-A activity (Figure 2B) were significantly upregulated in this tissue in obese Zucker rats after the treatment. AP-A activity in plasma (Figure 2C) as well as epididymal adipose tissue (Figure 2D) was not affected by HFI-419 administration.

Since hyperlipidemia-induced ROS production in skeletal muscle is involved in inhibition of insulin action, we evaluated the mRNA level of markers of oxidative stress and antioxidant defence mechanism in this tissue as well as in epididymal adipose tissue. In skeletal muscle, statistically significant upregulation of *Sod1* and *Sod2* mRNA levels were detected after HFI-419 administration (Figure 3A). A similar stimulating effect of HFI-419 was found in the case of SOD1 and SOD2 protein expression and SOD enzyme activity (Figures 3C,D). The expression of other genes encoding enzymes with antioxidant properties (*Sod3*, *Nfe2l2*, and *Nos3*) and NOX4 and P22PHOX subunit of NADPH oxidase (*Nox4* and *Cyba*) were not significantly affected by the treatment. In adipose tissue, the expression of prooxidant and

antioxidant genes was found unchanged except for *Cyba* mRNA level, which tended to decrease ( $p = 0.07$ ) in rats treated with HFI-419 (Figure 3B).

In skeletal muscle, significantly elevated level of transcription factor forkhead box protein O1 (*Foxo1*) mRNA, involved in regulation of redox balance, were detected after HFI-419 treatment (Figure 3E). Interestingly, increased protein content of SirT1, regulator of *Foxo* transcriptional activity, were observed in skeletal muscle after HFI-419 administration (Figure 3C). The gene expressions of transforming growth factor  $\beta$ -1 (*Tgfb1*), peroxisome proliferator-activated receptor gamma coactivator 1- $\alpha$  (*Ppargc1a*), involved in mitochondrial biogenesis, and type-2 angiotensin II receptor (*Agtr2*) were not changed in obese Zucker rats receiving HFI-419 (Figure 3E).

Regarding the adipose tissue metabolism, the effect of HFI-419 treatment on the gene expression of markers involved in adipogenesis and inflammation were detected in epididymal fat depot of obese Zucker rats. The *Fabp4* mRNA level was not changed while mesoderm-specific transcript homolog protein (*Mest*) and plasminogen activator inhibitor 1 (*Pai1*) mRNA levels were significantly reduced and C-C chemokine receptor type 2 (*Ccr2*) transcript level tended to decrease ( $p = 0.08$ ) in HFI-419-treated rats (Figure 3F).

## DISCUSSION

The genetically obese Zucker rats (fa/fa) represent a model of insulin resistance and prediabetes characterized by hyperinsulinemia, hyperlipidemia and peripheral glucose intolerance which is caused largely by an impairment of insulin-stimulated glucose uptake into skeletal muscle, the major site of insulin-mediated glucose disposal (Ionescu et al., 1985; King et al., 1992). We and other authors have previously shown that obesity is associated with dysregulation of IRAP activity in adipose tissue and skeletal muscle along with reduced plasma oxytocin due to increased peptide degradation by peripheral tissues (Gajdosechova et al., 2014; Alponi et al., 2015). A study on IRAP-knockout mice showed protective effect of aminopeptidase deficiency against development of obesity (Niwa et al., 2015). In order to investigate the impact

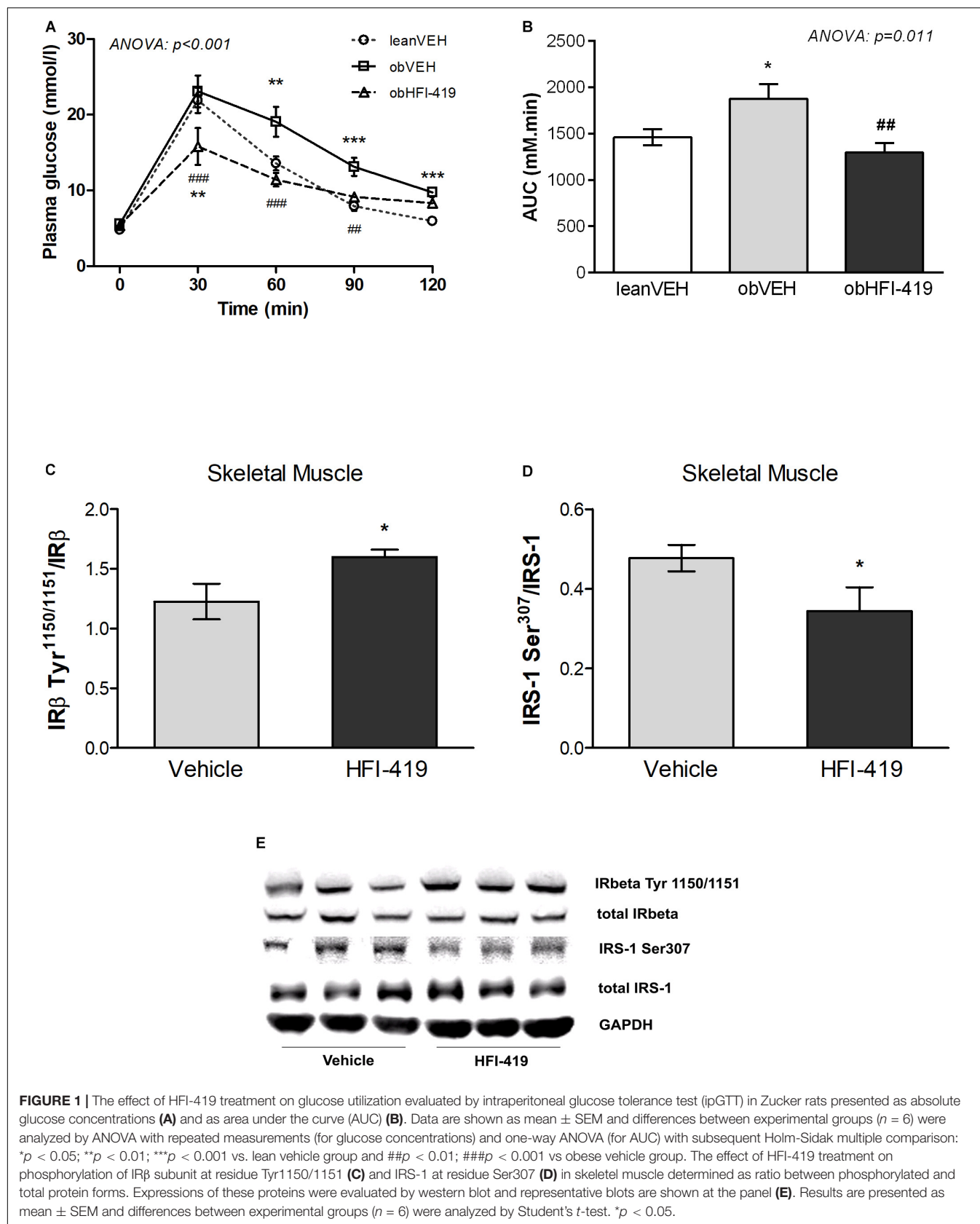
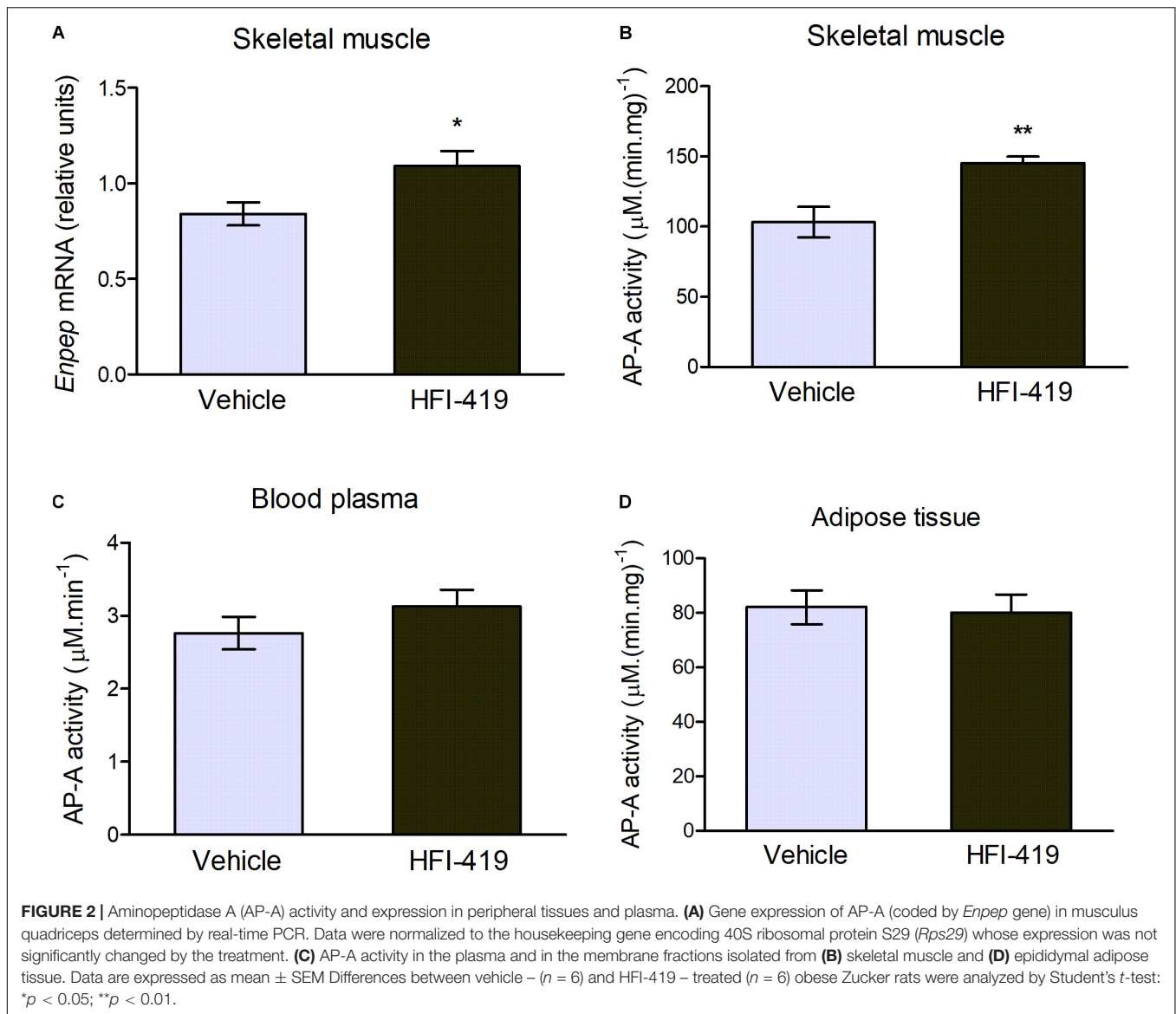


**FIGURE 1 |** The effect of HFI-419 treatment on glucose utilization evaluated by intraperitoneal glucose tolerance test (ipGTT) in Zucker rats presented as absolute glucose concentrations (**A**) and as area under the curve (AUC) (**B**). Data are shown as mean  $\pm$  SEM and differences between experimental groups ( $n = 6$ ) were analyzed by ANOVA with repeated measurements (for glucose concentrations) and one-way ANOVA (for AUC) with subsequent Holm-Sidak multiple comparison: \* $p < 0.05$ ; \*\* $p < 0.01$ ; \*\*\* $p < 0.001$  vs. lean vehicle group and ## $p < 0.01$ ; ### $p < 0.001$  vs obese vehicle group. The effect of HFI-419 treatment on phosphorylation of IR $\beta$  subunit at residue Tyr1150/1151 (**C**) and IRS-1 at residue Ser307 (**D**) in skeletal muscle determined as ratio between phosphorylated and total protein forms. Expressions of these proteins were evaluated by western blot and representative blots are shown at the panel (**E**). Results are presented as mean  $\pm$  SEM and differences between experimental groups ( $n = 6$ ) were analyzed by Student's  $t$ -test. \* $p < 0.05$ .



of IRAP inhibition on peripheral glucose tolerance and skeletal muscle and adipose tissue metabolism, we treated obese Zucker rats with HFI-419, a specific inhibitor of IRAP catalytic activity, for 2 weeks.

In our study, we confirmed reduced plasma oxytocin levels in obese eight-month-old rats compared with lean animals. The inhibition of aminopeptidase activity by HFI-419 resulted in a strong elevating tendency of circulating oxytocin level which was accompanied with marked amelioration of the glucose utilization during ipGTT in obese rats treated with IRAP inhibitor. Based on decrease of AUC and 2-h glycemia ( $p = 0.065$ ) to control values in HFI-419 – treated rats, we assume that inhibition of IRAP substantially improved glucose tolerance in obese rats. Decreased blood glucose level at 30 min in obese treated rats compared to both untreated obese and control lean rats during ipGTT may indicate that the HFI-419 treatment could enhance the insulin secretion after the glucose injection. However, plasma

insulin and C-peptide was not determined during ipGTT in our study. Regarding peripheral glucose tolerance, our results are consistent with previous observations in IRAP-deficient mice (*Irap*<sup>-/-</sup>) in which glucose and insulin tolerance tests have revealed that the glucose disposal and the hypoglycemic effect of insulin did not differ between groups of animals fed a normal diet but both of those are improved in *Irap*<sup>-/-</sup> mice after a high-fat diet challenge (Niwa et al., 2015). On the contrary, acute single administration of IRAP inhibitor HFI-419 did not affect peripheral whole-body glucose handling during the glucose and insulin tolerance tests, neither in control rats nor in the streptozotocin-induced experimental rat model of diabetes mellitus type I (Albiston et al., 2017). In keeping with these results, IRAP *in vitro* inhibition (30-min and 24-h) of both basal and insulin-stimulated L6GLUT4myc cells did not alter glucose uptake (Albiston et al., 2017). Thus, the effect of HFI-419 on glucose utilization seems to depend on metabolic status

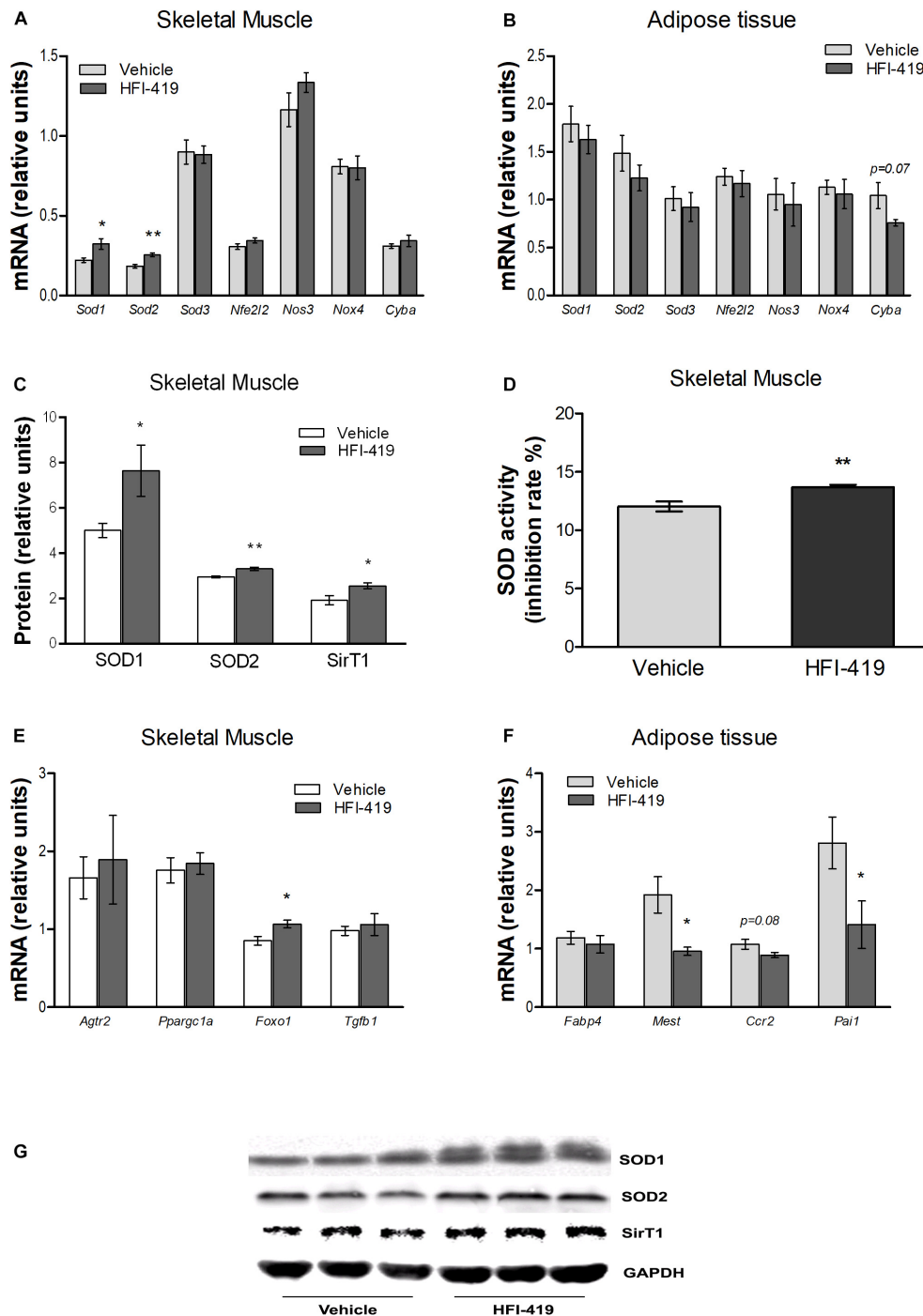


**FIGURE 3 |** Effect of HFI-419 treatment on expression of genes and proteins with pro-oxidant and antioxidant action and genes coding proteins involved in skeletal muscle and adipose tissue metabolism. Gene expression of superoxide dismutase [Cu-Zn] (*Sod1*), superoxide dismutase [Mn] (*Sod2*), extracellular superoxide dismutase [Cu-Zn] (*Sod3*), nuclear factor erythroid 2-related factor 2 (*Nfe2l2*), endothelial nitric oxid synthase (*Nos3*), NADPH oxidase (*Nox4*) and cytochrome b-245 light chain (*Cyba*), type-2 angiotensin II receptor (*Agtr2*), peroxisome proliferator-activated receptor gamma coactivator 1- $\alpha$  (*Ppargc1a*), forkhead box protein O1 (*Foxo1*), transforming growth factor  $\beta$ -1 (*Tgfb1*), fatty acid-binding protein 4 (*Fabp4*), mesoderm-specific transcript homolog protein (*Mest*), C-C chemokine receptor type 2 (*Ccr2*) and plasminogen activator inhibitor 1 (*Pai1*) in musculus quadriceps (**A,E**) and epididymal adipose tissue (**B,F**) of vehicle- and HFI-419-treated obese Zucker rats determined by real-time PCR. Data were normalized to the gene expression of 40S ribosomal protein S29 (*Rps29*) whose expression was not altered by the treatment. Protein expression of SOD1 and SOD2 and silent information regulator 1 (SirT1) (**C**) and SOD activity (**D**) in skeletal muscle of obese vehicle- and HFI-419-treated rats. Expression of proteins was evaluated by western blot and obtained data were normalized to loading control GAPDH whose expression was not altered by the treatment. Representative blots are shown at the panel (**G**). SOD activity is expressed as percentage of inhibition of tetrazolium salt WST-1 conversion to formazan dye and is related to 1 mg of tissue. Data are presented as mean  $\pm$  SEM and were analyzed by Student's *t*-test: \**p* < 0.05; \*\**p* < 0.01.



of the animals with the positive effect seen only in obese and insulin resistant ones.

With regard to potential mechanism for improvement of glucose utilization in HFI-419-treated animals we found beneficial changes in the insulin signaling cascade in the skeletal muscle. The ratio of phospho-IR $\beta$ (Tyr1150/1151)/IR $\beta$  was increased after HFI-419 administration. Insulin receptor subunit  $\beta$  phosphorylation in the Tyr1150/1151 has been demonstrated to be an important control site for transmission of the insulin signal (White et al., 1988). Next we found significantly decreased the ratio of phospho-IRS-1(Ser307)/IRS-1 and unaffected phospho-IRS-1(Ser612)/IRS-1 ratio in skeletal muscle of HFI-419-treated rats. Increased phosphorylation of IRS-1 on residues Ser307 and Ser612 have been suggested to be responsible for the desensitization mechanisms of insulin-stimulated signal transduction which plays an important role in insulin resistance in obesity (Aguirre et al., 2000). Thus, our results suggest that IRAP inhibition has a beneficial effect on glucose metabolism in the skeletal muscle.

We have recently detected obesity-associated significant decrease of membrane-bound AP-A (glutamyl aminopeptidase) activity in the skeletal muscle of Zucker rats accompanied by elevated plasma AP-A activity suggesting stimulated tissue AP-A autolysis due to dyslipidemia in obese phenotype (Lory et al., 2019). AP-A hydrolyses angiotensin II to the heptapeptide angiotensin III which has the highest relative affinity for AT2 receptor and is the most potent endogenous AT2 receptor agonist (Bosnyak et al., 2011). After HFI-419 treatment, we found a significant increase of AP-A gene expression along with a significant increase of membrane-bound AP-A activity in skeletal muscle. Such an upregulation of tissue AP-A activity was not observed in the plasma implicating that IRAP inhibitor has the potential to normalize obesity-impaired release of AP-A into the circulation and normalize the levels of its soluble form. In our previous study, we found a significant (10-fold) increase in AT2 receptor and a parallel decrease in AT1 receptor gene expression in obese 8-month-old Zucker rats (Lory et al., 2019). Regarding skeletal muscle physiology, AT2 receptor activation improves skeletal muscle perfusion, glucose uptake and oxygenation and is required for normal muscle microvascular and metabolic responses to insulin (Chai et al., 2011).

In relation to hyperlipidemia-induced ROS production and mitochondrial dysfunction associated with development of insulin resistance in skeletal muscle, we evaluated expression of genes encoding proteins with pro- and antioxidant properties and found out that HFI-419 treatment elevates the *Sod1* and *Sod2* mRNA levels while the expression of prooxidative genes (*Nox4* and *Cyba*) did not change. Increased superoxide dismutases gene expressions were also reflected in an increase in the SOD1 and SOD2 protein levels as well as in an increase in the SOD enzyme activity in the treated animals. The first line of antioxidant defense systems, critical in maintaining cellular redox balance, consists of superoxide dismutases (SODs), which eliminates superoxide to produce the less reactive H<sub>2</sub>O<sub>2</sub>: the cytosolic Cu/Zn-containing SOD (CuZnSOD encoded by *Sod1* gene), the mitochondrial Mn-containing SOD (MnSOD encoded by *Sod2* gene), and the extracellular SOD (EcSOD encoded by *Sod3* gene)

(Di Meo et al., 2017). Several lines of evidence have been provided that *Sod1* overexpression improves insulin-dependent glucose uptake into cells as well as peripheral glucose tolerance (Hoehn et al., 2009; Boden et al., 2012). Furthermore, *MnSOD*  $-/+$  mice displayed a significant impairment in glucose tolerance despite similar insulin levels to control mice (Hoehn et al., 2009). This upregulation of *Sod1* and *Sod2* genes observed in our study indicate that HFI-419 treatment has a beneficial effect on the skeletal muscle redox homeostasis, which is reflected by the improved glucose utilization. The up-regulation of antioxidant enzymes SOD1 and SOD2 observed in our study suggests that HFI-419 treatment has an improving effect on the skeletal muscle redox homeostasis, which might contribute to skeletal muscle insulin sensitivity.

A novel observation of the present study is that IRAP inhibition induced an elevation of *Foxo1* mRNA, transcription factor highly expressed in the major insulin target tissues, as well as protein content of SirT1, regulator of FoxO transcriptional activity in skeletal muscle of obese rats. It has been shown, that under pathophysiological conditions such insulin resistance and metabolic dysfunction FoxO1 expression may help drive the expression of genes involved in combating oxidative stress and that there is interplay between SirT1 and FoxO in ROS reduction. SirT1 also directly interacts with SOD, which could be regulated through FoxO (Gross et al., 2008; Zhang et al., 2017). It is tempting to speculate, that HFI-419-induced up-regulation of SirT1 protein may be involved in subsequent SOD upregulation and amelioration of oxidative stress in skeletal muscle of obese Zucker rats.

In relation to adipose tissue metabolism, plasminogen activator inhibitor 1 (PAI-1), a key component of fibrinolysis that has been demonstrated within adipose tissue being involved in adipose tissue expansion and insulin resistance was found to be reduced at the mRNA level after treatment with HFI-419. Study using *Irap* $-/-$  mice revealed that IRAP deficiency may lead to attenuated PAI-1 expression in differentiated preadipocytes isolated from inguinal fat pads of mice, since adipocyte *Pai1* mRNA as well as PAI-1 protein and its secretion into the culture medium were lower in adipocytes from *Irap* $-/-$  mice than those of wild-type mice (Wang et al., 2018). PAI-1 also contributes to the development of inflammation in adipose tissue during obesity by mechanism involving up-regulation of M1 (classically activated) macrophage numbers in visceral adipose depot (Wang et al., 2018). In addition to down-regulated *Pai1* mRNA in our study, the gene expression of C-C chemokine receptor type 2 (*Ccr2*), a marker of adipose tissue macrophage infiltration and accumulation (Kim et al., 2016), and mesoderm-specific transcript homolog protein (*Mest*), displayed clear tendency to decline by HFI-419 application. MEST is thought to play a role in the facilitation of lipid accumulation and fat storage in adipocytes, adipogenesis and adipocyte hypertrophy (Takahashi et al., 2005; Prudovsky et al., 2018). Our study confirmed *in vivo* previously observed *in vitro* changes in PAI-1 and has showed a role for IRAP in the regulation of these adipocyte markers.

In summary, our results show that the specific inhibitor of aminopeptidase activity of IRAP, HFI-419, ameliorated the obesity-induced metabolic disturbances in obese Zucker

rats. Beneficial effect was manifested by improvement of the peripheral whole-body glucose tolerance as well as activation of skeletal muscle antioxidant mechanisms and insulin signaling pathway. The results presented are likely to motivate further research as there is a gap in the knowledge regarding the regulation of IRAP/oxytocinase in order to reveal new approaches to modulate metabolism in obesity.

## DATA AVAILABILITY STATEMENT

The raw data supporting the conclusions of this article will be made available by the authors, without undue reservation.

## ETHICS STATEMENT

The animal study was reviewed and approved by the Jagiellonian University Ethical Committee on Animal Experiments.

## AUTHOR CONTRIBUTIONS

KK contributed to the study with the acquisition, analysis, and interpretation of the data, and wrote the first manuscript

draft. LB contributed to the conception and design of the study, and participated in the performance of experiments and acquisition of data. VD participated in the performance of animal experiments and acquisition of data. RO contributed to the conception and design of the study and supervised the experiments with animals. MS contributed to the conception and design of the study and participated in the performance of animal experiments. SC contributed to the conception and design of the study and participated in the methodology. ŠZ participated in the performance of experiments, supervised the research, contributed with the project administration, and provided critical revision of the final form of the manuscript. All authors contributed to the article and approved the submitted version.

## FUNDING

This study was supported by Scientific Grant Agency of the Ministry of Education, Science, Research and Sport of the Slovak Republic and the Slovak Academy of Sciences (VEGA 2/0160/20) and by the Slovak Research and Development Agency APVV (APVV-15-0229 and APVV-15-0565).

## REFERENCES

- Aguirre, V., Uchida, T., Yenush, L., Davis, R., and White, M. F. (2000). The c-Jun NH(2)-terminal kinase promotes insulin resistance during association with insulin receptor substrate-1 and phosphorylation of Ser(307). *J. Biol. Chem.* 275, 9047–9054. doi: 10.1074/jbc.275.12.9047
- Albiston, A. L., Cacador, M., Sinnayay, P., Burns, P., and Chai, S. Y. (2017). Insulin-regulated aminopeptidase inhibitors do not alter glucose handling in normal and diabetic rats. *J. Mol. Endocrinol.* 58, 193–198. doi: 10.1530/jme-17-0033
- Alponti, R. F., Viana, L. G., Yamanouye, N., and Silveira, P. F. (2015). Insulin-regulated aminopeptidase in adipocyte is Cys-specific and affected by obesity. *J. Mol. Endocrinol.* 55, 1–8. doi: 10.1530/jme-14-0321
- Boden, M. J., Brandon, A. E., Tid-Ang, J. D., Preston, E., Wilks, D., Stuart, E., et al. (2012). Overexpression of manganese superoxide dismutase ameliorates high-fat diet-induced insulin resistance in rat skeletal muscle. *Am. J. Physiol. Endocrinol. Metab.* 303, E798–E805.
- Bosnyak, S., Jones, E. S., Christopoulos, A., Aguilar, M.-I., Thomas, W. G., and Widdop, R. E. (2011). Relative affinity of angiotensin peptides and novel ligands at AT1 and AT2 receptors. *Clin. Sci. (Lond.)* 121, 297–303. doi: 10.1042/cs20110036
- Chai, S. Y., Fernando, R., Peck, G., Ye, S.-Y., Mendelsohn, F. A. O., Jenkins, T. A., et al. (2004). The angiotensin IV/AT4 receptor. *Cell Mol. Life Sci.* 61, 2728–2737. doi: 10.1007/s00018-004-4246-1
- Chai, W., Wang, W., Dong, Z., Cao, W., and Liu, Z. (2011). Angiotensin II receptors modulate muscle microvascular and metabolic responses to insulin in vivo. *Diabetes* 60, 2939–2946. doi: 10.2337/db10-1691
- Di Meo, S., Iossa, S., and Venditti, P. (2017). Skeletal muscle insulin resistance: role of mitochondria and other ROS sources. *J. Endocrinol.* 233, R15–R42.
- Dobroczyova, V., Slamkova, M., Krskova, K., Balazova, L., Suski, M., Olszanecki, R., et al. (2020). AVE0991, a nonpeptide angiotensin 1-7 receptor agonist, improves glucose metabolism in the skeletal muscle of obese Zucker rats: possible involvement of prooxidant/antioxidant mechanisms. *Oxid. Med. Cell Longev.* 2020:6372935.
- Eckertova, M., Ondrejčáková, M., Krskova, K., Zorad, S., and Jezov, D. (2011). Subchronic treatment of rats with oxytocin results in improved adipocyte differentiation and increased gene expression of factors involved in adipogenesis. *Br. J. Pharmacol.* 162, 452–463. doi: 10.1111/j.1476-5381.2010.01037.x
- Gajdosechova, L., Krskova, K., Segarra, A. B., Spolcova, A., Suski, M., Olszanecki, R., et al. (2014). Hypoxytocinaemia in obese Zucker rats relates to oxytocin degradation in liver and adipose tissue. *J. Endocrinol.* 220, 333–343. doi: 10.1530/joe-13-0417
- Gross, D. N., Farmer, S. R., and Pilch, P. F. (2004). Glut4 storage vesicles without Glut4: transcriptional regulation of insulin-dependent vesicular traffic. *Mol. Cell Biol.* 24, 7151–7162. doi: 10.1128/mcb.24.16.7151-7162.2004
- Gross, D. N., van den Heuvel, A. P., and Birnbaum, M. J. (2008). The role of FoxO in the regulation of metabolism. *Oncogene* 27, 2320–2336. doi: 10.1038/nc.2008.25
- Hoehn, K. L., Salmon, A. B., Hohnen-Behrens, C., Turner, N., Hoy, A. J., Maghzal, G. J., et al. (2009). Insulin resistance is a cellular antioxidant defense mechanism. *Proc. Natl. Acad. Sci. U.S.A.* 106, 17787–17792.
- Ionescu, E., Sauter, J. F., and Jeanrenaud, B. (1985). Abnormal oral glucose tolerance in genetically obese (fa/fa) rats. *Am. J. Physiol.* 248(5 Pt 1), E500–E506.
- Kim, J., Chung, K., Choi, C., Beloor, J., Ullah, I., Kim, N., et al. (2016). Silencing CCR2 in macrophages alleviates adipose tissue inflammation and the associated metabolic syndrome in dietary obese mice. *Mol. Ther. Nucleic Acids* 5:e280. doi: 10.1038/mtna.2015.51
- King, P. A., Horton, E. D., Hirshman, M. F., and Horton, E. S. (1992). Insulin resistance in obese Zucker rat (fa/fa) skeletal muscle is associated with a failure of glucose transporter translocation. *J. Clin. Invest.* 90, 1568–1575. doi: 10.1172/jci116025
- Lory, V., Balazova, L., Kršková, K., Horváthová, Ľ., Olszanecki, R., Suski, M., et al. (2019). Obesity and aging affects skeletal muscle renin-angiotensin system and myosin heavy chain proportions in pre-diabetic Zucker rats. *J. Physiol. Biochem.* 75, 351–365. doi: 10.1007/s13105-019-00689-1
- Morais, R. L., Hilzendeger, A. M., Visniauskas, B., Todiras, M., Alenina, N., Mori, M. A., et al. (2017). High aminopeptidase A activity contributes to blood pressure control in ob/ob mice by AT2 receptor-dependent mechanism. *Am. J. Physiol. Heart Circ. Physiol.* 312, H437–H445.
- Niwa, M., Numaguchi, Y., Ishii, M., Kuwahata, T., Kondo, M., Shibata, R., et al. (2015). IRAP deficiency attenuates diet-induced obesity in mice through increased energy expenditure. *Biochem. Biophys. Res. Commun.* 457, 12–18. doi: 10.1016/j.bbrc.2014.12.071

- Phillips, M. S., Liu, Q., Hammond, H. A., Dugan, V., Hey, P. J., Caskey, C. J., et al. (1996). Leptin receptor missense mutation in the fatty Zucker rat. *Nat. Genet.* 13, 18–19. doi: 10.1038/ng0596-18
- Prudovsky, I., Anunciado-Koza, R. P., Jacobs, C. G., Kacer, D., Siviski, M. E., Koza, R. A., et al. (2018). Mesoderm-specific transcript localization in the ER and ER-lipid droplet interface supports a role in adipocyte hypertrophy. *J. Cell Biochem.* 119, 2636–2645. doi: 10.1002/jcb.26429
- Ritchie, S. A., and Connell, J. M. (2007). The link between abdominal obesity, metabolic syndrome and cardiovascular disease. *Nutr. Metab. Cardiovasc. Dis.* 17, 319–326. doi: 10.1016/j.numecd.2006.07.005
- Takahashi, M., Kamei, Y., and Ezaki, O. (2005). Mest/Peg1 imprinted gene enlarges adipocytes and is a marker of adipocyte size. *Am. J. Physiol. Endocrinol. Metab.* 288, E117–E124.
- Wang, L., Chen, L., Liu, Z., Liu, Y., Luo, M., Chen, N., et al. (2018). PAI-1 exacerbates white adipose tissue dysfunction and metabolic dysregulation in high fat diet-induced obesity. *Front. Pharmacol.* 9:1087. doi: 10.3389/fphar.2018.01087
- White, M. F., Shoelson, S. E., Keutmann, H., and Kahn, C. R. (1988). A cascade of tyrosine autophosphorylation in the beta-subunit activates the phosphotransferase of the insulin receptor. *J. Biol. Chem.* 263, 2969–2980.
- Zhang, W., Huang, Q., Zeng, Z., Wu, J., Zhang, Y., Chen, Z., et al. (2017). Sirt1 inhibits oxidative stress in vascular endothelial cells. *Oxid. Med. Cell Longev.* 2017:7543973.
- Conflict of Interest:** The authors declare that the research was conducted in the absence of any commercial or financial relationships that could be construed as a potential conflict of interest.
- Copyright © 2020 Krskova, Balazova, Dobrocsyova, Olszanecki, Suski, Chai and Zorad. This is an open-access article distributed under the terms of the Creative Commons Attribution License (CC BY). The use, distribution or reproduction in other forums is permitted, provided the original author(s) and the copyright owner(s) are credited and that the original publication in this journal is cited, in accordance with accepted academic practice. No use, distribution or reproduction is permitted which does not comply with these terms.



OPEN ACCESS

**Edited by:**

Efstathios Stratikos,  
National and Kapodistrian University  
of Athens, Greece

**Reviewed by:**

Peter Michael Kloetzel,  
Charité – Universitätsmedizin Berlin,  
Germany  
Freidrich Cruz,  
University of Massachusetts Medical  
School, United States

**\*Correspondence:**

Peter van Endert  
peter.van-endert@inserm.fr  
Loredana Saveanu  
loredana.saveanu@inserm.fr

<sup>†</sup> These authors have contributed  
equally to this work

**\*Present address:**

Mirjana Weimershaus,  
Institut Imagine, Institut National de la  
Santé et de la Recherche Médicale,  
Paris, France  
Myriam Lawand,  
Institut Curie, Université Paris  
Sciences et Lettres, Institut National  
de la Santé et de la Recherche  
Médicale, Paris, France  
Loredana Saveanu,  
Institut National de la Santé et de la  
Recherche Médicale, Université  
de Paris, Centre National de la  
Recherche Scientifique, ERL 8252,  
Paris, France

**Specialty section:**

This article was submitted to  
Cellular Biochemistry,  
a section of the journal  
Frontiers in Cell and Developmental  
Biology

**Received:** 21 July 2020

**Accepted:** 04 November 2020

**Published:** 11 December 2020

**Citation:**

Weimershaus M, Mauvais F-X,  
Evnouchidou I, Lawand M, Saveanu L  
and van Endert P (2020) IRAP  
Endosomes Control Phagosomal  
Maturation in Dendritic Cells.  
Front. Cell Dev. Biol. 8:585713.  
doi: 10.3389/fcell.2020.585713

# IRAP Endosomes Control Phagosomal Maturation in Dendritic Cells

Mirjana Weimershaus<sup>1†</sup>, François-Xavier Mauvais<sup>1†</sup>, Irini Evnouchidou<sup>1,2</sup>,  
Myriam Lawand<sup>1†</sup>, Loredana Saveanu<sup>1\*†</sup> and Peter van Endert<sup>1\*†</sup>

<sup>1</sup> Institut National de la Santé et de la Recherche Médicale, Unité 1151, Université de Paris, Centre National de la Recherche Scientifique, UMR 8253, Paris, France, <sup>2</sup> Inovarian, Paris, France

Dendritic cells (DCs) contribute to the immune surveillance by sampling their environment through phagocytosis and endocytosis. We have previously reported that, rapidly following uptake of extracellular antigen into phagosomes or endosomes in DCs, a specialized population of storage endosomes marked by Rab14 and insulin-regulated aminopeptidase (IRAP) is recruited to the nascent antigen-containing compartment, thereby regulating its maturation and ultimately antigen cross-presentation to CD8<sup>+</sup> T lymphocytes. Here, using IRAP<sup>-/-</sup> DCs, we explored how IRAP modulates phagosome maturation dynamics and cross-presentation. We find that in the absence of IRAP, phagosomes acquire more rapidly late endosomal markers, are more degradative, and show increased microbicidal activity. We also report evidence for a role of vesicle trafficking from the endoplasmic reticulum (ER)–Golgi intermediate compartment to endosomes for the formation or stability of the IRAP compartment. Moreover, we dissect the dual role of IRAP as a trimming peptidase and a critical constituent of endosome stability. Experiments using a protease-dead IRAP mutant and pharmacological IRAP inhibition suggest that IRAP expression but not proteolytic activity is required for the formation of storage endosomes and for DC-typical phagosome maturation, whereas proteolysis is required for fully efficient cross-presentation. These findings identify IRAP as a key factor in cross-presentation, trimming peptides to fit the major histocompatibility complex class-I binding site while preventing their destruction through premature phagosome maturation.

**Keywords:** aminopeptidase, oxytocinase, phagosome maturation, GLUT4-storage vesicle, cross-presentation, ERGIC

## INTRODUCTION

Dendritic cells (DCs) are immune myeloid cells that exert prime functions in the initiation of adaptive immune responses. Key to the activation of cytotoxic CD8<sup>+</sup> T lymphocytes, the effector cells required for immunity against most viruses and cancer, is the generation of stable peptide-major histocompatibility complex class (MHC)-I complexes (pMHC) on the surface of DCs (Jung et al., 2002). While all nucleated cells generate pMHC loaded with peptides from proteins encoded in the cellular genome in a process referred to as the classical pathway of MHC-I antigen presentation, few cell types, including DCs, are able to “cross-present” and thus activate CD8<sup>+</sup> T lymphocytes with peptides derived from extracellular proteins. As the spatially restricted peptide-binding pocket on MHC-I molecules is best stabilized by 8-mer and 9-mer peptides, an appropriate



hydrolytic machinery in antigen-presenting cells is required in order to break down complex protein antigens into fragments of a suitable size (reviewed in Rock et al., 2010). While the C-terminus of most MHC-I-associated peptides is generated by the proteasome, different N-terminal trimming peptidases have been identified (reviewed in Weimershaus et al., 2013). In this context, we have discovered an unexpected role as trimming enzyme for insulin-regulated aminopeptidase (IRAP), a widely expressed enzyme best studied for its role in oxytocin and vasopressin cleavage and its colocalization with glucose transporter (GLUT) 4 to specific cytoplasmic insulin-responsive storage vesicles (GSVs; reviewed in Li et al., 2019).

Insulin-regulated aminopeptidase is structurally and ontogenetically closely related to the endoplasmic reticulum (ER) aminopeptidases (ERAPs). However, while ERAPs are soluble enzymes in the ER lumen, IRAP is a type II transmembrane protein located in specific endosomes that in DCs contain also the small guanosine triphosphatase (GTPase) Rab14. Its trafficking is regulated by cell type-specific extracellular signals and requires the short cytoplasmic tail of IRAP (Kandror and Pilch, 2011). While adipocytes and muscle cells mobilize IRAP vesicles in response to insulin, we have shown that in DCs, ligation of Fc receptors (FcRs) by immune complexes triggers phosphorylation and inactivation of the Rab14 GTPase-activating protein (GAP) AS160/Tbc1d4, resulting in the activation of Rab14 (Weimershaus et al., 2018). Active Rab14-GTP can form a complex with the kinesin Kif16b, which enables plus-end-directed transport of the vesicles on microtubules and promotes fusion with early endosomes and phagosomes (Weimershaus et al., 2018).

Thus, IRAP vesicle trafficking intersects with endocytic and phagocytic pathways. Phagocytosis is an evolutionary ancient process by which cells internalize extracellular particles and include them in membrane-bound organelles in a receptor-dependent manner. While generally targeted for destruction upon fusion with highly degradative lysosomes (Fairn and Grinstein, 2012), phagosomes in DCs display particular features with regard to their fusion and fission dynamics as well as in the composition of their enzymatic arsenal. Thus, the DC phago-endosomal system seems to be optimized in order to preserve peptides of suitable size for loading on MHC-I molecules for cross-presentation (Amigorena and Savina, 2010). Several studies have added to our mechanistical understanding how DC phagosome maturation and therefore cross-presentation are regulated by different intracellular membrane-modifying and fusion components. Rab GTPases and soluble N-ethylmaleimide-sensitive factor attachment protein receptor (SNARE) tethers are master regulators of vesicular trafficking (Stenmark, 2009). Several factors have been reported to interfere with phagosome maturation and cross-presentation in DCs: Rab27a that brings NADPH oxidase 2 (NOX2)-containing vesicles to the phagosome (Jancic et al., 2007); Rab39a regulating ER-Golgi-to-phagosome transport and stabilizing phagosomal NOX2 and MHC-I molecules (Cruz et al., 2020); Rab3b/c (Zou et al., 2009), Rab11, and Rab22 involved in Toll-like receptor (TLR)-triggered MHC-I delivery to phagosome (Nair-Gupta et al., 2014); Rab34 inducing lysosomal

clustering to the perinuclear region (Alloatti et al., 2015); and Rab43, a Golgi-related Rab controlling cross-presentation of phagocytized antigen *in vivo* (Kretzer et al., 2016). The SNARE protein Sec22b, by interaction with Stx4 on phagosomes, has been suggested to supply the latter with components of the peptide-loading complex and facilitate cross-presentation, although this role has been challenged by a second group using an *in vivo* model (Montealegre and van Endert, 2017; Wu et al., 2017).

A non-canonical role of proteins involved in autophagy also affects phagosome maturation, although the regulation of this pathway is incompletely understood. In this process, upon TLR or apoptotic cell receptor engagement, several components classically involved in macroautophagy sequentially associate with phagosomes and modulate their maturation. This so-called LC3-associated phagocytosis (LAP) is characterized by sustained recruitment of NOX2 and accelerated fusion with lysosomes leading to more efficient degradation of phagocytized substrates in murine macrophages and enhanced presentation of phagocytized antigens by MHC class II molecules (Sanjuan et al., 2007; Heckmann and Green, 2019).

While detrimental for cross-presentation when accelerated, phago-lysosomal fusion is the default end point of phagocytosis and required for peptide presentation on MHC-II and the destruction of internalized pathogens. The requirement to balance these functions against efficient cross-presentation underlines the importance for DCs of fine-tuning the endo-lysosomal system according to different cellular functions and extracellular cues (Samie and Cresswell, 2015).

Here we investigate how phagosome maturation specifically in DCs is controlled by fusion with an endosomal compartment marked by IRAP and Rab14, suggest that vesicle transport from the ER-Golgi intermediate compartment (ERGIC) affects IRAP vesicles, and confirm the role of IRAP peptidase activity in cross-presentation.

## MATERIALS AND METHODS

### Mice and Cells

Previously described IRAP<sup>-/-</sup> mice on an Sv129 background obtained from S. Keller were back-crossed up to 10 times to C57BL/6 mice obtained from Janvier (St. Quentin-Fallavier, France). While for some experiments mice with a lower number of back-crosses were used, cross-presentation experiments were always performed with mice on an identical genetic background. Control mice were either mixed background or C57BL/6 mice bred in our facility or C57BL/6 mice purchased from Janvier. Recombination-activating gene (RAG)1-deficient OT-1 T cell receptor transgenic mice were obtained from Taconic (Germantown, NY, United States) and bred in our animal facility. Animal experimentation was approved by the *Comité d'Éthique pour l'Expérimentation Animale* Paris Descartes (no P2.LS.156.10). Murine bone marrow-derived DCs (BM-DCs) were produced *in vitro* by culturing cells extruded from large bones for 6–8 days in complete medium [Iscove's modified Dulbecco's medium (IMDM) complemented with

10% fetal calf serum (FCS), 2 mM glutamine, 100 U/ml penicillin, 100 g/ml streptomycin, 50 mM  $\beta$ -mercaptoethanol supplemented with J558 supernatant containing 20  $\mu$ g/ml granulocyte-macrophage colony-stimulating factor (GM-CSF). Bone marrow-derived DC differentiation and activation were checked by staining with CD11c and CD80 antibodies as described (Weimershaus and van Endert, 2013).

## Antibodies

The following antibodies were used in this study.

### Fluorescence Microscopy

immunoaffinity purified rabbit antibodies specific for the cytosolic IRAP domain (Keller et al., 1995); mouse monoclonal IRAP antibodies (a kind gift from M. Birnbaum, University of Pennsylvania) (Garza and Birnbaum, 2000); goat polyclonal anti-EEA1 and anti-mouse transporter 1, ATP-binding cassette subfamily B member transporter associated with antigen processing (TAP1) (both Santa Cruz Biotechnologies); rat anti-mouse lysosome-associated membrane protein (LAMP1) clone 1D4B, mouse monoclonal anti-STX6, mouse monoclonal anti-GM130 (BD Pharmingen); rabbit polyclonal anti-STX6 (ProteinTech Group, Chicago, IL, United States); rat monoclonal anti-mouse mannose receptor, clone MR5D3 (AbD Serotec); rabbit polyclonal anti-Sec22b (Synaptic Systems); rabbit polyclonal anti-Rab14 (Sigma Aldrich); rat monoclonal anti-HA tag (Roche); rabbit polyclonal anti-LC3 (MBL). All secondary reagents were Alexa-coupled highly cross-adsorbed antibodies from Molecular Probes (Invitrogen).

### Immunoblotting

In addition to antibodies also used for microscopy, the following antibodies were used for immunoblots: rabbit polyclonal anti-MHC-I (P8, a gift from H. Ploegh); rabbit polyclonal anti-EEA1 (Abcam); rabbit polyclonal anti-TAP2 (a gift from Dr. J. Monaco); rabbit polyclonal anti-calnexin (Stressgen); rabbit polyclonal anti-V-ATPase subunit E and goat polyclonal anti-Cathepsin D (both Santa Cruz Biotechnologies).

### PhagoFACS Assays

PhagoFACS assays: (additional antibodies) rabbit polyclonal anti-ovalbumin (OVA) (Sigma Aldrich); mouse monoclonal anti-Rab7 (Abcam); rabbit polyclonal anti-BSA (Invitrogen).

### Flow Cytometry and Sorting

Flow cytometry and sorting: (additional antibodies) rat anti-mouse CD11b/PE-Cy7 (clone M1/70; BD Biosciences); hamster anti-mouse CD11c/eFluor450 (clone N418; eBioscience); rat anti-H2-K<sup>b</sup> (clone AF6-88.5; Biolegend); mouse IgG2a isotype control (clone MOPC-173, Biolegend); 7-actinomycin D (7-AAD, BD Biosciences).

### ELISAs

Capture: rat anti-mouse interleukin (IL)-2 (clone JES6-1A12); detection: rat anti-mouse IL-2/Biotin (clone JES6-5H4; both BD Biosciences).

## Fluorescence Microscopy

Bone marrow-derived DCs on day 7 were plated on fibronectin-coated 12-mm coverslips for 3 h in complete medium at 37°C. The cells were fixed in 4% paraformaldehyde (PFA) for 20 min at room temperature (RT), permeabilized in 0.2% saponin/0.2% bovine serum albumin (BSA) in phosphate buffered saline (PBS), quenched in 0.2 M glycine pH 7 and incubated with antibodies. For phagocytosis assays, the BM-DCs were seeded on IbiTreat channels (BioValley) for 3 h. Adherent cells were pulsed with latex beads (Polysciences) (dilution 1:100) or *Saccharomyces cerevisiae* cells expressing OVA attached to the cell wall ( $2 \times 10^8$ /ml) in complete medium for 5 min at 37°C. The free particles were removed by washing with cold PBS, and cells were chased in complete medium. At the end of each chase period, the cells were fixed, permeabilized, and stained.

Immunofluorescence images were acquired with a Leica SP8 confocal microscope using a 40 $\times$  oil immersion objective. Alternatively and where indicated, images were acquired with a Leica DMI 6000 microscope equipped with a piezoelectric-driven stage and Optophotonics XF100-2 [fluorescein isothiocyanate (FITC)], XF102-2 (Texas Red), and XF06 [4',6-diamidino-2-phenylindole (DAPI)] filters, and processed for 3D deconvolution using Metamorph<sup>TM</sup> 6.3.7.

## Image Analysis

Marker colocalization and signal intensity were evaluated using ImageJ. For each image, a stack of at least 10 planes was acquired, and only non-saturated images were measured. A manual threshold was established for each channel before image analysis. Individual cells were delimited with the freehand selection tool and considered as region of interest (ROI) in ImageJ. For colocalization studies, all images were first translated to a binary image (black pixel intensity = 0; white pixel intensity = 1). The binary images for green and red channels were multiplied to create a mask that encompasses the pixels present in both channels. The areas of green pixels, red pixels, and pixels of the mask were calculated using the plugin "measure stack" of ImageJ. The percentage of green pixels that colocalized with red pixels was calculated as the ratio of the sum of area of pixels in the mask divided by the sum of the area of green pixels.

For measurement of endosomal and Golgi STX6 intensity, a z-projection of the stack image was performed using the sum projection method. On the z-projection image, two individual ROIs were delimited for each cell analyzed, one for the Golgi stacks and one for the cellular area outside Golgi. Measurements performed with ImageJ were limited to threshold and included ROI area, ROI mean fluorescence intensity, and integrated density. The results were reported as mean of fluorescence or integrated density/area. Statistical analysis was performed with GraphPad Prism software using unpaired *t*-tests.

## Flow Cytometry and Sorting

Bone marrow-derived DCs were incubated on ice with fluorochrome- or biotin-conjugated CD11b, CD11c, and AF6-88.5 antibodies diluted in PBS with 2% FCS. APC/Cy7-streptavidin (Biolegend) was used as a secondary reagent

and 7-AAD (5  $\mu$ l/sample) to discriminate live and dead cells. BD Fortessa<sup>TM</sup> and fluorescence-activated cell sorting (FACS) ARIA-II<sup>TM</sup> machines were used for cell analysis and sorting, respectively.

## Immunoblots

Latex bead-containing phagosomes were prepared from BM-DCs by sucrose gradients according to published procedures (Desjardins et al., 1994). Briefly,  $1.5 \times 10^8$  BM-DCs were fed 0.5 ml deep-blue latex beads (Sigma). Cells were lysed mechanically, excess beads were removed by FCS flotation, and phagosomes were purified *via* a sucrose gradient by ultracentrifugation. Phagosomes were finally lysed in 1% 3-[(3-cholamidopropyl)dimethylammonio]-1-propanesulfonate hydrate (CHAPS), the protein concentration was measured with the Bradford reagent (BioRad), and the protein composition was analyzed by immunoblots.

## PhagoFACS

Here, 0.5 mg/ml OVA (Worthington) or ultrapure BSA (Sigma) were covalently coupled to 3 mm latex aminobeads (Biovalley). Bone marrow-derived DCs were pulsed with beads for 10 (Figure 4) or 20 (Figure 2A) min; the excess of non-phagocytized beads was removed by FCS flotation gradients, and the cells were harvested immediately or after another 10 min (Figure 4) or 40 min (Figure 2A) incubation of cells at 37°C. In the experiment shown in Figure 4, half of the BM-DCs were preincubated with 1  $\mu$ M IRAP inhibitor DG-026A for 2 h and the inhibitor was maintained during phagocytosis. After completion of the time course, the cells were mechanically lysed with a syringe in 250 mM sucrose, 3 mM imidazole, 1 mM dithiothreitol (DTT), and phagosomes were enriched by low-speed centrifugation, fixed in 1% PFA, stained with the lipid marker CellMask (Invitrogen) and Rab7, LAMP1, or OVA antibodies, and analyzed on a Canto II or Gallios cytometer.

## Phagosomal pH

The pH-sensitive dye carboxyfluorescein succinimidyl ester (CFSE) and the pH-insensitive dye AF647 were coupled to latex aminobeads (Polysciences) and added to DCs for phagocytosis. After removal of excess beads, the decrease of the CFSE-emitted fluorescence intensity was measured over time by flow cytometry. The signal was corrected for non-specific dye degradation with the AF647 signal. pH values were obtained by plotting the CFSE mean fluorescence intensity values to a calibration curve that was obtained by lysing phagosomes containing fluorochrome-conjugated beads in 1% Tween-20 solutions of known pH.

## Microbicidal Activity *in vitro*

Bone marrow-derived DCs were incubated with *Pseudomonas aeruginosa* or *S. cerevisiae* for 3 h at a microbe/DC ratio of 1. Then, microbes were washed away and the DCs were lysed in 0.1% Triton. The lysates were plated at different dilutions on yeast and bacterial culture plates, respectively, and colony formation was quantified after 18 h of culture. For *Aspergillus fumigatus* conidia phagocytosis, BM-DCs were incubated with

conidia at a conidia/DC ratio of 2, in 24-well plates. The plates were centrifuged at 4°C for 30 min followed by extensive washing with cold PBS to remove free conidia. The number of conidia bound to BM-DCs membrane was identical for wild-type (wt) and IRAP<sup>-/-</sup> cells. The BM-DCs were incubated for 5 h at 37°C in complete medium. Finally, the cells were lysed in 5 mM EDTA and 0.1% Tween 20 in H<sub>2</sub>O, and the lysates were plated on agar plates. *A. fumigatus* colonies were counted 48 h later.

## Phagosomal Peptide Transport Assay

Three-micron latex beads (Polysciences) were coated by passive adsorption with 100  $\mu$ g/ml rabbit immunoglobulin and incubated at a ratio of 3:1 for 20 min at 37°C for phagocytosis with BM-DCs. After elimination of free beads by FCS gradient, half of the preparation was disrupted immediately for phagosome preparation and the other half was incubated for another 20 min at 37°C to initiate phagosome maturation. Then, cells were disrupted mechanically in 220 mM sucrose, 3 mM imidazole, 1 mM DTT, and 5 mM MgCl<sub>2</sub>, and phagosomes were pelleted after removal of nuclei. Phagosomes were preincubated during 5 min with 0.9 mM ATP, 0.2 mg/ml creatine kinase, and 400 mM creatine phosphate and incubated for 15 min at 20°C or 4°C with 5  $\mu$ M peptide RRYNAC(FITC)TEL (R9L-FITC) obtained at ~80% purity from Pepscan or Sigma-Genosys. Finally, the phagosomes were washed with PBS, stained with 7.5  $\mu$ g/ml CellMask Deep Red<sup>TM</sup> membrane stain (Invitrogen) for 30 min at 4°C, and analyzed for peptide accumulation by FACS. Phagosomes incubated at 4°C served as negative controls.

## Cross-Presentation Assays

Here,  $2 \times 10^6$  BM-DCs were transfected on day 5 of culture with 2  $\mu$ g of plasmids encoding wt or mutant forms of IRAP or Rab14 using the Amaxa (Lonza) nucleofection kit for mouse immature DCs and program Y-001. On day 7, the cells were stained with CD11b and CD11c antibodies for 20 min, sorted as 7-AAD<sup>-</sup>CD11b<sup>+</sup>CD11c<sup>+</sup>GFP<sup>+</sup> cells, and seeded at a concentration of 15,000–20,000 cells/well into 96-well round-bottom culture plates. After 1 h, CD8<sup>+</sup> T cells purified from lymph nodes of OT-I mice were added to the culture for 20 h at a ratio T/BM-DCs: 1.5/1. To assess T cell activation, IL-2 concentration in supernatants was measured by sandwich ELISA using Nunc Maxisorp plates, streptavidin/horseradish peroxidase (Thermo Fisher Scientific), and OptEIA TMB substrate (BD Biosciences). Results represent the means of duplicate wells.

## Peptidase Activity Assays

IRAP<sup>-/-</sup> mouse epithelial fibroblasts were transfected with wt IRAP or the E465A mutant by electroporation. Two days later,  $2 \times 10^6$  surviving cells were lysed in 1% Triton, and IRAP was immunoprecipitated with specific mouse antibodies immobilized on Sepharose 4B beads. Half of the beads was resuspended in gel loading buffer and analyzed by immunoblot for IRAP content. The other half was used to prepare triplicate samples and incubated for 15 min with 50  $\mu$ M Arg-AMC with continuous measuring of the fluorescence signal at 460 nm using a Mithras<sup>TM</sup> fluorometer (Berthold).



## Cloning of Wild-Type and Mutant IRAP in pIRES2-eGFP

A cDNA coding for IRAP truncated by the 79 aminoterminal amino acids and extended by a carboxyterminal HA tag was amplified from mouse spleen cDNA using the following primers: 5'-ACC GGT GCC ACC ATG CTA CTA GTA AAT CAG TCA C (*AgeI* site underlined) and 5'-GAG CTC CTA GGC GTA GTC GGG CAC GTC GTA GGG GTA TCC CGA CAG CCA CTG GGA GAG-3' (HA tag in italics, *XhoI* site underlined). The PCR product was cloned in the pMAX-GFP vector (Lonza) between the *AgeI* and *XhoI* sites, thereby replacing the GFP cDNA and resulting in the plasmid pMAX-IRAP. The absence of errors was confirmed by sequencing. A cDNA encoding truncated inactive IRAP was obtained by the megaprimer method. A megaprimer of 235 bp was produced by PCR using pMAX-IRAP as template and the primers: 5'-CT AAA ATC ATT GCT CAC GCA CTG GCA CAT CAG TGG-3' (mutated base underlined) and 5'-GAA GAC TGA ACA GAT GAT GAT ATT GGA TGA-3', the latter primer being located downstream of an *EcoRI* site in the IRAP cDNA. A second PCR product was obtained using the megaprimer and the sense primer 5'-ACC GGT GCC ACC ATG CTA CTA GTA AAT CAG TCA C (*AgeI* site underlined). This PCR product was used to replace the fragment between the *AgeI* and *EcoRI* sites in pMAX-IRAP, creating pMAX-IRAP E465A, followed by sequencing to confirm the mutation. To obtain plasmids encoding full-length IRAP, the first 650 bp of IRAP were amplified using the primers 5'-GCT AGC GCC ACC ATG GAG TCC TTT ACC AAT GA-3' (*NheI* underlined) and 5'-TTG AAA TAT TAT GTC CTG TGC TAT-3', using as template the cDNA clone MGC\_144171 (plasmid IMAGE\_40098425, obtained from Open Biosystems) corresponding to Genbank accession number BC120926.1. The N-terminal IRAP fragment was cloned in pCR Blunt (Invitrogen) and sequenced. The C-terminal fragments of wt and inactive IRAP were removed from the pMAX plasmids using *EcoRV* and *XhoI* and cloned together with the N-terminal fragment, excised using *NheI* and *EcoRV*, between the *NheI* and *XhoI* sites in pCDH-EF1alpha vector (System Biosciences). Finally, the full-length IRAP inserts were transferred from pCDH-EF1alpha into pIRES2-EGFP (Clontech) as *NheI* and *XhoI* fragments.

## Lentivirus Production and Infection

The plasmids pLK0.1-puro carrying shRNA sequences specific for Sec22b (TRCN0000115089, also used by Cebrian et al., 2011) and a puromycin resistance gene were purchased from Open Biosystems. The control pLK0.1 plasmid carrying a non-targeting shRNA sequence (SHC002H) was purchased from Sigma Aldrich. The pLK0.1 plasmids were co-transfected with the packaging plasmids pCMVDelta8.2 and the envelope plasmid pMD2G into HEK-293-FT cells *via* calcium chloride transfection. Five hours post-transfection, the buffer was exchanged for complete Dulbecco's modified Eagle's medium (DMEM) and virus-containing supernatant was collected 24, 36, and 72 h post-transfection. The supernatants were concentrated in Centricon 70 devices (Millipore). To determine virus titers, NIH3T3 fibroblasts were transduced with several dilutions of viral

supernatants. Two days later, cells were harvested, genomic DNA was isolated, and the viral gene *fugw* was amplified by qPCR, and copy numbers were determined by plotting the obtained signal against dilutions of a *fugw*-encoding plasmid amplified in the same experiment.

Red blood cell-depleted bone marrow cells on day 3 of culture in the presence of GM-CSF were put in contact with lentiviral supernatants at a multiplicity of infection (MOI) of 10 supplemented with 8  $\mu$ g/ml polybrene and centrifuged for 100 min at 32°C. Subsequently, supernatants were washed off and replaced by BM-DC culture medium. Non-transduced cells were depleted by addition of 5  $\mu$ g/ml puromycin on day 5. Transduced cells were used on days 7–8 of culture. The efficiency of knockdown was confirmed by immunoblot and qPCR.

## Statistical Analysis

Statistical analyses including regression analysis, unpaired *t*-tests, and two-way ANOVA with *p*-values adjusted by Dunnett correction test (cross-presentation) were performed using GraphPad Prism™ software (version 7.0). For cross-presentation experiments, the mean values of four independent experiments were pooled and statistical significance was determined for every dose of antigen (parameter 1) and for every cell treatment (parameter 2) by comparing both the vector-IRAP<sup>+/+</sup> and the IRAP<sup>E465A</sup>-IRAP<sup>-/-</sup> conditions to the vector-IRAP<sup>-/-</sup> condition. For visual simplicity, the graph shows the *p* value applying to the three higher antigen concentrations.

## RESULTS

### Loss of Insulin-Regulated Amino-peptidase Accelerates Phagosome Maturation

Aiming to identify the peptidases involved in trimming the amino-terminus of MHC-I-presented antigenic peptides, we have previously reported that IRAP is rapidly recruited to newly formed phagosomes (Saveanu et al., 2009; Weimershaus et al., 2012, 2018). Here, comparing wt with IRAP<sup>-/-</sup> DCs lacking Rab14<sup>+</sup> storage endosomes, we set out to investigate in detail how this endosome species modulates the dynamic changes and molecular properties of phagosomes in the course of their maturation process. To this aim, we isolated latex-bead phagosomes from wt and IRAP<sup>-/-</sup> DCs and analyzed their content by immunoblot (**Figure 1A**). While neither the recruitment of the ER proteins Calnexin and TAP nor the amount of MHC-I molecules in phagosomes depended on the expression of IRAP, phagosomes from IRAP<sup>-/-</sup> DCs prematurely lost the early endosomal antigen (EEA) 1 and acquired more rapidly late endosomal and lysosomal markers such as cathepsin (Cat)D, the proton pump V-ATPase, and LAMP-1 (**Figure 1A**). To confirm these results by an alternative approach, we performed phagoFACS experiments, which allow for detection of selected membrane markers on bead-containing phagosomes at a given time point of maturation *via* flow cytometry (Savina et al., 2010). In



agreement with the results from the immunoblot analysis, FACS staining for the late endosomal/lysosomal markers LAMP-1 and Rab7 showed higher fluorescence intensities on phagosomes isolated from IRAP<sup>-/-</sup> DCs, indicating an accelerated phagosome maturation in these cells compared to wt DCs (**Figure 1B**). These changes in the presence of endosomal markers on the phagosomal membrane were accompanied by a stronger acidification measured in IRAP<sup>-/-</sup> phagosomes (**Figure 1C**).

Considering the published role of LAP in enhancing phagosome maturation, we wondered if IRAP<sup>-/-</sup> phagosomes displayed more LC3 on their membranes. Using phagoFACS and confocal imaging, we observed that early phagosomes from cells lacking IRAP showed stronger LC3 staining (**Figure 1D**). These results indicate that IRAP endosomes contribute to regulating phagosome maturation, stabilizing early endosomal markers and presumably a higher pH while limiting recruitment of a key element of the highly degradative LAP pathway.

As accelerated phagosome maturation and lower pH are generally associated with increased substrate degradation,

we next analyzed the proteolysis of two model substrates in phagosomes from IRAP<sup>-/-</sup> and wt DCs. Using OVA- and BSA-coated latex beads, respectively, we observed accelerated protein degradation in IRAP<sup>-/-</sup> phagosomes (**Figure 2A**). Similar results were obtained when monitoring accumulation of a reporter peptide in an *in vitro* assay of peptide transport into phagosomes: while peptide accumulated during 40 min in wt phagosomes, with greater amounts in later vesicles, peptide amounts decreased over time in IRAP<sup>-/-</sup> phagosomes. This was due to the more degradative milieu rather than diminished transport activity in IRAP<sup>-/-</sup> phagosomes, as addition of protease inhibitors increased the peptide amounts accumulating in the vesicles lacking IRAP, whereas it was without effect in IRAP<sup>+/+</sup> phagosomes (**Figure 2B**).

One physiological function of phagosome maturation is the inactivation and killing of potentially harmful content including microbes. We thus compared the intracellular survival of bacteria, fungi, and yeast upon phagocytosis by IRAP<sup>-/-</sup> and wt DCs. All three microbe species showed significantly

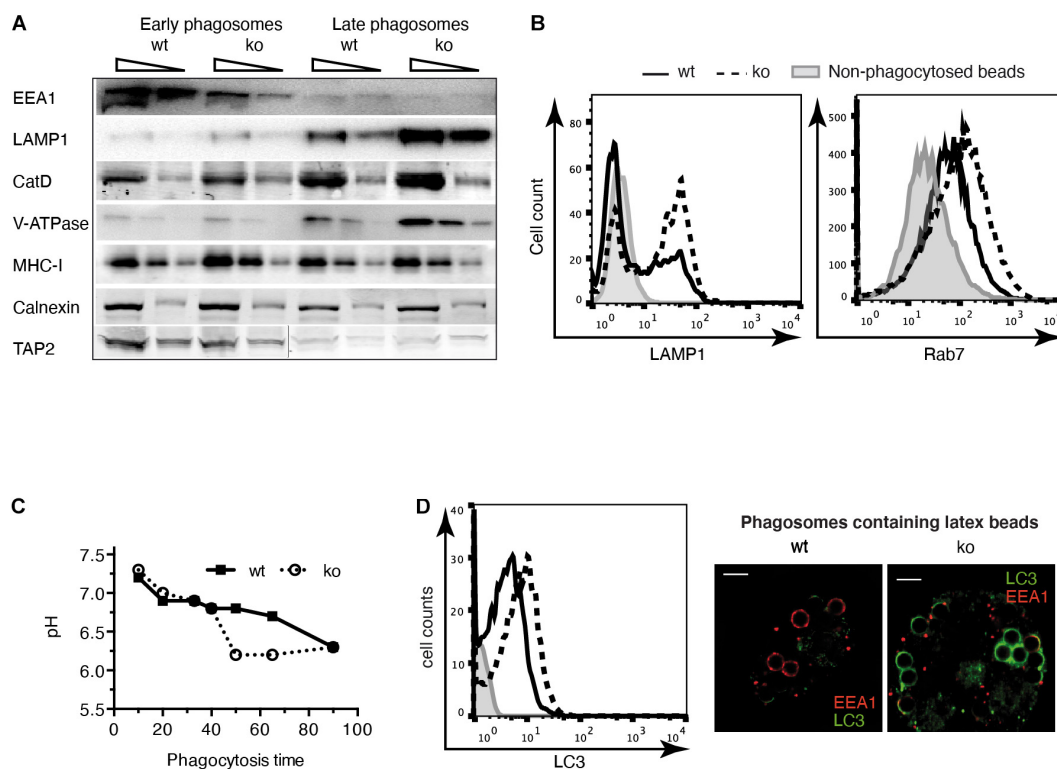
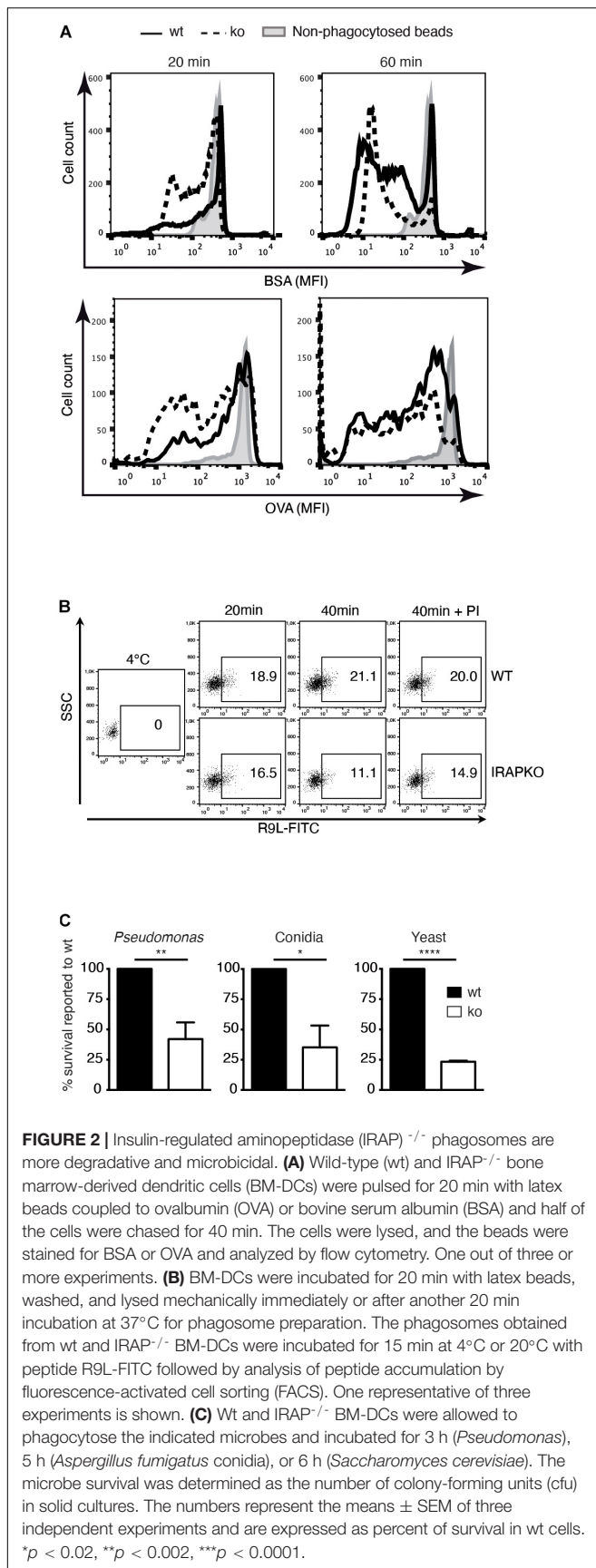


**FIGURE 1 |** Phagosome maturation is accelerated in insulin-regulated aminopeptidase (IRAP)<sup>-/-</sup> dendritic cells (DCs). **(A)** Latex bead phagosomes were isolated from wild-type (wt) or IRAP<sup>-/-</sup> bone marrow-derived DCs (BM-DCs) by sucrose gradients after a 20-min pulse (early) and after 120 min of chase (late). Equal protein amounts were analyzed by immunoblot for the markers indicated. One of three or more experiments. CatD, cathepsin D. **(B)** BM-DCs were pulsed for 20 min with latex beads and mechanically disrupted. Phagosomes in the post-nuclear supernatant were fixed, identified with the lipid marker Cellmask<sup>TM</sup>, stained for lysosome-associated membrane protein (LAMP)1 and Rab7, and analyzed by flow cytometry. One out of 10 (LAMP1) and three (Rab7) experiments. **(C)** The fluorescence intensity of phagocytosed latex beads conjugated to the pH-sensitive dye carboxyfluorescein succinimidyl ester (CFSE) and the pH-insensitive dye AF647 was monitored over time by flow cytometry. The ratio of CFSE to AF647 fluorescence was converted to pH values using a standard curve of beads in solutions of known pH. One of three similar experiments. **(D)** BM-DCs were pulsed for 20 min with latex beads, and LC3 staining of phagosomes containing single beads was performed as described in panel **(B)**. The images to the right show BM-DCs pulsed for 5 min with latex beads, chased for 15 min, and stained for LC3 and EEA1.



diminished survival in IRAP  $^{-/-}$  phagosomes, consistent with a more proteolytic and microbicidal content (**Figure 2C**).

## Insulin-Regulated Aminopeptidase Peptidase Activity Is Required for Antigen Presentation

We have previously shown that IRAP exerts trimming activity toward the amino-terminus of peptides in the MHC-I cross-presentation pathway. IRAP  $^{-/-}$  DCs fail to efficiently activate CD8 $^{+}$  T cells to cross-presented antigens (Saveanu et al., 2009). However, as accelerated phagosome maturation alone might be sufficient to hamper cross-presentation through increased destruction of antigenic peptides in the phagosome, we sought to dissect the contribution of IRAP peptidase activity to efficient cross-presentation as opposed to a merely structural, i.e., non-enzymatic role of IRAP in storage endosomes and their trafficking.

To this end, we generated a peptidase-dead IRAP variant carrying a single amino acid mutation in the catalytic site (E465A), which we overexpressed in IRAP  $^{-/-}$  DCs (**Figure 3A**, upper panel). As expected, in contrast to wt IRAP, the immunoprecipitated peptidase-dead mutant lacked hydrolytic activity toward the fluorogenic substrate Leu-AMC (**Figure 3A**). While peripheral endosomes staining for Stx6 and Rab14 were essentially absent in IRAP  $^{-/-}$  cells, the expression of the peptidase-dead mutant was sufficient to promote the appearance of peripheral endosomes staining for the storage endosome hallmark proteins Stx6, Rab14, EEA1, and mannose receptor (MR; **Figure 3B**). Wt and mutant IRAP colocalized to the same extent with the endosome markers analyzed, displaying the characteristic strong co-localization with Stx6 and Rab14 and weaker co-staining with EEA1 and MR (**Figure 3C**). However, while wt IRAP fully restored cross-presentation, the peptidase-dead mutant failed to rescue the cross-presentation defect observed in IRAP  $^{-/-}$  DCs (**Figure 3D**), consistent with a requirement of peptide trimming by IRAP for efficient CD8 $^{+}$  T cell priming.

However, it was still possible that protease-dead IRAP was sufficient to reconstitute storage endosomes but not normal, i.e., DC-typical attenuated phagosome maturation. Given the poor efficiency of full-length IRAP expression through transfection of BM-DCs, we were not able to obtain sufficient numbers of transfected BM-DCs to perform immunoblot and phagoFACS experiments for monitoring phagosome maturation. However, we reasoned that pharmacological IRAP inhibition should also reveal a potential requirement of proteolysis for physiologic phagosome maturation. We have previously shown that the inhibitor DG-026A reduces cross-presentation by wt BM-DCs to levels observed in IRAP  $^{-/-}$  DCs but has no effect on presentation in the latter, indicating selective inhibition of IRAP enzymatic activity in live cells (Kokkala et al., 2016). As expected, early phagosomes prepared from IRAP  $^{-/-}$  BM-DCs acquired higher levels of Lamp1 and Rab7 and contained somewhat lower levels of OVA than wt vesicles

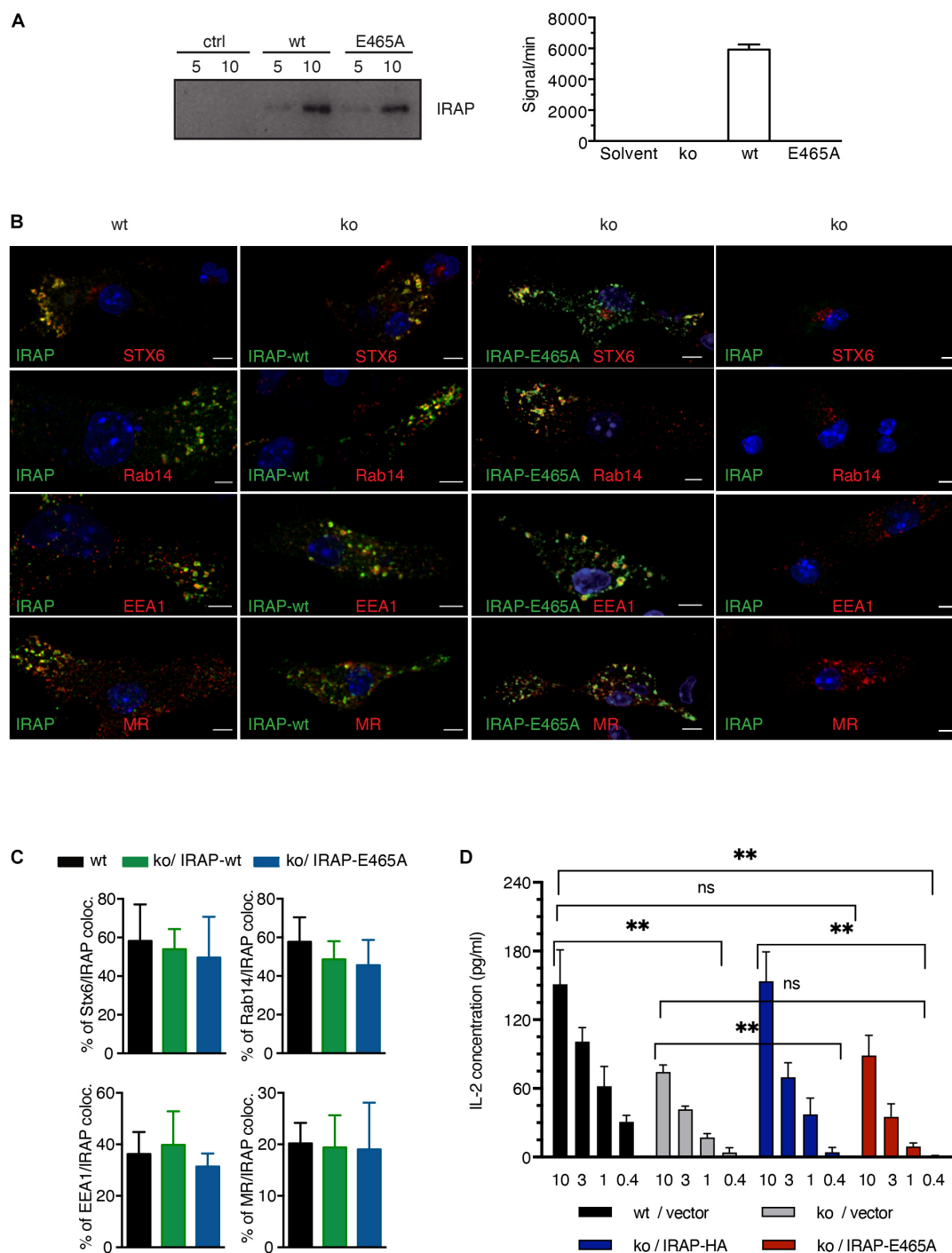


**FIGURE 3 |** Insulin-regulated aminopeptidase (IRAP) peptidase activity is required for efficient cross-presentation. **(A)** IRAP<sup>-/-</sup> mouse epithelial fibroblasts (MEFs) were transfected with full-length wild-type (wt) or mutant IRAP or mock-transfected (ctrl), followed by immunoprecipitation of IRAP 2 days later. The precipitates were analyzed for IRAP content by immunoblot and for peptidase activity toward the fluorogenic Arg-AMC substrate using mock-transfected cells as control. **(B)** IRAP<sup>-/-</sup> bone marrow-derived DCs (BM-DCs) were nucleofected with the plasmid pMAX-IRAP-E465A and analyzed 36 h later by confocal microscopy. Wt and untransfected IRAP<sup>-/-</sup> BM-DCs are shown as controls. **(C)** The colocalization of storage endosome markers in IRAP wt and IRAP<sup>-/-</sup> BM-DCs transfected with wt or protease-dead IRAP was analyzed for five representative cells. The graph shows mean co-localization  $\pm$  SEM. **(D)** IRAP<sup>+/+</sup> or IRAP<sup>-/-</sup> BM-DCs were nucleofected with empty pIRES2-GFP or the active site IRAP mutant E465A cloned in pIRES2-GFP. Live transfectants were sorted as GFP<sup>+</sup> 7AAD<sup>-</sup> CD11c<sup>+</sup> CD11b<sup>+</sup> cells and put in contact with graded amounts (mg/ml) of pre-formed complexes formed between MR antibodies and OVA fusion protein and with OT-I T cells. T cell stimulation was assessed by interleukin (IL)-2 ELISA. Histograms show the mean concentration of IL-2  $\pm$  SEM after subtraction of values obtained with control Glutamic acid decarboxylase (GAD) fusion protein from four independent experiments. \*\* $p < 0.01$ ; ns, not significant.

(Figure 4). However, incubation with DG-026A was without effect on acquisition of late endosome markers and OVA degradation not only in IRAP<sup>-/-</sup> phagosomes, as expected, but also in wt vesicles. Therefore, we were unable to find experimental evidence for a role of IRAP enzymatic activity in phagosome maturation.

### Insulin-Regulated Aminopeptidase Endosome Stability Depends on Sec22b

Efficient cross-presentation has been suggested to depend on the partial fusion of ER membranes with endosomal compartments

in a process relying on the ERGIC SNARE protein Sec22b and its phagosomal fusion partner Stx4 (Cebrian et al., 2011). In order to analyze the importance of Sec22b-mediated membrane fusion in phagosome maturation in IRAP<sup>-/-</sup> and wt DCs, we knocked down Sec22b expression using a lentivirus-expressed sequence also used by Cebrian and associates. To our surprise, abolishing Sec22b expression profoundly altered the organization of early endosomal structures. Specifically, immunofluorescence imaging revealed a near complete absence of peripheral endosomes staining for Stx6 or IRAP, while EEA1 staining was also slightly affected by Sec22b knockdown in BM-DCs (Figure 5A). Examining the correlation between

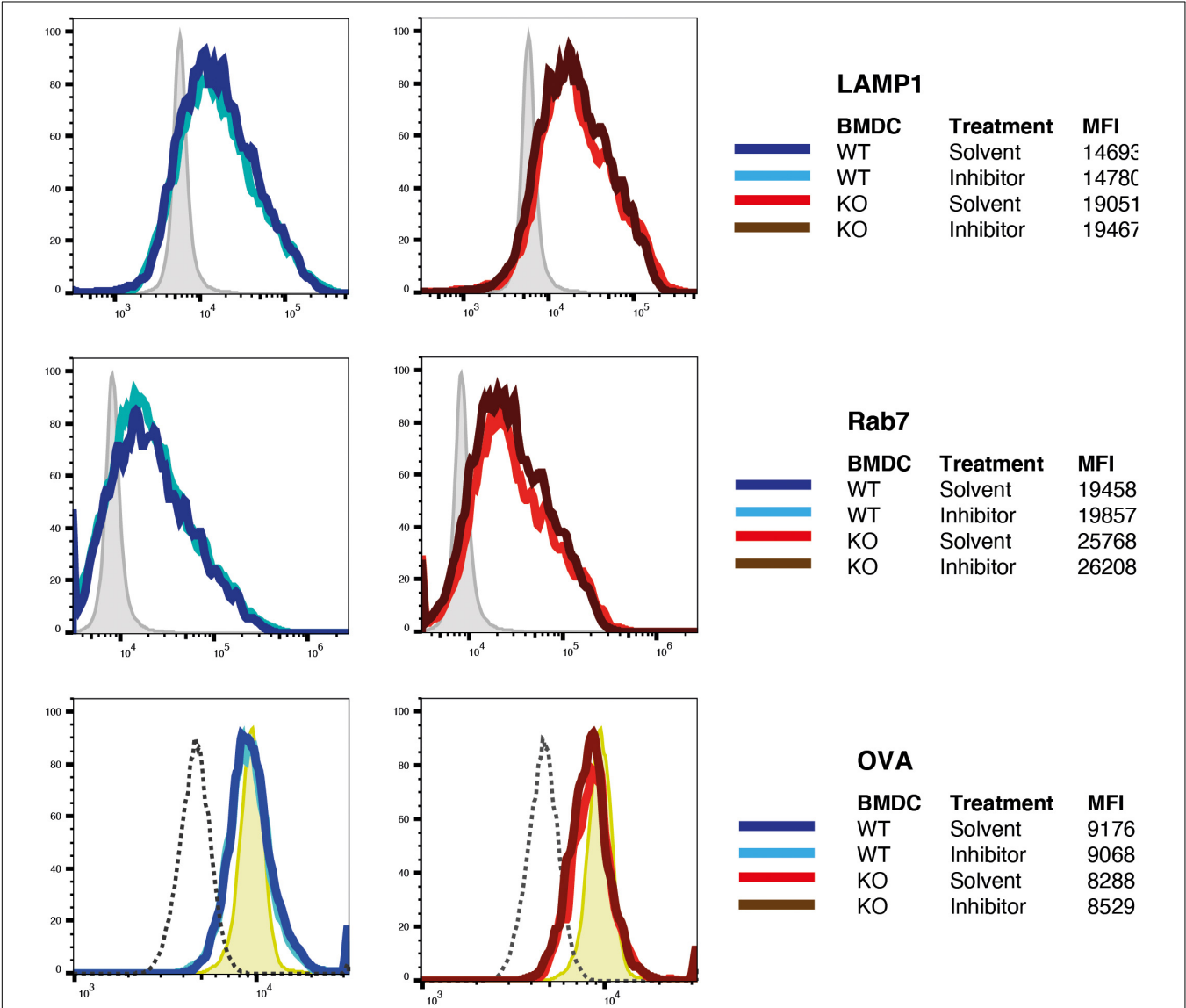


**FIGURE 4 |** Inhibition of insulin-regulated aminopeptidase (IRAP) protease activity does not alter phagosome maturation. Latex beads covalently coupled to ovalbumin (OVA) were fed to bone marrow-derived dendritic cells (BM-DCs) preincubated with the IRAP inhibitor DG-026A or solvent were incubated for 10 min with OVA-coated latex beads, washed, incubated in the presence of DG-026A for another 10 min at 37°C, and then lysed mechanically for preparation of phagosomes. Fixed phagosomes were stained for the late endosome markers Lamp1 and Rab7 and for OVA and analyzed by flow cytometry. One out of three experiments each performed in duplicate is shown. MFI, mean fluorescence intensity.



the endosomal staining intensity for these markers and the efficiency of Sec22b knockdown in individual cells, we observed a strong correlation between Sec22b expression and the presence of IRAP<sup>+</sup> and Stx6<sup>+</sup> endosomes, contrasting with a much weaker correlation for EEA1<sup>+</sup> endosomes (Figure 5A, right panels). TAP and LAMP staining was not affected by Sec22b knockdown. GM130 staining, in contrast, was inversely correlated with Sec22b expression, i.e., increased upon Sec22b deletion. As Stx6 is involved in vesicle traffic between the trans Golgi network (TGN) and endosomes, we asked whether its depletion was selective to endosomes. However, although Sec22b knockdown reduced Stx6 staining outside the Golgi more strongly than within, its distribution was not significantly altered (Figure 5B).

## DISCUSSION

The regulation of phagosomal maturation by myeloid cells is intimately linked to their specific role in the immune system. While macrophages excel in the intracellular destruction of phagocytosed cargo by rapid and efficient phagosome-lysosome fusion, it is widely accepted that the “mild” endosomal milieu in DCs promotes their capacity to cross-present. In this context, we have identified a cellular mechanism of regulated trafficking and fusion of Rab14<sup>+</sup>IRAP<sup>+</sup> storage endosomes with phagosomes in response to TLR4 engagement (Weimershaus et al., 2018). Here, we further characterize the trafficking dynamics during IRAP endosome-dependent phagosome maturation and report suggestive evidence relating it to previously described mechanisms regulating phagosome maturation such as LAP and the interaction of the ERGIC with post-Golgi vesicles.

We find that the absence of IRAP accelerates the loss of early and the acquisition of late endosomal markers. Consistent with this changed kinetics, IRAP<sup>-/-</sup> phagosomes display a lower luminal pH and an increased hydrolytic activity, which translates into increased killing of phagocytosed yeast, fungi, and bacteria, as well as increased TLR9 signaling (Babdor et al., 2017). Accelerated phagosome maturation most likely implicates the regulated movement of storage endosomes along microtubules: IRAP's N-terminus protrudes from the vesicular membrane to the cytosol where it physically interacts with the formin FHOD4, which anchors the endosomes to the actin cytoskeleton (Babdor et al., 2017). Additionally, we have previously shown that IRAP interacts with Tbc1d4/AS160, the Rab14 GAP in DCs (Weimershaus et al., 2018). Tbc1d4/AS160 activity is negatively regulated by the class I phosphoinositide 3-kinase (PI3K)/Akt signaling (Sadacca et al., 2013), a pathway known to be triggered by innate immune receptors and Fc receptors (Nair et al., 2011). Akt enzymatic activity leads to phosphorylation of Tbc1d4/AS160 and to guanosine diphosphate (GDP)-GTP exchange at Rab14. GTP-bound Rab14 associates with the kinesin Kif16b and promotes anterograde transport of IRAP endosomes to the cell periphery. The presence of IRAP and Rab14 in early phagosomes suggests that in DCs, phagocytosis

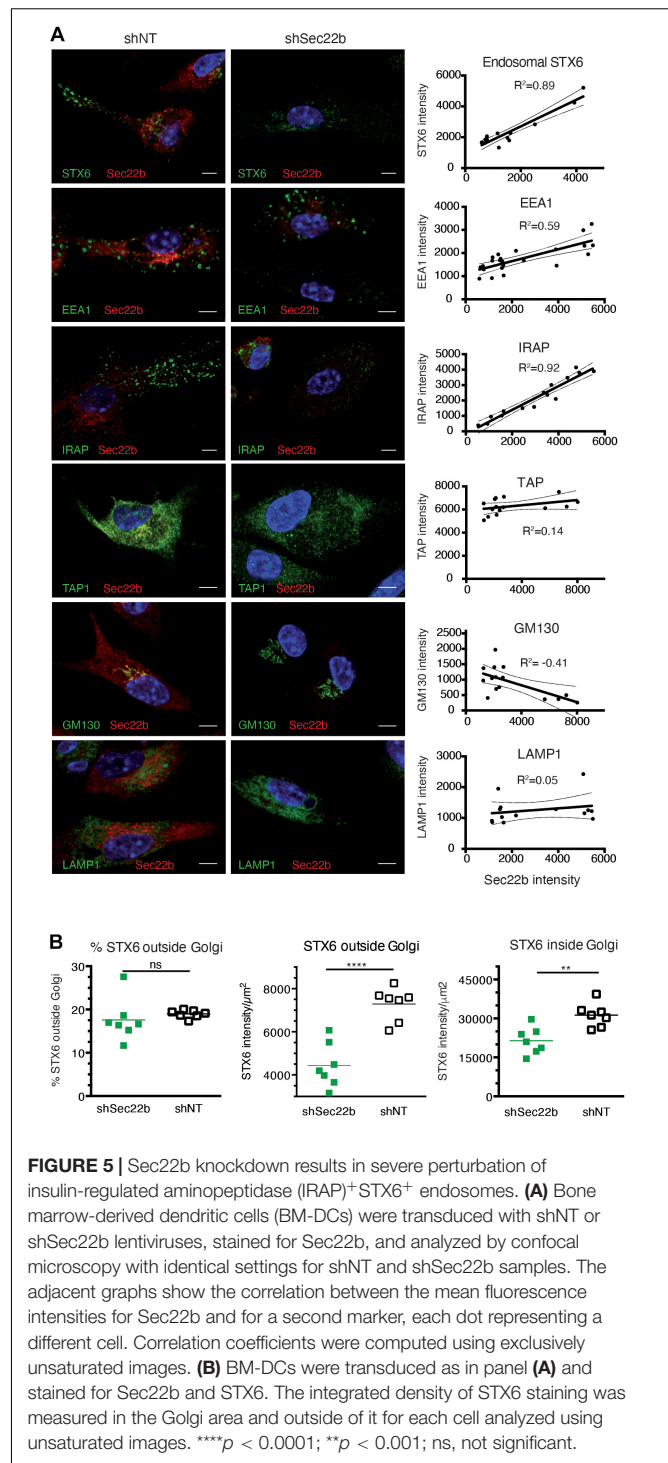


**FIGURE 5 |** Sec22b knockdown results in severe perturbation of insulin-regulated aminopeptidase (IRAP)<sup>+</sup>STX6<sup>+</sup> endosomes. **(A)** Bone marrow-derived dendritic cells (BM-DCs) were transduced with shNT or shSec22b lentiviruses, stained for Sec22b, and analyzed by confocal microscopy with identical settings for shNT and shSec22b samples. The adjacent graphs show the correlation between the mean fluorescence intensities for Sec22b and for a second marker, each dot representing a different cell. Correlation coefficients were computed using exclusively unsaturated images. **(B)** BM-DCs were transduced as in panel **(A)** and stained for Sec22b and STX6. The integrated density of STX6 staining was measured in the Golgi area and outside of it for each cell analyzed using unsaturated images. \*\*\*\* $p < 0.0001$ ; \*\* $p < 0.001$ ; ns, not significant.

is rapidly followed by fusion with storage endosomes, such that interaction of the two proteins with the cytoskeleton takes control of phagosome maturation (Saveanu et al., 2009; Weimershaus et al., 2012, 2018).

According to our findings in this and our previous report, the loss of IRAP and its static anchoring to the cytoskeleton is sufficient to promote destabilization of storage

endosomes and at the same time abolish plus-end-directed vesicle transport *via* the regulated Rab14-Kif16b hub, such that transport toward and fusion with lysosomes become dominant. In addition, *via* its recently discovered interaction with the retromer complex (Pan et al., 2017), IRAP might contribute to the retrieval of specific subdomains and cargos from early endosomes and phagosomes to trans-Golgi-derived vesicles, avoiding thus their targeting to lysosomes, a possibility that needs further investigation.

Interestingly, IRAP<sup>-/-</sup> phagosomes acquired more lipidated LC3 on their membranes. LC3-associated phagocytosis had first been described in murine macrophages as a non-canonical function of autophagy proteins (Sanjuan et al., 2007), resulting in accelerated phagosome maturation compared to phagocytosis without LC3 implication. Several membrane receptors have been described to trigger LAP, including TLR1/2/6, TLR4, TIM4, and FcR (Martinez, 2018). The initial signaling cascade, however, triggering the recruitment of the class III PI3K complex upstream of LC3 association, remains elusive, as well as the mechanisms through which the autophagy machinery promotes phagosome-lysosome fusion. Nevertheless, our findings suggest that the factors delivered to DC phagosomes by TLR4 or FcR-triggered fusion with IRAP storage endosomes “override” early signaling events leading to LC3 association with phagosomes because efficient LC3 association is only observed in IRAP<sup>-/-</sup> DCs. Analyzing the presence of Rubicon (a LAP-exclusive class III PI3K subunit) or the resulting phosphoinositide-3-phosphate levels on nascent phagosomes in IRAP<sup>-/-</sup> cells could provide further insight into the early membrane-modifying events that are regulated by IRAP.

The analysis of purified phagosomes did not reveal differences in the transport of MHC-I molecules to this compartment between wt and IRAP<sup>-/-</sup> cells. The exact relationship, however, between IRAP<sup>+</sup> storage endosomes and the DC endocytic recycling compartment (ERC) described by Nair-Gupta et al. (2014) remains unclear. This compartment is defined by VAMP3/VAMP8/Rab11 and harbors stocks of MHC-I molecules delivered upon TLR4 signaling for peptide loading to phagosomes. Note that despite the suggestive name of the ERC, the origin of its MHC-I molecules is unclear, as we have been unable to observe delivery of internalized recycling MHC-I molecules to it (Montealegre et al., 2019). IRAP deficiency did not affect the recruitment of ER-derived components (Calnexin, TAP) to phagosomes, which positions storage endosomes offside the trafficking and fusion events of ER membranes with phagosomes.

Interestingly, we observed that the knockdown of the ERGIC-SNARE Sec22b destabilized IRAP<sup>+</sup> storage endosomes in the steady-state. A role of this SNARE in intracellular IRAP trafficking has not been described; however, indirect evidence from studies on GSVs in insulin-responsive cells might help to explain our observations: in the absence of insulin signaling, GSVs are retained at a pre-Golgi location by the action of the Golgi tether proteins TUG, Golgin-160, and p115, the latter of which directly binds IRAP

(Hosaka et al., 2005; Williams et al., 2006). TUG, Golgin-160, and p115 localize to the cis-Golgi, ERGIC, and ER exit sites, where p115 has been shown to form stable complexes with Sec22b (Wang et al., 2015). Compromised formation of Sec22b-p115 complexes might result in misdirection of IRAP from the ERGIC or in its retrieval to the ER for eventual degradation; given the essential absence of IRAP in Sec22b knockdown BM-DCs, we favor the latter possibility. Whatever the mechanism underlying IRAP depletion upon Sec22b knockdown, our observation suggests a potential explanation for the previously unexplained accelerating effect of Sec22b knockdown on phagosome maturation (Cebrian et al., 2011). Next to affecting the delivery of ER membrane components to phagosomes, Sec22b may be required for correct formation of storage endosomes, which in turn regulate phagosome maturation.

Finally, we address the question of the dual role of IRAP as a trimming aminopeptidase and a constitutive component of storage endosomes in cross-presentation. We show that protease-dead IRAP fully reconstitutes IRAP<sup>+</sup> endosomes with a typical set of markers and that an IRAP inhibitor does not accelerate phenocopy IRAP knockout, i.e., does not accelerate phagosome maturation. Taken together, these findings suggest that IRAP has a structural role in storage endosomes and that this role is sufficient to mediate normal phagosome maturation. As DC-typical phagosome maturation has a well-documented importance in cross-presentation, it is plausible and likely that the structural role of IRAP has an independent effect on cross-presentation. Conversely, the fact that cross-presentation by BM-DCs expressing protease-dead IRAP is indistinguishable from cross-presentation by IRAP<sup>-/-</sup> cells lends credibility to a requirement of peptide trimming by IRAP for cross-presentation.

Interestingly, active proteasome complexes have recently been detected in endocytic DC vesicles, the precise identity of which remains to be determined (Sengupta et al., 2019). In our hands, cross-presentation of soluble, receptor-targeted, or particle-associated OVA is proteasome-dependent. Concerning TAP dependence, we have previously shown that the detrimental effect of TAP deficiency on cross-presentation of phagocytosed (but not receptor-targeted soluble) OVA by BM-DCs can be overcome by restoring cell surface class I levels through low-temperature incubation (Merzougui et al., 2011). In other words, particulate OVA cross-presentation by BM-DCs requires antigen degradation by proteasome complexes but not antigenic peptide transport by TAP, features shared by the experimental system employed by Sengupta et al. (2019). It is therefore conceivable that proteasome complexes reside in IRAP<sup>+</sup> vesicles, which then would contain a complete proteolytic chain for production of antigenic peptides. As the selectivity of IRAP trimming overlaps significantly with that of ER(A)P (Georgiadou et al., 2010; Mpakali et al., 2015), such a scenario would increase the likelihood that similar peptides are produced and presented in the endogenous and exogenous antigen presentation pathways, ensuring efficient recognition of tissue cells by CD8<sup>+</sup> T cells primed by cross-presenting DCs.

Collectively, our findings highlight the important and dual role of IRAP<sup>+</sup>Rab14<sup>+</sup> endosomes in optimizing cross-presentation and suggest that their availability may physiologically contribute to regulating the capacity of DCs to cross-prime CD8<sup>+</sup> T cell responses.

## DATA AVAILABILITY STATEMENT

The raw data supporting the conclusions of this article will be made available by the authors, without undue reservation.

## ETHICS STATEMENT

The animal study was reviewed and approved by Comité d'Éthique pour l'Expérimentation Animale Paris Descartes.

## REFERENCES

- Alloatti, A., Kotsias, F., Pauwels, A.-M., Carpiér, J.-M., Jouve, M., Timmerman, E., et al. (2015). Toll-like receptor 4 engagement on dendritic cells restrains phagolysosome fusion and promotes cross-presentation of antigens. *Immunity* 43, 1087–1100. doi: 10.1016/j.immuni.2015.11.006
- Amigorena, S., and Savina, A. (2010). Intracellular mechanisms of antigen cross presentation in dendritic cells. *Curr. Opin. Immunol.* 22, 109–117. doi: 10.1016/j.coi.2010.01.022
- Babdor, J., Descamps, D., Adiko, A. C., Tohmé, M., Maschalidi, S., Evnouchidou, I., et al. (2017). IRAP<sup>+</sup> endosomes restrict TLR9 activation and signaling. *Nat. Immunol.* 18, 509–518. doi: 10.1038/ni.3711
- Cebrian, I., Visentin, G., Blanchard, N., Jouve, M., Bobard, A., Moita, C., et al. (2011). Sec22b regulates phagosomal maturation and antigen crosspresentation by dendritic cells. *Cell* 147, 1355–1368. doi: 10.1016/j.cell.2011.11.021
- Cruz, F. M., Colbert, J. D., and Rock, K. L. (2020). The GTPase Rab39a promotes phagosome maturation into MHC-I antigen-presenting compartments. *EMBO J.* 39:e102020. doi: 10.15252/embj.2019102020
- Desjardins, M., Huber, L. A., Parton, R. G., and Griffiths, G. (1994). Biogenesis of phagolysosomes proceeds through a sequential series of interactions with the endocytic apparatus. *J. Cell Biol.* 124, 677–688. doi: 10.1083/jcb.124.5.677
- Fairn, G. D., and Grinstein, S. (2012). How nascent phagosomes mature to become phagolysosomes. *Trends Immunol.* 33, 397–405. doi: 10.1016/j.it.2012.03.003
- Garza, L. A., and Birnbaum, M. J. (2000). Insulin-responsive aminopeptidase trafficking in 3T3-L1 adipocytes. *J. Biol. Chem.* 275, 2560–2567. doi: 10.1074/jbc.275.4.2560
- Georgiadou, D., Hearn, A., Evnouchidou, I., Chroni, A., Leondiadis, L., York, I. A., et al. (2010). Placental leucine aminopeptidase efficiently generates mature antigenic peptides in vitro but in patterns distinct from endoplasmic reticulum aminopeptidase 1. *J. Immunol.* 185, 1584–1592. doi: 10.4049/jimmunol.0902502
- Heckmann, B. L., and Green, D. R. (2019). LC3-associated phagocytosis at a glance. *J. Cell Sci.* 132:jcs222984. doi: 10.1242/jcs.222984
- Hosaka, T., Brooks, C. C., Presman, L., Kim, S. K., Zhang, Z., Breen, M., et al. (2005). P115 interacts with the GLUT4 vesicle protein, IRAP, and plays a critical role in insulin-stimulated GLUT4 translocation. *Mol. Biol. Cell* 16, 2882–2890. doi: 10.1091/mbc.e05-01-0072
- Jancic, C., Savina, A., Wasmeier, C., Tolmachova, T., El-Benna, J., My-Chan Dang, P., et al. (2007). Rab27a regulates Phagosomal PH and NADPH oxidase recruitment to dendritic cell phagosomes. *Nat. Cell Biol.* 9, 367–378. doi: 10.1038/ncb1552
- Jung, S., Unutmaz, D., Wong, P., Sano, G.-I., De los Santos, K., Sparwasser, T., et al. (2002). In Vivo depletion of CD11c<sup>+</sup> dendritic cells abrogates priming of CD8<sup>+</sup> T Cells by exogenous cell-associated antigens. *Immunity* 17, 211–220. doi: 10.1016/s1074-7613(02)00365-5

## AUTHOR CONTRIBUTIONS

MW, F-XM, and LS designed, performed, and interpreted the experiments and co-wrote the manuscript. ML and IE performed the experiments. PE designed and interpreted the research and co-wrote the manuscript. All authors contributed to the article and approved the submitted version.

## FUNDING

This work was supported by institutional grants from INSERM and Université Paris Descartes, by grants 10-PPPP-1236 and 14-CE11-0014 from the *Agence Nationale de Recherche*, and by a grant Equipe DEQ20130326539 from the *Fondation pour la Recherche Médicale*.

- Kandror, K. V., and Pilch, P. F. (2011). The sugar is SIRVed: sorting glut4 and its fellow travelers. *Traffic* 12, 665–671. doi: 10.1111/j.1600-0854.2011.01175.x
- Keller, S. R., Scott, H. M., Mastick, C. C., Aebersold, R., and Lienhard, G. E. (1995). Cloning and characterization of a novel insulin-regulated membrane aminopeptidase from Glut4 vesicles. *J. Biol. Chem.* 270, 23612–23618. doi: 10.1074/jbc.270.40.23612
- Kokkala, P., Mpakali, A., Mauvais, F. X., Papakyriakou, A., Daskalaki, I., Petropoulou, I., et al. (2016). Optimization and structure-activity relationships of phosphinic pseudotriptide inhibitors of aminopeptidases that generate antigenic peptides. *J. Med. Chem.* 59, 9107–9123. doi: 10.1021/acs.jmedchem.6b01031
- Kretzer, N. M., Theisen, D. J., Tussiwand, R., Briseo, C. G., Grajales-Reyes, G. E., Wu, X., et al. (2016). RAB43 facilitates cross-presentation of cell-associated antigens by CD8α<sup>+</sup> Dendritic cells. *J. Exp. Med.* 213, 2871–2883. doi: 10.1084/jem.20160597
- Li, D. T., Estifanos, N., Habtemichael, O. J., Sales, C. I., Westergaard, X. O., DeVries, S. G., et al. (2019). GLUT4 storage vesicles: specialized organelles for regulated trafficking. *Yale J. Biol. Med.* 92, 453–470.
- Martinez, J. (2018). LAP it up, fuzz ball: a short history of LC3-associated phagocytosis. *Curr. Opin. Immunol.* 55, 54–61. doi: 10.1016/j.coi.2018.09.011
- Merzougui, N., Kratzer, R., Saveanu, L., and van Endert, P. (2011). A proteasome-dependent, TAP-independent pathway for cross-presentation of phagocytosed antigen. *EMBO Rep.* 12, 1257–1264. doi: 10.1038/embor.2011.203
- Montealegre, S., Abramova, A., Manceau, V., de Kanter, A. F., and van Endert, P. (2019). The role of MHC Class I recycling and Arf6 in cross-presentation by murine dendritic cells. *Life Sci. Alliance* 2:e201900464. doi: 10.26508/lsa.201900464
- Montealegre, S., and van Endert, P. (2017). MHC Class I Cross-presentation: stage lights on Sec22b. *Trends Immunol.* 38, 618–621. doi: 10.1016/j.it.2017.07.002
- Mpakali, A., Saridakis, E., Harlos, K., Zhao, Y., Kokkala, P., Georgiadis, D., et al. (2015). Crystal structure of insulin-regulated aminopeptidase with bound substrate analogue provides insight on antigenic epitope precursor recognition and processing. *J. Immunol.* 195, 2842–2851. doi: 10.4049/jimmunol.1501103
- Nair, P., Amsen, D., and Magarian Blander, J. (2011). Co-ordination of incoming and outgoing traffic in antigen-presenting cells by pattern recognition receptors and T Cells. *Traffic* 12, 1669–1676. doi: 10.1111/j.1600-0854.2011.01251.x
- Nair-Gupta, P., Baccarini, A., Tung, N., Seyffer, F., Florey, O., Huang, Y., et al. (2014). TLR signals induce phagosomal MHC-I Delivery from the endosomal recycling compartment to allow cross-presentation. *Cell* 158, 506–521. doi: 10.1016/j.cell.2014.04.054
- Pan, X., Zaarur, N., Singh, M., Morin, P., and Kandror, K. V. (2017). Sortilin and retromer mediate retrograde transport of Glut4 in 3T3-L1 adipocytes. *Mol. Biol. Cell* 28, 1667–1675. doi: 10.1091/mbc.E16-11-0777

- Rock, K. L., Farfán-Arribas, D. J., and Shen, L. (2010). Proteases in MHC Class I presentation and cross-presentation. *J. Immunol.* 184, 9–15. doi: 10.4049/jimmunol.0903399
- Sadacca, L. A., Bruno, J., Wen, J., Xiong, W., and McGraw, T. E. (2013). Specialized sorting of GLUT4 and its recruitment to the cell surface are independently regulated by distinct rabs. *Mol. Biol. Cell* 24, 2544–2557. doi: 10.1091/mbc.E13-02-0103
- Samie, M., and Cresswell, P. (2015). The transcription Factor TFEB acts as a molecular switch that regulates exogenous antigen-presentation pathways. *Nat. Immunol.* 16, 729–736. doi: 10.1038/ni.3196
- Sanjuan, M. A., Dillon, C. P., Tait, S. G. W., Moshiah, S., Dorsey, F., and Connell, S. (2007). Toll-like receptor signalling in macrophages links the autophagy pathway to phagocytosis. *Nature* 450, 1253–1257. doi: 10.1038/nature06421
- Saveanu, L., Carroll, O., Weimershaus, M., Guernonprez, P., Firat, E., Lindo, V., et al. (2009). IRAP identifies an endosomal compartment required for MHC Class I cross-presentation. *Science* 325, 213–217. doi: 10.1126/science.1172845
- Savina, A., Vargas, P., Guernonprez, P., Lennon, A.-M., and Amigorena, S. (2010). Measuring PH, ROS production, maturation, and degradation in dendritic cell phagosomes using cytofluorometry-based assays. *Meth. Mol. Biol.* 595, 383–402. doi: 10.1007/978-1-60761-421-0\_25
- Sengupta, D., Graham, M., Liu, X., and Cresswell, P. (2019). Proteasomal degradation within endocytic organelles mediates antigen cross-presentation. *EMBO J.* 38:e99266.
- Stenmark, H. (2009). Rab GTPases as coordinators of vesicle traffic. *Nat. Rev. Mol. Cell Biol.* 10, 513–525. doi: 10.1038/nrm728
- Wang, T., Grabski, R., Sztul, E., and Hay, J. C. (2015). P115-SNARE interactions: a dynamic cycle of P115 Binding monomeric SNARE motifs and releasing assembled bundles. *Traffic* 16, 148–171. doi: 10.1111/tra.12242
- Weimershaus, M., Evnouchidou, I., Saveanu, L., and van Endert, P. (2013). Peptidases trimming MHC Class I ligands. *Curr. Opin. Immunol.* 25, 90–96. doi: 10.1016/j.coi.2012.10.001
- Weimershaus, M., Maschalidi, S., Sepulveda, F., Manoury, B., van Endert, P., and Saveanu, L. (2012). Conventional dendritic cells require IRAP-Rab14 endosomes for efficient cross-presentation. *J. Immunol.* 188, 1840–1846. doi: 10.4049/jimmunol.1101504
- Weimershaus, M., Mauvais, F. X., Saveanu, L., Adiko, C., Babdor, J., Abramova, A., et al. (2018). Innate immune signals induce anterograde endosome transport promoting MHC Class I Cross-presentation. *Cell Rep.* 24, 3568–3581. doi: 10.1016/j.celrep.2018.08.041
- Weimershaus, M., and van Endert, P. (2013). Preparation of dendritic cells by in vitro cultures. *Meth. Mol. Biol.* 960, 351–357. doi: 10.1007/978-1-62703-218-6\_25
- Williams, D., Hicks, S. W., Machamer, C. E., and Pessin, J. E. (2006). Golgin-160 is required for the golgi membrane sorting of the insulin-responsive glucose transporter GLUT4 in adipocytes. *Mol. Biol. Cell* 17, 5346–5355. doi: 10.1091/mbc.e06-05-0386
- Wu, S. J., Niknafs, Y. S., Kim, S. H., Oravec-Wilson, K., Zajac, C., Toubai, T., et al. (2017). A critical analysis of the role of SNARE Protein SEC22B in antigen cross-presentation. *Cell Rep.* 19, 2645–2656. doi: 10.1016/j.celrep.2017.06.013
- Zou, L., Zhou, J., Zhang, J., Li, J., Liu, N., Chai, L., et al. (2009). The GTPase Rab3b/3c-positive recycling vesicles are involved in cross-presentation in dendritic cells. *Proc. Natl. Acad. Sci. U.S.A.* 106, 15801–15806. doi: 10.1073/pnas.0905684106

**Conflict of Interest:** The authors declare that the research was conducted in the absence of any commercial or financial relationships that could be construed as a potential conflict of interest.

Copyright © 2020 Weimershaus, Mauvais, Evnouchidou, Lawand, Saveanu and van Endert. This is an open-access article distributed under the terms of the Creative Commons Attribution License (CC BY). The use, distribution or reproduction in other forums is permitted, provided the original author(s) and the copyright owner(s) are credited and that the original publication in this journal is cited, in accordance with accepted academic practice. No use, distribution or reproduction is permitted which does not comply with these terms.





# Serum IRAP, a Novel Direct Biomarker of Prediabetes and Type 2 Diabetes?

Candice Trocmé<sup>1</sup>, Nicolas Gonnet<sup>2</sup>, Margaux Di Tommaso<sup>3</sup>, Hanen Samouda<sup>3</sup>, Jean-Luc Cracowski<sup>2,4,5</sup>, Claire Cracowski<sup>2</sup>, Stéphanie Lambert-Porcheron<sup>6,7</sup>, Martine Laville<sup>6,7,8</sup>, Estelle Nobécourt<sup>9</sup>, Chiraz Gaddhab<sup>10</sup>, Allan Le Lay<sup>11</sup>, Torsten Bohn<sup>3</sup>, Christine Poitou<sup>12,13</sup>, Karine Clément<sup>12,13</sup>, Fahd Al-Mulla<sup>14</sup>, Milad S. Bitar<sup>14,15</sup> and Serge P. Bottari<sup>3,16,17,18\*</sup>

<sup>1</sup> Department of Biochemistry, Molecular Biology and Environmental Toxicology, Centre Hospitalier Grenoble-Alpes, La Tronche, France, <sup>2</sup> Centre d'Investigation Clinique, Centre Hospitalier Grenoble-Alpes, La Tronche, France, <sup>3</sup> Population Health Department, Nutrition and Health Research Group, Luxembourg Institute of Health, Luxembourg, Luxembourg, <sup>4</sup> Medical School, Université Grenoble Alpes, La Tronche, France, <sup>5</sup> INSERM U1042 Laboratoire Hypoxie et Physiopathologies cardiovasculaires et respiratoires (HP2), Grenoble, France, <sup>6</sup> Centre de Recherche en Nutrition Humaine Rhône-Alpes, Pierre-Bénite, France, <sup>7</sup> CH Lyon Sud, Lyon, France, <sup>8</sup> INSERM U1060 Laboratoire de Recherche en Cardiovasculaire, Métabolisme, diabétologie et Nutrition, Oullins, France, <sup>9</sup> Department of Endocrinology, Metabolic Diseases and Nutrition, Centre Hospitalier Universitaire de La Réunion, Saint-Denis, France, <sup>10</sup> Department of Pediatrics, Diabetes and Endocrinology Care, Centre Hospitalier de Luxembourg, Luxembourg, Luxembourg, <sup>11</sup> CHU Grenoble-Alpes, Department of Biochemistry, Molecular Biology and Environmental Toxicology, Grenoble, France, <sup>12</sup> INSERM UMR-S 1269, NutriOmics, Paris, France, <sup>13</sup> Medical School, Sorbonne Universités, Paris, France, <sup>14</sup> Department of Genomics and Bioinformatics, Dasman Diabetes Institute, Kuwait City, Kuwait, <sup>15</sup> Department of Pharmacology, Faculty of Medicine, Kuwait University, Kuwait City, Kuwait, <sup>16</sup> GREPI, UMR5525 Techniques de l'Ingénierie Médicale et de la Complexité Informatique, Mathématiques et Applications, Grenoble (TIMC-IMAG), La Tronche, France, <sup>17</sup> Faculté de Médecine, Université Grenoble Alpes, La Tronche, France, <sup>18</sup> Centre Hospitalier Grenoble-Alpes, La Tronche, France

## OPEN ACCESS

### Edited by:

Jonathan Bogan,  
National and Kapodistrian University  
of Athens, Greece

### Reviewed by:

Loredana Saveanu,  
Institut National de la Santé et de la  
Recherche Médicale  
(INSERM), France  
Paul Richard Gard,  
University of Brighton,  
United Kingdom

### \*Correspondence:

Serge P. Bottari  
serge.bottari@univ-grenoble-alpes.fr

### Specialty section:

This article was submitted to  
Cellular Biochemistry,  
a section of the journal  
Frontiers in Molecular Biosciences

**Received:** 18 August 2020

**Accepted:** 23 November 2020

**Published:** 16 February 2021

### Citation:

Trocmé C, Gonnet N, Di Tommaso M, Samouda H, Cracowski J-L, Cracowski C, Lambert-Porcheron S, Laville M, Nobécourt E, Gaddhab C, Le Lay A, Bohn T, Poitou C, Clément K, Al-Mulla F, Bitar MS and Bottari SP (2021) Serum IRAP, a Novel Direct Biomarker of Prediabetes and Type 2 Diabetes? *Front. Mol. Biosci.* 7:596141. doi: 10.3389/fmolb.2020.596141

Insulin resistance (IR), currently called prediabetes (PD), affects more than half of the adult population worldwide. Type 2 diabetes (T2D), which often follows in the absence of treatment, affects more than 475 million people and represents 10–20% of the health budget in industrialized countries. A preventive public health policy is urgently needed in order to stop this constantly progressing epidemic. Indeed, early management of prediabetes does not only strongly reduce its evolution toward T2D but also strongly reduces the appearance of cardiovascular comorbidity as well as that of associated cancers. There is however currently no simple and reliable test available for the diagnosis or screening of prediabetes and it is generally estimated that 20–60% of diabetics are not diagnosed. We therefore developed an ELISA for the quantitative determination of serum Insulin-Regulated AminoPeptidase (IRAP). IRAP is associated with and translocated in a stoichiometric fashion to the plasma membrane together with GLUT4 in response to insulin in skeletal muscle and adipose tissue which are the two major glucose storage sites. Its extracellular domain (IRAPs) is subsequently cleaved and secreted in the blood stream. In T2D, IRAP translocation in response to insulin is strongly decreased. Our patented sandwich ELISA is highly sensitive ( $\geq 10.000$ -fold “normal” fasting concentrations) and specific, robust and very cost-effective. Dispersion of fasting plasma concentration values in a healthy population is very low ( $101.4 \pm 15.9 \mu\text{g/ml}$ ) as compared to those of insulin ( $21\text{--}181 \text{ pmol/l}$ ) and C-peptide ( $0.4\text{--}1.7 \text{ nmol/l}$ ). Results of pilot studies indicate a clear correlation between IRAPs levels and insulin sensitivity. We

therefore think that plasma IRAPs may be a direct marker of insulin sensitivity and that the quantitative determination of its plasma levels should allow large-scale screening of populations at risk for PD and T2D, thereby allow the enforcement of a preventive health policy aiming at efficiently reducing this epidemic.

**Keywords:** IRAP, diabetes, biomarker, prediabetes, diagnosis, screening, GLUT4

## STATE OF THE ART AND CURRENT ISSUES

Type 2 diabetes (T2D) is a severe chronic disease whose incidence has been increasing continuously over the past decades becoming a major public health and socio-economic issue (Herman and Zimmet, 2012; Menke et al., 2015; International Diabetes Federation, 2019). T2D does not develop abruptly, but is preceded by a gradually worsening impaired glucose tolerance or insulin resistance, now generally referred to as prediabetes (Perreault, 2000; Edwards and Cusi, 2016). This disease which is essentially asymptomatic, is due to the progressive appearance of a resistance of target tissues to the metabolic actions of insulin (Kahn, 1996). One of the most extensively characterized initial signs of prediabetes is a reduction of the rate of glucose uptake by the insulin responsive cells after a meal (Garvey et al., 1998; Jung and Lee, 1999). This together with increased hepatic gluconeogenesis leads to higher levels of postprandial glycemia and to a delayed return to basal glycemia levels. These two phenomena are usually accompanied by increased postprandial insulin levels. Additional features are usually hypertriglyceridemia, mild hypertension and overweight.

The situation generally worsens with time over a period which can take several years, to finally result in fasting hyperglycemia which is the definition of type 2 diabetes (Geiss et al., 2010).

Contrary to type 1 diabetes which is due to a severe decrease in insulin secretion by the pancreas, type 2 diabetes is due to defects in signal transduction between the insulin receptor and the molecular mechanisms involved in glucose uptake and other metabolic actions of insulin. These defects, make the cells resistant to the metabolic actions of insulin (Kahn, 1992, 1996). Whereas, not all tissues, e.g., the brain and the liver, depend on insulin for glucose uptake, the major glucose storage tissues, i.e., skeletal muscle and adipose tissue do. In addition, insulin is no longer able to inhibit gluconeogenesis, especially by the liver, thereby contributing to the progressive worsening of hyperglycemia. Numerous studies have shown that in the absence of early and adequate management of insulin-resistance, prediabetes almost invariably evolves to T2D (Perreault, 2000; Herman and Zimmet, 2012; Kerrison et al., 2017; Braga et al., 2019). Currently the International Diabetes Foundation (IDF) estimates that more than 460 million people have diabetes worldwide. Seventy five percent of the individuals having diabetes (> 350 million) are aged between 20 and 64 years and are therefore part of the working age population which explains the huge socio-economic burden of the disease (International Diabetes Federation, 2019).

T2D is the first cause of death in adults worldwide, namely about 4.2 million people, i.e., 11.3% of deaths. It is also a major cause of disability (Gregg et al., 2016; International Diabetes Federation, 2019).

It is now widely recognized that prediabetes carries an equal risk of morbi-mortality as T2D (Huang et al., 2016; Casagrande et al., 2018b) with regard to cardiovascular diseases (Balakumar et al., 2016; Strain et al., 2018) and/or cancer (Scappaticcio et al., 2017). Current IDF estimations emphasize that more than 375 million people worldwide have prediabetes (Bullard et al., 2018; International Diabetes Federation, 2019). The total number of people living with a high risk of developing insulin-resistance associated diseases, essentially cardiovascular diseases and cancer, is therefore  $\geq 835$  million individuals. Moreover, the IDF considers that approximately half of the population having diabetes is undiagnosed and therefore unaware of having the disease (International Diabetes Federation, 2019).

Finally, about 16% of the pregnant women, i.e., more than 20 million women worldwide, develop diabetes during pregnancy. This gestational diabetes often results in potentially severe complications either during pregnancy or at the parturition and even later on in life both for the infant and the mother (Chiefari et al., 2017; Casagrande et al., 2018a; Plows et al., 2018).

From an economic point of view, the IDF estimated last year's worldwide direct cost of diabetes at 760 billion USD and its indirect costs at 455 billion USD (in 2015) (International Diabetes Federation, 2019).

Despite these impressive figures and the grim projections of the progression of the prevalence of these diseases for the next decades, there is so far no simple, reliable, and cost-effective diagnostic test for T2D and even less so for prediabetes (Muniyappa et al., 2008; Malkani and DeSilva, 2012; Wolffenbuttel et al., 2013; Xiang et al., 2014; Gloyn and Drucker, 2018).

Currently, all diagnostic tests for T2D are based either on the determination of glycemia, insulin or its secreted precursor C-peptide levels or on the assessment of the consequences of hyperglycemia, e.g., hemoglobin glycation (HbA1c levels). The most common screening test used is random plasma glucose testing (RPG). In an elegant paper, Herman's group showed that this method results in an extremely high overestimation of the incidence of T2D using a cut-off value of 130 mg/dl (Johnson et al., 2005). In order to try to standardize screening it has been recommended to assay fasting plasma glucose levels instead. It turned out that using a cut-off value of 126 mg/dl, the sensitivity of FPG ranges between 35 and 59% and the specificity between 85 and 95%, comparable to the sensitivity and specificity of an RPG cut-off point of 160 mg/dl (Blunt et al.,

1991; Borthey et al., 1994; Engelgau et al., 2000). Another, more logical approach for the screening of T2D considering that it is due to insulin resistance, is to measure post-prandial glycemia (PPG). The major drawback of this method is the considerable inter-individual and intra-individual variability of PPG (Venn and Green, 2007; Rohling et al., 2019) due to high interpersonal variability in post-prandial glycemic responses to the same food (Zeevi et al., 2015). It is thus obvious now that these tests cannot be used for screening for T2D and even less so for PD (Bansal, 2015).

Another parameter whose measurement has been proposed for screening of T2D, is HbA1c. The rationale behind it is that HbA1c should reflect an integrated measurement of glycemia over a period of ~3 months as compared to the real time punctual information represented by FPG and PPG. Unfortunately, HbA1c levels are also strongly determined by genetic factors (Cohen et al., 2006; Bloomgarden et al., 2008; Cavagnoli et al., 2017) and do therefore show important interindividual variability independently of glycemia. In agreement with this, a lack of correlation with FPG and PPG have been consistently reported (Bonora et al., 2001; E. van 't et al., 2010; Cavagnoli et al., 2011; Nathan et al., 2014), as well as other discrepancies (Gomez-Perez et al., 1998; Bonora and Tuomilehto, 2011; Tucker, 2020).

Therefore, whereas it is a useful marker for the follow-up of glycemia in T2D patients, each patient acting as his own control, it obviously cannot be used as a diagnostic neither as a screening assay (Gomez-Perez, 2015).

Considering the lack of sensitivity and specificity of these static markers, dynamic tests have been and are currently being used. The most widely used is the oral glucose tolerance test (OGTT) first described by JW Conn in 1940, in which patients are challenged with glucose after which their glycemia and insulinemia are monitored for 2 h or more (Matthews et al., 1985; American Diabetes Association, 2020). Based on the glycemia and insulinemia values during the 2-h duration of OGTT, Matsuda has proposed an equation which fits better with the data obtained using the euglycemic hyperinsulinemic clamp, considered to be the gold standard (Matsuda and DeFronzo, 1999). This index has further been improved using the AUCs for both parameters (Abdul-Ghani et al., 2007). Nevertheless, the intrinsic problem of this dynamic test is the important intra- and interindividual variability of glycemia and insulinemia, even if this issue is somewhat alleviated by integrating the values measured at several time points. Thus, whereas OGTT may represent an improvement for the diagnosis of T2D, the immobilization of the patients for more than 2 h it requires, precludes it from being used for screening purposes. This is even more so for the euglycemic hyperinsulinemic clamp which can only be used in research settings.

In an attempt to find a solution to this issue, an index based on the mathematical modeling of the steady-state basal plasma glucose and insulin concentrations feedback loop has been developed. It has been proposed by the authors that comparison of a patient's fasting values with the model's predictions allows a quantitative assessment of the contributions of insulin resistance and deficient beta-cell function to the fasting hyperglycaemia

(homeostasis model assessment, HOMA) (Matthews et al., 1985). However, as indicated by the authors, "The low precision of the estimates from the model (coefficients of variation: 31% for insulin resistance and 32% for beta-cell deficit) limits its use (Matthews et al., 1985)." Most important are, as stated by the authors, the facts that 1° The HOMA model is a model of the glucose-insulin feedback system in the homeostatic (overnight-fasted) state and 2° it has been designed to predict pancreatic  $\beta$ -cell function (% $\beta$ ) and insulin sensitivity (IS) in the fasting steady state. Its initial aim was to provide an accurate representation of physiology and successfully predict the homeostatic responses to an intravenous glucose infusion (Levy et al., 1998).

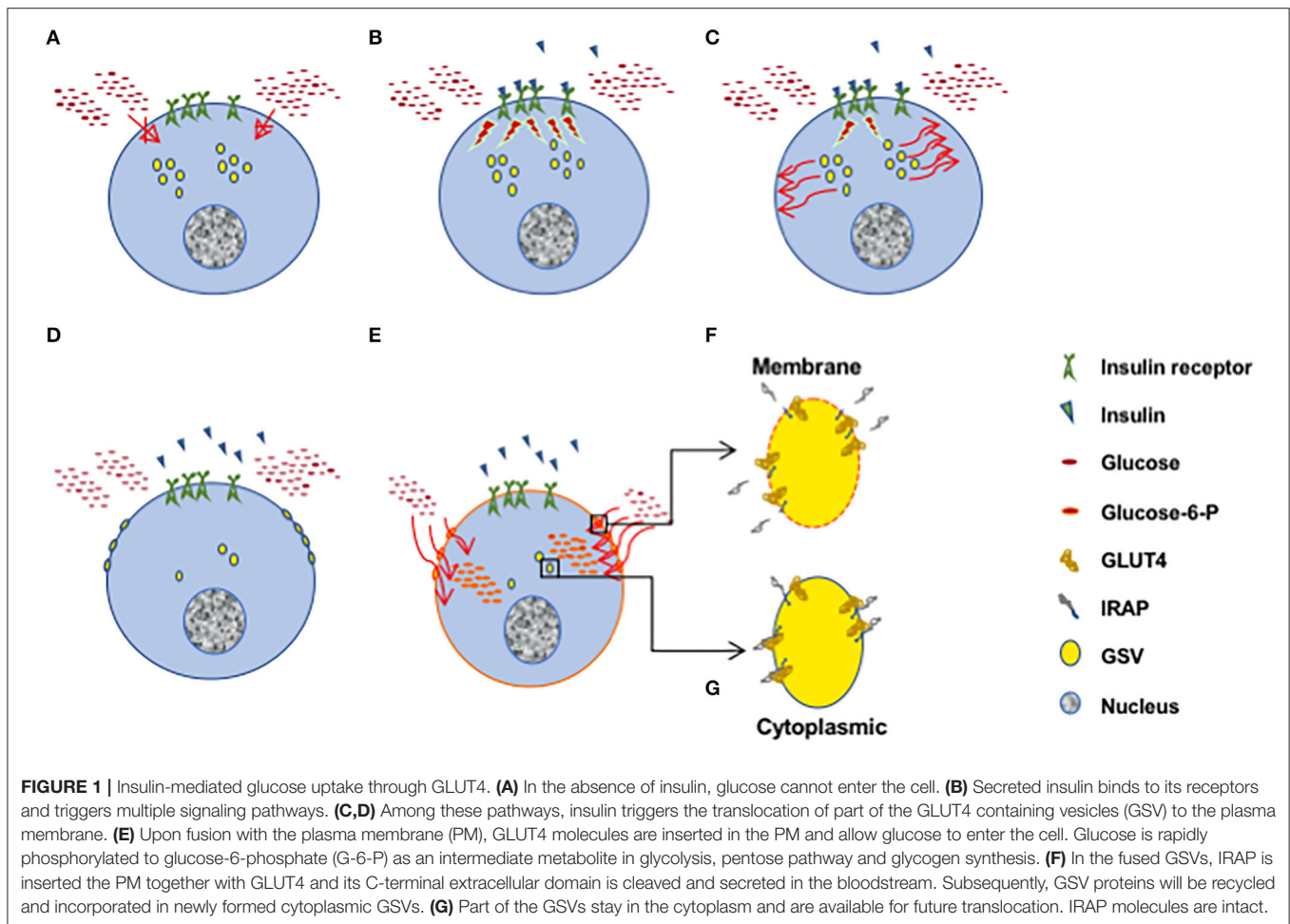
This model has been extrapolated to a clinical use to determine IS and % $\beta$  and from there to diagnose diabetes despite the caveats and inappropriate uses pointed out by the authors (Wallace et al., 2004). Obviously, the value of the HOMA index essentially depends on the quality of the sample measurements (Matthews et al., 1985) which brings us back to the issue of FPG with its high degree of intra- and interindividual variability which also holds for insulinemia.

Many other indices have been proposed based on direct, i.e., insulin infusion-based tests, and indirect, i.e., insulinemia measurements, methods. The advantages and caveats of the major indices for clinical purposes has been reviewed in detail by Matsuda in 2010 (Matsuda, 2010). The correlations of 35 indices with IS and 1/IS obtained from IVGTT and standard hyperglycemic breakfast test have been reported and are indicative of the important discrepancies between most of them (Aloulou et al., 2006). More interesting even is the comparison of several of these indices in similar settings between diabetics and healthy subjects (Brun et al., 2013). The data reported unambiguously show that whereas there is a good correlation of some indices in healthy subjects, this is not the case in patients with diabetes. This thus once more raises the issue of extrapolating indices which reflect physiological glucose homeostasis to clinical settings.

In summary, all available methods used so far for the diagnosis of T2D suffer from more or less serious drawbacks and particularly the tests based on single time point determinations. This is obviously even more true for PD where increases in glycemia and insulinemia are less pronounced than in T2D.

The most reliable diagnostic test being OGTT based, there is thus as yet no reliable method available allowing for the screening of T2D and PD.

Recent work aimed at finding novel biomarkers of PD and T2D has resulted in the identification of copeptin, which is the C-terminal fragment of pre-pro-vasopressin (Enhorning et al., 2011; Wannamethee et al., 2015; Roussel et al., 2016; Jensen et al., 2019). The mechanisms which link the secretion of copeptin to insulin-resistance are however still unclear. It is possible that increased copeptin levels in T2D are due to decreased translocation of IRAP which has been reported to degrade vasopressin, thereby triggering the secretion of its precursor pre-pro-vasopressin. Interestingly however copeptin appears to be an interesting independent marker of renal and cardiovascular complications in T2D (Riphagen et al., 2013; Velho et al., 2013; Bar-Shalom et al., 2014; Zhu et al., 2016; Potier et al., 2019).



## A NOVEL DIAGNOSTIC APPROACH

Our approach has therefore been to shift from an integrative parameter, glycemia, to a specific and exclusively insulin-dependent parameter, glucose uptake. Indeed, insulin resistance which is the defect underlying prediabetes, T2D and gestational diabetes, always involves altered insulin-mediated glucose uptake (Kahn, 1996).

The mechanism through which insulin stimulates cellular glucose uptake, is by inducing the translocation of the vesicles which contain the glucose transporter GLUT4, from the cytoplasm to the plasma membrane (Bryant et al., 2002). As a result, these vesicles fuse with the plasma membrane and the GLUT4 proteins become inserted there. Since there is an important concentration gradient of glucose from the extracellular fluid to the cytosol, glucose will enter the cell by passive diffusion and will be instantaneously phosphorylated to enter the metabolic pathways. Thus, cytosolic glucose concentrations always remain extremely low, maintaining the concentration gradient.

Apart from this pathway, there is no other additional or alternative way for glucose to enter cells in an insulin-dependent fashion. Certain cells and organs like the brain and the liver

do not rely on insulin for glucose uptake and express other glucose transporter isoforms which are located constitutively in the plasma membrane.

The major issue with this approach was to find the appropriate biomarker. Indeed, determining plasma membrane vs. vesicular GLUT4, is not only complex but also invasive as it requires muscle or adipose tissue biopsies. Such an approach is obviously not suitable for routine and large-scale screening or diagnosis of insulin resistance.

The challenge was thus to find a plasmatic or serum biomarker of GLUT4 vesicle translocation.

GLUT4 vesicles contain a series of other proteins, most of which are essentially involved in the translocation process (Bogan and Kandror, 2010).

Interestingly, among these vesicular proteins, there is an aminopeptidase which appears to be closely associated with GLUT4 in a stoichiometric fashion. A peculiarity of this protein called Insulin-Regulated AminoPeptidase (IRAP) which was identified and cloned in 1994 (Mastick et al., 1994; Keller et al., 1995; Ross et al., 1996), is that its large 160 kDa extracellular domain is cleaved by metalloproteases, ADAM 9 and 12 and thus secreted in the bloodstream (Figure 1) (Ito et al., 2004), similar to angiotensin-converting enzyme (ACE) (Costerousse et al., 1992).



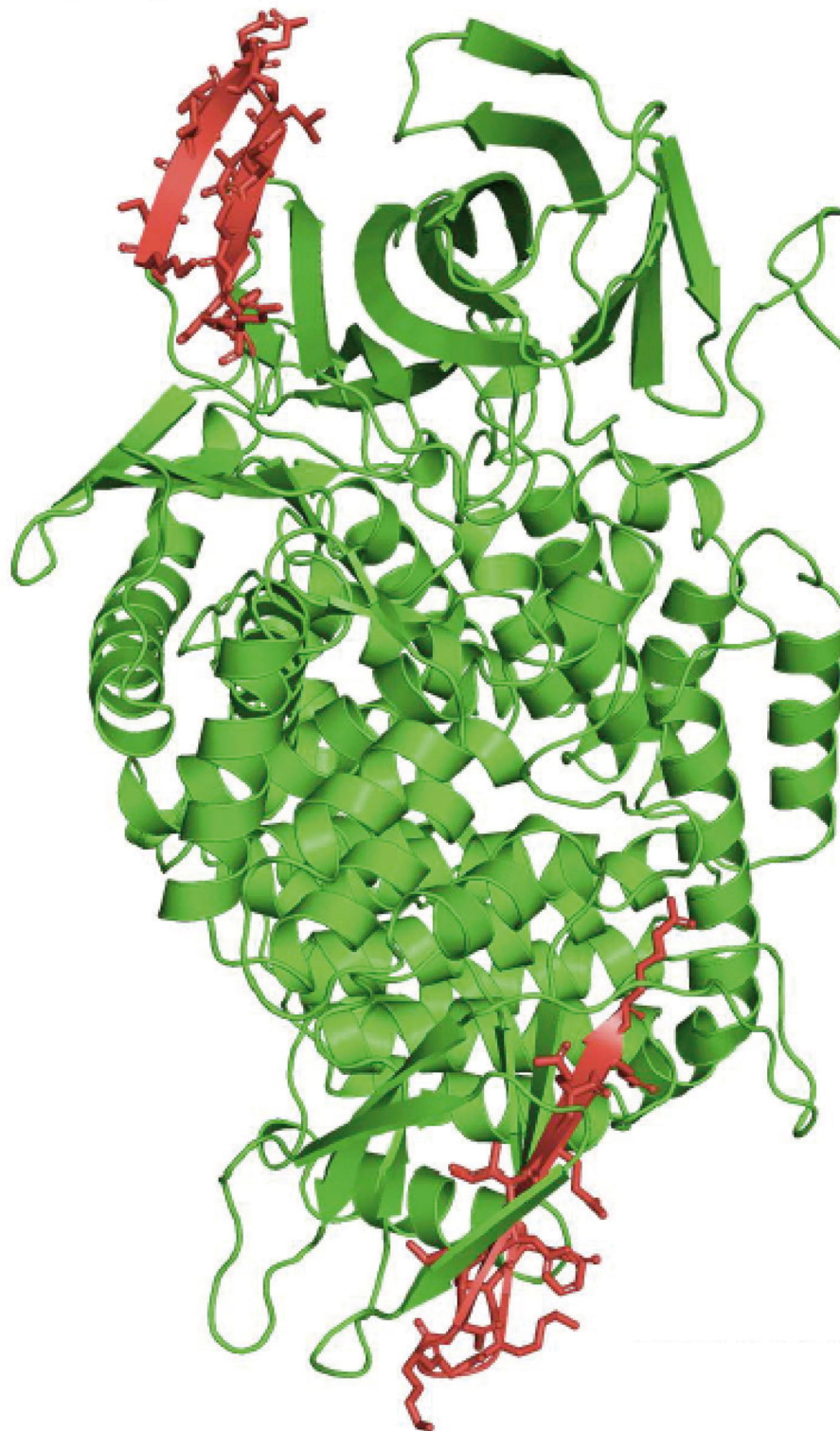


**FIGURE 2 |** Structure of the cleaved extracellular domain of IRAP: 3-dimensional model of the cleaved extracellular domain of IRAP. Epitopes recognized by the monoclonal antibodies used in the ELISA are in red.

Since insulin triggers the translocation of the GLUT4 vesicles to the plasma membrane, the circulating levels of IRAP should reflect the amount of IRAP and GLUT4 which are translocated to the plasma membrane (**Figure 1**) and hence reflect the degree of insulin sensitivity.

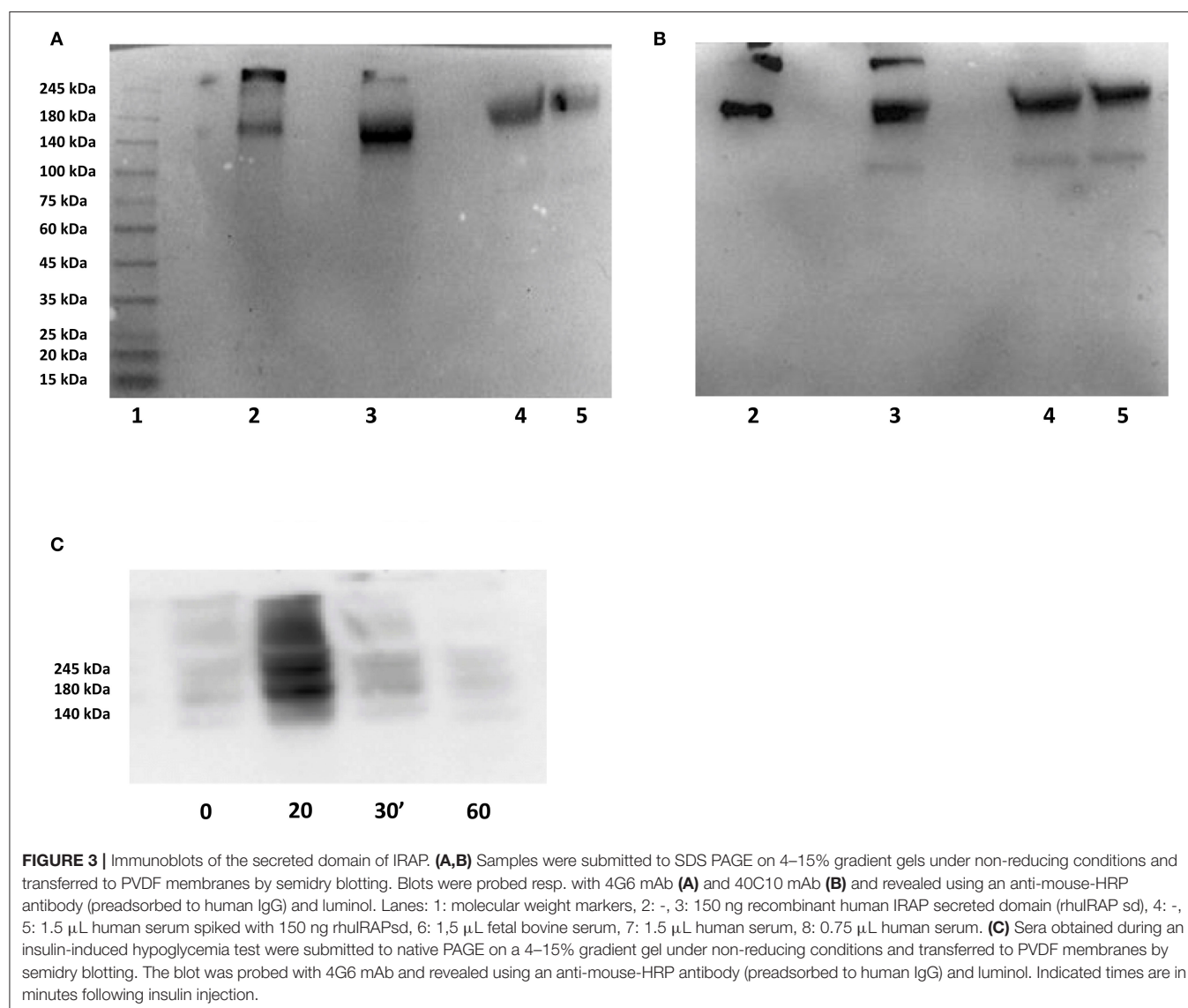
In agreement with this hypothesis, data from the literature indicate a decrease of IRAP translocation in response to insulin in adipocytes and skeletal muscle in diabetic rats (Takeuchi et al., 2006) and in patients with type 2 diabetes (Garvey et al., 1998; Maianu et al., 2001). It is therefore reasonable to assume that circulating IRAP (IRAPs) levels will be decreased in people having prediabetes or diabetes.

IRAPs may therefore be a direct marker of insulin response and sensitivity. Accordingly, its quantitative determination by a simple and robust method could allow the screening of populations at risk for prediabetes, type 2 diabetes and gestational diabetes.

Similar to what had been done previously by other investigators for measuring circulating angiotensin-converting enzyme (ACE) (Danilov et al., 1996), we attempted to develop an assay for the quantitative determination of IRAPs in serum.

After having investigated and tried different techniques, we chose to further develop a sandwich ELISA using two monoclonal antibodies directed against two epitopes of the globular extracellular domain of IRAP (**Figure 2**) identified by 3-D modeling (Mpakali et al., 2015). The ELISA is calibrated with recombinant human IRAPs obtained through (over)expression in mammalian cells.

The assay is highly specific for IRAP and does not display any cross-reactivity with other related aminopeptidases under the analytical conditions. Its sensitivity is 10 ng/ml for reference values around 100 µg/ml in healthy volunteers under fasting conditions. This assay and the diagnostic applications of IRAP



have been patented under the reference PCT/FR2009/05133 and published as WO 2010/001079.

Clinical trials to validate the diagnostic interest of this assay are currently under way. Preliminary data from pilot studies indicated that IRAPs is cleared from the circulation within 1 hr and that (Figure 3), in healthy individuals, its levels appear to follow glycemia and insulinemia (Figure 4). Interestingly, the dispersion of the IRAP concentrations determined in healthy volunteers under fasting conditions using this assay is low ( $101.4 \pm 15.9 \mu\text{g/ml}$ ) as compared to glycemia, insulinemia ( $21\text{--}181 \text{ pmol/l}$ ) or C-peptide ( $0.4\text{--}1.7 \text{ nmol/l}$ ), adding to its potential clinical value as a biomarker.

## PRELIMINARY RESULTS

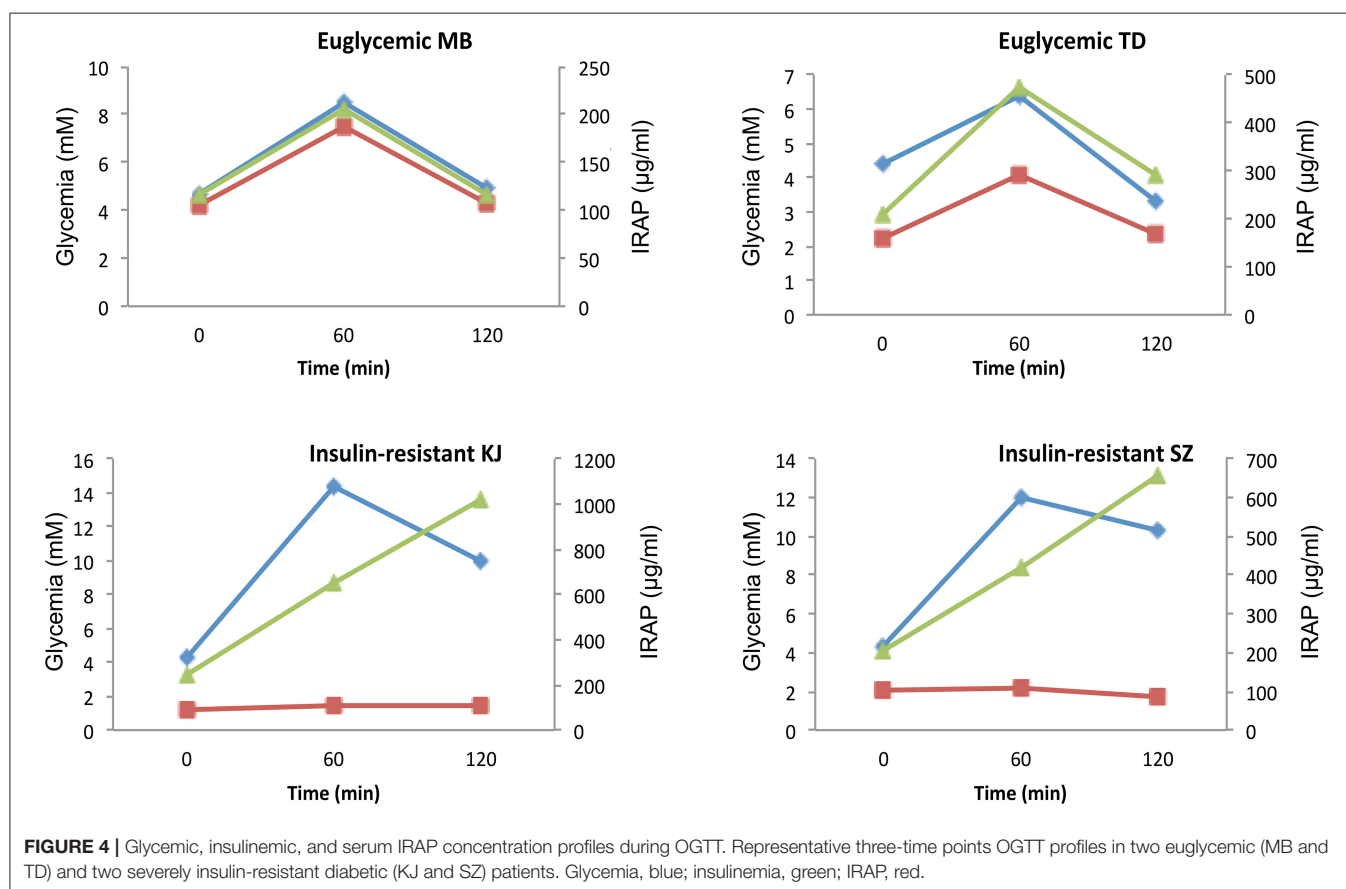
As shown in Figures 3A,B, immunolabeling of serum IRAP after SDS-PAGE with either of both monoclonal antibodies used in the ELISA, i.e., 4G6 for capture and 40C10 for detection, reveals a major band with an apparent molecular weight ( $M_r$ ) of approximately 160 kDa. Another band with a higher  $M_r$  between 300 and 400 kDa seen in the recombinant human IRAP secreted domain preparation probably corresponds to dimerization. Conversely, bovine serum does not show any detectable IRAP, in agreement with the absence of a proteolytic cleavage site required for its shedding. Interestingly, the mAb

40C10 also detects a minor band with an  $M_r$  of  $\sim 100 \text{ kDa}$  which may correspond to a proteolytic fragment.

Figure 3C shows that in serum samples obtained during an insulin-induced hypoglycemia test, IRAP reaches a peak concentration within 20 min after insulin injection and is cleared within 60 min. The mechanisms involved in IRAP clearance are not elucidated yet but probably involves proteolysis as we observed a proteolytic fragment with one of the monoclonal antibodies (Figure 3B). The PAGE performed under “native” conditions shown in this figure also indicates that IRAP forms oligomers. These dissociate in the presence of SDS, yielding a single band with an apparent molecular weight of approximately 160 kDa as shown in Figures 3A,B. Effective dissociation of the oligomers is obviously a key feature of the ELISA.

As expected, IRAP levels do not follow insulinemia in severe insulin resistance. Figure 4 shows typical glycemia, insulinemia and serum IRAP concentration profiles during OGTT in two euglycemic and two severely insulin-resistant diabetic patients. Whereas, serum IRAP levels correlate with glycemia and insulinemia in the two euglycemic patients, IRAP levels do not increase in response to increased insulinemia be it at 60 or 120 min after glucose intake.

These observations are in agreement with the hypothesis that IRAP translocation and shedding are strongly dependent upon insulin sensitivity.



## CONCLUSIONS

Type 2 diabetes and its preceding condition, prediabetes, are two major health issues worldwide, considering the dramatically increasing number of people having these conditions and the associated growing socioeconomic burden (Herman and Zimmet, 2012).

Interestingly and as opposed to other important health issues like cancer and infectious diseases, the major issue with T2D and PD is not so much their treatment, which is very cost-effective if started at an early stage and in constant progress with the advent of novel drugs, but timely diagnosis. The use of glycemia to screen for T2D and even more so for PD, has proven delusive probably due to its complex regulation and so are HbA1c and insulinemia.

IRAP, a protein associated with GLUT4 and directly involved in insulin-mediated glucose uptake, appears to be an interesting candidate biomarker for insulin-resistance.

We developed a highly specific and sensitive ELISA allowing the quantitative measurement of the circulating domain of IRAP in plasma and serum. The currently ongoing clinical trials will tell whether this test is a valuable tool for the screening and diagnosis of the insulin-resistance dependent diseases: prediabetes, type 2 diabetes and gestational diabetes.

## REFERENCES

- Abdul-Ghani, M. A., Matsuda, M., Balas, B., and DeFronzo, R. A. (2007). Muscle and liver insulin resistance indexes derived from the oral glucose tolerance test. *Diabetes Care* 30, 89–94. doi: 10.2337/dc06-1519
- Aloulou, I., Brun, J. F., and Mercier, J. (2006). Evaluation of insulin sensitivity and glucose effectiveness during a standardized breakfast test: comparison with the minimal model analysis of an intravenous glucose tolerance test. *Metabolism* 55, 676–690. doi: 10.1016/j.metabol.2006.01.002
- American Diabetes Association. (2020). Classification and diagnosis of diabetes: standards of medical care in diabetes-2020. *Diabetes Care* 43(Suppl 1):S14–31. doi: 10.2337/dc20-S002
- Balakumar, P., Maung, U. K., and Jagadeesh, G. (2016). Prevalence and prevention of cardiovascular disease and diabetes mellitus. *Pharmacol. Res.* 113(Pt A), 600–609. doi: 10.1016/j.phrs.2016.09.040
- Bansal, N. (2015). Prediabetes diagnosis and treatment: a review. *World J. Diabetes* 6, 296–303. doi: 10.4239/wjcd.v6.i2.296
- Bar-Shalom, D., Poulsen, M. K., Rasmussen, L. M., Diederichsen, A. C., Sand, N. P., Henriksen, J. E., et al. (2014). Plasma copeptin as marker of cardiovascular disease in asymptomatic type 2 diabetes patients. *Diab. Vasc. Dis. Res.* 11, 448–450. doi: 10.1177/1479164114544464
- Bloomgarden, Z. T., Inzucchi, S. E., Karnieli, E., and Le Roith, D. (2008). The proposed terminology 'A(1c)-derived average glucose' is inherently imprecise and should not be adopted. *Diabetologia* 51, 1111–4. doi: 10.1007/s00125-008-1027-7
- Blunt, B. A., Barrett-Connor, E., and Wingard, D. L. (1991). Evaluation of fasting plasma glucose as screening test for NIDDM in older adults. Rancho Bernardo Study. *Diabetes Care* 14, 989–993. doi: 10.2337/diacare.14.11.989
- Bogan, J. S., and Kandror, K. V. (2010). Biogenesis and regulation of insulin-responsive vesicles containing GLUT4. *Curr. Opin. Cell Biol.* 22, 506–512. doi: 10.1016/j.ceb.2010.03.012
- Bonora, E., Calcaterra, F., Lombardi, S., Bonfante, N., Formentini, G., Bonadonna, R. C., et al. (2001). Plasma glucose levels throughout the day and HbA(1c) interrelationships in type 2 diabetes: implications for treatment and monitoring of metabolic control. *Diabetes Care* 24, 2023–2029. doi: 10.2337/diacare.24.12.2023

## DATA AVAILABILITY STATEMENT

The raw data supporting the conclusions of this article will be made available by the authors, without undue reservation.

## ETHICS STATEMENT

The studies involving human participants were reviewed and approved by Comité de protection des personnes Sud-Ouest et Outre-Mer III, NUMERO D'ENREGISTREMENT SICNIPH:ID 2360 n°18.12.11.65552, NUMÉRO ID-RCB: 2018-A03158-47. The patients/participants provided their written informed consent to participate in this study.

## AUTHOR CONTRIBUTIONS

CT, NG, AL, J-LC, CC, SL-P, ML, CG, KC, and SB participated to the studies. CG, HS, TB, FA-M, MB, and SB participated to the writing of the manuscript. MB and SB are the senior authors. All authors contributed to the article and approved the submitted version.

- Bonora, E., and Tuomilehto, J. (2011). The pros and cons of diagnosing diabetes with A1. *Diabetes Care* 34(Suppl 2):S184–90. doi: 10.2337/dc11-s216
- Borthey, A. L., Malerbi, D. A., and Franco, L. J. (1994). The ROC curve in the evaluation of fasting capillary blood glucose as a screening test for diabetes and IG. *Diabetes Care* 17, 1269–1272. doi: 10.2337/diacare.17.11.1269
- Braga, T., Kraemer-Aguilar, L. G., Docherty, N. G., and Le Roux, C. W. (2019). Treating prediabetes: why and how should we do it? *Minerva Med.* 110, 52–61. doi: 10.23736/S0026-4806.18.05897-4
- Brun, J. F., Ghanassia, E., Fedou, C., Bordenave, S. E., Raynaud M., and Mercier, J. (2013). Assessment of insulin sensitivity (S I) and glucose effectiveness (S G) from a standardized hyperglucidic breakfast test in type 2 diabetics exhibiting various levels of insulin resistance. *Acta Diabetol.* 50, 143–153. doi: 10.1007/s00592-010-0232-2
- Bryant, N. J., Govers, R., and James, D. E. (2002). Regulated transport of the glucose transporter GLUT4. *Nat. Rev. Mol. Cell Biol.* 3, 267–277. doi: 10.1038/nrm782
- Bullard, K. M., Cowie, C. C., Lessem, S. E., Saydah, S. H., Menke, A., Geiss, L. S., et al. (2018). Prevalence of diagnosed diabetes in adults by diabetes type - United States, 2016. *MMWR Morb. Mortal. Wkly. Rep.* 67, 359–361. doi: 10.15585/mmwr.mm6712a2
- Casagrande, S. S., Linder, B., and Cowie, C. C. (2018a). Prevalence of gestational diabetes and subsequent Type 2 diabetes among U.S. women. *Diabetes Res. Clin. Pract.* 141, 200–208. doi: 10.1016/j.diabres.2018.05.010
- Casagrande, S. S., Menke, A., Linder, B., Osganian, S. K., and Cowie, C. C. (2018b). Cardiovascular risk factors in adolescents with prediabetes. *Diabet Med.* 5:10.1111/dme.13661. doi: 10.1111/dme.13661
- Cavagnoli, G., Comerlato, J., Comerlato, C., Renz, P. B., Gross, J. L., and Camargo, J. L. (2011). HbA(1c) measurement for the diagnosis of diabetes: is it enough? *Diabet. Med.* 28, 31–35. doi: 10.1111/j.1464-5491.2010.03159.x
- Cavagnoli, G., Pimentel, A. L., Freitas, P. A., Gross, J. L., and Camargo, J. L. (2017). Effect of ethnicity on HbA1c levels in individuals without diabetes: systematic review and meta-analysis. *PLoS ONE* 12:e0171315. doi: 10.1371/journal.pone.0171315
- Chieffari, E., Arcidiacono, B., Foti, D., and Brunetti, A. (2017). Gestational diabetes mellitus: an updated overview. *J. Endocrinol. Invest.* 40, 899–909. doi: 10.1007/s40618-016-0607-5
- Cohen, R. M., Snieder, H., Lindsell, C. J., Beyan, H., Hawa, M. I., Blinko, S., et al. (2006). Evidence for independent heritability of the glycation gap (glycosylation



- gap) fraction of HbA1c in nondiabetic twins. *Diabetes Care* 29, 1739–1743. doi: 10.2337/dc06-0286
- Costerousse, O., Jaspard, E., Wei, L., Corvol, P., and Alhenc-Gelas, F. (1992). The angiotensin I-converting enzyme (kininase II): molecular organization and regulation of its expression in humans. *J. Cardiovasc. Pharmacol.* 20(Suppl 9):S10–15. doi: 10.1097/00005344-199200209-00004
- Danilov, S., Savoie, F., Lenoir, B., Jeunemaitre, X., Azizi, M., Tarnow, L., and Alhenc-Gelas, F. (1996). Development of enzyme-linked immunoassays for human angiotensin I converting enzyme suitable for large-scale studies. *J. Hypertens* 14, 719–727. doi: 10.1097/00004872-199606000-00007
- Edwards, C. M., and Cusi, K. (2016). Prediabetes: a worldwide epidemic. *Endocrinol. Metab. Clin. North Am.* 45, 751–764. doi: 10.1016/j.ecl.2016.06.007
- Engelgau, M. M., Narayan, K. M., and Herman, W. H. (2000). Screening for type 2 diabetes. *Diabetes Care* 23, 1563–1580. doi: 10.2337/diacare.23.10.1563
- Enhörning, S., Struck, J., Wirfalt, E., Hedblad, B., Morgenthaler, N. G., and Melander, O. (2011). Plasma copeptin, a unifying factor behind the metabolic syndrome. *J. Clin. Endocrinol. Metab.* 96, E1065–E1072. doi: 10.1210/jc.2010-2981
- E. van 't, R., Alsema, M., Rijkkelikhuisen, J. M., Kostense, P. J., Nijpels, G., and Dekker, J. M. (2010). Relationship between A1C and glucose levels in the general Dutch population: the new Hoorn study. *Diabetes Care* 33, 61–66. doi: 10.2337/dc09-0677
- Garvey, W. T., Maianu, L., Zhu, J. H., Brechtel-Hook, G., Wallace, P., and Baron, A. D. (1998). Evidence for defects in the trafficking and translocation of GLUT4 glucose transporters in skeletal muscle as a cause of human insulin resistance. *J. Clin. Invest.* 101, 2377–2386. doi: 10.1172/JCI1557
- Geiss, L. S., James, C., Gregg, E. W., Albright, A., Williamson, D. F., and Cowie, C. C. (2010). Diabetes risk reduction behaviors among U.S. adults with prediabetes. *Am. J. Prev. Med.* 38, 403–409. doi: 10.1016/j.amepre.2009.12.029
- Gloyn, A. L., and Drucker, D. J. (2018). Precision medicine in the management of type 2 diabetes. *Lancet Diabetes Endocrinol.* 6, 891–900. doi: 10.1016/S2213-8587(18)30052-4
- Gomez-Perez, F. J. (2015). Glycated hemoglobin, fasting, two-hour post-challenge and postprandial glycemia in the diagnosis and treatment of diabetes mellitus: are we giving them the right interpretation and use? *Rev. Invest. Clin.* 67, 76–79.
- Gomez-Perez, F. J., Aguilar-Salinas, C. A., Lopez-Alvarenga, J. C., Perez-Jauregui, J., Guillen-Pineda, L. E., and Rull, J. A. (1998). Lack of agreement between the World Health Organization Category of impaired glucose tolerance and the American Diabetes Association category of impaired fasting glucose. *Diabetes Care* 21, 1886–1888. doi: 10.2337/diacare.21.11.1886
- Gregg, E. W., Sattar, N., and Ali, M. K. (2016). The changing face of diabetes complications. *Lancet Diabetes Endocrinol.* 4, 537–547. doi: 10.1016/S2213-8587(16)30010-9
- Herman, W. H., and Zimmet, P. (2012). Type 2 diabetes: an epidemic requiring global attention and urgent action. *Diabetes Care* 35, 943–944. doi: 10.2337/dc12-0298
- Huang, Y., Cai, X., Mai, W., Li, M., and Hu, Y. (2016). Association between prediabetes and risk of cardiovascular disease and all cause mortality: systematic review and meta-analysis. *BMJ* 355:i5953. doi: 10.1136/bmj.i5953
- International Diabetes Federation (2019). *IDF Diabetes Atlas. 9th Edn.* In: Ed Diabetes data portal.
- Ito, N., Nomura, S., Iwase, A., Ito, T., Kikkawa, F., Tsujimoto, M., et al. (2004). ADAMs, a disintegrin and metalloproteinases, mediate shedding of oxytocinase. *Biochem. Biophys. Res. Commun.* 314, 1008–1013. doi: 10.1016/j.bbrc.2003.12.183
- Jensen, T., Bjørnstad, P., Johnson, R. J., Sippl, R., Rewers, M., and Snell-Bergeon, J. K. (2019). Copeptin, and estimated insulin sensitivity in adults with and without type 1 diabetes: the CACTI study. *Can J Diabetes* 43, 34–39. doi: 10.1016/j.cjcd.2018.03.006
- Johnson, S. L., Tabaei, B. P., and Herman, W. H. (2005). The efficacy and cost of alternative strategies for systematic screening for type 2 diabetes in the U.S. population 45–74 years of age. *Diabetes Care* 28, 307–311. doi: 10.2337/diacare.28.2.307
- Jung, C. Y., and Lee, W. (1999). Glucose transporters and insulin action: some insights into diabetes management. *Arch. Pharm. Res.* 22, 329–334. doi: 10.1007/BF02979053
- Kahn, B. B. (1992). Alterations in glucose transporter expression and function in diabetes: mechanisms for insulin resistance. *J. Cell Biochem.* 48, 122–128. doi: 10.1002/jcb.240480203
- Kahn, B. B. (1996). Lilly lecture 1995. Glucose transport: pivotal step in insulin action. *Diabetes* 45, 1644–1654. doi: 10.2337/diab.45.11.1644
- Keller, S. R., Scott, H. M., Mastick, C. C., Aebersold, R., and Lienhard, G. E. (1995). Cloning and characterization of a novel insulin-regulated membrane aminopeptidase from Glut4 vesicles. *J. Biol. Chem.* 270, 23612–23618. doi: 10.1074/jbc.270.40.23612
- Kerrison, G., Gillis, R. B., Jiwani, S. I., Alzahrani, Q., Kok, S., Harding, S. E., et al. (2017). The effectiveness of lifestyle adaptation for the prevention of prediabetes in adults: a systematic review. *J. Diabetes Res.* 2017:8493145. doi: 10.1155/2017/8493145
- Levy, J. C., Matthews, D. R., and Hermans, M. P. (1998). Correct homeostasis model assessment (HOMA) evaluation uses the computer program. *Diabetes Care* 21, 2191–2192. doi: 10.2337/diacare.21.12.2191
- Maianu, L., Keller, S. R., and Garvey, W. T. (2001). Adipocytes exhibit abnormal subcellular distribution and translocation of vesicles containing glucose transporter 4 and insulin-regulated aminopeptidase in type 2 diabetes mellitus: implications regarding defects in vesicle trafficking. *J. Clin. Endocrinol. Metab.* 86, 5450–5456. doi: 10.1210/jcem.86.11.8053
- Malkani, S., and DeSilva, T. (2012). Controversies on how diabetes is diagnosed. *Curr. Opin. Endocrinol. Diabetes Obes.* 19, 97–103. doi: 10.1097/MED.0b013e32835168c0
- Mastick, C. C., Aebersold, R., and Lienhard, G. E. (1994). Characterization of a major protein in GLUT4 vesicles. Concentration in the vesicles and insulin-stimulated translocation to the plasma membrane. *J. Biol. Chem.* 269, 6089–6092.
- Matsuda, M. (2010). Measuring and estimating insulin resistance in clinical and research settings. *Nutr. Metab. Cardiovasc. Dis.* 20, 79–86. doi: 10.1016/j.numecd.2009.07.007
- Matsuda, M., and DeFronzo, R. A. (1999). Insulin sensitivity indices obtained from oral glucose tolerance testing: comparison with the euglycemic insulin clamp. *Diabetes Care* 22, 1462–1470. doi: 10.2337/diacare.22.9.1462
- Matthews, D. R., Hosker, J. P., Rudenski, A. S., Naylor, B. A., Treacher, D. F., and Turner, R. C. (1985). Homeostasis model assessment: insulin resistance and beta-cell function from fasting plasma glucose and insulin concentrations in man. *Diabetologia* 28, 412–419. doi: 10.1007/BF00280883
- Menke, A., Casagrande, S., Geiss, L., and Cowie, C. C. (2015). Prevalence of and trends in diabetes among adults in the United States, 1988–2012. *JAMA* 314, 1021–1029. doi: 10.1001/jama.2015.10029
- Mpakali, A., Saridakis, E., Harlos, K., Zhao, Y., Papakyriakou, A., Kokkala, P., et al. (2015). Crystal structure of insulin-regulated aminopeptidase with bound substrate analogue provides insight on antigenic epitope precursor recognition and processing. *J. Immunol.* 195, 2842–2851. doi: 10.4049/jimmunol.1501103
- Muniyappa, R., Lee, S., Chen, H., and Quon, M. J. (2008). Current approaches for assessing insulin sensitivity and resistance in vivo: advantages, limitations, and appropriate usage. *Am. J. Physiol. Endocrinol. Metab.* 294, E15–E26. doi: 10.1152/ajpendo.00645.2007
- Nathan, D. M., McGee, P., Steffes, M. W., Lachin, J. M., and DER Group. (2014). Relationship of glycated albumin to blood glucose and HbA1c values and to retinopathy, nephropathy, and cardiovascular outcomes in the DCCT/EDIC study. *Diabetes* 63, 282–290. doi: 10.2337/db13-0782
- Perreault, L. (2000). Prediabetes. In: *Endotext*. Ed Feingold KR, Anawalt B, Boyce A, Chrousos G, Dungan K, Grossman A, Hershman JM, Kaltsas G, Koch C, Kopp P, Korbonits M, McLachlan R, Morley JE, New M, Perreault L, Purnell J, Rebar R, Singer F, Trencle DL, Vinikand AP. Wilson, MA: South Dartmouth.
- Plows, J. F., Stanley, J. L., Baker, P. N., Reynolds, C. M., and Vickers, M. H. (2018). The pathophysiology of gestational diabetes mellitus. *Int. J. Mol. Sci.* 19:3342. doi: 10.3390/ijms19113342
- Potier, L., Roussel, R., Marre, M., Bjørnstad, P., Cherney, D. Z., El Boustany, R., et al. (2019). Plasma copeptin and risk of lower-extremity amputation in type 1 and type 2 diabetes. *Diabetes Care* 42, 2290–2297. doi: 10.2337/dc19-1062
- Ripphagen, I. J., Boertien, W. E., Alkhalaf, A., Kleefstra, N., Gansevoort, R. T., Groenier, K. H., et al. (2013). Copeptin, a surrogate marker for arginine vasopressin, is associated with cardiovascular and all-cause mortality in

- patients with type 2 diabetes (ZODIAC-31). *Diabetes Care* 36, 3201–3207. doi: 10.2337/dc12-2165
- Rohling, M., Martin, T., Wonnemann, M., Kragl, M., Klein, H. H., Heinemann, L., et al. (2019). Determination of postprandial glycemic responses by continuous glucose monitoring in a real-world setting. *Nutrients* 11:2305. doi: 10.3390/nu11102305
- Ross, S. A., Scott, H. M., Morris, N. J., Leung, W. Y., Mao, F., Lienhard, G. E., et al. (1996). Characterization of the insulin-regulated membrane aminopeptidase in 3T3-L1 adipocytes. *J Biol Chem*, 271, 3328–3332. doi: 10.1074/jbc.271.6.3328
- Roussel, R., El Boustany, R., Bouby, N., Potier, L., Fumeron, F., Mohammadi, K., et al. (2016). Plasma Copeptin, AVP gene variants, and incidence of type 2 diabetes in a cohort from the community. *J. Clin. Endocrinol. Metab.* 101, 2432–2439. doi: 10.1210/jc.2016-1113
- Scappaticcio, L., Maiorino, M. I., Bellastella, G., Giugliano, D., and Esposito, K. (2017). Insights into the relationships between diabetes, prediabetes, and cancer. *Endocrine* 56, 231–239. doi: 10.1007/s12020-016-1216-y
- Strain, W. D., and Paldanius, P., M. (2018). Diabetes, cardiovascular disease and the microcirculation. *Cardiovasc Diabetol.* 17:57. doi: 10.1186/s12933-018-0703-2
- Takeuchi, M., Itakura, A., Okada, M., Mizutani, S., and Kikkawa, F. (2006). Impaired insulin-regulated membrane aminopeptidase translocation to the plasma membrane in adipocytes of Otsuka Long Evans Tokushima Fatty rats. *Nagoya J. Med. Sci.* 68, 155–63. doi: 10.1016/j.jep.2007.10.040
- Tucker, L. A. (2020). Limited agreement between classifications of diabetes and prediabetes resulting from the OGTT, hemoglobin A1c, and fasting glucose tests in 7412 U.S. Adults. *J. Clin. Med.* 9:2207. doi: 10.3390/jcm9072207
- Velho, G., Bouby, N., Hadjadj, S., Matallah, N., Mohammadi, K., Fumeron, F., et al. (2013). Plasma copeptin and renal outcomes in patients with type 2 diabetes and albuminuria. *Diabetes Care* 36, 3639–3645. doi: 10.2337/dc13-0683
- Venn, B. J., and Green, T. J. (2007). Glycemic index and glycemic load: measurement issues and their effect on diet-disease relationships. *Eur. J. Clin. Nutr.* 61(Suppl 1), S122–S131. doi: 10.1038/sj.ejcn.1602942
- Wallace, T. M., Levy, J. C., and Matthews, D. R. (2004). Use and abuse of HOMA modeling. *Diabetes Care* 27, 1487–1495. doi: 10.2337/diacare.27.6.1487
- Wannamethee, S. G., Welsh, P., Papacosta, O., Lennon, L., Whincup, P. H., and Sattar, N. (2015). Copeptin, insulin resistance, and risk of incident diabetes in older men. *J. Clin. Endocrinol. Metab.* 100, 3332–3339. doi: 10.1210/JC.2015-2362
- Wolffenbuttel, B. H., Herman, W. H., Gross, J. L., Dharmalingam, M., Jiang, H. H., and Hardin, D. S. (2013). Ethnic differences in glycemic markers in patients with type 2 diabetes. *Diabetes Care* 36, 2931–2936. doi: 10.2337/dc12-2711
- Xiang, A. H., Watanabe, R. M., and Buchanan, T. A. (2014). HOMA and Matsuda indices of insulin sensitivity: poor correlation with minimal model-based estimates of insulin sensitivity in longitudinal settings. *Diabetologia* 57, 334–338. doi: 10.1007/s00125-013-3121-8
- Zeevi, D., Korem, T., Zmora, N., Israeli, D., Rothschild, D., Weinberger, A., et al. (2015). Personalized nutrition by prediction of glycemic responses. *Cell* 163, 1079–1094. doi: 10.1016/j.cell.2015.11.001
- Zhu, F. X., Wu, H. L., Tu, K. S., Chen, J. X., Zhang, M., and Shi, C. (2016). Serum levels of copeptin are associated with type 2 diabetes and diabetic complications in Chinese population. *J. Diabetes Complicat.* 30, 1566–1570. doi: 10.1016/j.jdiacomp.2016.07.017

**Conflict of Interest:** The authors declare that the research was conducted in the absence of any commercial or financial relationships that could be construed as a potential conflict of interest.

Copyright © 2021 Trocmé, Gonnet, Di Tommaso, Samouda, Cracowski, Cracowski, Lambert-Porcheron, Laville, Nobécourt, Gaddhab, Le Lay, Bohn, Poitou, Clément, Al-Mulla, Bitar and Bottari. This is an open-access article distributed under the terms of the Creative Commons Attribution License (CC BY). The use, distribution or reproduction in other forums is permitted, provided the original author(s) and the copyright owner(s) are credited and that the original publication in this journal is cited, in accordance with accepted academic practice. No use, distribution or reproduction is permitted which does not comply with these terms.



# Structural Basis of Inhibition of Human Insulin-Regulated Aminopeptidase (IRAP) by Benzopyran-Based Inhibitors

Sudarsana Reddy Vanga<sup>1</sup>, Johan Åqvist<sup>1</sup>, Anders Hallberg<sup>2</sup> and Hugo Gutiérrez-de-Terán<sup>1,3\*</sup>

<sup>1</sup> Department of Cell and Molecular Biology, BMC, Uppsala University, Uppsala, Sweden, <sup>2</sup> Department of Pharmaceutical Chemistry, BMC, Uppsala University, Uppsala, Sweden, <sup>3</sup> Science for Life Laboratory, Uppsala University, Uppsala, Sweden

## OPEN ACCESS

### Edited by:

Megha Agrawal,  
University of Illinois at Chicago,  
United States

### Reviewed by:

Krishna Mohan Poluri,  
Indian Institute of Technology  
Roorkee, India  
Beihong Ji,  
University of Pittsburgh, United States

### \*Correspondence:

Hugo Gutiérrez-de-Terán  
hugo.gutierrez@icm.uu.se

### Specialty section:

This article was submitted to  
Molecular Diagnostics  
and Therapeutics,  
a section of the journal  
Frontiers in Molecular Biosciences

**Received:** 10 November 2020

**Accepted:** 10 March 2021

**Published:** 01 April 2021

### Citation:

Vanga SR, Åqvist J, Hallberg A  
and Gutiérrez-de-Terán H (2021)  
Structural Basis of Inhibition  
of Human Insulin-Regulated  
Aminopeptidase (IRAP) by  
Benzopyran-Based Inhibitors.  
Front. Mol. Biosci. 8:625274.  
doi: 10.3389/fmolb.2021.625274

Inhibition of the insulin-regulated aminopeptidase (IRAP) improves memory and cognition in animal models. The enzyme has recently been crystallized and several series of inhibitors reported. We herein focused on one series of benzopyran-based inhibitors of IRAP known as the HFI series, with unresolved binding mode to IRAP, and developed a robust computational model to explain the structure-activity relationship (SAR) and potentially guide their further optimization. The binding model here proposed places the benzopyran ring in the catalytic binding site, coordinating the Zn<sup>2+</sup> ion through the oxygen in position 3, in contrast to previous hypothesis. The whole series of HFI compounds was then systematically simulated, starting from this binding mode, using molecular dynamics and binding affinity estimated with the linear interaction energy (LIE) method. The agreement with experimental affinities supports the binding mode proposed, which was further challenged by rigorous free energy perturbation (FEP) calculations. Here, we found excellent correlation between experimental and calculated binding affinity differences, both between selected compound pairs and also for recently reported experimental data concerning the site directed mutagenesis of residue Phe544. The computationally derived structure-activity relationship of the HFI series and the understanding of the involvement of Phe544 in the binding of this scaffold provide valuable information for further lead optimization of novel IRAP inhibitors.

**Keywords:** free energy perturbation (FEP), linear interaction energy (LIE), molecular dynamics (MD), Insulin regulated aminopeptidase (IRAP), benzopyran

## INTRODUCTION

Insulin-regulated aminopeptidase (IRAP, EC 3.4.11.3), also known as leucyl-cystinyl aminopeptidase, placental leucine aminopeptidase, and oxytocinase is a transmembrane zinc metalloenzyme that belongs to the M1 family of aminopeptidases (Lew et al., 2003). High levels of IRAP expression are found in areas of the brain associated with cognitive function including the hippocampus (Harding et al., 1992; Roberts et al., 1995; Chai et al., 2000), and it has been associated with several biological functions such as antigenic peptide processing for MHC Class I cross-presentation (Saveanu et al., 2009; Segura et al., 2009), GLUT4 regulation and transportation

(Albiston et al., 2007), and regulation of oxytocin and vasopressin levels in the brain (Chai et al., 2004; Stragier et al., 2008; Hattori and Tsujimoto, 2013). In 2001, angiotensin IV (Ang IV) was identified as a potential inhibitor of IRAP (Albiston et al., 2001) along with LVV-hemorphin-7 (LVVYPWTQRF, a degradation product of  $\beta$ -globin) (Lee et al., 2003; Lew et al., 2003), both with  $K_i$  values in the nanomolar range.

It has been shown that inhibiting IRAP with Ang IV (1, **Figure 1**) and other structurally related peptidomimetics like HA08 (2) (Diwakarla et al., 2016b) is linked with improved memory and learning *in vivo* (Braszkowski et al., 1988; Wright et al., 1993, 1996, 1999; O'Malley et al., 1998; De Bundel et al., 2009; Fu et al., 2012), including enhancement of dendritic spine density (DSD) exerted by HA08 in hippocampal cells (O'Malley et al., 1998; Fu et al., 2012), as well as drug mitigation and lesion-induced memory deficits in rodents (Vauquelin et al., 2002; Albiston et al., 2003; Chai et al., 2004). Endogenous IRAP substrates such as the macrocyclic peptides oxytocin (3) and vasopressin (4, **Figure 1**) also improve cognitive parameters in the brain (Chai et al., 2004; Stragier et al., 2008). Consequently, it is not surprising that during the last 10–15 years, considerable efforts have been devoted to the discovery of small molecule IRAP inhibitors as potential cognitive enhancers. Comprehensive reviews are now available, and existing IRAP inhibitors reported include drug-like scaffolds like sulfonamides (5) or benzopyrans (6–9, **Figure 1**) (Hallberg, 2009; Barlow and Thompson, 2020; Georgiadis et al., 2020; Hallberg and Larhed, 2020). The later scaffold was identified in 2008 by virtual screening, and subsequently optimized resulting in a series coined as HFI (Howard Florey Institute) (Albiston et al., 2008). The most potent inhibitors present affinity values within the nanomolar range, and include either a 4-(pyridin-3-yl) or a 4-(isoquinolin-3-yl) substituent at the benzopyran and also a 2-amino or 2-acetamido substitution (**Figure 1**; Albiston et al., 2008). Recently it was demonstrated that HFI compounds, exemplified by HFI-419 (8), enhance spatial working memory possibly by promoting the formation of functional dendritic spines by facilitating GLUT4-mediated glucose uptake into hippocampal neurons (Seyer et al., 2020).

A binding mode and derived SAR of the inhibitory mechanism of the HFI series was initially proposed on the basis of a homology model of the catalytic domain of IRAP, which was built on the template of the equivalent domain of leukotriene A4 hydrolase (E.C. 3.3.2.6; LTA4H, PDB ID: 1HS6) (Thunnissen et al., 2001). Benzopyrans are chiral molecules, and the model proposed presented the *S*-isomer as the active enantiomer, with two well defined binding poses for pyridinyl and the quinolinyl derivatives, respectively (Albiston et al., 2010); while the pyridinyl derivatives would coordinate the  $Zn^{2+}$  ion through the benzopyran oxygen, for the quinolinyl compounds the coordination was predicted to occur through the nitrogen in this ring. Based on this model, a full series of HFI compounds was synthesized and pharmacologically characterized in 2014 (Mountford et al., 2014). However, the crystal structures of IRAP reveal a more open binding crevice as compared to other aminopeptidases. In the first crystal structure of IRAP (PDB code 4PJ6), the particular conformation of the GAMEN loop was

related to the IRAP specificity for hydrolyzing cyclic peptides (Hermans et al., 2015). Even the last crystal structure of IRAP with the macrocyclic inhibitor HA08 (2), reported during the preparation of this manuscript, shows a binding site more open than in LTA4H, since the partially closed GAMEN loop is compensated with a rearrangement of the topology of some helical domains (Mpakali et al., 2020).

A computational docking study of HFI compounds performed right after the release of the first IRAP crystal structure suggested this time the *R*-enantiomer as the bioactive one, showing a unified binding orientation across the whole series in contrast to the previous models. In this new modeling, the  $Zn^{2+}$  ion would be coordinated by the oxygen of the hydroxyl group from the benzopyran ring, while the chromene ring remained packed against the GAMEN loop (Hermans et al., 2015). A later crystal structure of the closed conformation of IRAP (PDB ID: 5MJ6), was recently used to propose a different binding pose for compound 9 (HFI-437) (Mpakali et al., 2017). However, none of the binding modes proposed so far could explain the SAR of the HFI series, which motivated the present study. In addition to the SAR, we were interested in the role of specific residues in ligand binding. To accomplish these goals, we designed an approach combining molecular docking, molecular dynamics (MD) and binding free energy calculations utilizing both linear interaction energy (LIE) and free energy perturbation (FEP) approaches. These models were analyzed on their capacity to reproduce and explain the available experimental affinity data of the HFI inhibitor series for the wild type (WT) IRAP (Mountford et al., 2014), as well as the mutagenesis data of position Phe544 for a subseries of HFI compounds (Albiston et al., 2010). Our results suggest a unified binding mode that is compatible with all the (SAR) data available for this series, allowing a better understanding of the molecular details involved in inhibitor binding to IRAP.

## MATERIALS AND METHODS

### Preparation of the IRAP Structure and Ligand Docking

The crystal structure of human IRAP was retrieved from the protein data bank (PDB code 4PJ6) (Hermans et al., 2015), and monomer A from the crystal dimer was retained for docking and molecular dynamics (MD) simulations. The structure was prepared with the *protein preparation wizard* utility in Maestro v. 9.2. (Schrödinger, LLC; NY, United States), involving addition of hydrogens and rotamer assignment of Asn, Gln, and His sidechains to optimize the H-bonding pattern. The F544I and F544V mutants were model on this structure using the Prime tool in Maestro, which allows adapting side chain conformation for neighboring residues to the modeled mutation. The 3D structures of all ligands (6–9, 15a–g, 16–18, see **Figure 1** and **Table 1**) were built in Maestro and prepared with the LigPrep utility, which includes hydrogen addition considering most probable tautomers and isoelectric species and generation of independent stereoisomers, with a final optimization of the 3D structure.



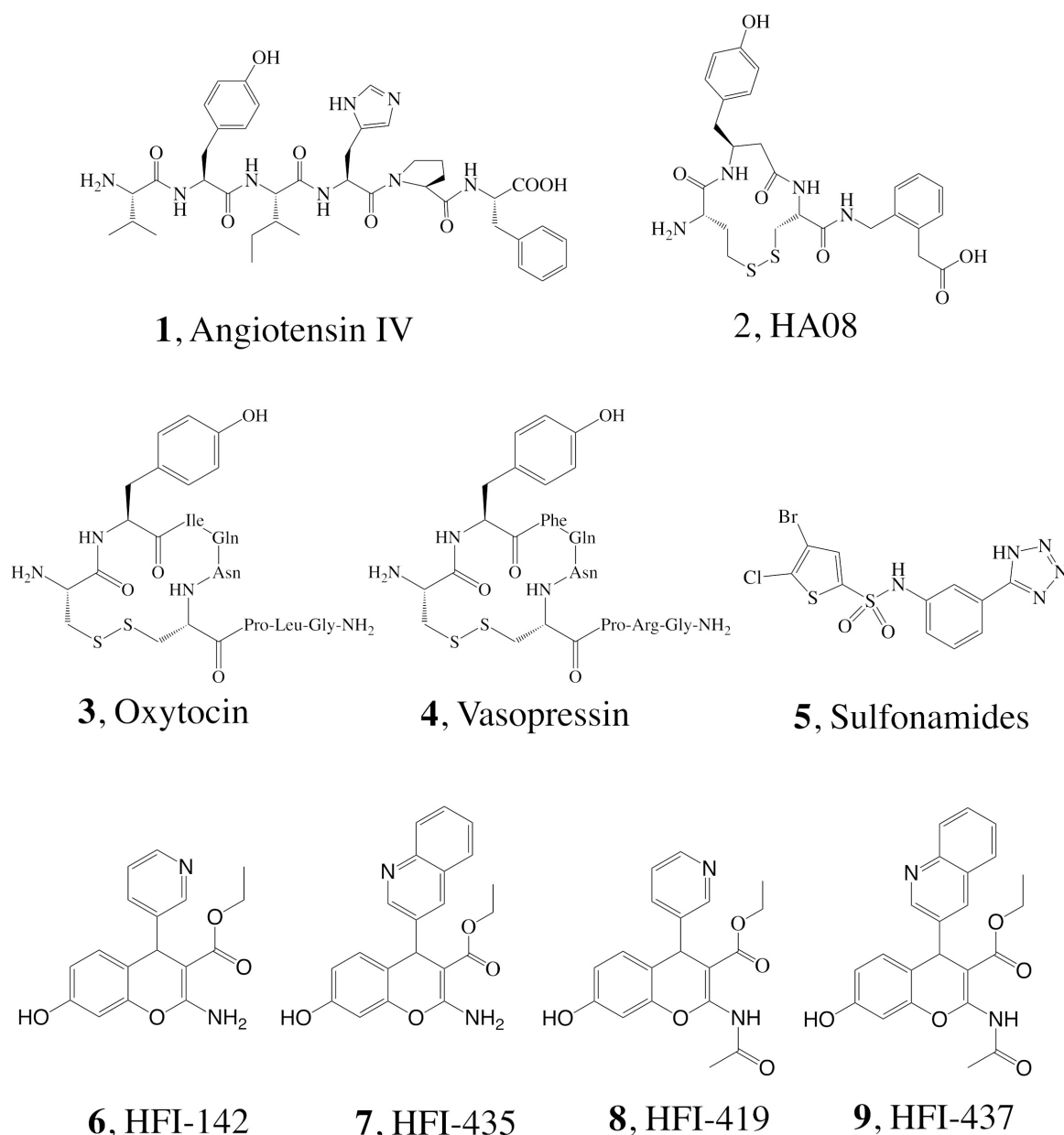


**FIGURE 1** | Structure of IRAP inhibitors and substrates.

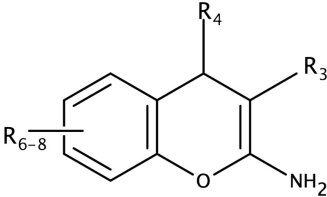
Docking explorations of subset 6–9 were performed with GLIDE-XP (Halgren et al., 2004) on a 30 Å cubic grid centered on the equivalent position of the C $\alpha$  atom of His in Ang IV (Diwakarla et al., 2016b). These settings were applied in two separate docking approaches: (i) without constraints, and (ii) with constraints, where H-bond/Metal and Metal Coordination constraints against the Zn<sup>2+</sup> ion were used in the receptor grid generation, to ensure a metal–ligand interaction preserving the initial metal coordination. Once one binding mode was determined for this subset, it was used as a template to dock the entire HFI-series of compounds (15a–g, 16a–r, 17a–g, 18d–h, see **Table 1**) in analogous orientation on the wt-IRAP using the Flexible Ligand

Alignment in Maestro v. 9.2. All docking poses resulted from the docking calculations were retained for further analysis and MD calculations.

### Molecular Dynamics (MD) Simulations

Molecular dynamic simulations were performed with spherical boundary conditions using the program Q (Marelius et al., 1998), optimized for efficient sampling suitable for the free energy calculations for ligand series or protein mutations (Boukharta et al., 2014; Shamsudin Khan et al., 2015). The OPLS-AA force field for proteins was used (Jorgensen et al., 1996), in combination with compatible parameters for Zn<sup>2+</sup> ion and

TABLE 1 | LIE-Calculated and experimental binding free energies of HFI-series compounds.



Compound	R <sub>3</sub>	R <sub>4</sub>	R <sub>6-8</sub>	K <sub>i</sub> (μM) <sup>a</sup>	ΔG Calc <sup>b</sup>	ΔG Exp <sup>c</sup>
15a	CN	4-methoxyphenyl	7-OH	>100	−5.26 ± 0.12	> −5.45
15b	CN	3-methoxyphenyl	7-OH	>100	−5.35 ± 0.11	> −5.45
15c	CN	3,4-dimethoxyphenyl	7-OH	50	−5.56 ± 0.12	−5.86
15d	CN	3,5-dimethoxyphenyl	7-OH	>100	−5.83 ± 0.14	> −5.45
15e	CN	3,4,5-trimethoxyphenyl	7-OH	>100	−6.05 ± 0.17	> −5.45
15f	CN	pyridin-3-yl	7-OH	>100	−5.03 ± 0.26	> −5.45
15g	CN	4-N,N-dimethylaminophenyl	7-OH	>100	−5.40 ± 0.14	> −5.45
16a	CO <sub>2</sub> Et	phenyl	7-OH	>100	−5.46 ± 0.17	> −5.45
16b	CO <sub>2</sub> Et	2-cyanophenyl	7-OH	>100	−5.61 ± 0.19	> −5.45
16c	CO <sub>2</sub> Et	pyridin-2-yl	7-OH	2.9	−6.67 ± 0.19	−7.55
16d	CO <sub>2</sub> Et	quinolin-2-yl	7-OH	3	−7.64 ± 0.09	−7.53
16e	CO <sub>2</sub> Et	2-nitrophenyl	7-OH	42	−7.01 ± 0.08	−5.96
16f	CO <sub>2</sub> Et	3-chlorophenyl	7-OH	35	−7.15 ± 0.14	−6.07
16g	CO <sub>2</sub> Et	3-cyanophenyl	7-OH	3.2	−7.37 ± 0.11	−7.49
16h	CO <sub>2</sub> Et	2,4-dichloropyridine-3-yl	7-OH	14	−7.38 ± 0.18	−6.61
16i	CO <sub>2</sub> Et	4-methylphenyl	7-OH	>100	−5.24 ± 0.10	> −5.45
16j	CO <sub>2</sub> Et	4-bromophenyl	7-OH	>100	−6.00 ± 0.11	> −5.45
16k	CO <sub>2</sub> Et	4-chlorophenyl	7-OH	>100	−5.86 ± 0.16	> −5.45
16l	CO <sub>2</sub> Et	4-cyanophenyl	7-OH	11	−7.55 ± 0.08	−6.76
16m	CO <sub>2</sub> Et	pyridin-4-yl	7-OH	3.7	−7.23 ± 0.07	−7.40
16n	CO <sub>2</sub> Et	quinolin-4-yl	7-OH	0.9	−7.93 ± 0.17	−8.24
16o	CO <sub>2</sub> Et	4-nitrophenyl	7-OH	7.7	−7.83 ± 0.22	−6.97
16p	CO <sub>2</sub> Et	4-(pyridin-2-yl)phenyl	7-OH	>100	−5.96 ± 0.18	> −5.45
16q	CO <sub>2</sub> Et	4-N,N-dimethylaminophenyl	7-OH	5.3	−7.57 ± 0.20	−7.19
16r	CO <sub>2</sub> Et	3,4-dimethoxyphenyl	7-OH	6.2	−7.72 ± 0.21	−7.10
17a	CO <sub>2</sub> Me	pyridin-3-yl	7-OH	4.9	−6.86 ± 0.07	−7.24
17b	CO <sub>2</sub> Pr	pyridin-3-yl	7-OH	1.6	−7.13 ± 0.14	−7.90
17c	CO <sub>2</sub> n-But	pyridin-3-yl	7-OH	2.6	−7.07 ± 0.17	−7.61
17d	CO <sub>2</sub> t-But	pyridin-3-yl	7-OH	11.9	−7.15 ± 0.15	−6.71
17e	CO <sub>2</sub> -(CH <sub>2</sub> ) <sub>2</sub> -O-CH <sub>3</sub>	pyridin-3-yl	7-OH	4	−6.97 ± 0.20	−7.36
17g	CO <sub>2</sub> -Bz	pyridin-3-yl	7-OH	1.7	−7.31 ± 0.08	−7.86
18d	CO <sub>2</sub> Et	pyridin-3-yl	6-Cl, 7-OH	5.6	−7.33 ± 0.24	−7.16
18f	CO <sub>2</sub> Et	pyridin-3-yl	8-OH	9.8	−6.79 ± 0.21	−6.83
18g	CO <sub>2</sub> Et	pyridin-3-yl	7-8, fused phenyl	>100	−7.47 ± 0.10	> −5.45
18h	CO <sub>2</sub> Et	pyridin-3-yl	5-6, fused phenyl	>100	−5.49 ± 0.21	> −5.45

<sup>a</sup>Experimental data extracted fromMountford et al. (2014). <sup>b</sup>Energies in kcal mol<sup>−1</sup>, obtained from the optimized LIE model, with α = 0.285, β = 0.138, γ = −1.2 and expressed as mean ± 1 SEM from the replicate simulations. Average unsigned error is 0.5 kcal mol<sup>−1</sup> (considering only compounds with experimentally determined K<sub>i</sub>). <sup>c</sup>Experimental values obtained as ΔG<sub>bind</sub><sup>exp</sup> RTlnK<sub>i</sub>.

automatic parametrization of the ligands within the same force field, performed with MacroModel version 10.6 (Schrödinger, LLC; NY, United States). A simulation sphere of 25 Å radius centered on the equivalent position of the Cα atom of His4 in Ang IV was built as previously described (Diwakarla et al., 2016a,b; Vanga et al., 2018). The sphere was solvated with TIP3P water molecules (Jorgensen et al., 1983) and subjected

to polarization and radial constraints according to the surface constrained all-atom solvent (SCAAS) model (King and Warshel, 1989; Marelus et al., 1998) to mimic the properties of bulk water at the sphere surface. Protein atoms outside the simulation sphere were restrained to their initial positions and only interacted with the system through bonds, angles, and torsions. Excluding His, all other titratable residues within 20 Å of the Zn<sup>2+</sup> ion were treated

in their charged form. In addition, the residues Lys520, Lys726, Glu767, Asp773, Arg817, Glu818, Arg820, Glu825, Arg858, Glu887, Lys890, Lys892, Glu895, Arg933, and Glu1002, within the 20–25 Å layer of the sphere were also treated as ionized since they are forming salt bridges, while all other ionizable residues within this layer were treated as neutral to avoid insufficient dielectrical screening. With this setup, the simulation sphere was overall neutral, thus avoiding the consideration of additional Born terms in the calculation of free energies of charged ligands as compared to bulk solvent. Non-bonded interactions were calculated explicitly up to a 10 Å cutoff, except for the ligand atoms for which no cutoff was used. Beyond the direct cutoff, long-range electrostatics were treated with the local reaction field (LRF) multipole expansion method (Lee and Warshel, 1992). During a 175 ps equilibration stage, the system was slowly heated to the target temperature of 310 K while initial positional restraints on all solute heavy atoms were gradually released. The subsequent data collection phase consisted of 10 replicate MD simulations of 2 ns each, with randomized initial velocities, accounting for a total of 20 ns sampling trajectories where the ligand-surrounding energies were collected for binding affinity calculations. A time step of 1 fs was used and no positional restraints were applied. Solvent bonds and angles were constrained using the SHAKE algorithm (Ryckaert et al., 1977). Non-bonded pair lists were updated every 25 steps, and the ligand-surrounding interaction energies were sampled every 50 steps. In order to estimate free energies of binding, the same setup was used for the reference state calculations. For the LIE and ligand-FEP simulations, this involves sampling the ligand-surrounding energies in parallel MD simulations of the ligand solvated in water, while for the residue FEP simulations the reference MD simulations involve the apo state of the protein, i.e., without the ligand complexed.

## Linear Interaction Energy (LIE) Calculations

Binding free energies for every compound were calculated for every docked ligand using the linear interaction energy (LIE) method as (Aqvist et al., 1994; Hansson et al., 1998)

$$\Delta G_{bind}^{calc} = \alpha \Delta \langle U_{l-s}^{vdW} \rangle + \beta \Delta \langle U_{l-s}^{el} \rangle + \gamma \quad (1)$$

where,  $\Delta \langle U_{l-s}^{vdW} \rangle$  and  $\Delta \langle U_{l-s}^{el} \rangle$  are the differences in the average nonpolar and polar ligand-surrounding interaction energies in the two states, that is, water solvated (free ligand) and in complex with the protein (bound ligand). The coefficients  $\alpha$  and  $\beta$  are scaling parameters (Hansson et al., 1998; Almlöf et al., 2004, 2007) for the nonpolar and polar terms, respectively. In the standard LIE model,  $\alpha$  has a value of 0.18, while  $\beta$  depends on the chemical nature of the ligand. The IRAP active site has a divalent  $Zn^{2+}$  ion together with a cluster of carboxylates, causing very large electrostatic interaction energies with the ligands. Because these interaction energies, particularly those involving the  $Zn^{2+}$  ion, will be very sensitive to the force field parameters, we follow a protocol used earlier for binding sites containing ions (Mishra et al., 2012) and treated  $\beta$  as a free parameter. The reported non-bonded energies correspond to average values over

10 replicate MD simulations on each state (free and bound), and the corresponding errors are calculated as the standard error of the mean (SEM).

Experimental binding free energies ( $\Delta G_{bind}^{exp}$ ) were extracted from inhibition constant ( $K_i$ ) experimental values as

$$\Delta G_{bind}^{exp} = RT \ln K_i \quad (2)$$

## Free Energy Perturbation (FEP) Simulations

### Ligand FEP

The relative binding free energy between selected pairs of ligands, A and B, was calculated using the free energy perturbation (FEP) method. In this method ligand A is transformed into B in parallel MD simulations in both the protein-bound ligand and the free (water-solvated) reference state. The construction of a closed thermodynamic cycle connecting these processes allows the estimation of the relative binding free energy between the pair of ligands ( $\Delta \Delta G_{bind, hboxB-A}$ ), as the difference in the free energy of each transformation of  $A \rightarrow B$ , as

$$\Delta G_{bind}^B - \Delta G_{bind}^A = \Delta \Delta G_{bind} = \Delta G_{bound}^{A \rightarrow B} - \Delta G_{free}^{A \rightarrow B} \quad (3)$$

The free energy difference associated with each ligand transformation was calculated using Zwanzig's exponential formula (Zwanzig, 1954)

$$\begin{aligned} \Delta G^{A \rightarrow B} &= \Delta G_B - \Delta G_A \\ &= -\beta^{-1} \sum_{m=1}^{n-1} \ln \langle \exp(-\beta^{-1}(U_{m+1} - U_m)) \rangle_m \end{aligned} \quad (4)$$

where  $U_m$  denotes the effective potential energy function of a particular FEP window and  $n$  is the number of intermediate states.  $U_m$  is constructed as a linear combination of the initial (A) and final (B) potentials

$$U_m = (1 - \lambda_m)U_A + \lambda_m U_B \quad (5)$$

where the coupling parameter  $\lambda_m$  is stepwise incremented from 0 to 1, in our case divided into 51  $\lambda$ -windows, where every window is sampled for 30 ps.

### Residue FEP

Similar to the ligand FEP method, relative binding free energies associated with amino acid side-chain mutations are calculated following Eq. 4–6, but instead the two states (A and B) correspond to the wild-type (wt) and mutant (mut) versions of the enzyme. This protocol is based on a computational alanine scanning protocol developed in our lab, which makes use of the additive property of thermodynamic cycles sharing a common leg to allow non-alanine mutations (Boukharta et al., 2014; Keränen et al., 2015). During annihilation of a side-chain, each atom group will undergo three consecutive transformations (i) annihilation of partial charges, (ii) introduction of a soft-core potential for the van der Waals (Lennard-Jones) potential to prevent singularities, and (iii) annihilation of the soft-core potential. Depending on the nature of the starting sidechain, and the number of atom-groups

therein defined, this involves a number of stages that varies from 4 (for simple cases like Set to Ala) to 11 (i.e., Trp to Ala). Each of these stages is performed over a number of FEP windows (51  $\lambda$ -windows, each sampled for 30 ps), assuring enough sampling to achieve converged results. The full transformation (wt  $\rightarrow$  Ala) is performed in 10 replica molecular dynamics (MD) simulations for each state, which in this case involves the receptor in complex with the ligand (*holo*) and the free (*apo*) receptor. The difference in ligand binding free energy between the wt and Ala (mut) versions of the receptor ( $\Delta\Delta G_{bind}^{wt-ala}$ ) can be estimated by solving the associated thermodynamic cycle. It follows that, for non-alanine mutations, one can start the same set of annihilations to Alanine starting from the modeled (mut) state, and calculate the associated ( $\Delta\Delta G_{bind}^{mut-ala}$ ). The relative free energy associated with non-Ala mutations (in our case, F544I and F544V) will be the result of the combination of the corresponding thermodynamic cycles as

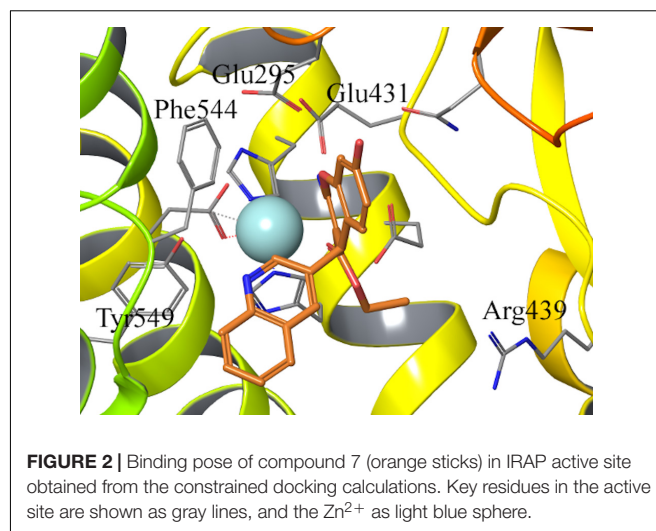
$$\Delta\Delta G_{bind}^{mut-wt} = \left( \Delta G_{holo}^{wt} - \Delta G_{apo}^{wt} \right) - \left( \Delta G_{holo}^{mut} - \Delta G_{apo}^{mut} \right) \quad (7)$$

When performing several mutations for the same position, the wt  $\rightarrow$  Ala of the cycle needs to be calculated only once and can be reused for any mutation at that position. Hysteresis as a measure of convergence is calculated as the absolute difference between forward and reverse pathways of each subperturbation. The total hysteresis is the sum of the hysteresis values for each subperturbation of the transformation.

## RESULTS

### Docking, MD and LIE Calculations

The binding mode of compound 6–9 was explored with two independent docking protocols, and the poses obtained for each ligand were followed by MD relaxation. This stage allowed discarding any binding orientation that did not show structural stability. In particular, none of the binding poses obtained with the “no constraints” docking with GLIDE (Halgren et al., 2004) showed any direct contact with the  $Zn^{2+}$ , despite being in the vicinity of the ion, and the simulations confirmed unstable binding modes in all cases, with protein-ligand interactions lost during the MD sampling. Conversely, the docking pose obtained for *R*-isomer of ligand 7 (HFI-435) by imposing an interaction with the cation as a constraint, revealed itself as a stable binding mode after the MD stage. This binding mode showed coordination to the  $Zn^{2+}$  through the ester carbonyl oxygen, while the benzopyran ring formed a stable  $\pi$ -stacking interaction with Phe544, accompanied by frequent polar interactions of the exocyclic 2-amino group with Glu431 and Glu295. The quinolone ring in  $R_4$  displayed  $\pi$ -stacking with Tyr549 (Figure 2). This binding mode was then retained and used as a template to build the entire HFI-series of compounds (Mountford et al., 2014) (15a-g, 16a-r, 17a-g, 18d-h, see Table 1) in analogous orientation on the wt-IRAP. Additionally, for ligands 6–9 we also generated the corresponding complex with the two IRAP mutants here investigated (F544I and F544V). The next step was the estimation of the ligand binding affinities to the wt-IRAP for the whole



series. For this, the same MD sampling used in the previous stage was replicated 10 times per ligand-IRAP complex, accompanied by the same MD sampling of each ligand in a similar water sphere, all of which was used as a basis to calculate the binding free energy with the linear interaction energy (LIE) method (Aqvist et al., 1994).

All compounds were stable during these MD simulations, maintaining the key coordination of the  $Zn^{2+}$  through the carbonyl oxygen of the 3-ethyl ester, with the exception of the 3-cyano derivatives 15a-g. For these compounds, it was found that the 3-cyano group could not be accommodated near the metal while preserving other key protein-ligand interactions, resulting in instability of the initial binding pose (see **Supplementary Table 1**, indicating average ligand RMSD along the MD trajectories) and consequently low values for the LIE estimated binding free energies, due to loss of key interactions with IRAP. This observation is in line with the experimental data, showing ligands 15a-g as inactive compounds (only 15c has measured  $K_i$ , but as low as 50  $\mu M$ ). Compounds 8 and 9 showed an edge to face  $\pi$ -stacking interactions with Phe544 (Figure 3A). In these compounds, the hydroxyl group at the position 7 of the benzopyran ring interacts with Arg439 via a water molecule, while Tyr549 makes  $\pi$ -stacking with the 3-pyridyl (8) or 3-quinoliny (9) rings (Figure 3A). In compounds 7 and 8, the central core ring is stabilized by  $\pi$ -stacking interactions with Phe544 (parallel  $\pi$ -stacking) and Tyr549 (edge-to-edge), while the free 2-amino group makes H-bonds with Glu295 and Glu431. Interestingly, along the MD simulations of all 2-amino compounds the role of His464 and His468 in coordination of the  $Zn^{2+}$  ion was replaced with two water molecules (Figure 3B).

Owing to the strong electrostatic ligand interactions with the  $Zn^{2+}$  ion, which is very sensitive to given force field parameters, it was found necessary in previous LIE calculations to determine the parameters  $\alpha$ ,  $\beta$ , and  $\gamma$  (Diwakarla et al., 2016a,b; Vanga et al., 2018) empirically. The earlier derived LIE parameters were based on a few chemically diverse compounds. In the present series, 25 out of 39 compounds have experimentally determined  $K_i$  values



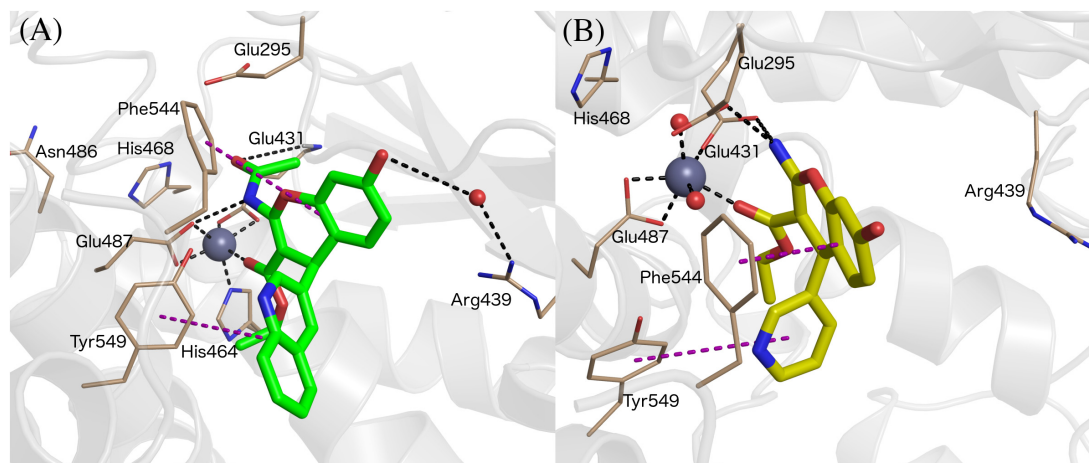


**FIGURE 3 |** Binding mode of compound 9 (panel **A**, green sticks), and 6 (panel **B**, yellow sticks) in IRAP as determined from the MD simulations used for LIE calculations.  $\text{Zn}^{2+}$  and water molecules are shown as gray and red spheres, respectively. All of the figures shown are extracted from representative snapshots of 2 ns MD simulations. H-bonds are shown as black dotted line, and  $\pi$  – stacking interactions in the purple color dashed line.

for the wild-type enzyme, while the remaining compounds (non-binders) have  $K_i$  values  $> 100 \mu\text{M}$ . Hence, we selected this subset of 25 compounds to optimize the LIE model by independent fitting. We applied the resulting LIE parameterization to estimate the affinities to wt-IRAP for the entire series, including the known non-binders. The results, summarized in **Table 1**, show excellent agreement with the experimental data, with a calculated mean unassigned error (MUE) for the 25 compounds with measured  $K_i$  as low as was 0.50 kcal/mol.

For compounds 6–9, binding free energies were estimated not only with wt-IRAP, but also with the F544I and F544V modeled mutants, for which experimental data was available (Albiston et al., 2010). Replacement of Phe544 with either Ile or Val led to the loss of the  $\pi$ -stacking between the wt sidechain and the benzopyran, partially explaining the significant decline in binding affinity observed in most cases (see **Table 2**). Indeed, the correlation of the LIE-calculated with the experimental values for the mutations on these four ligands was quite remarkable (**Table 2**), with a calculated MUE of 0.5, 0.68, and 0.5 kcal/mol for wt-IRAP, F544I, and F544V, respectively.

The overall results of the LIE model are summarized in **Figure 4**, showing the correlation between calculated and experimental binding free affinities for the HFI compounds with experimental  $K_i$  values for both wt (triangles) and mutants (stars). This model not only shows very small average deviations from experimental values (overall MUE = 0.51 kcal/mol), but the relative ranking within the series, which is key to assess further optimization efforts, is excellent with a Pearson correlation coefficient,  $R = 0.71$ .

## Free Energy Perturbation Calculations

To further confirm the binding mode proposed for the HFI series and the derived SAR, we designed a set of free energy perturbation (FEP) transformations between selected pairs of ligands, following the experimental design illustrated in **Figure 5**.

The advantage of this approach is that, by estimation of the relative binding free energies ( $\Delta\Delta G$ ) between four pairs of compounds, one can not only compare with the corresponding experimental differences in affinity, but also estimate the error of such calculations, since the overall energy change along the closed thermodynamic cycle is  $\Delta G = 0$  kcal/mol. The vertical legs of the

**TABLE 2 |** LIE calculated and experimentally binding free energies ( $\Delta G$ , in kcal/mol) for compounds 6–9 in wild type and mutant IRAP.

Compound	$\Delta G$ (kcal mol <sup>-1</sup> ) <sup>a</sup>	
	LIE <sup>b</sup>	Experimental <sup>c</sup>
<b>wt-IRAP</b>		
6	$-8.17 \pm 0.4$	$-7.76 \pm 0.26$
7	$-8.73 \pm 0.4$	$-8.83 \pm 0.43$
8	$-8.56 \pm 0.1$	$-8.35 \pm 0.41$
9	$-9.09 \pm 0.2$	$-10.23 \pm 0.13$
<b>F544I</b>		
6	$-7.71 \pm 0.4$	$-6.52 \pm 0.33$
7	$-7.29 \pm 0.1$	$-7.40 \pm 0.17$
8	$-7.53 \pm 0.1$	$-7.82 \pm 0.19$
9	$-8.09 \pm 0.2$	$-9.13 \pm 0.15$
<b>F544V</b>		
6	$-6.61 \pm 0.4$	$-7.34 \pm 0.02$
7	$-7.54 \pm 0.2$	$-7.63 \pm 0.21$
8	$-8.26 \pm 0.1$	$-8.41 \pm 0.20$
9	$-8.34 \pm 0.2$	$-8.95 \pm 0.30$

<sup>a</sup>Energies are expressed as mean  $\pm$  S.E.M. estimated from independent experiments (Albiston et al., 2010) or replicate MD simulations (LIE). <sup>b</sup>Optimized LIE model, with  $\alpha = 0.285$ ,  $\beta = 0.138$ ,  $\gamma = -1.2$ . <sup>c</sup>Experimental values are extracted from Albiston et al. (2010).

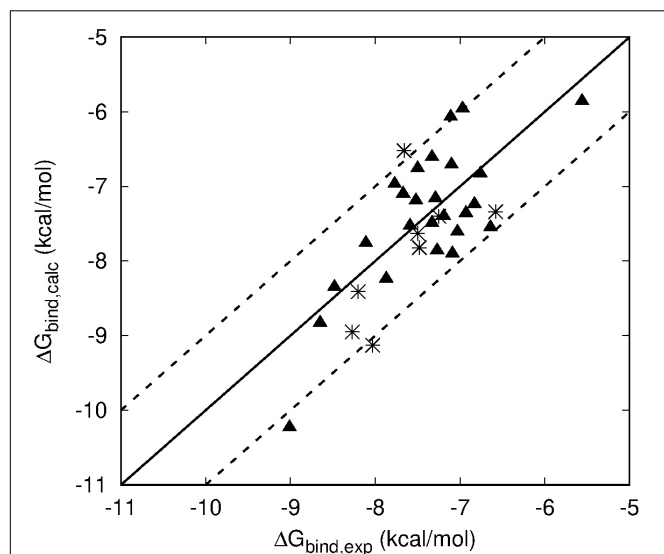


**FIGURE 4** | Scattered plot of LIE calculated (Y axis) and experimental (X-axis) binding affinities of all HFI compounds that have experimentally determined  $K_i$  values for WT (triangles) and F544I/V mutant version (stars) of IRAP. Main line denotes perfect agreement with experiments, while the two dashed lines are  $\pm 1 \text{ kcal}\cdot\text{mol}^{-1}$ .

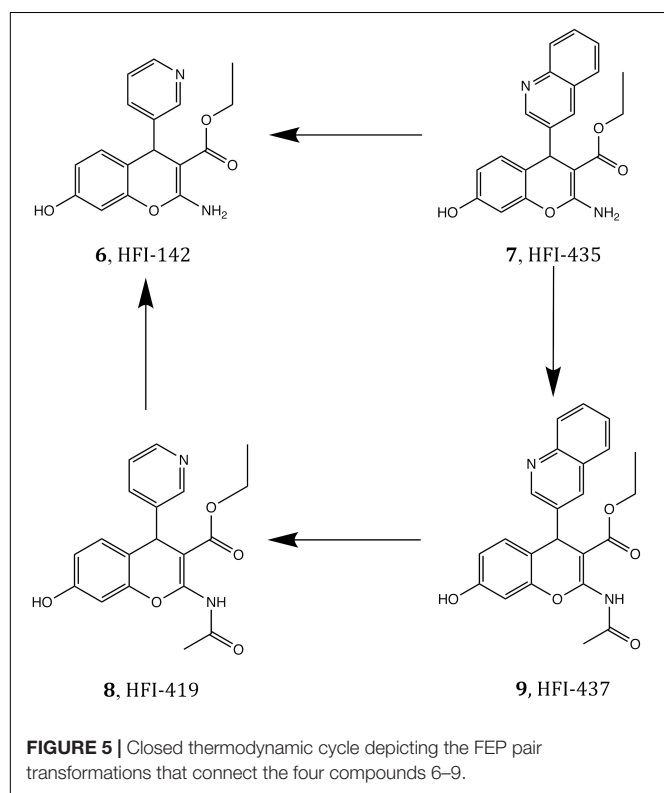


**FIGURE 5** | Closed thermodynamic cycle depicting the FEP pair transformations that connect the four compounds 6–9.

closed thermodynamic cycle shown in **Figure 5** explore the effect of replacing the acetamide by a free amino group in position 2 of the benzopyran ring, while the horizontal legs refer to the change of replacing 3-quinoline by 3-pyridyl.

The results of these FEP simulations are summarized in **Table 3** and **Figure 6**. The detrimental effect of replacing the acetamide by a free amino group in position 2 of the benzopyran ring was observed in both  $9 \rightarrow 7$  and  $8 \rightarrow 6$  FEP transformations. Our model reproduces the experimental effect very accurately, and assigns this effect to the loss of the interaction established between acetamide oxygen with the Glu431 backbone (**Figure 6D**). Interestingly, the detrimental effect of replacing 3-quinoline by 3-pyridyl (transformation of  $9 \rightarrow 8$  and  $7 \rightarrow 6$ ) was indirect, inducing the loss of the  $\pi$ -stacking interactions between the ligand and Phe544, while no significant effect was observed in the region of the substituent changed. During the transformation  $9 \rightarrow 8$ , these changes were accompanied by a replacement of the interaction of the acetamide oxygen with the backbone of Glu431, to establish a new interaction with Gln293, as shown in **Figure 6A**. These structural rearrangements explain the large experimental shifts in relative binding affinities between compounds 9 and 8, which were captured in our FEP simulations (**Table 3**). Overall, the calculated relative affinity change between the four compound pairs is in excellent agreement with the experimental data, with a MUE = 0.04 kcal/mol and an equally negligible cycle closure error of 0.09 kcal/mol, reinforcing the ability of this binding mode to explain the SAR of this series.

The next question was to evaluate the mutagenesis effects with FEP simulations. A first approach was to perform the four transformations illustrated in **Figure 5** but considering the F544I

**TABLE 3** | Experimental and FEP calculated relative binding free energies between ligand within the subset of compounds 6–9, both in wild type and mutant versions of IRAP.

Transformation	$\Delta\Delta G (B - A, \text{kcal mol}^{-1})^a$	
	FEP	Experimental <sup>b</sup>
<b>wt-IRAP</b>		
8→6	$0.68 \pm 0.70$	$0.58 \pm 0.34$
7→6	$1.10 \pm 0.46$	$1.07 \pm 0.36$
9→8	$1.90 \pm 0.18$	$1.89 \pm 0.30$
9→7	$1.38 \pm 0.50$	$1.40 \pm 0.32$
<b>F544I-IRAP</b>		
8→6	$1.44 \pm 0.98$	$1.30 \pm 0.27$
7→6	$0.87 \pm 0.29$	$0.88 \pm 0.26$
9→8	$1.39 \pm 0.20$	$1.31 \pm 0.17$
9→7	$0.74 \pm 0.37$	$1.73 \pm 0.16$
<b>F544V-IRAP</b>		
8→6	$1.04 \pm 0.65$	$1.07 \pm 0.14$
7→6	$0.61 \pm 0.24$	$0.29 \pm 0.15$
9→8	$0.78 \pm 0.30$	$0.54 \pm 0.26$
9→7	$1.40 \pm 0.25$	$1.32 \pm 0.26$

<sup>a</sup>Energies are expressed as mean  $\pm$  S.E.M. estimated from independent experiments (Albiston et al., 2010) or replicate MD simulations (FEP). <sup>b</sup> Experimental energies obtained from  $K_i$  values (Albiston et al., 2010) using the relation  $\Delta\Delta G_{\text{bind,exp}}^0 = RT \ln \left( \frac{K_i(B)}{K_i(A)} \right)$ .

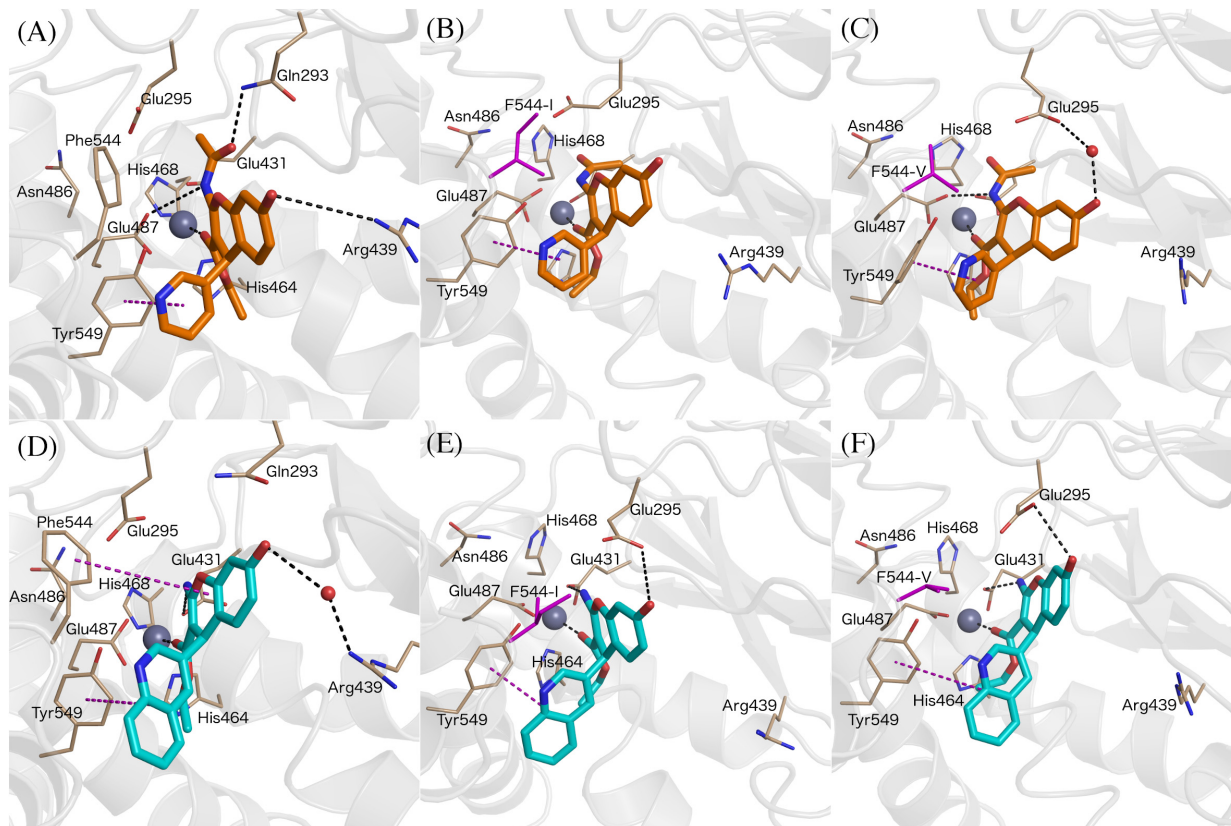


**FIGURE 6 |** Binding modes of compound 8 (**A**, orange sticks) and 7 (**D**, cyan sticks) in wt-IRAP active site determined by FEP simulations. Binding mode of compound 8 in F544I (**B**) and F544V (**C**). Binding mode of compound 7 in F544I (**E**) and F544V (**F**). All of the figures shown are extracted from representative snapshot simulations. Residues playing a role in ligand binding are explicitly shown, while residues F544I and F544V are represented in magenta color. The remaining atom representations and protein-ligand interactions following the scheme as in **Figure 3**.

and F544V IRAP mutants. While the four ligands bound in a conserved way as compared to the wt-IRAP, several important interactions are missing. For example, as shown in **Figure 6B**, compound 8 shows only two direct interactions, with  $\text{Zn}^{2+}$  and a  $\pi$ -stacking with Tyr549. The experimental reduction in binding affinity can thus be assigned to the loss of critical interactions such as  $\pi$ -stacking with Phe544 and H-bonds with Arg439. The obtained relative binding free energies from the FEP transformations in the mutant versions of IRAP are again in excellent agreement with the experimental data (**Table 3**), with MUE values of 0.31 kcal/mol (F544I) and 0.17 kcal/mol (F544V), and calculated cycle closure errors of 1.22 (F544I) and  $-0.19$  (F544V). The larger error observed for the F544I simulations is found to arise from the  $9 \rightarrow 7$  transformation, which is off by about 1 kcal/mol from the experimental value.

The above calculations were further complemented with a direct simulation of the Phe544 mutation both to Val and Ile. The protocol to perform such *in silico* site-directed mutagenesis approach has been recently automated (Jespersen et al., 2019) and thoroughly applied in our lab to characterize the site-directed mutagenesis effects on ligand binding for a number of GPCRs (Boukharta et al., 2014; Keränen et al., 2014, 2015). Here, one needs to perform the residue transformation both in

the presence and in the absence of the bound ligand to fulfill the thermodynamic cycle, obtaining an estimated shift in the binding affinity of the ligand involved, due to the mutation examined. The FEP protocol is based on successive annihilation of the sidechain atoms to the common intermediate of alanine, which is performed once from the wt sidechain, and in parallel simulations for each of the modeled mutant sidechains, so that the two thermodynamic cycles can be joined and the total effect of wt  $\rightarrow$  mutant calculated. The results, summarized in **Table 4**, show again excellent agreement with the experimental mutagenesis data, with MUE of 0.17 and 0.18 kcal/mol for Phe544Ile and Phe544Val, respectively, further confirming the validity of the proposed binding mode. It can be appreciated that for the case of the Phe  $\rightarrow$  Ile transformation, the effect on ligand binding was more accurately described by this approach (i.e., *in silico* mutagenesis) rather than comparing the ligand transformations performed in wt and mutant versions of the enzyme. As opposed to the end-point LIE simulations, the FEP simulations show a maintained interaction between the ligand and Arg439 along the wt-IRAP transformations ( $8 \rightarrow 6$  and  $9 \rightarrow 7$ , **Figures 6A,D**). The fact that this interaction is selectively lost in the simulations on the two IRAP mutants provides a molecular mechanism to the reduced affinity besides

**TABLE 4** | Experimental and FEP calculated shifts in binding free energies due to point mutations of IRAP, for the subset of compounds 6–9.  $\Delta\Delta G$  (mut – WT, kcal mol<sup>−1</sup>)<sup>a</sup>.

Compd	$\Delta\Delta G$ (mut – WT, kcal mol <sup>−1</sup> ) <sup>a</sup>						
	F544A	I544A	V544A	F544I		F544V	
	FEP			FEP	exp	FEP	exp
6	0.93 ± 0.20	−0.35 ± 0.19	0.41 ± 0.18	1.28 ± 0.19	1.24 ± 0.29	0.52 ± 0.19	0.42 ± 0.18
7	0.92 ± 0.20	−0.73 ± 0.20	−0.59 ± 0.29	1.66 ± 0.20	1.43 ± 0.33	1.51 ± 0.25	1.20 ± 0.34
8	0.31 ± 0.17	−0.21 ± 0.21	0.36 ± 0.11	0.52 ± 0.19	0.53 ± 0.32	−0.06 ± 0.15	−0.07 ± 0.32
9	1.10 ± 0.22	−0.41 ± 0.18	−0.48 ± 0.15	1.51 ± 0.20	1.10 ± 0.14	1.58 ± 0.19	1.28 ± 0.23

<sup>a</sup>Energies are expressed as mean ± S.E.M. estimated from independent experiments (Albiston et al., 2010) or replicate MD simulations (FEP).

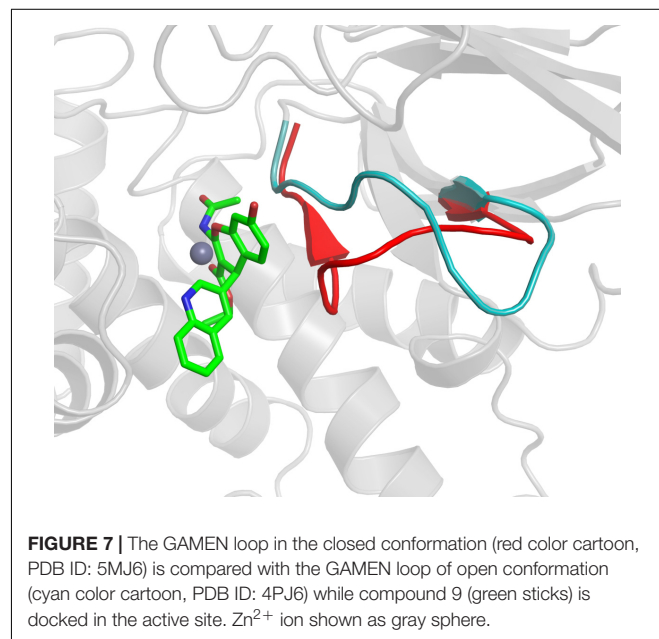
the weakened interactions with the mutant (Val or Ile) sidechains replacing Phe544. The simulations also allowed to envisage the reasons of high affinity of compound 9, which when transformed to either compound 8 or 7, consistently loses interactions with Glu431 and Glu487 or with Glu295, respectively, on both mutant or the mutant versions of IRAP (**Figure 6**).

## DISCUSSION

The benzopyran-based small molecule IRAP inhibitors (HFI series) constitute a promising chemotype for the development of first-in-class drugs for dementia and related diseases. Understanding the molecular mechanism of IRAP inhibition is thus crucial for the further hit-to-lead and lead optimization process of the existing collection of HFI compounds. In the absence of a crystal structure of any IRAP-HFI complex, we conducted an exhaustive docking study on the most potent compounds using the crystal structure of the semi-open conformation of IRAP (PDB 4PJ6). The selection of this conformation of the enzyme was based on the fact that it presents a different orientation of the GAMEN loop, as compared to the latest closed conformation structure of IRAP (PDB ID: 5MJ6). The superposition of the HFI-complex here determined with the closed conformation of IRAP, depicted in **Figure 7**, shows, however, no predicted steric clashes with the closed configuration of the GAMEN loop, thus suggesting that the HFI-series of compounds may bind to different IRAP conformations. The validity of the binding pose was further assessed by systematic estimation of the binding affinity for the complete series with the LIE approach, showing excellent agreement with the experimental data ( $R = 0.71$ , MUE = 0.5 Kcal/mol). More important, this binding mode allowed for a consistent interpretation of the full SAR for this series, in contrast with previous proposals in the literature. Such binding poses were proposed based on homology model (Albiston et al., 2010), semi-open (Hermans et al., 2015), and closed conformations (Mpakali et al., 2017) of IRAP, but all of them failed in explaining some intriguing features of this series. One particularly intriguing aspect not solved in the previous models was the role of 3-position substitutions on the chromene ring and the inactivity of 3-cyano compounds. Our binding pose of the HFI chemotype can explain this inactive series by highlighting the role of the oxygen

of the ester group in position 3 in coordinating the Zn<sup>2+</sup> ion. Thus, the 3-cyano series (15a–g) show instability of the predicted binding pose (high ligand RMSD values as compared to the compounds with measurable affinity), losing the key interactions with the enzyme and consequently the trajectories resulted in low LIE predicted free energies of binding. The LIE model also captures the observed tolerance for the aliphatic chain of the ester, even admitting an aromatic chain (17g) once the substituent at position 4 is fixed on the pyridine-3-yl substituent (series 17a–g, **Table 2**). Finally, the role of the hydroxy substituent in the chromone scaffold is also tuned down in our model, presenting this group toward a solvent-exposed area with polar residues in the vicinity, in agreement with the experimental SAR showing that this substituent can be swapped between positions 7 and 8 of the benzopyran ring (18f) while a fused phenyl ring is absolutely detrimental for the affinity (compounds 18g, 18h).

One common aspect with previous binding models is the role of residue Phe544, an important anchoring point through  $\pi$  – stacking with the benzopyran ring (**Figure 3**). The experimental mutagenesis data on this residue (Albiston et al., 2010) was here





computed in different ways, providing further support for this interaction but quantifying its effect. LIE simulations reveal that the interactions with the  $\text{Zn}^{2+}$  are maintained in the Phe544 mutant versions, explaining the moderate effect of mutation of this position to hydrophobic sidechains. However, moderate changes in affinity due to marked structural changes, as is a sidechain mutation or the type of the chemical modifications within series 6–9 (topological changes on a ring, amide versus substituted acetamide) might fall out of the sensibility of LIE modeling. For this reason, we investigated the 6–9 series and the mutagenesis effects with FEP simulations. The use of complementary FEP transformations (i.e., ligand perturbations on different enzyme forms, and receptor mutation upon binding of different ligands) provides “two sides of the same coin” that provide a comprehensive perspective of the ligand binding process, as recently showed for the elucidation of the binding mode of  $\text{A}_{2\text{A}}$  adenosine receptor antagonists (Jespers et al., 2020). In the IRAP system, these simulations allowed to identify interactions that were selectively lost on the mutant versions of the enzyme (i.e., between the ligand and Arg439), or differences in ligand binding consistently observed within wt and mutant versions of the enzyme, as the case of the interactions of compound 9 with the network of glutamic acid residues (Figure 6). These simulations also showed the role of residues like Tyr549 and Glu295 and Glu431, suggesting further site directed mutagenesis experiments to probe this model.

In summary, the binding model for the HFI series here presented, which is supported by different methods of free energy calculations, provides a unified model across the series that satisfactorily explains the observed SAR of the series. Moreover, this binding model points to a relatively promiscuity for the conformations of IRAP, and sets the grounds for further structure-based optimization.

## REFERENCES

- Albiston, A. L., McDowall, S. G., Matsacos, D., Sim, P., Clune, E., Mustafa, T., et al. (2001). Evidence that the angiotensin IV (AT4) receptor is the enzyme insulin-regulated aminopeptidase. *J. Biol. Chem.* 276, 48623–48626. doi: 10.1074/jbc.C100512200
- Albiston, A. L., Morton, C. J., Ng, H. L., Pham, V., Yeatman, H. R., Ye, S., et al. (2008). Identification and characterization of a new cognitive enhancer based on inhibition of insulin-regulated aminopeptidase. *FASEB J.* 22, 4209–4217. doi: 10.1096/fj.08-112227
- Albiston, A. L., Mustafa, T., McDowall, S. G., Mendelsohn, F. A. O., Lee, J., and Chai, S. Y. (2003). AT4 receptor is insulin-regulated membrane aminopeptidase: potential mechanisms of memory enhancement. *Trends Endocrinol. Metabol.* 14, 72–77. doi: 10.1016/S1043-2760(02)00037-1
- Albiston, A. L., Peck, G. R., Yeatman, H. R., Fernando, R., Ye, S., and Chai, S. Y. (2007). Therapeutic targeting of insulin-regulated aminopeptidase: heads and Tails? *Pharmacol. Therapeut.* 116, 417–427. doi: 10.1016/j.pharmthera.2007.07.006
- Albiston, A. L., Pham, V., Ye, S., Ng, L., Lew, R. A., Thompson, P. E., et al. (2010). Phenylalanine-544 plays a key role in substrate and inhibitor binding by providing a hydrophobic packing point at the active site of insulin-regulated aminopeptidase. *Mol. Pharmacol.* 78, 600–607. doi: 10.1124/mol.110.065458
- Almlöf, M., Brandsdal, B. O., and Åqvist, J. (2004). Binding affinity prediction with different force fields: examination of the linear interaction energy method. *J. Comput. Chem.* 25, 1242–1254. doi: 10.1002/jcc.20047
- Almlöf, M., Carlsson, J., and Åqvist, J. (2007). Improving the accuracy of the linear interaction energy method for solvation free energies. *J. Chem. Theory Comput.* 3, 2162–2175. doi: 10.1021/ct700106b
- Åqvist, J., Medina, C., and Samuelsson, J. E. A. (1994). New method for predicting binding affinity in computer-aided drug design. *Protein Eng.* 7, 385–391.
- Barlow, N., and Thompson, P. E. (2020). IRAP inhibitors: M1-aminopeptidase family inspiration. *Front. Pharmacol.* 11:585930. doi: 10.3389/fphar.2020.585930
- Boukharta, L., Gutiérrez-de-Terán, H., and Åqvist, J. (2014). Computational prediction of alanine scanning and ligand binding energetics in G-Protein coupled receptors. *PLoS Comput. Biol.* 10:e1003585. doi: 10.1371/journal.pcbi.1003585
- Braszkowski, J. J., Kupryszewski, G., Witczuk, B., and Wiśniewski, K. (1988). Angiotensin Ii-(3–8)-hexapeptide affects motor activity, performance of passive avoidance and a conditioned avoidance response in rats. *Neuroscience* 27, 777–783. doi: 10.1016/0306-4522(88)90182-0
- Chai, S. Y., Bastias, M. A., Clune, E. F., Matsacos, D. J., Mustafa, T., Lee, J. H., et al. (2000). Distribution of angiotensin IV binding sites (AT4 Receptor) in the human forebrain, midbrain and pons as visualised by in vitro receptor autoradiography. *J. Chem. Neuroanat.* 20, 339–348. doi: 10.1016/S0891-0618(00)00112-5
- Chai, S. Y., Fernando, R., Peck, G., Ye, S.-Y., Mendelsohn, F. A. O., Jenkins, T. A., et al. (2004). What's new in the renin-angiotensin system? The angiotensin IV/AT4 receptor. *Cell. Mol. Life Sci.* 61, 2728–2737. doi: 10.1007/s00018-004-4246-1

## DATA AVAILABILITY STATEMENT

The raw data supporting the conclusions of this article will be made available by the authors, without undue reservation.

## AUTHOR CONTRIBUTIONS

SV designed, performed and analyzed the experiments, and wrote the first draft. HG-D-T designed and analyzed the experiments and wrote the manuscript. JÅ and AH designed the experiments and contributed to the final writing of the manuscript. All authors contributed to the article and approved the submitted version.

## FUNDING

This work was supported from the Swedish Research Council (VR) and the Swedish Network for e-sciences (eSENCE) is gratefully acknowledged.

## ACKNOWLEDGMENTS

The simulations were performed on resources provided by Swedish National Infrastructure for Computing (SNIC) at HPC2N and C3SE.

## SUPPLEMENTARY MATERIAL

The Supplementary Material for this article can be found online at: <https://www.frontiersin.org/articles/10.3389/fmolb.2021.625274/full#supplementary-material>

- De Bundel, D., Smolders, I., Yang, R., Albiston, A. L., Michotte, Y., and Chai, S. Y. (2009). Angiotensin IV and LVV-haemorphin 7 enhance spatial working memory in rats: effects on hippocampal glucose levels and blood flow. *Neurobiol. Learn. Mem.* 92, 19–26. doi: 10.1016/j.nlm.2009.02.004
- Diwakarla, S., Nylander, E., Grönbladh, A., Vanga, S. R., Khan, Y. S., Gutiérrez-de-Terán, H., et al. (2016a). Aryl sulfonamide inhibitors of insulin-regulated aminopeptidase enhance Spine density in primary hippocampal neuron cultures. *ACS Chem. Neurosci.* 7, 1383–1392. doi: 10.1021/acscchemneuro.6b00146
- Diwakarla, S., Nylander, E., Grönbladh, A., Vanga, S. R., Khan, Y. S., Gutiérrez-de-Terán, H., et al. (2016b). Binding to and inhibition of insulin-regulated aminopeptidase (IRAP) by macrocyclic disulfides enhances spine density. *Mol. Pharmacol.* 89, 413–424. doi: 10.1124/mol.115.102533
- Fu, M., Yu, X., Lu, J., and Zuo, Y. (2012). Repetitive motor learning induces coordinated formation of clustered dendritic spines in Vivo. *Nature* 483, 92–95. doi: 10.1038/nature10844
- Georgiadis, D., Ziotopoulou, A., Kaloumenou, E., Lelis, A., and Papasava, A. (2020). The Discovery of insulin-regulated aminopeptidase (IRAP) inhibitors: a literature review. *Front. Pharmacol.* 11:585838. doi: 10.3389/fphar.2020.585838
- Halgren, T. A., Murphy, R. B., Friesner, R. A., Beard, H. S., Frye, L. L., Pollard, W. T., et al. (2004). Glide: a new approach for rapid, accurate docking and scoring. 2. Enrichment factors in database screening. *J. Med. Chem.* 47, 1750–1759. doi: 10.1021/jm030644s
- Hallberg, M. (2009). Targeting the insulin-regulated Aminopeptidase/AT4 receptor for cognitive disorders. *Drug News Perspect.* 22, 133–139. doi: 10.1358/dnp.2009.22.3.1325032
- Hallberg, M., and Larhed, M. (2020). From angiotensin IV to small peptidomimetics inhibiting insulin-regulated aminopeptidase. *Front. Pharmacol.* 11:590855. doi: 10.3389/fphar.2020.590855
- Hansson, T., Marelus, J., and Åqvist, J. (1998). Ligand binding affinity prediction by linear interaction energy methods. *J. Comput. Aided Mol. Des.* 12, 27–35.
- Harding, J. W., Cook, V. I., Miller-Wing, A. V., Hanesworth, J. M., Sardinia, M. F., Hall, K. L., et al. (1992). Identification of an AII(3–8) [AIV] binding site in guinea pig hippocampus. *Brain Res.* 583, 340–343. doi: 10.1016/S0006-8993(10)80047-2
- Hattori, A., and Tsujimoto, M. (2013). Endoplasmic reticulum aminopeptidases: biochemistry, physiology and pathology. *J. Biochem.* 154, 219–228. doi: 10.1093/jb/mvt066
- Hermans, S. J., Ascher, D. B., Hancock, N. C., Holien, J. K., Michell, B. J., Chai, S. Y., et al. (2015). Crystal structure of human insulin-regulated aminopeptidase with specificity for cyclic peptides. *Protein Sci.* 24, 190–199. doi: 10.1002/pro.2604
- Jespersen, W., Isaksen, G. V., Andberg, T. A. H., Vasile, S., van Veen, A., Åqvist, J., et al. (2019). QresFEP: an automated protocol for free energy calculations of protein mutations in Q. *J. Chem. Theory Comput.* 15, 5461–5473. doi: 10.1021/acs.jctc.9b00538
- Jespersen, W., Verdon, G., Azuaje, J., Majellaro, M., Keränen, H., García-Mera, X., et al. (2020). X-Ray crystallography and free energy calculations reveal the binding mechanism of A2A adenosine receptor antagonists. *Angew. Chem. Int. Ed.* 59, 16536–16543. doi: 10.1002/anie.202003788
- Jorgensen, W. L., Chandrasekhar, J., Madura, J. D., Impey, R. W., and Klein, M. L. (1983). Comparison of simple potential functions for simulating liquid water. *J. Chem. Phys.* 79, 926–935. doi: 10.1063/1.445869
- Jorgensen, W. L., Maxwell, D. S., and Tirado-Rives, J. (1996). Development and testing of the OPLS all-atom force field on conformational energetics and Properties of organic liquids. *J. Am. Chem. Soc.* 118, 11225–11236. doi: 10.1021/ja9621760
- Keränen, H., Åqvist, J., and Gutiérrez-de-Terán, H. (2015). Free energy calculations of A2A adenosine receptor mutation effects on agonist binding. *Chem. Commun.* 51, 3522–3525. doi: 10.1039/C4CC09517K
- Keränen, H., Gutiérrez-de-Terán, H., and Åqvist, J. (2014). Structural and energetic effects of A2A adenosine receptor mutations on agonist and antagonist binding. *PLoS One* 9:e108492. doi: 10.1371/journal.pone.0108492
- King, G., and Warshel, A. A. (1989). Surface constrained all-atom solvent model for effective simulations of polar solutions. *J. Chem. Phys.* 91, 3647–3661. doi: 10.1063/1.456845
- Lee, F. S., and Warshel, A. A. (1992). Local reaction field method for fast evaluation of long-range electrostatic interactions in molecular simulations. *J. Chem. Phys.* 97, 3100–3107. doi: 10.1063/1.462997
- Lee, J., Mustafa, T., McDowall, S. G., Mendelsohn, F. A. O., Brennan, M., Lew, R. A., et al. (2003). Structure-activity study of LVV-hemorphin-7: angiotensin AT4 receptor ligand and inhibitor of insulin-regulated aminopeptidase. *J. Pharmacol. Exp. Ther.* 305, 205–211. doi: 10.1124/jpet.102.045492
- Lew, R. A., Mustafa, T., Ye, S., McDowall, S. G., Chai, S. Y., and Albiston, A. L. (2003). Angiotensin AT4 ligands are potent, competitive inhibitors of insulin regulated aminopeptidase (IRAP). *J. Neurochem.* 86, 344–350. doi: 10.1046/j.1471-4159.2003.01852.x
- Marelius, J., Kolmodin, K., Feierberg, I., and Åqvist, J. Q. (1998). A Molecular dynamics program for free energy calculations and empirical valence bond simulations in biomolecular systems. *J. Mol. Graph. Model* 16, 213–225, 261.
- Mishra, S. K., Sund, J., Åqvist, J., and Koëa, J. (2012). Computational prediction of monosaccharide binding free energies to lectins with linear interaction energy models. *J. Comput. Chem.* 33, 2340–2350. doi: 10.1002/jcc.23081
- Mountford, S. J., Albiston, A. L., Charman, W. N., Ng, L., Holien, J. K., Parker, M. W., et al. (2014). Synthesis, structure-activity relationships and brain uptake of a novel series of benzopyran inhibitors of insulin-regulated aminopeptidase. *J. Med. Chem.* 57, 1368–1377. doi: 10.1021/jm401540f
- Mpakali, A., Saridakis, E., Giastas, P., Maben, Z., Stern, L. J., Larhed, M., et al. (2020). Structural basis of inhibition of insulin-regulated aminopeptidase by a macrocyclic peptidic inhibitor. *ACS Med. Chem. Lett.* 11, 1429–1434. doi: 10.1021/acsmchemlett.0c00172
- Mpakali, A., Saridakis, E., Harlos, K., Zhao, Y., Kokkala, P., Georgiadis, D., et al. (2017). Ligand-induced conformational change of insulin-regulated aminopeptidase: insights on catalytic mechanism and active site plasticity. *J. Med. Chem.* 60, 2963–2972. doi: 10.1021/acs.jmedchem.6b01890
- O'Malley, A., O'Connell, C., and Regan, C. M. (1998). Ultrastructural analysis reveals avoidance conditioning to induce a transient increase in hippocampal dentate spine density in the 6hour post-training period of consolidation. *Neuroscience* 87, 607–613. doi: 10.1016/S0306-4522(98)00178-X
- Roberts, K. A., Krebs, L. T., Kramár, E., Shaffer, M. J., Harding, J. W., and Wright, J. W. (1995). Autoradiographic identification of brain angiotensin IV binding sites and differential C-Fos expression following intracerebroventricular injection of angiotensin II and IV in rats. *Brain Res.* 682, 13–21. doi: 10.1016/0006-8993(95)00289-3
- Ryckaert, J.-P., Ciccotti, G., and Berendsen, H. J. C. (1977). Numerical integration of the cartesian equations of motion of a system with constraints: molecular dynamics of n-alkanes. *J. Comp. Phys.* 23, 327–341. doi: 10.1016/0021-9991(77)90098-5
- Saveanu, L., Carroll, O., Weimershaus, M., Guermontprez, P., Firat, E., Lindo, V., et al. (2009). IRAP Identifies an endosomal compartment required for MHC class I cross-presentation. *Science* 325, 213–217. doi: 10.1126/science.1172845
- Segura, E., Albiston, A. L., Wicks, I. P., Chai, S. Y., and Villadangos, J. A. (2009). Different cross-presentation pathways in steady-state and inflammatory dendritic cells. *Proc. Nat. Acad. Sci. U.S.A.* 106, 20377–20381. doi: 10.1073/pnas.0910295106
- Seyer, B., Diwakarla, S., Burns, P., Hallberg, A., Grönbladh, A., Hallberg, M., et al. (2020). Insulin-regulated aminopeptidase inhibitor-mediated increases in dendritic spine density are facilitated by glucose uptake. *J. Neurochem.* 153, 485–494. doi: 10.1111/jnc.14880
- Shamsudin Khan, Y., Kazemi, M., Gutiérrez-de-Terán, H., and Åqvist, J. (2015). Origin of the enigmatic stepwise tight-binding inhibition of cyclooxygenase-1. *Biochemistry* 54, 7283–7291. doi: 10.1021/acs.biochem.5b01024
- Stragier, B., Bundel, D. D., Sarre, S., Smolders, I., Vauquelin, G., Dupont, A., et al. (2008). Involvement of insulin-regulated aminopeptidase in the effects of the renin-angiotensin fragment angiotensin IV: a review. *Heart Fail. Rev.* 13, 321–337. doi: 10.1007/s10741-007-9062-x
- Thunnissen, M. M. G. M., Nordlund, P., and Haeggström, J. Z. (2001). Crystal Structure of human leukotriene A<sub>4</sub> hydrolase, a bifunctional enzyme in inflammation. *Nat. Struct. Mol. Biol.* 8, 131–135. doi: 10.1038/84117
- Vanga, S. R., Sävmarker, J., Ng, L., Larhed, M., Hallberg, M., Åqvist, J., et al. (2018). Structural basis of inhibition of human insulin-regulated aminopeptidase (IRAP) by Aryl sulfonamides. *ACS Omega* 3, 4509–4521. doi: 10.1021/acsomega.8b00595
- Vauquelin, G., Michotte, Y., Smolders, I., Sarre, S., Ebinger, G., Dupont, A., et al. (2002). Cellular targets for angiotensin II fragments: pharmacological

- and molecular evidence. *J. Renin Angiotensin Aldosterone Syst.* 3, 195–204. doi: 10.3317/jraas.2002.041
- Wright, J. W., Clemens, J. A., Panetta, J. A., Smalstig, E. B., Weatherly, L. S., Kramár, E. A., et al. (1996). Effects of LY231617 and angiotensin IV on ischemia-induced deficits in circular water maze and passive avoidance performance in rats. *Brain Res.* 717, 1–11. doi: 10.1016/0006-8993(95)01454-3
- Wright, J. W., Miller-Wing, A. V., Shaffer, M. J., Higginson, C., Wright, D. E., Hanesworth, J. M., et al. (1993). Angiotensin II(3–8) (ANG IV) hippocampal binding: potential role in the facilitation of memory. *Brain Res. Bull.* 32, 497–502. doi: 10.1016/0361-9230(93)90297-O
- Wright, J. W., Stubley, L., Pederson, E. S., Kramár, E. A., Hanesworth, J. M., and Harding, J. W. (1999). Contributions of the brain angiotensin IV–AT4 receptor subtype system to spatial learning. *J. Neurosci.* 19, 3952–3961.
- Zwanzig, R. W. (1954). High-temperature equation of state by a perturbation method. I. nonpolar gases. *J. Chem. Phys.* 22, 1420–1426. doi: 10.1063/1.1740409
- Conflict of Interest:** The authors declare that the research was conducted in the absence of any commercial or financial relationships that could be construed as a potential conflict of interest.

Copyright © 2021 Vanga, Åqvist, Hallberg and Gutiérrez-de-Terán. This is an open-access article distributed under the terms of the Creative Commons Attribution License (CC BY). The use, distribution or reproduction in other forums is permitted, provided the original author(s) and the copyright owner(s) are credited and that the original publication in this journal is cited, in accordance with accepted academic practice. No use, distribution or reproduction is permitted which does not comply with these terms.

# Advantages of publishing in Frontiers



## OPEN ACCESS

Articles are free to read  
for greatest visibility  
and readership



## FAST PUBLICATION

Around 90 days  
from submission  
to decision



## HIGH QUALITY PEER-REVIEW

Rigorous, collaborative,  
and constructive  
peer-review



## TRANSPARENT PEER-REVIEW

Editors and reviewers  
acknowledged by name  
on published articles

## Frontiers

Avenue du Tribunal-Fédéral 34  
1005 Lausanne | Switzerland

Visit us: [www.frontiersin.org](http://www.frontiersin.org)

Contact us: [frontiersin.org/about/contact](http://frontiersin.org/about/contact)



## REPRODUCIBILITY OF RESEARCH

Support open data  
and methods to enhance  
research reproducibility



## DIGITAL PUBLISHING

Articles designed  
for optimal readership  
across devices



## FOLLOW US

@frontiersin



## IMPACT METRICS

Advanced article metrics  
track visibility across  
digital media



## EXTENSIVE PROMOTION

Marketing  
and promotion  
of impactful research



## LOOP RESEARCH NETWORK

Our network  
increases your  
article's readership